THE Mg_2 INDEX
FOR
STELLAR POPULATION STUDIES

Thesis submitted to the
International School for Advanced Studies, Trieste, Italy
– *Astrophysics Sector* –
in partial fulfilment of the requirements for the degree of

Doctor Philosophiae

Candidate:
Ravi Kumar Gulati

Supervisor:
Prof. Dennis W. Sciama
Co-Supervisor:
Prof. Maria L. Malagnini

Academic Year 1990/91

to my parents

and

to my wife

Contents

List of Tables

List of Figures

Acknowledgements

First and foremost, I would like to express my gratitude to my co-supervisor, Professor M.L. Malagnini, for suggesting me the topic of the research and for her invaluable guidance and support throughout the course of this project. Dr. C. Morossi deserves much credit for friendly guidance and for critical reading of the thesis. My thanks are also due to my supervisor, Professor D.W. Sciama and to Professor M. Hack for giving me inspirations and general support. This research would have been impossible without the support of Dr. R.L. Kurucz, who has kindly provided me with his latest models and line data before publication. Also I am thankful for his hospitality and guidance rendered to me during my visit to CfA, Cambridge, where a part of the thesis work was done. I am also grateful to Dr. F. Castelli for allowing me to use Kurucz' ATLAS and SYNTHE and her own computer programs and for the same reasons I thank Dr. G. Vladilo.

Thanks are also due to Dr. Buzzoni, Dr. Gariboldi and Dr. Mantegezza for providing me the observed stellar data and for their collaboration. This work has been greatly benefited from my visit to Brazil, from the funds of Professor M.L. Malagnini (CNR bilateral grant number 89.0003702), for attending IAU symposium 149 on The Stellar Populations of Galaxies. There I have benefited from the discussion with Professor S. Faber, who has given me the data for stars prior to publication.

I acknowledge the hospitality and computing facilities offered by Osservatorio Astronomico di Trieste and Dipartimento di Astronomia dell' Università degli Studi di Trieste.

Last but not least, I thank my wife, Neena, for her unflagging support throughout the difficult course of this dissertation research. Finally a great contribution to this work has come from the love and best wishes of our families.

Abstract

Since the improvement in the observational techniques, it has become possible to acquire a large number of photometric and spectrophotometric observations not only for stellar systems, but also for individual stars in nearby stellar systems, i.e. clusters and galaxies. In order to understand the evolutionary history and chemistry of these stellar systems in the context of evolutionary population models, it is essential to use spectral features, since models based on broad-band and intermediate-band photometric systems alone are inadequate to disentangle the effect of age from that due to metallicity, in the sense that old systems of metal poor composition exhibit the same colors as young systems of metal rich chemical composition. These spectral features must be selected considering that they should be easily identified in distant stellar systems, and should underlie the relationships with fundamental parameters that characterize stellar populations. A list of useful spectral features, observed in the visible and near-infrared regions, is given by Faber (1973), Spinrad and Taylor (1971) and Rose (1984). One of these features, which is strong in spectra of globular clusters and elliptical galaxies and conspicuous even at large distances, is measured in the form of the so-called Mg_2 index. It is centered around 5176 Å and is mainly composed of lines of the Mg b triplet and molecular bands of MgH.

Its relevance for the study of stellar populations in old stellar systems

has been emphasized by Burstein (1985). Since the Mg_2 index is considered to be a good indicator of metallicity for old stellar systems and indicator of surface gravities for cool stars, it has been observed widely for stellar systems and for selected samples of stars (*e.g.* Faber *et al.*, 1985, Gorgas *et al.*, 1990, Brodie and Huchra, 1991, Buzzoni *et al.*, 1991).

On the theoretical side, Mould (1978) was the first who attempted to synthesize an Mg index by using model atmospheres from different sources available at that time. In our previous studies (Gulati *et al.*, 1991), we investigated the synthetic Mg_2 index based on model atmospheres computed by us in an homogenous way in the case of solar chemical composition. At present, Kurucz (1991a) has provided us with a new computed by taking into account the contribution to opacity from a new and very large collection not only of atomic, but also of molecular line data, and a refined treatment of atmospheric convection. In addition to model improvements, line parameters for the line data referring to the wavelength region of the Mg_2 index have been improved by us. These parameters were derived after carefully matching the observed solar central intensity spectrum with the one predicted theoretically. Using the new grid of Kurucz models and our line list, we have now set up a comprehensive library of synthetic spectra in the wavelength range of 4850–5400 Å, covering a wide range of temperature, surface gravity, and metallicity for representing different stellar populations. We have studied the behaviour of spectral features involved in the region of the Mg_2 index with respect to basic atmospheric parameters and other parameters that control the spectral energy distribution in the synthetic spectra.

We have discussed the results of synthetic spectra and index in the light of our observations of reference field stars at the moderate resolution. We have calibrated the synthetic Mg_2, computed from the library of synthetic stellar spectra, against basic stellar atmospheric parameters which will allow us to populate the stellar systems with certain prescription of evolutionary isochrones and initial mass functions.

The results we obtained and relevant applications can be outlined in the following points:

- Synthetic stellar spectra, based on Kurucz new models that take into account the contribution of molecular opacities, reproduce very well the observational spectral behaviour of cool stars at moderate resolution in the region of the Mg_2 index.
- The synthetic Mg_2 index is shown to depend both on effective temperature and surface gravity for models of three different metallicities.
- The new line list derived in the region of the Mg_2 index will be an asset for high resolution spectroscopic analysis.
- The library of synthetic stellar fluxes that we have computed for models representative of cool stars can be profitably compared with observations in order to estimate the basic atmospheric parameters effective temperature, surface gravity and metallicity.
- The library of synthetic stellar fluxes can be used to derive other spectral indices, namely Mg *b* λ5177 Å, Fe λ5270 Å, and Mg_1, for stellar populations studies.

We present here our theoretical calibration of the Mg_2 index with respect to effective temperature and surface gravity, for different values of metallicities, thus providing the fundamental tool for evaluating the integrated theoretical Mg_2 index of stellar systems by using stellar population synthesis models.

Chapter 1

Introduction

The main information concerning the structure of the universe is carried out by the radiation emitted by stellar systems. Most of our knowledge about stellar populations in stellar systems is based on statistical analysis of data for individual stars. Current concept of stellar populations relies on the determination of stellar metallicities, ages, positional and dynamical properties. With the exception of few nearby stellar system, it is impossible to perform star-by-star analysis. Therefore, the other approach to study stellar populations of distant stellar systems is through their integrated light.

The problem of disentangling the composite light from galaxy spectra was first faced by Whipple (1935), who developed techniques to synthesize absorption lines strengths and profiles in galaxy spectra. He showed that different types of stars may provide comparable contributions to the integrated spectra at a given wavelength. A composite nature is a fundamental characteristic of integrated light, and meaningful results can not be obtained unless it is properly modeled through population synthesis techniques.

From the technical point of view, population synthesis techniques flow in two streams. On one hand, one starts with a color-magnitude (CM) diagram and predicts the integrated spectral energy distributions. This technique is known as evolutionary population synthesis (Barbaro and Olivi, 1986, Renzini and Buzzoni, 1986, Buzzoni, 1989). On the other hand, one starts from

an observed spectral energy distribution and estimates the color-magnitude diagram that fits it best. This technique is called "optimizing synthesis" (O'Connell, 1980, Pickles, 1985).

In both these approaches, it is highly desirable to have a complete and fully tested grid of stellar evolutionary tracks and a library of spectral energy distributions (SED's) which may either be theoretical or observed ones. The theoretical evolutionary tracks can be successfully used only when accurate tests prove their ability to reproduce characteristics of real stars and stellar systems. Several sets of stellar iscochrones have become available (VandenBerg, 1985, Green *et al.* 1987) which can be complemented with the observations (*e.g.* Frogel and Whitford, 1987) of advanced stages of stellar evolution, where our theoretical knowledge is yet poor.

In order to synthesize the spectra of stellar systems it is necessary to have spectral energy distributions available for the whole range of stellar parameters (mass, age, chemical composition, etc.). In principle, one must provide the complete coverage of SED's in each non-void box of the CM diagram and a complete link between theoretical physical parameters and observable or empirical quantities needed to compare models and stars. Moreover, the observed SED's can be replaced by the ones computed from theoretical models only after the comparison between observed and computed SED's within acceptable limits on errors. In addition to this, the library of SED's should cover the entire wavelength range accessible with the present instruments as the contribution to the total energy from different stellar components depends on the evolutionary status of stellar systems. For instance, from young stellar systems, due to the presence of early-type stars, the overwhelming contribution of energy is in the uv- and far uv-regions.

Population synthesis models based on the current knowledge of stellar evolution and stellar atmospheres have been evolved into two generations.

The first generation of evolutionary stellar populations models were based on broad-band photometric colors so as to give integrated colors of galaxies.

The so-called photometric models were initiated by Tinsley (1972,1975) for interpreting visible colors of galaxies of the Hubble sequence in the color-color diagram in the form of (U-B) vs (B-V). Such kind of models were later improved upon after the prediction of various processes such as nebular components (Huchra, 1977), metal deficiency effect and far-UV colors (Rocca-Volmerange *et al.* 1981), and continuous metallicity effect (Arimoto and Yoshi, 1986). Despite the fact that these models have been applied to stellar systems successfully, still there remains the problem of disentangling the interdependence of metallicity and age on the resulting integrated spectral energy distributions, in the sense that the increasing of metal abundance produces the same effect one obtains by increasing the age of more metal-poor population.

A second generation of models were built by using the empirical library of stellar spectra in the visible and infrared wavelength regions obtained at intermediate resolution by O'Connell (1980) and by Pickles (1985). They demonstrated that with the careful selection of continuum and absorption line strength bandpasses one can separate the age effects from the metallicity ones. The importance of the study of the optical region in the spectra of galaxies has long been recognized, since this is the part of the spectrum where old stellar populations emit most of their energy (Spinrad and Taylor, 1969, Faber, 1973). This spectral range has been observed extensively for spectroscopic studies in the past few years by using CCD detectors. It contains few absorption features which can readily be observed in distant stellar systems and will provide useful information about them. A useful list of such spectral features, observed for a large sample of K-giant stars in view of understanding early-type stellar systems, has been given by Faber *et al.* (1985). In particular, the feature around 5176 Å, composed of mainly Mg b and MgH lines, has been observed for a large number of old stellar systems such as globular clusters and elliptical galaxies (*e.g.* Burstein *et al.*, 1984; Davies *et al.*, 1987, Brodie and Huchra, 1990, Buzzoni *et al.*, 1991), and for

field stars (Faber *et al.* 1985). The Mg_2 index [1], which is used to measure the above mentioned feature, is considered to be an indicator of metallicity for stellar systems.

The Mg index has been interpreted empirically by large number of people. Although this kind of approach is quite good qualitatively, one can certainly understand better the details of sensitivities of the index by taking advantage of the control given by the spectrum synthesis technique. In a first attempt to synthesize an Mg index for a set of chemically homogenous model galaxies, Mould (1978) computed the synthetic spectra based on model atmospheres and line data available at that time, and calculated the theoretical indices on the system of Spinrad and Taylor (1971). Recently, Barbuy (1989) and ourselves (Gulati *et al.*, 1991) have investigated the behavior in the spectral region 4800-5400 Å using synthetic spectra based on models of Gustaffson *et al.* (1975) and models we computed extending Kurucz (1979b) grid to low temperatures, respectively.

Kurucz (1991a) has now computed a new grid of model atmospheres based on new calculations of statistical opacity distribution functions derived from his most comprehensive line list. This updated line list is the most complete available at present (58 million against about 1 million available in the recent past), and takes into account the contribution of molecules which are the most important source of opacity for cool stars. By using this grid of models, we have revisited the region of the Mg_2 index and have computed the new grid of synthetic spectra in the wavelength range 4850–5400 Å, and consequently the grid of Mg_2 index for models representative of cool stars of different chemical composition. We have derived the set of relationships of Mg_2 vs. atmospheric parameters to be used in stellar population synthesis models to predict synthetic integrated Mg_2 for stellar systems.

The structure of the present thesis is as follows:

[1]The Mg_2 index is defined as the ratio of the integrated flux in the central band ($\lambda\lambda$ 5156.00-5197.25 Å) to the flux at the local continuum (which is interpolated between sideband intervals $\lambda\lambda$ 4897.00-4958.25 Å, $\lambda\lambda$ 5303.00-5366.75 Å) expressed in magnitude

In the first chapter, we discuss the ingredients involved in preparing the library of synthetic spectra in the wavelength range $\lambda\lambda$ 4850-5400 Å. A large part of this chapter is devoted to the description of the method used to compute synthetic spectra based on new models and line data. Much of our contribution in this chapter is to derive the line parameters of line data in a semi-empirical way and to investigate sensitivity of the features, in the region of the Mg_2 index, to the input parameters.

Chapter second describes in some detail the computational aspects of the synthetic Mg_2 index. We present the dependence of the synthetic Mg_2 index on the basic atmospheric parameters, effective temperature and surface gravity, and the calibration of the index with respect to them for different values of metallicity. The implications of the calibration of the Mg_2 against basic atmospheric parameters are indicated for the study of stellar systems.

In the third chapter, we present briefly the observational stellar data, obtained at the ESO Observatory, used for comparing with theoretical predictions, and derivation of instrumental profile.

Finally in chapter four, we examine the library of synthetic spectra in the light of our observational sample. Much of our current research centers around the comparison of observed and synthetic stellar spectra to verify the reliability of the synthetic spectra which will make up our "stellar library". We also compare the predicted integrated fluxes in the continuum as well as in the central bandpasses of the index with those of observed ones. We investigate the consistency of the grid of synthetic Mg_2 for solar chemical composition by comparing it with our and other empirical determinations.

Chapter 2

Spectrum Synthesis

The reliability of stellar atmospheric models can be ensured by properly reproducing the observed fluxes, colors and line profiles. Moreover, the careful interpretation of the observations of stars require the use of detailed model atmospheres which can be used to calibrate the empirically derived data in terms of atmospheric parameters. Comprehensive grids of blanketed flux constant model atmospheres available are those of Kurucz (1979a,1991a) or Gustaffson *et al.* (1975). Kurucz (1979a) models have been proved to faithfully reproduce the stellar continuum of B, A and F stars in the visible and ultraviolet wavelength regions (Malagnini and Morossi, 1988, and reference therein), whereas, Kurucz (1991a) new grid of models is extended down to K stars and provides fluxes and colors for F, G and K type stars. However, these models give the surface fluxes at step of $\Delta\lambda \sim 25$ Å, or $\Delta\lambda \sim 10$ Å, which is inadequate to resolve the important spectral features observed even at moderate resolution. Hence we need a technique which enables us to obtain simultaneously all the lines observed. This technique is known as spectrum synthesis technique. It was originally applied to compare the synthetic spectrum with the high resolution observations in a portion of the solar spectrum and to derive chemical abundance (Ross and Aller, 1968). With the advent of modern computers this technique has been revolutionized, since large set of line data can be used simultaneously to generate synthetic spectra in a wide wavelength range. This technique has been applied not only to high

resolution stellar data, but also to much lower resolution data for the study of stellar populations of distant systems in terms of their individual stellar components (Tripicco and Bell, 1990).

In this chapter we describe the ingredients involved in the computation of synthetic spectra, in particular we present the way we derived the line parameters of line data to be used in the spectrum synthesis. We have investigated the effect of parameters such as computational resolution, line list, and model from different grids, on the behaviour of line profiles in the region of Mg_2 index.

2.1 Model atmospheres

The first step in the process of synthesizing a synthetic spectrum for a given star is to identify a star with a particular atmospheric model. These atmospheric models are considered to be realistic ones, when the observed spectral features are reproduced by the predicted ones. It is common practice to use Kurucz (1979a) and Gustaffson *et al.* (1975), hereafter called GBEN, models for analysing cool stars. The main differences between these models are that the former are computed with opacity distribution functions that use one million atomic lines in Kurucz and Peytremann (1975) line list, while the latter use 50,000 atomic lines and a number of molecular lines "many times greater" (Gustaffson and Bell, 1979).

More recently, Kurucz (1991a) has computed new model atmospheres using an updated version of computer code, *i.e.* ATLAS9, which can handle his additional sources of continuum and line opacities. For technical description of ATLAS code, we refer to Kurucz (1970). Each new model has been computed with statistical line opacity distribution functions that are based on his more comprehensive line list of over 58 million atomic and molecular lines. The model atmospheres employed in our current synthetic spectrum calculations are a sub set of Kurucz (1991a) models (hereafter K91 models),

kindly provided to us by Dr. Kurucz. We have used these models due to the following reasons:
1) the new models are based on the line blanketing which is the most complete available at present and includes the contribution of molecular opacity, which is the most important component for cool stars;
2) opacity and model flux calculations are performed with the narrow frequency intervals *i.e.* in the new code there are 1221 frequency intervals as compared to 332 in the old one;
3) the K91 models refer to a more refined treatment of convection, which plays a relevant role in the atmospheres of cool stars;
4) the K91 grid of models is extended down to K stars, and provide photometric colors for F, G and K stars.

The atmospheric models used here are computed under the classical assumptions *i.e.* they incorporate the principles of hydrostatic equilibrium, conservation of energy flux and local thermodynamic equilibrium (LTE) in horizontally plane parallel layers. The fundamental information provided by the calculation of the models is the atmospheric structure. The structure is represented by the run of temperature, and other basic thermodynamics quantities, namely gas pressure, and electron density, as a function of depth in the atmosphere. As an example, Figure 2.1 shows the temperature stratification, *i.e.* the dependence of the temperature on the Rosseland optical depth (τ_R), for one of K91 models ; the steepening of temperature with depth in the constant flux models is due to the difficulties the flux experiences leaving the star in the presence of opacity contributed by the lines. In the case of gray atmospheres in radiative equilibrium, the temperature at the Rosseland optical depth of 2/3 corresponds to the effective temperature of the model. The effect of the temperature gradient is quite significant when translated into the behaviour of spectral features having different depth of formation. The following sub-section describes our experience with the grid of models we computed using Kurucz 8th version of ATLAS code (hereafter referred to as GMM models), and with the current grid of models.

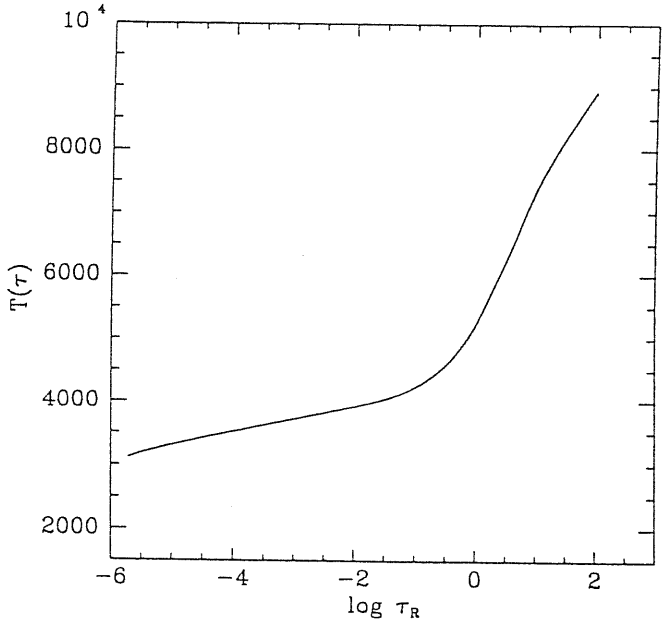

Figure 2.1: Temperature stratification for one of the K91 models with atmospheric parameters, 4750/4.5/0.0.

2.1.1 Grid of models

Previous work was devoted to compute the library of synthetic spectra starting from GMM models, in order to synthesize the Mg_2 index (Gulati *et al.*, 1991). The grid of model atmospheres was chosen in such a way so as to represent main sequence and giant intermediate type stars of solar chemical composition; therefore we chose the surface gravity values, in the form of log g, 4.5 and 3.0, effective temperature, T_{eff}, in the range of 4000–6250 K at 250 K step, and metallicity, [M/H] = 0.0 (where [M/H] = log (M/H)-log $(M/H)_\odot$). The choice of these atmospheric parameters, T_{eff} and log g, was dictated by the need to cover the characteristics of stellar populations in old stellar systems of solar chemical composition.

Since the available Kurucz (1979a,b) models were limited to $T_{eff} \geq 5500$ K, we extended the grid down to $T_{eff} = 4000$ K by using the VAX version 8 of ATLAS computer code (Kurucz, 1970, 1979a), as described in Castelli (1988). The computed models had the same characteristics as those of Kurucz (1979b) models : they take into account the optical thin formulation of

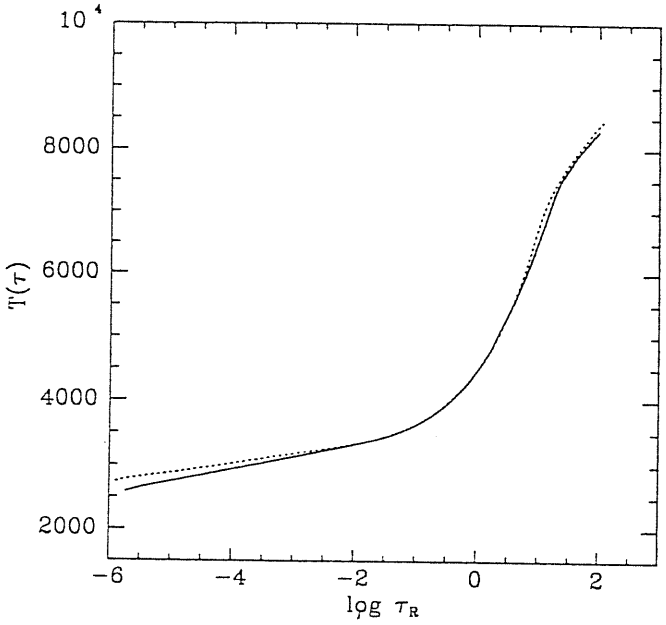

Figure 2.2: Comparison of temperature structure for K91 (solid line) and GMM (dotted line) model with atmospheric parameters 4000/1.5/0.0.

mixing length theory, with α, the ratio of mixing length to the pressure scale height, equal to 1; 64 optical depth points are considered in the computations. The opacity distribution functions refer to microturbulence velocity ξ = 2 km s^{-1}. Each model was computed with as many iterations as needed to ensure the convergence with errors at each depth point within 3 % for the flux, and 10 % on its derivatives. In this way we had set up a grid of models covering the temperature range 4000–6250 K with step of 250 K and gravity values of 3.0 and 4.5, for solar chemical composition.

Our recent grid is part of K91 model atmospheres. This grid covers the effective temperature range of 4000-6000 K with step of 250 K, surface gravity values in the range of 1.5 to 4.5 with step of 0.5 dex, and for metallicities [M/H] = -0.5, 0.0, 0.5. The range in atmospheric parameters selected in the current study will allow us to span stellar populations characteristic of old stellar systems. The new grid is composed of 189 models as shown in Table 2.1. As regards the microturbulence velocity of these models, each model was computed by Kurucz using new opacity distribution functions with microturbulence velocity of 2 km/s; the structure of the model atmospheres

Table 2.1: The grid of K91 models for metallicities [M/H] = -0.5, 0.0 and 0.5 used in the present study

	log g	1.5	2.0	2.5	3.0	3.5	4.0	4.5
T_{eff}								
6000		x	x	x	x	x	x	x
5750		x	x	x	x	x	x	x
5500		x	x	x	x	x	x	x
5250		x	x	x	x	x	x	x
5000		x	x	x	x	x	x	x
4750		x	x	x	x	x	x	x
4500		x	x	x	x	x	x	x
4250		x	x	x	x	x	x	x
4000		x	x	x	x	x	x	x

includes this depth-independent microturbulence velocity in an explicit way. The convection was treated using mixing-length to scale-height ratio of 1.5. The abundance of each element, in the new models that represents the solar chemical composition, comes from Anders and Grèvesse (1989) and models for other metallicities are scaled to these values. The role of complete atomic and molecular line blanketing in the computation of model atmospheres is shown in Figure 2.2, where we compare the temperature distribution of one of K91 models with one computed by us (see GMM) using ATLAS8 code. It is evident from this figure, that due to presence of much more line blanketing in the new model, the temperature structure, shown by solid line, is modified at the surface and deep in the atmospheres, where temperatures are lower than those predicted by the old model as shown with dotted line. This effect is translated into the behaviour of spectral energy distributions in the synthetic spectra where the strength of spectral features are expected to increase with the new model as compared to that with the old model.

2.2 Spectrum synthesis method

The underlying philosophy of this method is to compute the spectrum that makes use of already computed model atmospheres together with line data associated with line parameters relevant for absorption processes in the wavelength region of interest. A concise analytical description involved in the calculations of synthetic spectrum is given below.

2.2.1 Analytical description

For the classical atmospheres, the monochromatic flux at the surface, contributed both from the line and continuum sources at the different layers of the atmospheres and flux from the depth forming a continuum are given by:

$$F_\nu^{c+l}(0) = 2\int_0^\infty S_\nu^{c+l} E_2(\tau_\nu^{c+l})\, d\tau_\nu^{c+l} \tag{2.1}$$

$$F_\nu^{c}(0) = 2\int_0^\infty S_\nu^{c} E_2(\tau_\nu^{c})\, d\tau_\nu^{c} \tag{2.2}$$

where $F_\nu^{c+l}(0)$ and $F_\nu^{c}(0)$ are the surface and continuum fluxes respectively, $E_2(\tau_\nu)$ is the second exponential integral and S_ν^c and S_ν^{c+l} are the source functions for continuum and for both continuum and line opacities. A general form of the source function is:

$$S_\nu^{c+l} = \frac{\sum_i \kappa_{\nu_i}^c S_{\nu_i}^c + \sum_i l_{\nu_i} S_{\nu_i}^l + \sigma_\nu^c R_1 + \sigma_\nu^1 R_2}{\kappa_\nu^c + l_\nu + \sigma_\nu^c + \sigma_\nu^l} \tag{2.3}$$

where:

$\kappa_\nu^c = \sum_i \kappa_{\nu_i}$ is the sum of the continuum absorption coefficients, κ_{ν_i} of the individual species i, and $S_{\nu_i}^c$ are the corresponding continuous source functions.

$l_\nu^c = \sum_i l_{\nu_i}$ is the total line absorption coefficient, given by the sum of the individual line absorption coefficient,

l_{ν_i}, and $S^l_{\nu_i}$ are the corresponding line source functions.
$\sigma^c_\nu = \sum_i \sigma_{\nu_i^c}$ is the sum of individual continuous scattering coefficients.
$\sigma^l_\nu = \sum_i \sigma_{\nu_i^c}$ is the sum of individual line scattering coefficients.
$R_1 = \int \int_0^\infty I_{\nu'} n' R^c(\nu', n'; \nu, n) d\nu' d\omega' / 4\pi$
$R_2 = \int \int_0^\infty I_{\nu'} n' R^l(\nu', n'; \nu, n) d\nu' d\omega' / 4\pi$ where $R^c(\nu', n'; \nu, n)$ and $R^l(\nu', n'; \nu, n)$ are the redistribution functions for scattering in the continuum and in the lines respectively. They may be approximated with different functions for different cases. For a special case, where the continuum scattering coefficient is coherent and isotropic, and the line scattering is represented by isotropic complete redistribution over a line profile, the continuum scattering emission coefficient is given by $j_\nu = \sigma^c_\nu J_\nu$ and line scattering emission coefficient is given by $j_\nu = \sigma^l_\nu \int_0^\infty l_{\nu'} J_{\nu'} d\nu'$, with $\sigma^l_\nu = (1 - \epsilon) l_\nu$, where ϵ is a function that allows treatment of part of the line opacity as scattering.

In this case the source function is given by:

$$S^{c+l}_\nu = \frac{\sum_i \kappa^c_{\nu_i} S^c_{\nu_i} + \sum l_{\nu i} S^l_{\nu_i} + \sigma^c_\nu J_\nu + (1 - \epsilon) l_\nu \int_0^\infty l_\nu J_\nu d\nu}{\kappa^c_\nu + l_\nu + \sigma^c_\nu} \tag{2.4}$$

The optical depths τ^c_ν and τ^{c+l}_ν are given by:

$$\tau^{c+l}_\nu = \int_x (\kappa^c_\nu + \sigma^c_\nu + l_\nu) \rho dx \tag{2.5}$$

and

$$\tau^c_\nu = \int_x (\kappa^c_\nu + \sigma^c_\nu) \rho dx \tag{2.6}$$

where ρ is the density of the stellar material, and x is the geometrical height.

The general form of the line absorption coefficient is:

$$l_{\nu_i} = N_{il} \frac{\pi e^2}{m_e c} f_{lu} \phi_\nu \tag{2.7}$$

where N_{il} is the number density of atoms of the i specie in the lower level l involved in the transition, f_{lu} is the oscillator strength for the transition

from the lower l level to upper u level, and ϕ_ν is line absorption profile, which is represented by different function depending on the kind of the line. For example, for metallic lines:

$$l_{\nu_i} = N_{il}\frac{\sqrt{\pi e^2}}{m_e c}\frac{f_{lu}}{\Delta\nu_D}\, H(\alpha, v) \tag{2.8}$$

The profile function is the Voigt function $H(\alpha, v)$, which accounts for the broadening mechanism of the spectral lines, such as the Doppler broadening (which includes microturbulence velocity), and the radiative, quadratic Stark and van der Waals broadening. In the Voigt function the variables are $\alpha = \lambda_\gamma/4\pi v_D$ and $v = \Delta\nu/\Delta\nu_D$. γ is the damping parameter and v_D is the Doppler velocity including microturbulence. $\delta\nu_D = \nu V_D/c$ is the Doppler width.

The lines dominated by the linear Stark effect, such as the hydrogen lines and some strong lines, have different line source function. The Stark profiles are computed with several theories (Kepple and Griem, 1968, Vidal *et al.*, 1970,1973) taking into account the broadening both by ions and electrons. The resulting Stark profile are available in tabular form. Autoionization lines may have Fano (1961) profiles with autoionization broadening from Artru and Lanz (1987).

The line profile may be computed in LTE or NLTE approximations. In LTE, the number densities N_{i_l} are derived from Saha and Boltzmann equations and the $S^c_{\nu_i}$ and $S^l_{\nu_i}$ source functions are Planck function B_ν. To compute the line absorption coefficient we need to know the line oscillator strengths and broadening constants. In NLTE, the populations N_{il} and the departure coefficients for upper and lower energy levels are computed by solving the statistical equilibrium and radiative transfer equations in a consistent way. Then the departure coefficients are inserted into the formula used for the LTE case, as in the partition functions, in the Saha and Boltzmann equations, in the opacities, so that the LTE $N_i l$ values are replaced by NLTE ones. NLTE analyses require atomic models, and therefore the knowledge of both

of all the relevant levels and of more atomic data than in the LTE case, such as photo-ionization cross sections and the electron-collision cross sections.

2.2.2 The library of synthetic spectra

From the above descriptions, it appears that all the quantities are a function of the depth in the atmosphere and therefore depend on the atmospheric structure. This means that the intensity of a line depends upon, in a first place, on the temperature (which is the main variable affecting both the state of the gas and intensity of the radiation field), in the second place on the electron density (which affects the degree of ionization) and thirdly on the abundance of the elements from which the atmospheric gas is formed.

Thus depending on the model atmospheres, source functions, atomic parameters, and the method for the solution of the radiative transfer and state equations, results with different degree of approximation can be obtained.

For carrying out the above calculations, Kurucz spectrum-synthesis computer program (SYNTHE code, Kurucz and Avrett, 1981) was used. The accuracy of synthetic spectrum depends on the model atmospheres and the line data used to compute the flux at each wavelength point. The model atmospheres in the computation of synthetic spectra were employed from the grid of models, given in Sec. 1.1. During the computation of spectra, the contribution of molecular opacity were also considered in the treatment of equation of state and to derive number densities; a total of 152 different species were included of which 84 refer to atoms and 68 to molecules, both in neutral as well as ionized form. For each model atmosphere in the grid, the synthetic spectrum in the wavelength range of 4850-5400 Å which includes the region of Mg_2 index was computed. A total of 189 synthetic spectra were computed.

As regards the line data, in the following sub-section we discuss in detail the set used in the present study. We assumed microturbulence velocity

of 2 km/s. In each case, we computed the intensity spectrum for 17 emergent angles with resolution of $R = \lambda/\Delta\lambda = 250,000$. The intensity spectra were then interpolated and integrated over the stellar disk to produce a flux spectrum for an assumed projected rotational velocity of 0 km/s.

2.2.3 Line data

As far as the line list is concerned, in the calculation of spectrum we need an extensive line list in the wavelength range of our interest for each element in the different ionization states, with known laboratory wavelengths, excitation potential for lower and upper levels, reliable oscillator strength values, $log\ gf$, and broadening parameters.

As regards atomic line data, we have used Kurucz line list (1988); and the molecular data, which refer to all hydrides, CN and C_2 molecular lines, are from Kurucz (1987,1990b). We do not include TiO molecular data in the synthesis of stellar spectra for the grid of models between 4000-6000 K, since, according to Jaschek and Jaschek (1990), this molecule appears at λ = 4954 Å in the blue bandpass of the Mg_2 index for spectral type later than K5.

The lines have oscillator strength values either extracted from the literature or determined by Kurucz in a semi-empirical manner. The values for radiative, Stark , and van der Waals damping constants for all lines from Ca III to Ni are all determined by Kurucz (1981). For all other lines, damping constants are either taken from the literature or are computed by Kurucz and Avrett (1981). This line list is considered to be the most complete available so far for the synthesis work.

We improved the line parameters, such as oscillator strengths and damping constants, for the line data relevant in the spectral region of our interest. These parameters were determined in a semi-empirical way as follows:
Since the Sun is the laboratory for verifying the computed line data, we used

the best available solar model, the "empirical solar model " (Maltby *et al.*, 1986) that includes the depth dependent microturbulence velocity. By using this model, the normalized central intensity spectrum was computed with the resolving power $\lambda/\Delta\lambda$ = 500,000, in the wavelength range of 4850-5400 Å, using the line data as described above. The resulting spectrum was made comparable to the observed one by taking into account solar macroturbulence velocity of 1.5 km/s. Then the predicted central intensity spectrum in the wavelength region of the Mg_2 index was compared to the observed high resolution FTS solar central intensity spectrum observed by Brault at the Kitt Peak Observatory and digitized by Kurucz. We compared the observed central intensity rather than the solar flux, because in the latter case some lines get blended after integrating through all solid angles. The oscillator strength and damping constants, in particular van der Waals damping constant, of the predicted solar lines in the region of the index Mg_2 were adjusted until the synthetic spectral features match satisfactorily with the observed ones.

In Figure 2.3 we demonstrate the one of the Mg *b* features in the central band of the index at the wavelength 517.2684 *nm*, which shows a large discrepancy between the predicted and the observed line profile. In this figure, the residual intensities of the synthetic and observed spectra, *i.e.* the intensities normalized to the continuum level, are displayed as a function of wavelength (where the wavelength is expressed in *nm*). On the top of each panel, the label indicates the last three decimal places of the line wavelength, the atomic number along with the ionization degree of the element or the code number designated to molecules, lower energy level in cm^{-1}, and the residual flux of the unbroadened spectrum.

The spectrum in the upper panel was computed by using a value of van der Waal damping constant, Γ_{vw}, equal to -7.12 (from Kurucz line list) and in the lower panel the spectrum was computed after applying a correction of -0.20 to this constant: this correction removes the discrepancy between the predicted and observed profile. In some lines, both damping and oscillator strength parameters were needed to be modified simultaneously so as to

match the predicted profile with the observed one.

For reference, we present in Appendix A an atlas of solar intensity spectrum generated with empirical solar model and the line list modified for line parameters in bandpasses of the Mg_2 together with the observed solar intensity spectrum. In order to examine closely the strong as well as very weak atomic and molecular components involved in the region of the Mg_2, we labeled all those line for which the residual intensity is lower than 0.990. As the intensity spectrum is not affected by rotational broadening, the lines are narrower and less blended than in flux spectra, so it provides detailed information about the atomic and molecular components contributing to the Mg_2 index. This information is useful for high resolution spectroscopic studies. (The line list is available in the format used in creating synthetic spectra with Kurucz' spectrum synthesis program).

Here we are dealing with the study of spectral features in stellar populations, we are interested in setting up the library of stellar spectra to represent the real stars which are the point sources from which we get the fluxes. Therefore, we tested our line list by comparing also the solar flux spectrum, computed using the empirical model, with the observed solar flux spectrum (Kurucz *et al.*, 1984), again in the wavelength region of the Mg_2. For illustration, we present in Appendix B the atlas of predicted solar flux spectrum together with the observed one in the three regions of the index. To mark most of the lines in the atlas we set threshold of residual flux at 0.990. Few weak unpredictable spectral features were found to be present in the observed spectra, in the regions of our interest, but they can hardly affect the integrated behaviour of bandpasses. On the whole, the agreement between the observed solar flux is generally very good, thus giving credibility to our line data for syntheses of the library of spectra.

Since our grid of models is extended down to the lowest temperature of 4000 K, the lines predicted by models cooler than the solar one should also be incorporated in the synthesis of spectra. Towards this end, we analysed the

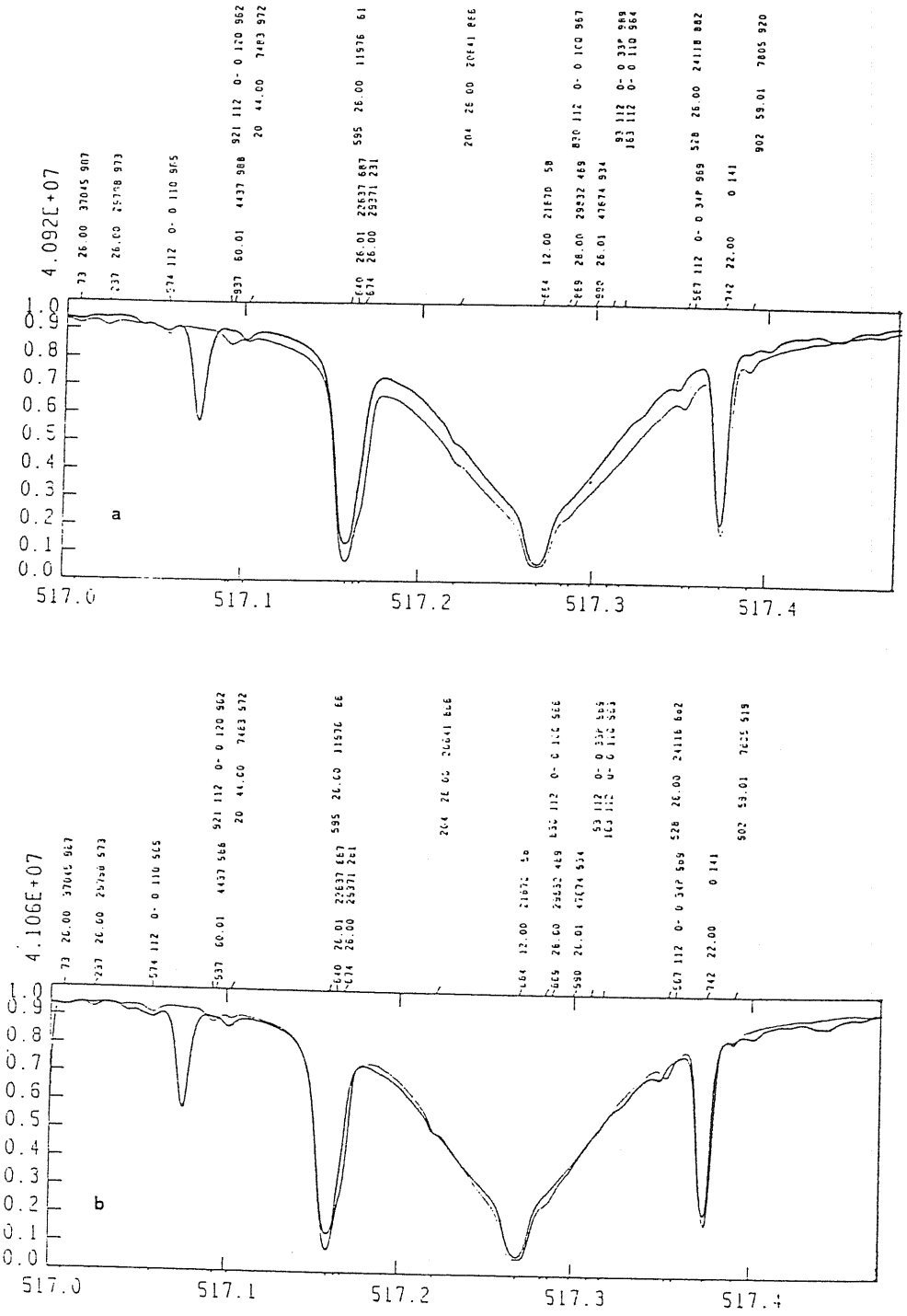

Figure 2.3: One of the components of Mg *b* triplet in the central bandpass of the Mg_2 (a) before and (b) after adjusting line parameters.

set of lines predicted by the Arcturus model of Peterson *et al.* (1991), who have shown that their model can reproduce very well the observed flux distribution while comparing to Griffin atlas of Arcturus in the visible wavelength region. The atmospheric parameters they used to synthesize the spectrum for Arcturus are the following: T_{eff}=4300 K, log g = 1.5, [M/H] = -0.5, microturbulence velocity = 1.7 km/s, and convection parameter 1.25. In Appendix C, we demonstrate the comparison between observed Arcturus spectra, observed by Griffin (1968) and digitized by Kurucz, and Arcturus model spectra in the central bandpass of the Mg_2. Our experience with the Arcturus model has shown more lines than those predicted by the solar empirical model because of different photospheric conditions at the lower temperature. In the input line data we include these lines also, so as to properly synthesize the spectra also of stars cooler than the Sun. Besides, one can ask about the lines not predicted by the solar and the Arcturus model; should they be included in the line list while synthesizing spectra for stars unlike Sun and Arcturus ? Though these lines could not be verified due to lack of high resolution observations for stars cooler than Arcturus, we chose to include all other lines present in the current Kurucz line list in the wavelength range 4850-5400 Å. We cannot ignore these lines in our synthetic spectrum computation, because we might expect some of them to show up for stars with photospheric conditions different from the solar and Arcturus models.

Hence our line list includes two sets of data:

1) the first group has been derived for the present project: it is a combination of the lines predicted by the solar model, and very well matched with the detailed observed solar spectrum, and by the best Arcturus model. This line list is composed of 13,403 lines in the wavelength range 4850–5400 Å. This set of lines should be considered as a reliable one, since this was derived after carefully matching the synthetic solar central intensity spectrum with the observed one ;

2) second group, which contains lines other than those present in group one, but existing in the Kurucz current line list, forms a total of 30,518 lines. We

will refer to the complete line list in the following analyses, unless otherwise stated.

This part of the work has been done in CfA, Cambridge, USA, in collaboration with Dr. Kurucz.

In the following subsections we investigate the effect of the parameters on the behaviour of flux distributions in the wavelength range of our interest.

2.2.4 Dependence on computational resolution

One of the parameters that can be varied in generating synthetic spectra is the computational resolution, expressed in resolving power $\lambda/\Delta\lambda$, where $\Delta\lambda$ is the wavelength step for computing the fluxes. One can set this parameter to as high a limit as one wants, depending on the availability of computer CPU time, and space for storing the output data. In fact, one can learn more physics that enter into stellar model atmospheres and spectrum synthesis from the comparison of high resolution synthetic and observed spectra. Unfortunately, this kind of refined analysis is limited to a handful of stars for which one can get very high resolution observations with the present available instruments. On the other hand, if one wants to extend this approach to the spectral analysis of stellar populations in distant stellar systems, where the loss of spectral information is expected due to velocity dispersion effects, high resolution cannot be achieved. In order to synthesize integrated spectral energy distributions of these stellar systems, one needs either an observed stellar library of energy distributions or a library of synthetic stellar spectra degraded to the observational resolution. For instance, Tripicco and Bell (1990) have recently investigated CN-sensitive spectral indices using a library of synthetic spectra computed at the wavelength step $\Delta\lambda = 0.1$ Å. During the M.Phil. project (Gulati, 1989), we made several tests for the selection of this parameter. We concluded that after degrading the synthetic spectra computed with R = 50,000 we do not lose spectral features observed at the resolution of our observation. Therefore to save computational time

we used this value of the computational resolution.

After getting new models and revising line lists, we have again investigated this parameter critically both from qualitative and quantitative points of view. For the model (5000/4.5/0.0), (hereafter introducing a shorthand, *e.g.* 5000/4.5/0.0 designates the model having the following parameter values: T_{eff} = 5000, log g = 4.5, [M/H] =0.0), with line lists as described above, we computed the synthetic spectra with computational resolutions 50,000 as well as at the resolution of 250,000. As an illustration, Figure 2.2.4 shows the effect of resolution in a small portion of the synthetic spectrum. In the upper panel, we present the synthetic spectrum computed for the model with $R = 50,000$ and in the lower panel we show the spectrum computed with resolution $R = 250,000$. Our experiments using these resolutions have shown that the computational time to compute synthetic spectra increases by three times when we use $R = 250,000$ instead of $R = 50,000$ and at the same time the space requirements for storing the final results increase. It is a matter of taste, when we have low resolution observational data where features get diluted, one can compute synthetic spectra at smaller resolution without significant losses in the final results (see Gulati (1989) M.Phil. thesis). On the contrary, if we are dealing with observational data of very high quality which are available for few objects and likely to extend with sophisticated space instruments, we certainly need synthetic spectra computed at very high resolution. For instance, one can distinguish the doublet features of MgI at 5165.321 Å and FeI at 5167.487 Å, in the synthetic spectra computed at $R = 250,000$, not at $R = 50,000$ (see Figure 2.2.4) and so if someone is interested in analysing these features individually one certainly needs a synthetic spectrum computed with the high resolution.

Recently, Lester (1990) has investigated the effect of spectral resolution using Kurucz's old model for abundance analysis and he has shown that there is an insignificant change of abundance when the resolution increases from 50,000 to 75,000. However, we decided to use $R = 250,000$ resolution with new models, so as to store maximum information once obtained for fur-

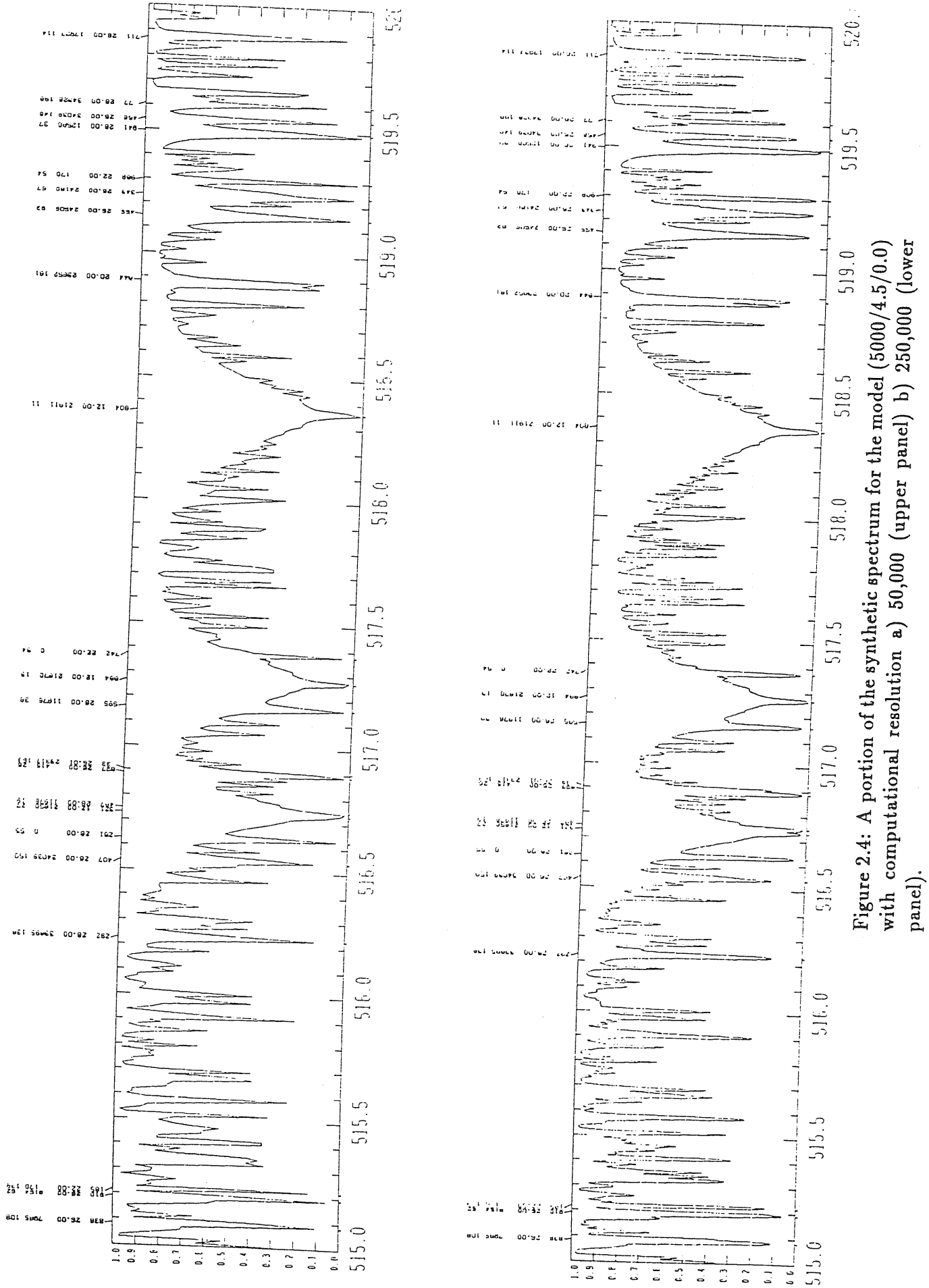

Figure 2.4: A portion of the synthetic spectrum for the model (5000/4.5/0.0) with computational resolution a) 50,000 (upper panel) b) 250,000 (lower panel).

ther detailed analysis and avoiding unnecessary inaccuracies in the computed spectra as far as possible.

2.2.5 Dependence on the grid of models

Since the synthetic spectrum for a particular line list depends upon the model, the effect of different grids of model atmospheres on the synthetic spectrum is worth investigating. Of the existing grids of models in the temperature range 4000-6000 K, we selected the model (4000/1.5/0.0) from K91 models, GBEN and GMM models for comparison. In order to be consistent with the new model, we computed all the synthetic spectra by setting micro-turbulence velocity equal to 2 km/s. We compare in Figure 2.5 the segment of normalized unbroadened flux spectrum based on GBEN model (upper panel) with the one based on K91 (lower panel). Note that lines with residual flux values less than 0.2 are labeled in this figure, in order to distinguish the strong lines. As can be seen from the figure, the values of residual flux of strong lines in the wavelength range of 5150-5200 Å is higher in case of GBEN than in case of K91 model. This suggests that the strength of spectral features is more enhanced in K91 model than in GBEN model, which indicates that K91 models takes into account comparatively more complete line blanketing.

On comparing (Figure 2.6) the synthetic spectrum based on GMM model (upper panel) with the one computed with the K91 model (lower panel), we noticed the same effect as in the case of GBEN model but to a greater extent for some lines. Our model predicts smaller line strength than the new model, since GMM models do not take into account the contribution of molecular opacity.

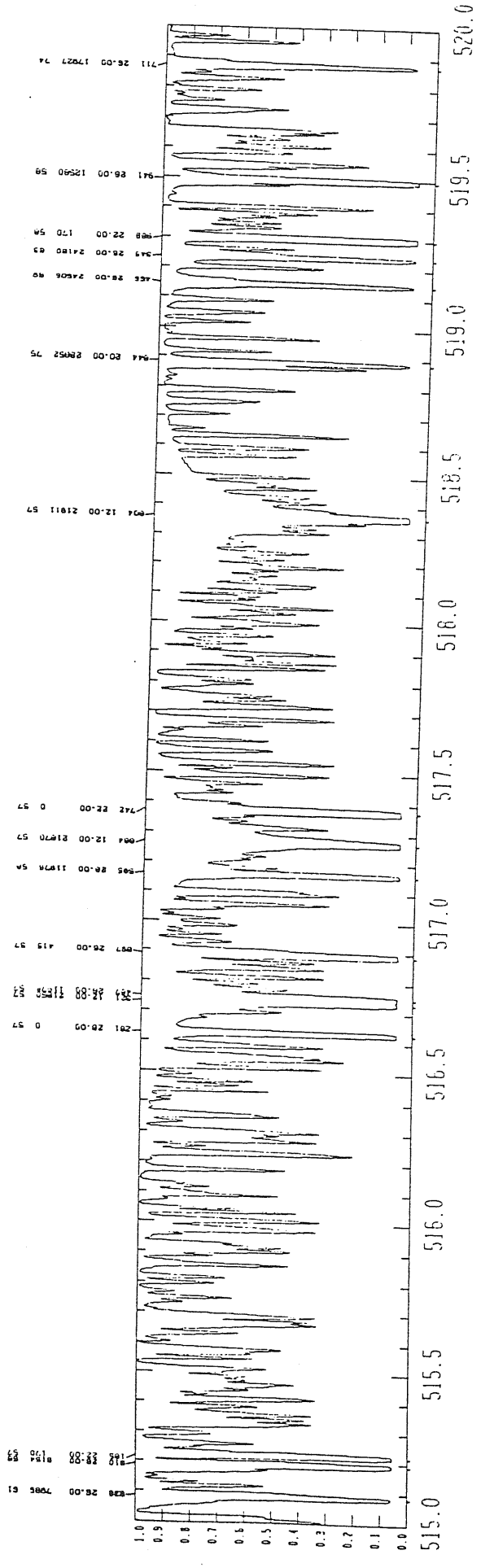

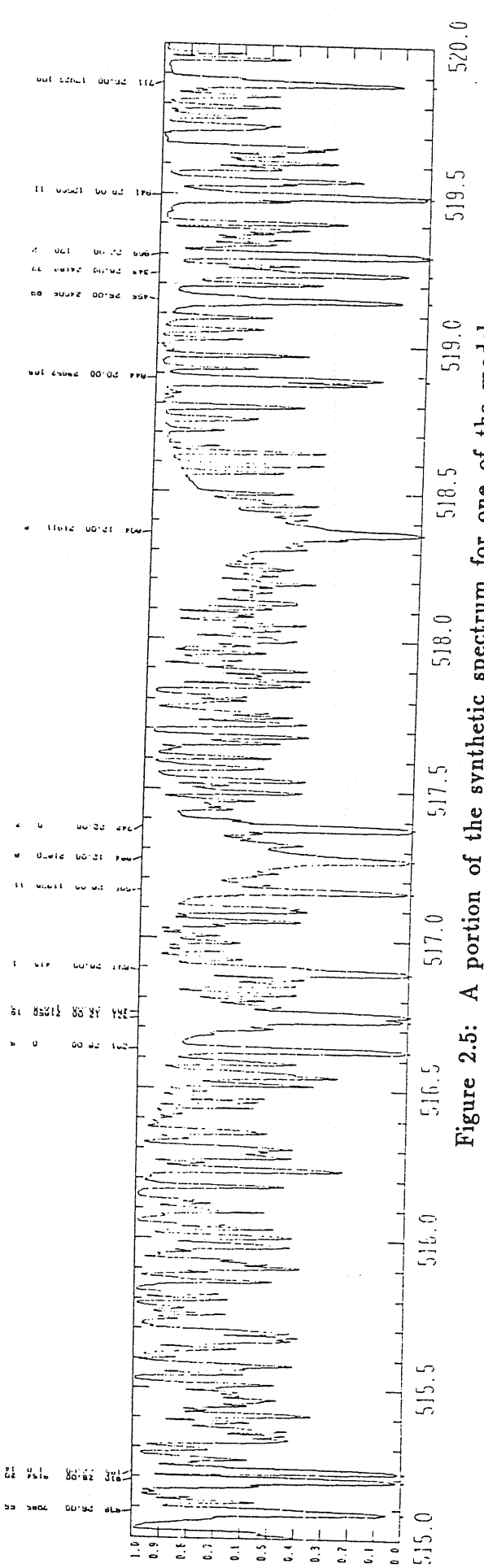

Figure 2.5: A portion of the synthetic spectrum for one of the models (4000/1.5/0.0) in GBEN grid and K91 grid (a) GBEN model (upper panel), (b) K91 model (lower panel).

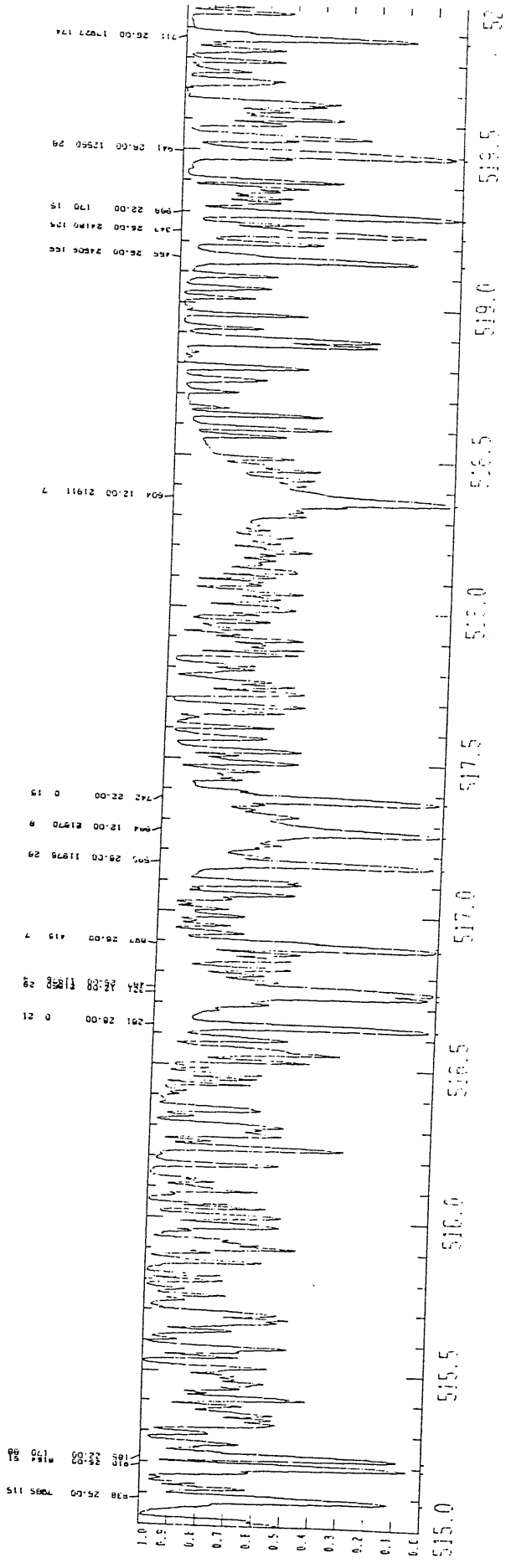

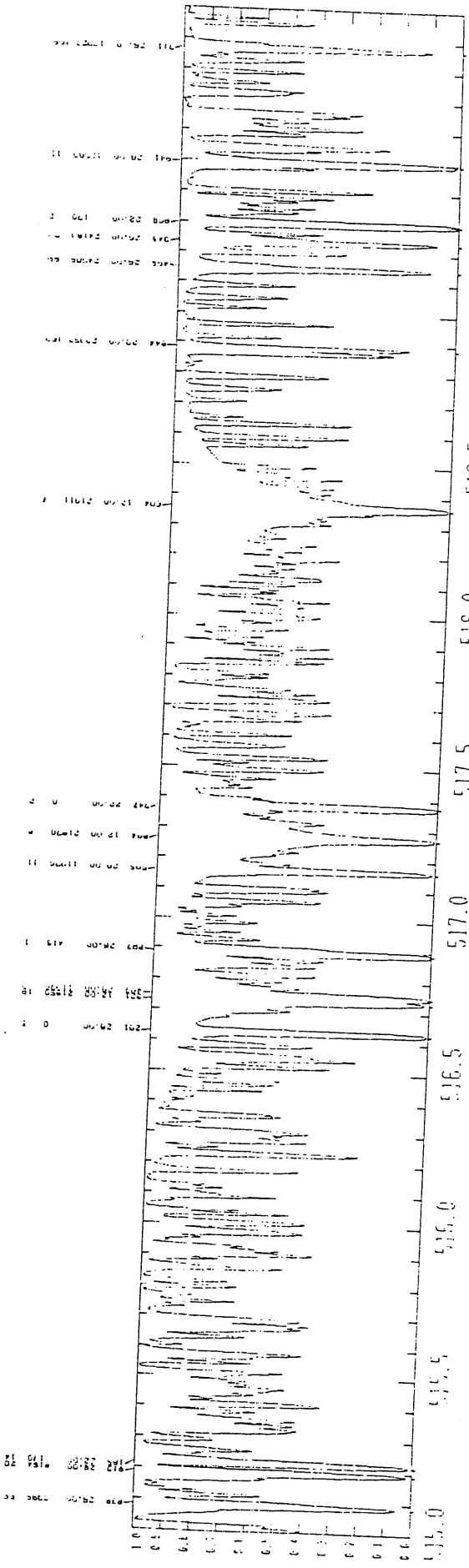

Figure 2.6: A portion of the synthetic spectrum for GMM and K91 model (4000/1.5/0.0) a) GMM model (upper panel) b) K91 model (lower panel).

2.2.6 Dependence on line data

In this subsection, we investigate the effect of line data on the synthetic spectrum from a qualitative point of view. As explained above, our line list is composed of two groups: one which is predicted by the solar and the Arcturus model, and another, which is derived from Kurucz current line list (auxiliary line list).

The effect of the auxiliary line list on the resulting synthetic spectra for the given model is shown in Figure 2.7, where in the upper panel we plot the segment of the synthetic spectra computed without auxiliary line list, and in the lower panel the same part of synthetic spectrum computed with auxiliary line list for the model (5000/4.5/0.0). At the threshold of residual flux equal to 0.2, the contribution of auxiliary lines can not be singled out, however at higher levels of residual flux, we did see the contribution of auxiliary lines in the central region of the index. We replot synthetic spectra given in the lower panel of Figure 2.8 by setting the threshold of residual flux at 0.9. Mark that the wavelengths of lines from auxiliary line list are followed by the symbol ':'.

Even though the inclusion of auxiliary line list increase the computational time by three times, it is essential to include them, since we may expect the contribution of these lines under the atmospheric conditions different from the solar and the Arcturus models.

2.3 Synthetic spectra and atmospheric parameters

The key parameters that determine the spectral energy distribution of stars are effective temperature, surface gravity and metallicity. In this section we investigate the effect of these basic parameters on the regions of the Mg_2 index, in particular in the central bandpass, $\lambda\lambda$ 5156.00-5197.25 Å, which

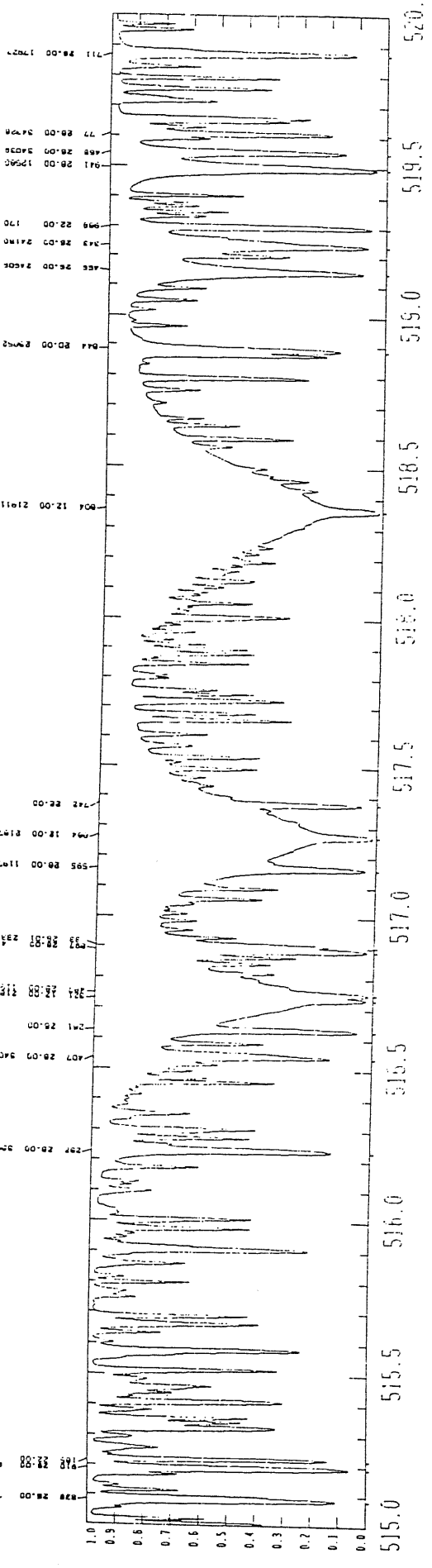

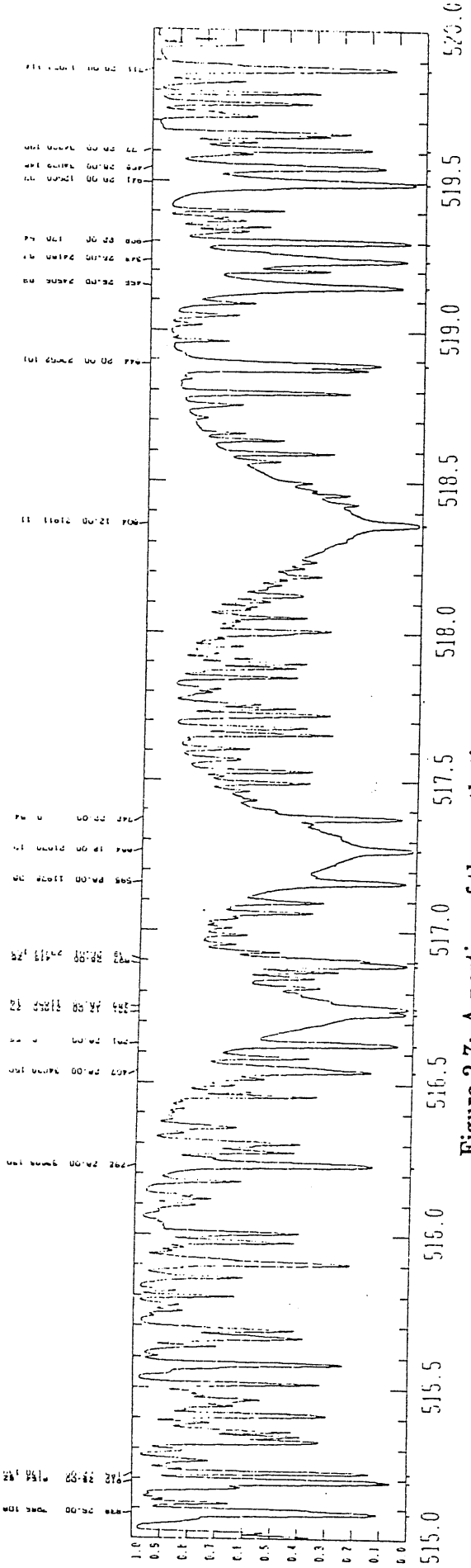

Figure 2.7: A portion of the synthetic spectra showing the effect of line data for the K91 model (5000/4.5/0.0) a) without auxiliary line list (upper panel) b) with auxiliary line list (lower panel).

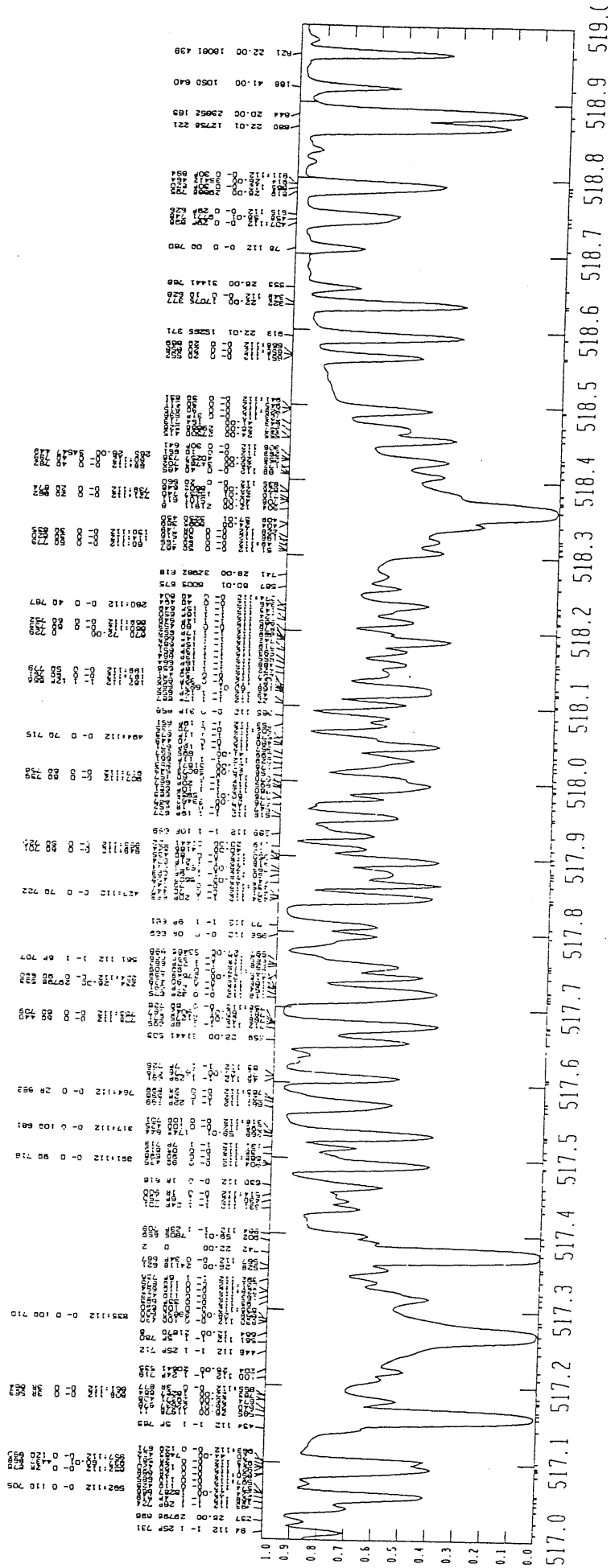

Figure 2.8: Same as in the lower panel of Figure 2.7a, but the labeling is for residual fluxes below 0.9.

has strong absorption features. Additional physical parameters, such as microturbulence velocity, and abundance anomalies have not been considered, since they play a role at a lower level.

In order to look into the effects of atmospheric parameters on the behaviour of spectral energy distributions in the central band, we plotted normalized flux spectra in the wavelength range $\lambda\lambda$ 515.0-520.0 *nm* for different sets of effective temperatures, surface gravities and metallicities (Figures 2.9, 2.10, and 2.11).

In Figure 2.9 we show the temperature effect by plotting the unbroadened synthetic flux for the model (6000/4.5/0.0) in the upper panel and the model (4000/4.5/0.0) in the lower panel. This figure shows clearly that at the lower temperature there is an increase in the strength of Mg b triplet and of other lines. In addition, the MgH molecular lines start contributing at the lower temperature, and further enhance the spectral strength in the central bandpass. For demonstrating the effect of gravity on the flux distributions in the central bandpass, in Figure 2.10 we plotted synthetic spectral fluxes of models (4750/1.5/0.0) (upper panel) and (4750/4.5/0.0) (lower panel) respectively. The sensitivity of the MgH lines to surface gravity can be inferred from this figure. The appearance of the (1,1) vibrational transition of MgH molecule around 5182 Å in the central bandpass of synthetic spectrum at high gravity strengthens the spectral features. The sensitivity of the intensity of MgH lines to gravity is discussed in detail by Bell *et al.* (1985).

As regards the metallicity, we plotted in Figure 2.11 the synthetic spectra in the central portion of the Mg_2 index for models (4750/4.5/0.0) (upper panel) and for (4750/4.5/-0.5) (lower panel) respectively. This figure shows that as the metallicity decreases, the strength of Mgb triplet and other lines in the central bandpass of the index decreases.

In this chapter we saw the effect of parameters on the unbroadened synthetic spectra, while in the following we will discuss in detail the behaviour of these spectra when broadened to the resolution of our observations.

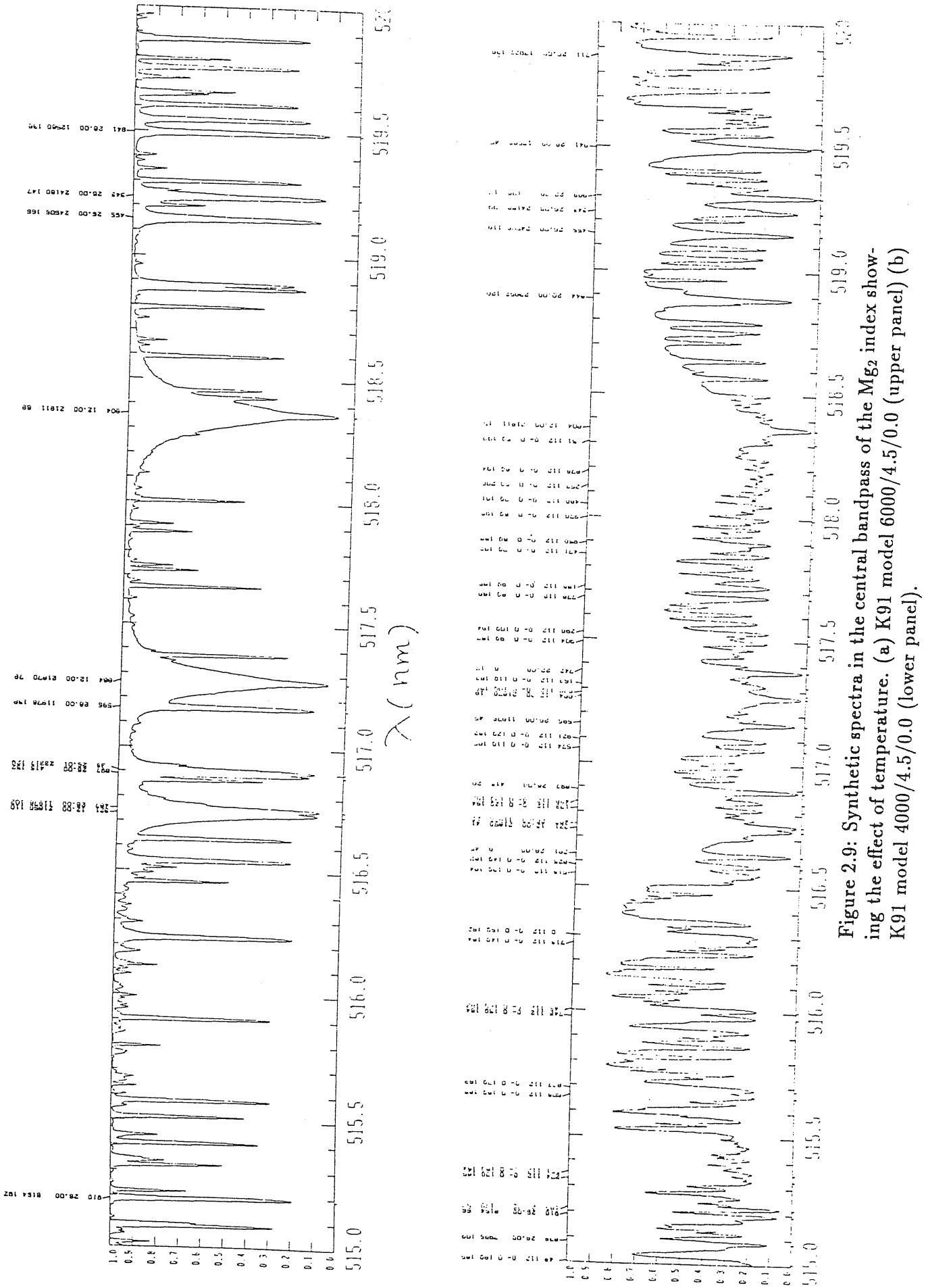

Figure 2.9: Synthetic spectra in the central bandpass of the Mg_2 index showing the effect of temperature. (a) K91 model 6000/4.5/0.0 (upper panel) (b) K91 model 4000/4.5/0.0 (lower panel).

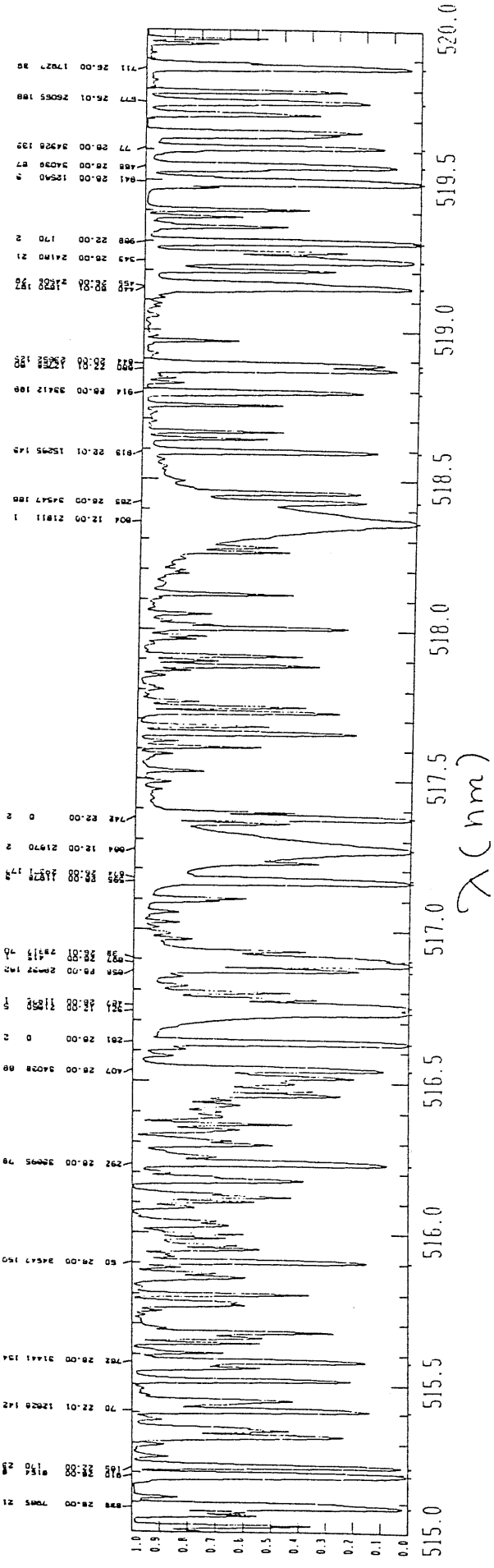

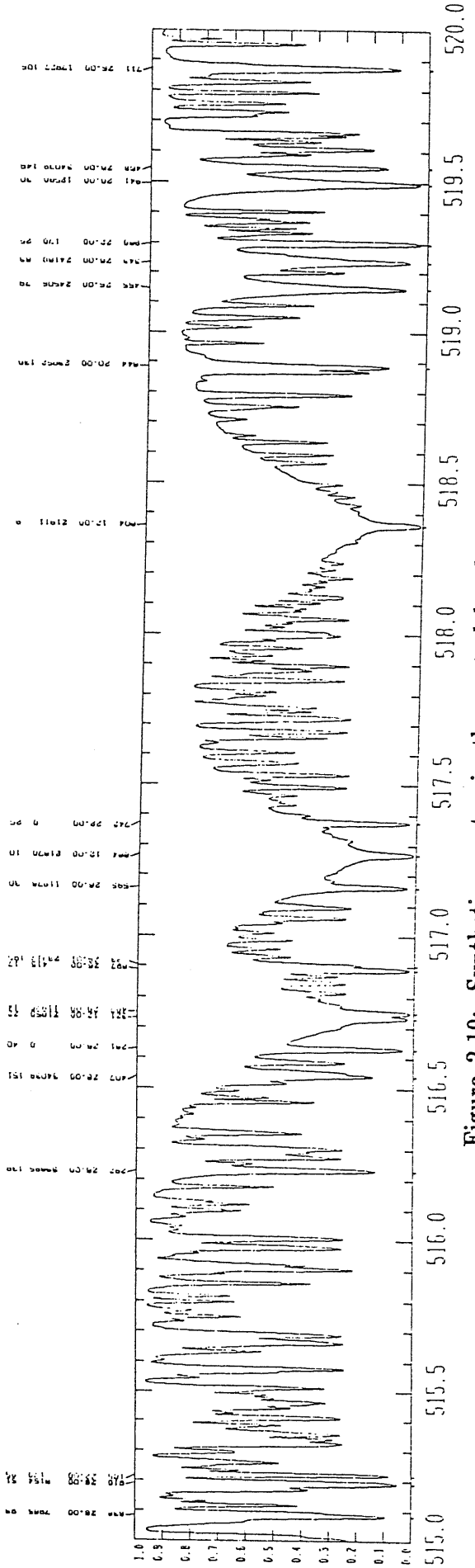

Figure 2.10: Synthetic spectra in the central bandpass of the Mg_2 index showing the effect of surface gravity. (a) K91 model 4750/1.5/0.0 (upper panel) (b) K91 model 4750/4.5/0.0 (lower panel).

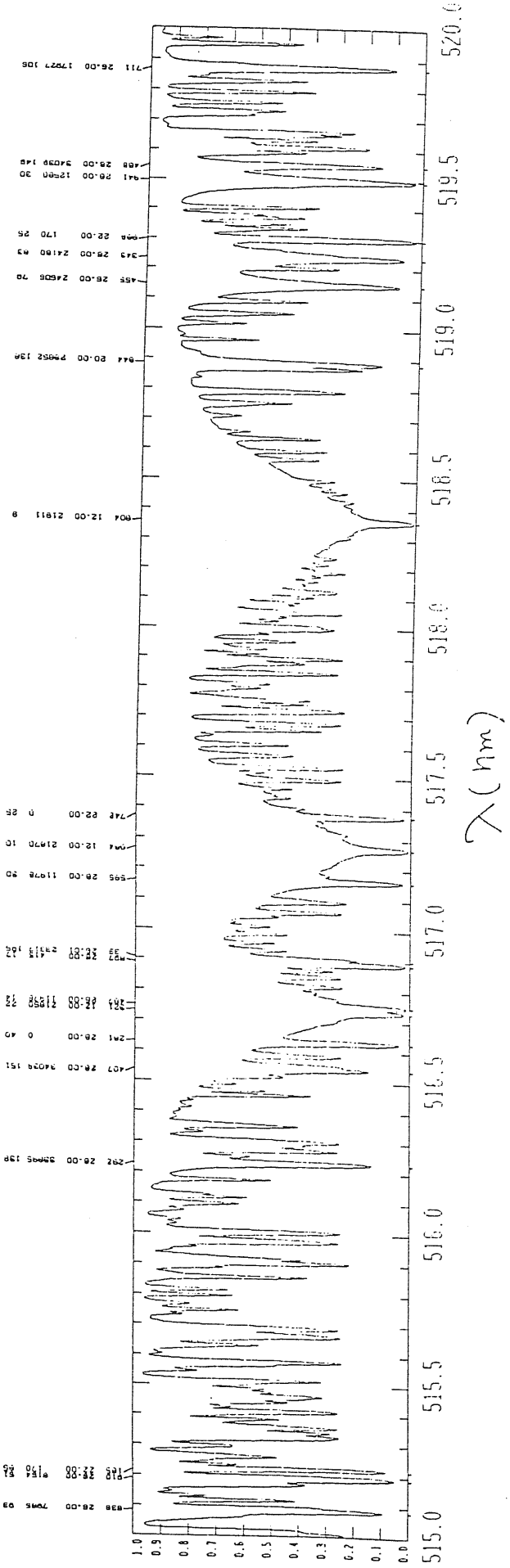

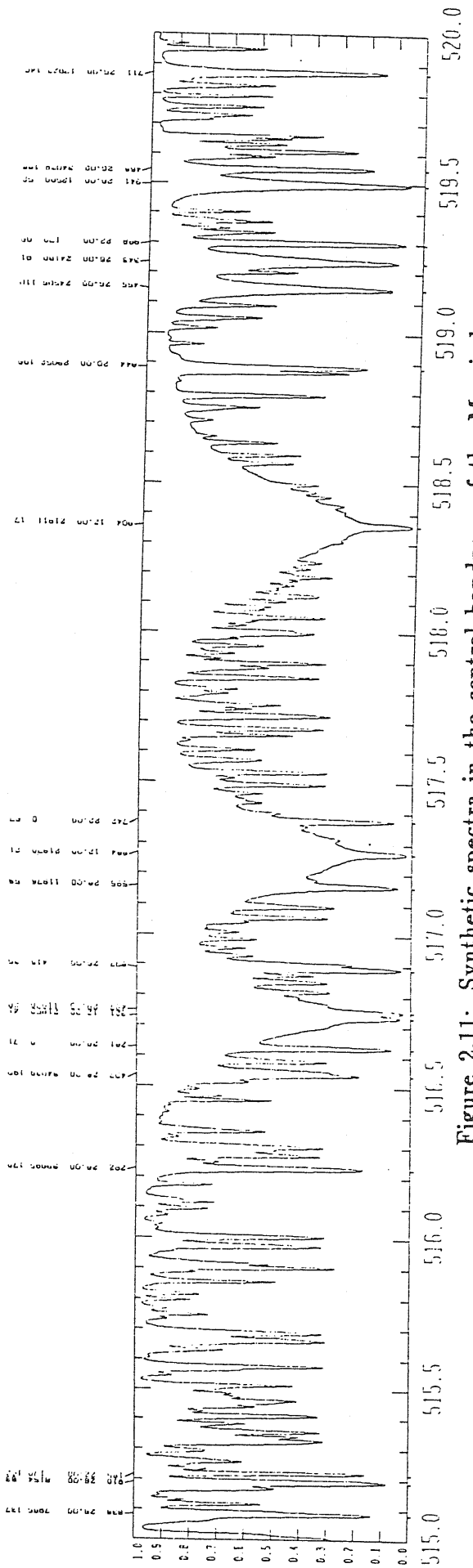

Figure 2.11: Synthetic spectra in the central bandpass of the Mg_2 index showing the effect of metallicity. (a) K91 model 4750/4.5/0.0 (upper panel) (b) K91 model 4750/4.5/-0.50 (lower panel).

2.4 Applications

So far we have built up a library of synthetic stellar fluxes based on K91 models and representative of cool stars of different metallicities in the wavelength range of 4850-5400 Å. The large surveys of stellar populations in the our galaxy and nearby galaxies is based on photometric techniques. However, the analysis of stellar populations using low resolution spectra spanning a large wavelength range should give more information on the stellar characteristics than the photometric systems. After the advent of multi-aperture spectrographs, it has become possible to observe spectroscopically large number of stars.

Our library, stored on optical disks, can be used for interpreting observations of high as well as low resolution data after degrading synthetic spectra to the resolution of observations. In particular, it can be used for determining the atmospheric parameters of stars by comparing the observed spectra with the library of synthetic spectra. Quantitative methods, as described by Malagnini and Morossi (1983), Thévnin and Foy (1983), and Cayrel *et al.* (1991), can be used to this aim. The advantage of using the synthetic stellar library over any empirical library of spectra is that the library provides a complete and very narrow coverage of atmospheric parameters.

Another fundamental application of the library of synthetic spectra is to investigate the behaviour of spectral indices in the wavelength range of 4850-5400 Å with respect to atmospheric parameters. According to Faber *et al.* (1985), the spectral indices lying in this wavelength region are Mg*b*, Feλ, Mg_1 and Mg_2 and are powerful diagnostics for stellar population studies. In my M.Phil. thesis I have investigated the dependence of synthetic Mg*b* index, measured as equivalent width, on atmospheric parameters. In next chapters, we will concentrate on the Mg_2 index which has been strongly emphasized for study of stellar systems due its relationship with the metallicity.

Chapter 3

Mg_2 index

The magnesium triplet is one of the strongest features in the visible spectra of cool stars. Ohman (1936) was the first to recognize its usefulness as temperature and luminosity indicator for cool stars. Thackery (1939,1949), however, was first to give a quantitative account of the luminosity effect shown by the triplet. Deeming's (1960) extensive spectrophotometric survey of the Mg b features of 539 G and K stars confirmed this effect, and showed that the strength of the Mg b lines provided a good luminosity criterion for stars with spectral types between G8 and K5. This luminosity dependence has been confirmed by Spinrad and Wood (1965), Price (1966), O'Connell (1973), Pritchet and van den Berg (1977) and Faber *et al.* (1985) also. Guinan and Smith (1984) have measured the strength of Mgb and MgH features, "magnesium features", using two 70 Å FWHM interference filters and a single channel photometer, for a large sample of solar neighbourhood stars, ranging in spectral type from B to M. They have also shown that the strength of the features depends on effective temperature and surface gravity. Faber (1973) has observed these features on intermediate-band photometric systems and she has shown the features are very well correlated with metallicity in elliptical galaxies. In order to unravel the underlying correlation between strength of Mg features and metallicity in elliptical galaxies, Faber *et al.* (1977) have made the spectroscopic observations at the intermediate resolution. In order to understand these systems in terms of individual stars,

Faber *et al.* (1985) have observed features in the wavelength range 4000–6200 Å for a large set of K-giant stars at the spectroscopic resolution of 9 Å. Apart from other indices, they measured Mg b and MgH features in the form of Mg_2 index, and have investigated the effect of atmospheric parameters on the Mg_2 index. Large observational survey of this parameter has been done for Galactic and M31 globular clusters by Burstein *et al.* (1984) and Brodie and Huchra (1990) in order to investigate the correlation between Mg_2 index with other indices.

In this chapter, we describe the definition which we follow and quantitative account of the synthetic Mg_2 index and show the dependence of input and atmospheric parameters on the Mg_2 index.

3.1 Definition

The so-called Mg_2 index, as a measure of strength of the features around 5176 Å, is mainly composed of the Mg b triplet at 5167.327 Å, 5172.698 Å, 5183.619 Å and the band head of MgH (2,2) around wavelength 5182 Å. The index definition with reference to a typical synthetic spectrum for the model atmospheric parameters: T_{eff} = 6000, log g = 4.5 and [M/H] = 0.0 is illustrated in Figure 3.1, where we label the positions of side-bands and the central band. We designate the blue sideband, the central band and the red sideband by symbols F_1, F_2 and F_3 respectively. The actual intervals of side-bands and the central band are given in Table 3.1.

The wavelength intervals of each band in the Mg_2 index are defined in such way so as to match broadened galaxy spectra rather than stars. Therefore, the sideband intervals are quite large and include contribution from many weak absorption lines, which reduces the index dilution even at large values of the velocity dispersion, this being an important consideration for interpretation of galaxy spectra. According to Faber *et al.* (1985), the Mg_2 index is defined as the ratio of the integrated flux at the central band to

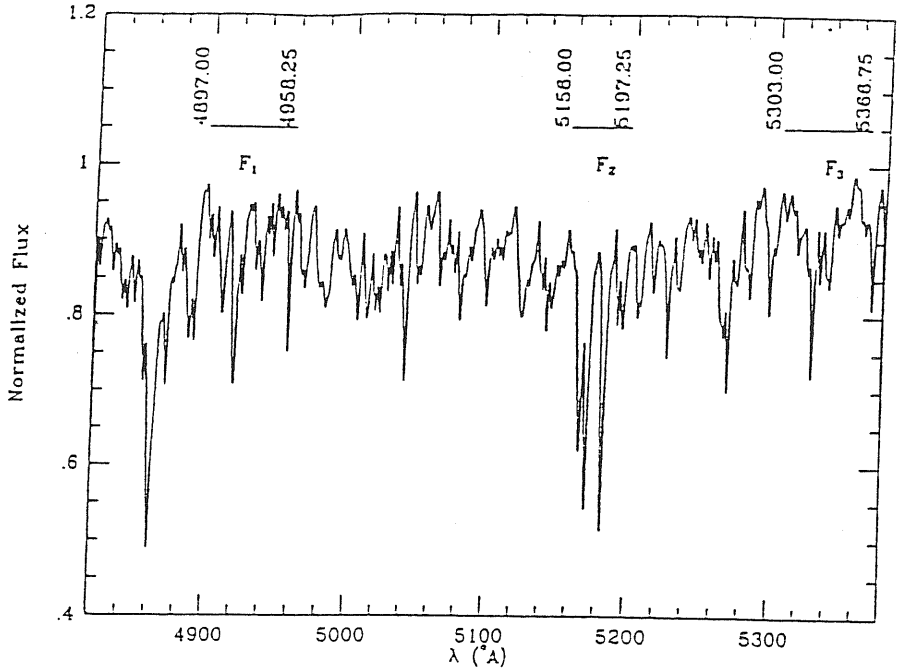

Figure 3.1: Figure showing the spectral bands in the definition of Mg_2.

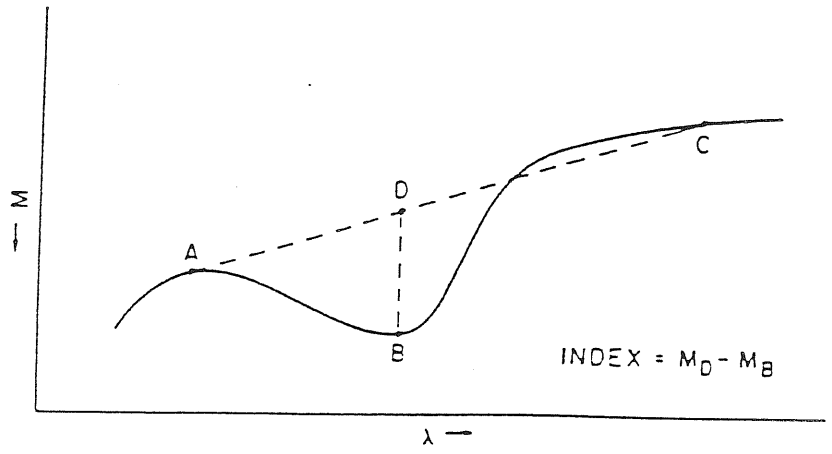

Figure 3.2: Figure showing the schematic representation of the Mg index.

Table 3.1: Observational spectral features diagnostic of for stellar populations in the wavelength range 4850–5400 Å

Identification	Features Measured	Central Bandpass	Continuum Bandpasses
	Equivalent Widths		
$Mgb\lambda5177$	Mgb	5162.00-5193.25	5144.50-5162.00
			5193.25-5207.00
$Fe\lambda5270$	FeI, CaI	5248.00-5286.75	5235.50-5249.25
			5288.00-5319.25
	Molecular Bands		
	Molecular Bands		
Mg_1	MgH	5071.00-5134.75	4897.00-4958.25
			5303.00-5366.75
Mg_2	$MgH+Mgb$	5156.00-5197.25	4897.00-4958.25
			5303.00-5366.75

the flux at local continuum interpolated between the blue and the red continuum bandpasses expressed in magnitude. The schematic representation of the Mg_2 index is given in Figure 3.2. In this figure points, A, B and C, represent the magnitudes at the average values of blue, central and red bandpasses respectively. The point, D, represents the magnitude at the local continuum derived from the interpolation between side continua. The difference of magnitude between the point D and B gives the index.

Analytical expression of this index is:

$$Mg_2 = -2.5log\frac{F_2}{F_1 + (F_3 - F_1)0.61} \tag{3.1}$$

The error in computation of the Mg_2 index can be estimated following the standard theory of error propagation:

$$\Delta Mg_2 = 1.0857[(\frac{\Delta F_2}{F_2})^2 + (\frac{\Delta F_3}{F_3 + 0.39F_1})^2 + (\frac{1.078\Delta F_1}{F_3 + 0.39F_1})^2]^{\frac{1}{2}} \tag{3.2}$$

where $\Delta F_1, \Delta F_2$, and ΔF_3 are errors on the fluxes in each bandpass.

The Mg_2 index involves the integrated fluxes over the side-bands and the central band that we compute from the distribution of fluxes over the region

Table 3.2: A grid of Mg_2 index for models of metallicity [M/H] =0.0

	log g	1.5	2.0	2.5	3.0	3.5	4.0	4.5
T_{eff}								
6000		0.063	0.063	0.065	0.071	0.082	0.098	0.122
5750		0.073	0.074	0.079	0.087	0.102	0.123	0.154
5500		0.088	0.090	0.097	0.109	0.129	0.158	0.199
5250		0.109	0.114	0.124	0.140	0.167	0.207	0.265
5000		0.137	0.143	0.157	0.183	0.225	0.286	0.365
4750		0.166	0.180	0.208	0.254	0.320	0.400	0.493
4500		0.205	0.240	0.294	0.363	0.443	0.531	0.622
4250		0.253	0.317	0.391	0.470	0.552	0.634	0.699
4000		0.260	0.346	0.433	0.517	0.597	0.658	0.668

of the index. Following the relationship (3.1), we computed the synthetic Mg_2 index from the library of synthetic fluxes convolved with the gaussian profile of FWHM =1.65 Å (see section 4.2). We list the values of the Mg_2 index computed for models of solar chemical composition, about one-third of the solar composition and three times the solar chemical composition in Tables 3.2, 3.3, and 3.4, respectively.

In the previous chapter, we discussed the qualitative treatment of the region contributing to the Mg_2 index and showed the effect of computational resolution, line data, instrumental profile, and atmospheric parameters on the behaviour of features contributing to the central bandpass of the index. Here we present the effects of these parameter on the global quantity, *i.e.* the Mg_2 index.

3.2 Effect of computational resolution on Mg_2

To investigate the effect of computational resolution on the global behaviour of the synthetic fluxes in the region of the index, we computed Mg_2 for models at selected points of the grid with different R's. In particular, we computed residual fluxes for K91 models (4000/4.5/0.0) and (6000/4.5/0.0)

Table 3.3: A grid of Mg_2 index for models of [M/H] = -0.50

	log g	1.5	2.0	2.5	3.0	3.5	4.0	4.5
T_{eff}								
6000		0.047	0.047	0.049	0.052	0.059	0.070	0.086
5750		0.053	0.054	0.056	0.062	0.072	0.087	0.109
5500		0.061	0.062	0.068	0.077	0.091	0.111	0.141
5250		0.072	0.076	0.084	0.098	0.118	0.148	0.191
5000		0.091	0.097	0.109	0.129	0.161	0.208	0.273
4750		0.114	0.126	0.149	0.185	0.239	0.311	0.397
4500		0.151	0.181	0.227	0.289	0.365	0.454	0.551
4250		0.226	0.283	0.352	0.430	0.514	0.599	0.627
4000		0.317	0.393	0.470	0.548	0.614	0.615	0.608

Table 3.4: A grid of Mg_2 index for models of [M/H] =0.50

	log g	1.5	2.0	2.5	3.0	3.5	4.0	4.5
T_{eff}								
6000		0.097	0.090	0.094	0.102	0.117	0.139	0.171
5750		0.109	0.111	0.116	0.129	0.146	0.174	0.214
5500		0.135	0.138	0.145	0.160	0.183	0.219	0.272
5250		0.166	0.170	0.179	0.198	0.231	0.282	0.354
5000		0.197	0.202	0.218	0.249	0.300	0.373	0.463
4750		0.222	0.238	0.271	0.325	0.399	0.486	0.580
4500		0.234	0.276	0.336	0.411	0.495	0.583	0.669
4250		0.208	0.278	0.362	0.451	0.539	0.623	0.699
4000		0.156	0.234	0.329	0.430	0.526	0.613	0.684

Table 3.5: Effect of computational resolution on the Mg_2 index

R	6000/4.5/0.0	4000/4.5/0.0
50,000	0.122 *mag*	0.667 *mag*
250,000	0.122 *mag*	0.668 *mag*

at the resolution of 50,000 in order to compare with the results at R =250,000 In the case of the stellar model (6000/4.5/0.0), there is no difference in the index value either computed with resolution 50,000 or with resolution 250,000 (Table 3.5). It was expected that the Mg_2 index of the model at the low temperature might be significantly affected by the value of computational resolution, as the contribution due to molecular opacity is stronger than at higher temperatures. Indeed, the difference in the index value is higher than in the previous case, but it is on the order of 0.001 *mag*, which is well within the observational error quoted by Faber *et al.* (1985) on the basis of their repeated observations of some standard stars. So we conclude that computation of Mg_2 is not affected due to the choice of resolution, so long the resolution takes into account the spectral features in the region of Mg_2.

3.3 Dependence of Mg_2 on grids of models

In chapter 2, we discussed the model atmospheric parameters (4000/1.5/0.0) from three different grids, namely GBEN, GMM and K91. The choice of this model for comparison derives from the fact that model atmospheres at low temperatures are blanketed not only due to atomic line opacities, but also to molecular opacities that were deficient in GMM models, so we expect more discrepancies among the different sets of models.

As a consequence of different amounts of opacities in different grids of models, we obtained Mg_2 values given in Table 3.6. It is obvious from this table that the model which lacks in molecular opacities sources gives the Mg_2 significantly different from that take into account the contribution of

Table 3.6: Effect of grids on the Mg_2

Grid	Mg_2
GMM	0.216 *mag*
GBEN	0.254 *mag*
K91	0.260 *mag*

this component. A word of caution was given by Gustaffson (1991) for the use of his grid of models for supermetal rich stars, where there is possibility of lack of opacity. He recommended that one should use K91 models which account for large opacity contributions for analysis of such stars.

3.4 Dependence of Mg_2 on line data

We investigated the dependence of the line list on the resulting Mg_2 index at selected points of the grid of models. As we have seen in Chapter 2 our line lists are composed of two groups of line data: one is composed of lines predicted from the solar-empirical model and the Arcturus model, and the second list is composed of all other lines present in the range of 4850-5400 Å, ("auxiliary line list").

The reliability of the current line lists was tested by computing the Mg_2 index values from the fluxes computed with the empirical solar model and the observed solar fluxes. We obtained the Mg_2 value of 0.135 *mag* from the observed fluxes and 0.137 *mag* for the model fluxes. The difference between these values is within the error on the order of ± 0.007 *mag* given by Faber *et al.* (1985). So, the resulting Mg_2 values in both cases agree very well, lending credibility to the line data. To look into the effect of the auxiliary line list on the Mg_2 index for models, we computed synthetic spectra for models at the border points of the grid with and without the auxiliary line list. In Figure 3.3 we show the effect of the auxiliary line list on the Mg_2 index by plotting Mg_2 based on synthetic fluxes computed with and without the auxiliary line list

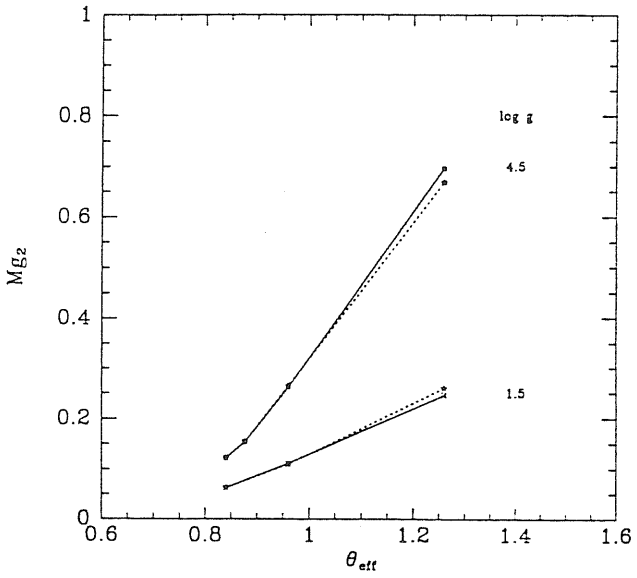

Figure 3.3: Mg_2 for models computed with (solid lines) and without auxiliary line (dashed lines).

Table 3.7: Effect of line data on the Mg_2 index

Model	F_2	F_2^{aux}	Mg_2	Mg_2^{aux}
4000/1.5/0.0	0.125	0.122	0.246	0.260
4000/4.5/0.0	0.079	0.073	0.696	0.668
5750/4.5/0.0	0.144	0.143	0.154	0.154
6000/4.5/0.0	0.150	0.150	0.122	0.122

for selected models as a function of $\theta_{eff} = 5040/T_{eff}$. The integrated fluxes in the bandpasses of the Mg_2 index for models with parameters different from the solar and Arcturus models, are lower when computed with the auxiliary line list than those computed without auxiliary line list. It is worth mentioning that the Mg_2 index is not always directly proportional to the integrated fluxes in the central bandpass (see Table 3.7). Although the stellar model (4000/4.5/0.0) gives lower integrated fluxes in the central bandpass of the index, this model is bluer in Mg_2 index. The differences in the index are clearly dependent on T_{eff}, while are not significantly related to log g values. They are on the order of 5 %, so it is hard to verify line lists using the current

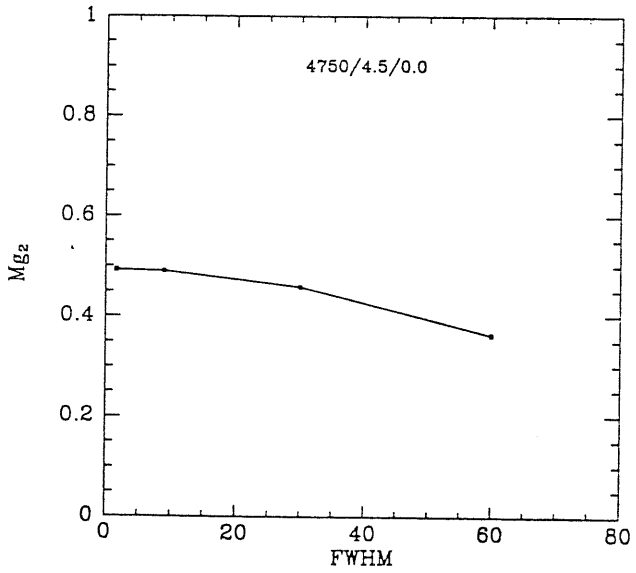

Figure 3.4: Mg_2 as a function of FWHM for the model (4750/4.5/0.0).

observations. For instance, it is very difficult to observe the coolest dwarfs at the moderate resolution, because of their low magnitude. Therefore, for the sake of completeness we preferred to use the complete line list in the computation of synthetic spectra for the grid of models.

3.5 Dependence on Mg_2 index on the instrumental resolution

In sec. 2.2.4, we accounted for the effect of instrumental broadening on the spectral energy distribution qualitatively. In order to look into the effect of instrumental broadening on the Mg_2 index, we convolved the normalized flux spectra with Gaussian profiles with different values of FWHM. As an illustration, we plot in Figure 3.4 the computed synthetic Mg_2 as a function of FWHM of the Gaussian profiles with which the spectra were convolved. The Mg_2 index is not affected by the instrumental broadening corresponding to the value of resolution of our observed sample, *i.e.* 1.65 Å, or resolution

of 9.00 Å, the resolution at which Faber and co-workers obtain their stellar and elliptical galaxies spectra. This suggests that the grid of synthetic Mg_2 indices obtained at the resolution of 1.65 Å, can be directly comparable to the observations obtained at the resolution of 9.00 Å. The Mg_2 index is clearly affected by higher values of FWHM, thus implying the use of the proper instrumental resolution to compare synthetic values with the observed ones.

3.6 Dependence of Mg_2 on atmospheric parameters

In Figure 3.5 we show the global behavior of the Mg_2 index with respect to the reciprocal of effective temperature $\theta_{eff} = 5040/T_{eff}$ for the grid of solar chemical composition models.

The different lines in this figure indicate the synthetic Mg_2 values as measured from the library of synthetic spectra for different gravity values. It is obvious that the Mg_2 index shows a biparametrical behaviour, in the sense that this index depends upon both T_{eff} and log g. The strength of the index increases with the decrease of temperature, while at the same temperature there is clear demarcation of Mg_2 indices with gravity for cool stars. The maximum separation between synthetic Mg_2 values of dwarfs and giants at the same temperature is on the order of 0.4 *mag*. There is a tendency of saturation in the Mg_2 values below 4250 K. The Mg_2 index, which measures mainly the strength of Mg b and MgH features, shows increase in the strength of these features with the increase in gravity and decrease in temperature. The dependence of the Mg_2 on surface gravity is stronger for stellar models with effective temperature lower than 5000 K. There is an inversion in the value of the Mg_2 index for the model (4000/4.5/0.0) with respect to the model (4250/4.5/0.0). Not only there is an inversion in Mg_2, but the integrated flux in the central bandpass of the index also show the same behaviour, in the sense that the model (4000/4.5/0.0) predicts higher flux than the model (4250/4.5/0.0). Barbuy *et al.* (1991) recently

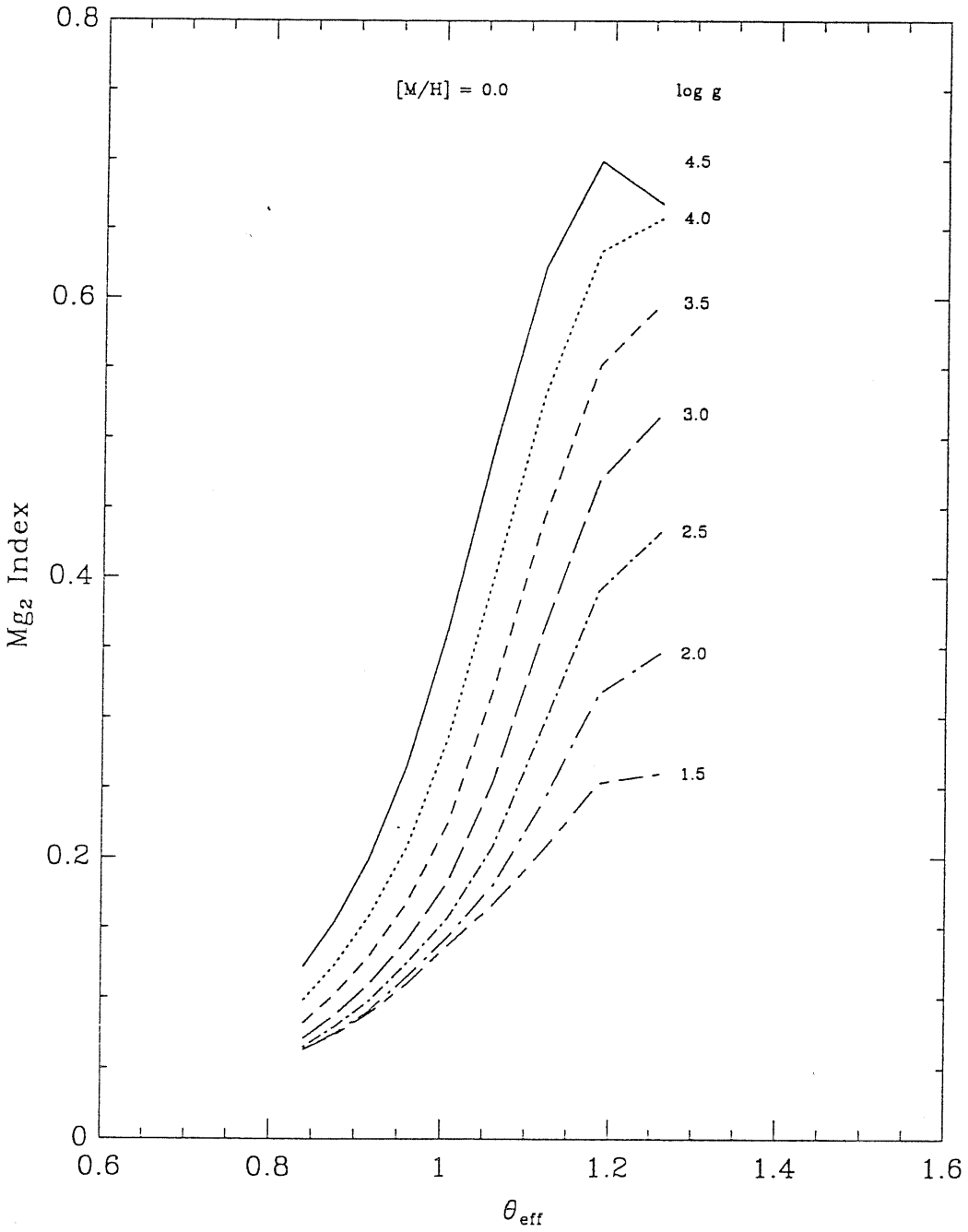

Figure 3.5: The Mg_2 as function of reciprocal of effective temperature, (θ_{eff}), for the grid of solar chemical composition.

investigated the effect of synthetic Mg_1, Mg_2 and Mgb indices on the basic stellar atmospheric parameters using GBEN models and their line list. In their figure 4, showing the dependence of integrated flux in the central band of the Mg_2 on metallicity for different temperatures, we see the same effect. So we conclude that this behaviour is not model and line data dependent.

The trend of Mg_2 with the temperature for the grid of models of metallicity [M/H]=-0.5 (about one-third the solar chemical composition) is shown in Figure 3.6. There is a similar tendency of the index with temperature as illustrated for models of solar chemical composition, except for the fact that models with temperature lower than 4250 K and surface gravity values less than 4.0 do not show saturation in the index with temperature. Note that the index in the model (4000/4.5/-0.5) becomes smaller than the value of the model (4000/3.5/-0.5).

In Figure 3.7 we plotted the response of the Mg_2 to temperature for models of chemical composition about three times the solar composition (Again the tendency of the index with temperature is the same as for models of solar and one-third of solar chemical composition. For models with low temperatures and low gravities, the Mg_2 index instead of getting saturated continues to decrease.

3.7 Theoretical calibrations of the index

As seen before, for models of different gravity and metallicity the theoretical behaviour of the Mg_2 index with respect to reciprocal θ_{eff} follows a certain trend. For understanding the integrated Mg_2 index of a given stellar system in the context of population synthesis models (Buzzoni, 1989, Charlot, S. and Bruzual, 1991), it is desirable to have a continuous description of the index with respect to the atmospheric parameters. Towards this aim, we present here the theoretical calibrations of the index with respect to temperature based on our grid of the index for models of different gravity and metallicity

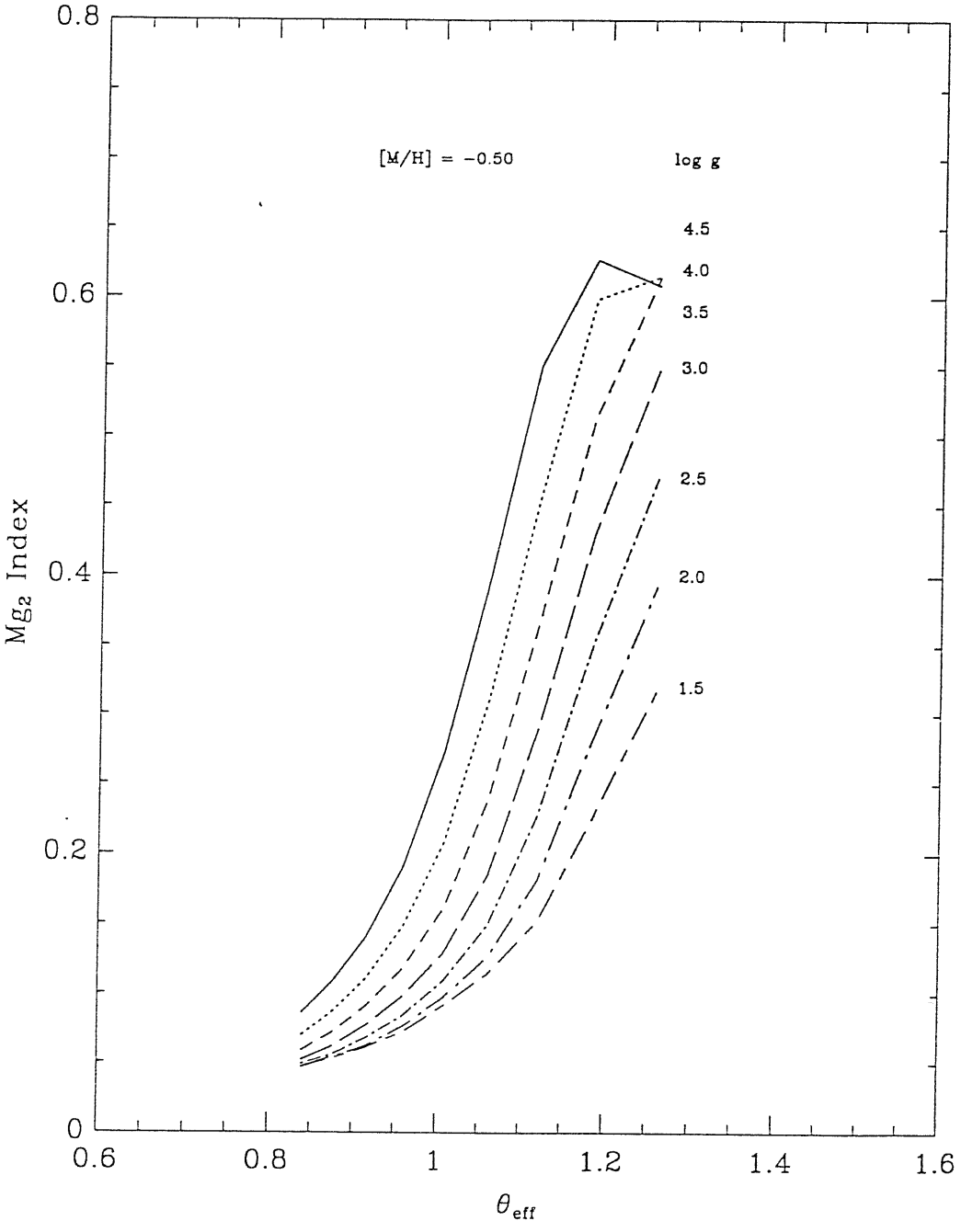

Figure 3.6: The Mg_2 as function of reciprocal of effective temperature (θ_{eff}) for the grid of [M/H] = -0.50.

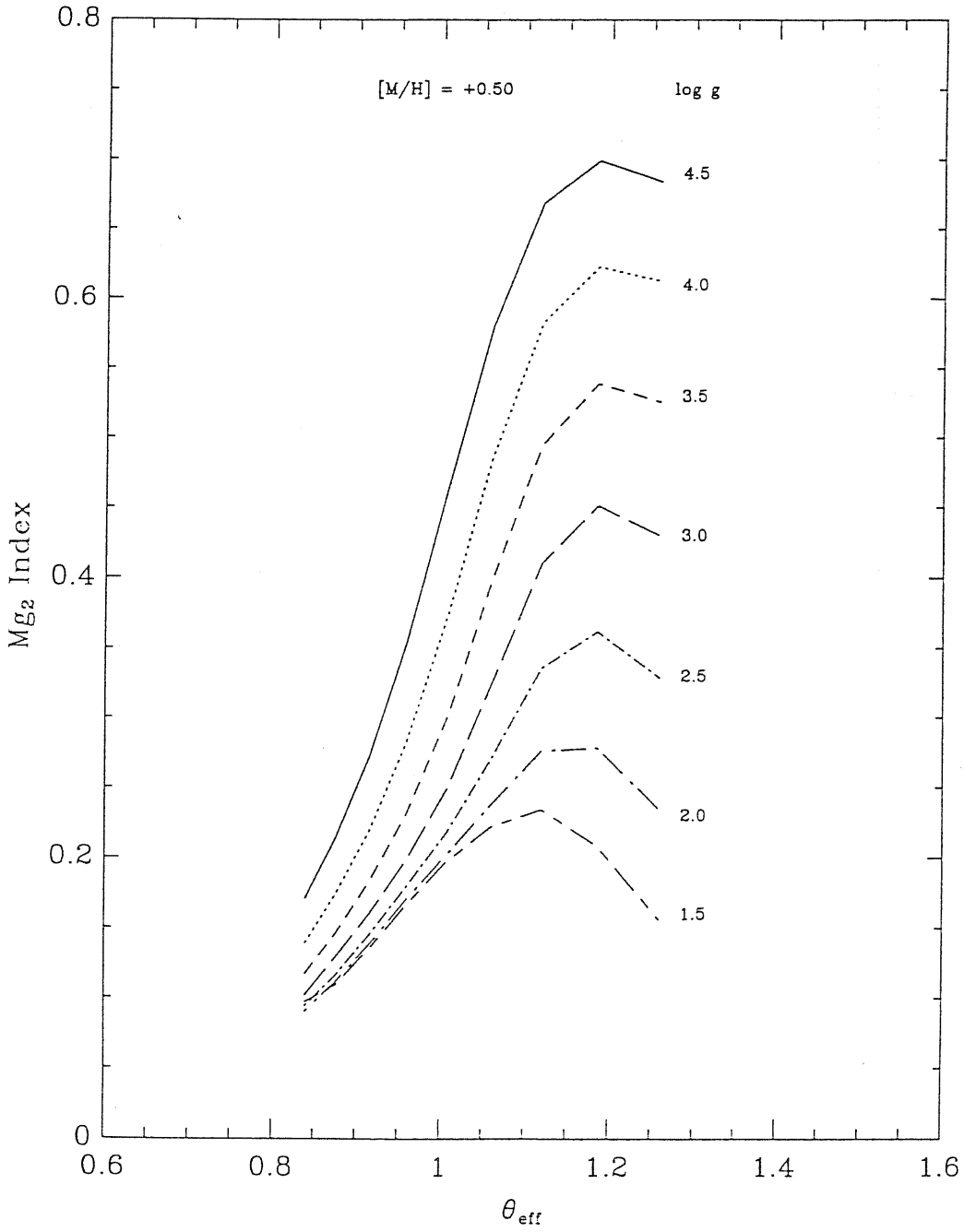

Figure 3.7: The Mg_2 as function of reciprocal of effective temperature θ_{eff} for the grid of [M/H] = 0.50.

Table 3.8: Coefficients A, B, C and D in the relation between Mg_2 index and θ_{eff} for the grid of [M/H]=0.0 together with RMSE and correlation coefficient r

log g	A	B	C	D	RMSE	r
1.5	1.139	-3.453	3.319	-0.874	0.001	1.003
2.0	-0.442	1.842	-2.612	1.348	0.001	1.003
2.5	0.146	0.455	-1.744	1.295	0.003	1.001
3.0	3.575	-9.760	8.204	-1.839	0.006	0.995
3.5	8.579	-25.149	23.732	-6.939	0.007	1.002
4.0	13.977	-42.115	41.270	-12.852	0.007	1.001
4.5	20.211	-62.198	62.601	-20.259	0.007	0.999

values.

The behaviour of the index with respect to temperature may be best modeled by fitting a third order polynomial through points excluding the point at temperature 4000 K ($\theta_{eff} = 1.26$) in Figures 3.5, 3.6, and 3.7. The exclusion of Mg_2 at $\theta_{eff} = 1.26$ derives from the following argument: for grid of different values of gravity and metallicity, the index at this temperature shows a sudden break in its trend, which is also noticed by Buzzoni *et al.* (1991) who attribute it to the presence of TiO blends affecting the blue continuum bandpass. At present, since we do not include TiO molecules in the synthesis of spectra, so we are uncertain about the strength of the index at this temperature.

The general relationships between Mg_2 and θ_{eff} for different surface gravities and metallicity values is as follows:

$$Mg_2 = A + B\theta_{eff} + C\theta_{eff}^2 + D\theta_{eff}^3 \tag{3.3}$$

where A, B, C and D are the fitting coefficients and they are given in Tables 3.8, 3.9, 3.10. The correlation coefficient(r) together with the root mean square error (RMSE) of the cubic polynomial fit is also given in Tables 3.8, 3.9, 3.10. The values of r, which are closer to 1, suggest the best representation of data points by the third order polynomial. The good-

Table 3.9: Coefficients A, B, C and D in the relation between Mg_2 index and θ_{eff} for [M/H]=-0.50 together with RMSE and r

log g	A	B	C	D	RMSE	r
1.5	-3.090	10.168	-11.167	4.174	0.002	0.999
2.0	-4.570	15.122	-16.696	6.235	0.002	0.995
2.5	-4.680	15.860	-17.964	6.887	0.001	0.997
3.0	-3.099	11.316	-13.802	5.710	0.003	1.003
3.5	1.006	-1.067	-1.575	1.794	0.005	1.001
4.0	7.352	-20.594	18.189	-4.741	0.007	0.997
4.5	20.739	-62.565	61.652	-19.555	0.013	0.998

Table 3.10: Coefficients A, B, C and D in the relation between Mg_2 index and θ_{eff} for the grid of [M/H]=0.50 together with RMSE and r

log g	A	B	C	D	RMSE	r
1.5	7.446	-24.267	26.135	-9.123	0.001	1.000
2.0	5.188	-7.012	18.299	-6.276	0.003	1.005
2.5	6.554	-20.635	21.277	-6.980	0.005	0.999
3.0	9.907	-30.637	31.002	-10.024	0.007	1.003
3.5	15.105	-46.695	47.299	-15.412	0.007	1.004
4.0	19.320	-60.222	61.597	-20.330	0.006	0.996
4.5	20.938	-66.360	69.010	-23.141	0.003	1.001

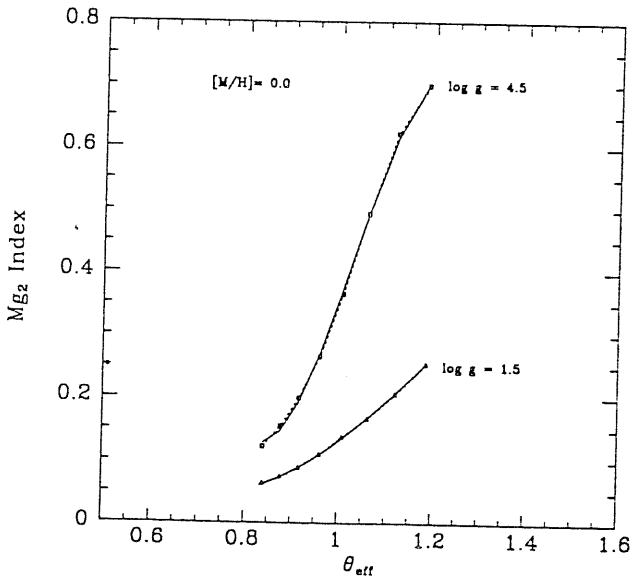

Figure 3.8: A plot of Mg_2 vs. θ_{eff} for gravity values of log g =4.5 and 1.5 for the grid of [M/H] = 0.0 together with the best fitted cubic polynomial.

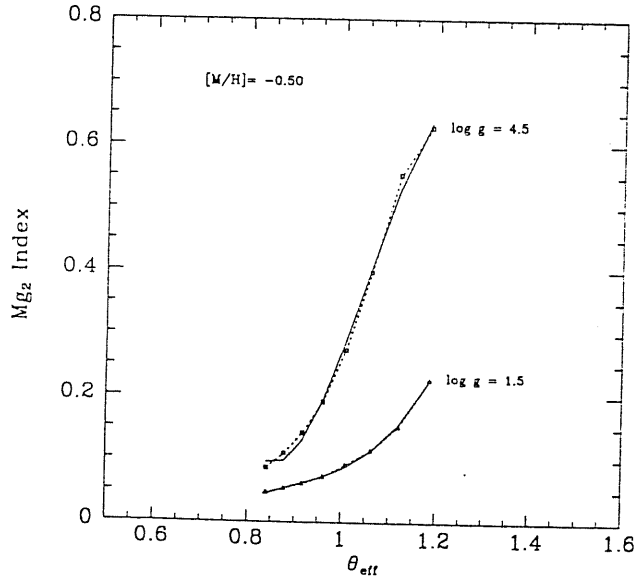

Figure 3.9: Same as in Figure 3.8, but for the grid of [M/H] = -0.50.

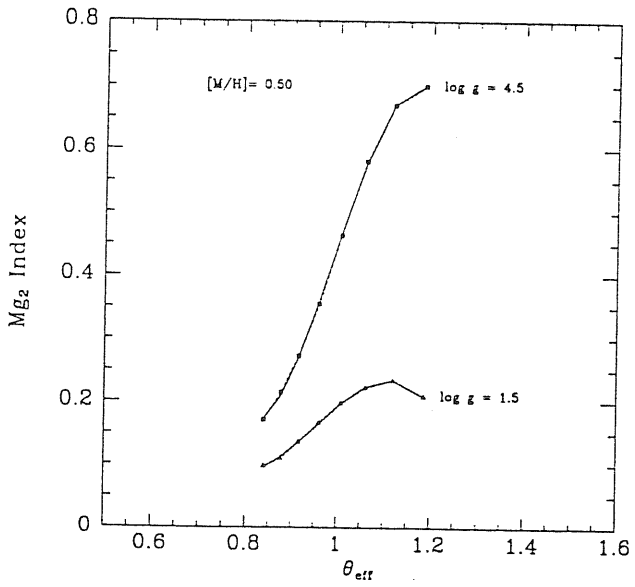

Figure 3.10: Same as in Figure 3.8, but for the grid of [M/H] = 0.50.

ness of the fit can also be judged from Figures 3.8, 3.9, and 3.10, where for an illustration we show the theoretical Mg_2 values as a function of θ_{eff} for models of 1.5 and 4.5 gravity and for metallicity [M/H]= 0.0, -0.5 and 0.5. The dashed lines in these figures represent the connection of grid Mg_2 values indicated with filled squares for log g = 4.5 and filled triangles for log g = 1.5, while the best cubic polynomial fits are represented by solid lines.

In order to look into the dependence of surface gravity separately, in Figure 3.11, we plot the Mg_2 index as a function of surface gravity for models at the different temperatures. As can be seen from this figure, the Mg_2 index is almost independent of surface gravity for stellar models with temperature higher than 5250 K ($\theta_{eff} < 0.96$). The Mg_2 index is strongly dependent on the gravity for stars with effective temperature less than 5000 K ($\theta_{eff} > 1.01$), which supports the conclusion empirically derived by Faber *et al.* (1985) that the Mg_2 index is a good indicator of surface gravity for K-giants.

The metallicity effect can be visualized in Figure 3.12, where we plot Mg_2 index as a function of θ_{eff} for three metallicity values for log g = 3.0. For temperature above 4500 K ($\theta_{eff} < 1.12$), the separation among the loci of

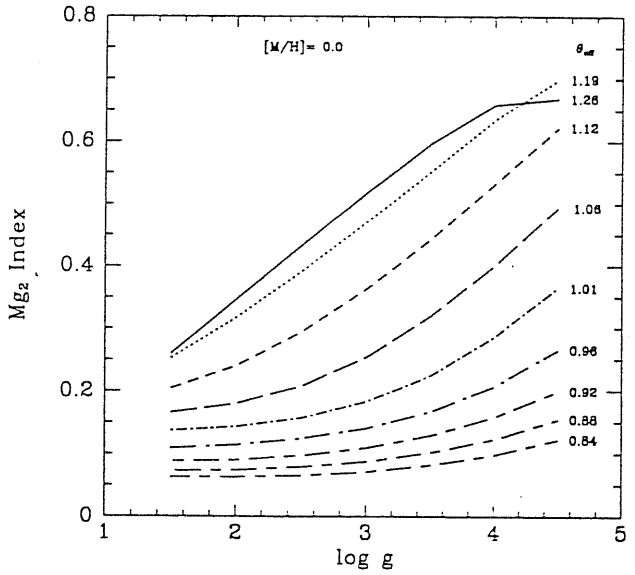

Figure 3.11: The Mg_2 as a function of log of surface gravity for the grid of solar chemical composition at different temperature values.

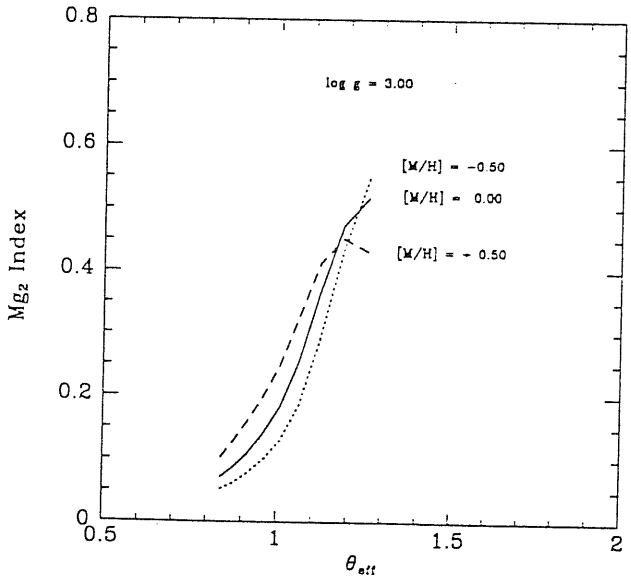

Figure 3.12: The Mg_2 as function of reciprocal of effective temperature (θ_{eff} for the grid of different metallicity values.

three metallicities is clear. However, the crossing of Mg_2 value below this temperature makes it hard to establish conclude the dependence of Mg_2 on metallicity below temperature 4250 K ($\theta_{eff} > 1.19$). In the range of metallicity we considered here, we can say that the Mg_2 increases with metallicity for stellar models with T_{eff} ranging from 4250 K to 6000 K ($0.84 \leq \theta_{eff} \leq 1.19$). For example, for a grid of log g = 3.0 at 5000 K ($\theta_{eff} = 1.01$) there is a increase of the Mg_2 by 0.110 *mag* as the global metallicity [M/H] changes from -0.50 *dex* to 0.50 *dex*. On the average, the variation of the index with respect to metallicity is on the order of 0.087, which is consistent with empirical determination by FFBG.

Chapter 4

Observations

In this chapter, we describe the observational data of field stars observed as a result of a joint ESO proposal by A. Buzzoni (Merate Observatory, Milano) as principal investigator, L. Mantegazza (University of Pavia), M.L. Malagnini (Trieste University), C. Morossi (Trieste Observatory), and F. Castelli (CNR). We will use these data as a guide to check the synthetic stellar spectra and consequently the derived synthetic Mg_2 index.

4.1 Observational data

Observations of a set of field stars were made by L. Mantegazza, at the ESO observatory, La Silla, Chile, with the 1.52 m telescope equipped with Boller and Chivens spectrograph, RCA high resolution CCD detector(ESO CCD no. 13) and grating giving a dispersion of 59.5 Å/mm (ESO grating no. 26). During the observations, a standard source of He-Ar lamp was observed with the same configuration for wavelength calibration of the observed data. The characteristics of the instrument used to obtain observations are presented in Table 4.1. The observations cover the wavelength range of 4500-5500 Å, which includes the region of the Mg_2 index and H_β. In all, 87 stars were observed, of which 79 stars were observed during four nights of observations in December 1988 and 8 red dwarf selected from Gliese catalogue were observed

Table 4.1: Principal characteristics of the optical telescope and B & C spectrograph

Telescope Aperture	1.52 m
Focal ratio of telescope	14.9
Focal ratio of B & C	7.0
Focal length of collimator	630 mm
Focal length of Schmidt camera	127 mm

in the second run of observations in April 1989 to extend the data base to very cool stars. The latter observations were obtained with the same equipment, but due to change in the configuration of Schmidt camera spectrograph the reciprocal dispersion of the spectra increased to 65 Å/mm.

Data reduction was done in Milan, by using ESO MIDAS package (see MIDAS Users Guide, Image Processing Group, ESO V4.3, 1988). Correction for flat field were applied in order to remove spurious CCD high-frequency features in the raw spectra. The data were calibrated in wavelength using the He-Ar reference spectra, and sampled at 0.8 Å. No standard stars were observed so that absolute fluxes can not be directly obtained. In the following, we will refer to already processed data.

In Tables 4.2, 4.3, 4.4, we list the stellar data base with their identification code. Most of them have effective temperature, surface gravity and metallicity published in Cayrel de Strobel *et al.* (1985) compilation, however, where more than one values of these parameters are given, we report an average value. For stars taken from Gliese catalogue, the effective temperatures and gravities were derived from infrared indices by using calibrations of Veeder (1975). The adopted atmospheric parameters are listed in columns 3 to 5 of Table 2. With these atmospheric parameters, the observational sample spans a range of the effective temperature from 3210 to 6072 K, spectral type from M1 to F8, the surface gravity from 0.2 to 4.8 and metal abundance, [Fe/H], (where [Fe/H] = log(Fe/H)-log$(Fe/H)_{\odot}$) in the range of -2.60 to 1.80. The distribution of basic atmospheric parameters compiled from

Table 4.2: A list of program stars

HD	V	T_{eff}	log g	[Fe/H]
1581	4.23	6000	4.50	-0.10
1835	6.39	5793	4.45	0.05
3443	5.57	5419	4.57	-0.16
10380	4.44	4000	1.50	-0.30
10700	3.50	5305	4.46	-0.34
13611	4.37	5143	3.00	0.00
13974	4.87	5600	4.50	-0.30
14802	5.20	5929	4.40	0.00
17925	6.04	5091	4.50	-0.15
18322	3.89	4710	2.80	0.20
20630	4.83	5793	4.45	0.23
20766	5.54	5600	4.00	-0.16
20794	4.27	5362	4.40	-0.25
20807	5.24	5727	4.50	-0.20
20894	5.52	5091	3.10	-0.20
22049	3.73	5040	4.40	-0.23
22484	4.28	6000	3.96	0.04
30495	5.51	6000	4.50	0.10
30562	5.78	5860	3.75	0.13
32147	6.22	4755	4.45	0.02
33793	8.89	3524	4.87	-0.50
36395	7.97	3626	4.80	0.60
37160	4.09	4667	2.57	-0.21
37763	5.19	5040	3.00	0.35
39091	5.65	5663	3.94	0.00
39364	3.81	4383	9.99	-0.36
39523	4.51	4667	1.90	0.15
44033	5.69	3294	9.99	-0.07
45829	6.63	4200	0.20	-0.08
46407	6.38	4990	2.55	0.03

Table 4.3: Table 4.2 continued

HD	V	T_{eff}	log g	[Fe/H]
47205	3.95	4941	3.08	0.07
50778	4.07	3877	1.90	-0.12
50877	3.78	4200	0.40	0.05
56577	4.79	4383	1.30	0.16
60219	8.50	4800	1.70	-0.50
62576	4.59	4308	1.30	0.01
62644	5.06	5143	3.12	-0.35
63302	6.35	4500	0.20	0.17
65699	5.11	4846	1.50	-0.20
76151	6.00	5600	4.40	-0.02
83548	5.50	5091	2.00	0.10
84810	3.69	4941	1.50	0.30
84903	–	4500	0.80	-2.60
88218	6.13	5538	3.36	-0.42
88284	3.61	5040	2.86	0.10
89388	3.40	4500	1.60	0.54
91324	4.89	6072	3.90	-0.60
91805	6.08	4846	2.00	0.00
95272	4.08	4032	2.48	-0.12
95345	4.84	4667	2.00	-0.05
96918	3.91	5727	0.40	0.32
97907	5.32	3818	2.07	-0.17
98430	3.56	4846	2.48	-0.33
99491	6.50	5600	4.60	0.09
100407	3.54	4846	2.20	0.00
102365	4.91	5419	4.09	-0.59
102634	6.15	6072	4.30	0.12
102870	3.61	6072	4.30	0.21
111631	8.48	3907	4.50	0.10
188510	8.81	5305	3.80	1.80

Table 4.4: Table 4.2 continued

HD	V	T_{eff}	log g	[Fe/H]
189567	6.07	5727	4.08	-0.28
190248	3.56	5600	4.31	0.30
191408	5.32	4893	4.60	-0.07
192310	5.76	4941	4.50	-0.08
192947	3.57	4990	3.00	0.12
196378	5.12	6072	4.10	-0.30
203638	5.77	4541	1.50	0.35
208776	6.94	5929	4.00	-0.14
209100	4.69	4500	4.70	0.04
211391	4.16	4941	2.80	-0.07
212330	5.32	5793	4.20	0.00
213009	3.97	4800	2.00	-0.20
215104	4.85	4755	2.30	-0.20
216437	6.05	5929	4.40	0.10
216763	4.21	4893	2.50	-0.20
221148	6.25	3210	2.60	0.07
225212	5.16	4200	1.00	0.00
GL 229	-	3652	4.75	-
GL 234	-	3000	4.92	-
GL 273	-	3252	4.85	-
GL 488	-	3877	4.70	-
GL 551	-	2625	5.03	-
GL 699	-	3170	4.87	-
GL 729	-	3111	4.89	-

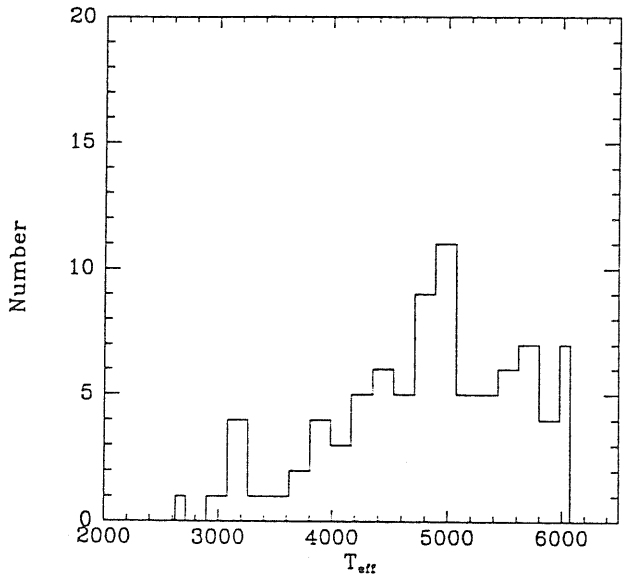

Figure 4.1: A histogram showing the number distributions of program star with respect to T_{eff}.

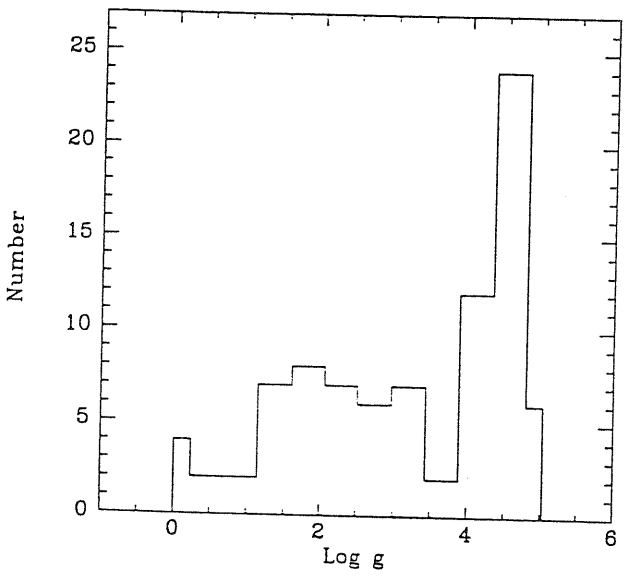

Figure 4.2: A histogram showing the number distributions of program star with respect to log g.

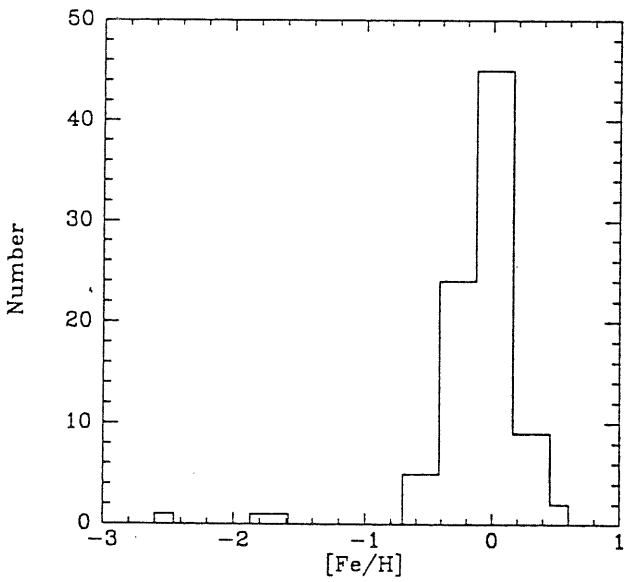

Figure 4.3: A histogram showing the number distributions of program star with respect to metallicity.

Cayrel and co-workers catalogue is displayed in Figures 4.1, 4.2 and 4.3.

Most of the stars have effective temperature higher than 4800 K and there are very few stars with temperature lower than 4000 K (Figure 4.1). The distribution of surface gravity is dominated by dwarfs, and giants and there are few supergiants (see Figure 4.2). The metallicity of the observed sample in most of the stars lie about the solar value with a spread of about ± 1 dex and there are only a few very metal-poor members (see Figure 4.3)

4.2 Determination of instrumental profile

Distortion and blurring of stellar spectrum are caused not only by the projected rotational velocity and macroturbulence velocity of the star, but also by instrumental effects, such as detector resolution, diffraction and aberration. In all cases the structure of the spectrum is degraded. Measurements of the instrumental profile tell us how much degradation has occurred and to some extent allows us to degrade the synthetic spectrum to the resolution of the observation. Instrumental profile is of paramount importance in

the measurement of line profiles and comparing observations with theoretical predictions.

The instrumental profile is generally represented by a Gaussian profile, and is usually determined from the best fit of the monochromatic line in the standard lamp with the gaussian profile. We tried different Gaussian profiles over one of the emission lines in the He-Ar lamp in the wavelength range of our interest. As a result we derived the Gaussian profile, which fits best the observed line of the lamp source, having FWHM equal to 2.07 Å. From the monochromatic lines it is very difficult to deconvolve the intrinsic broadening of lines obtained from the instrumental broadening in the observed spectrum. Another way to determine this parameter of the Gaussian profile is by tuning full width at half maximum (FWHM) in the synthetic spectra until the synthetic line profiles matches very well with the observed ones. The effect of instrumental broadening on the behaviour of synthetic spectra is demonstrated in Figure 4.4, where we have plotted the portion of the synthetic spectrum, in the upper panel, before broadening due to instrumental profile and in the lower panel after broadening with gaussian profile of full width at half maximum (FWHM) equal to 1.65 Å. The broadening of synthetic spectra causes the smoothing out the features, however it does not affect the equivalent width of spectral features.

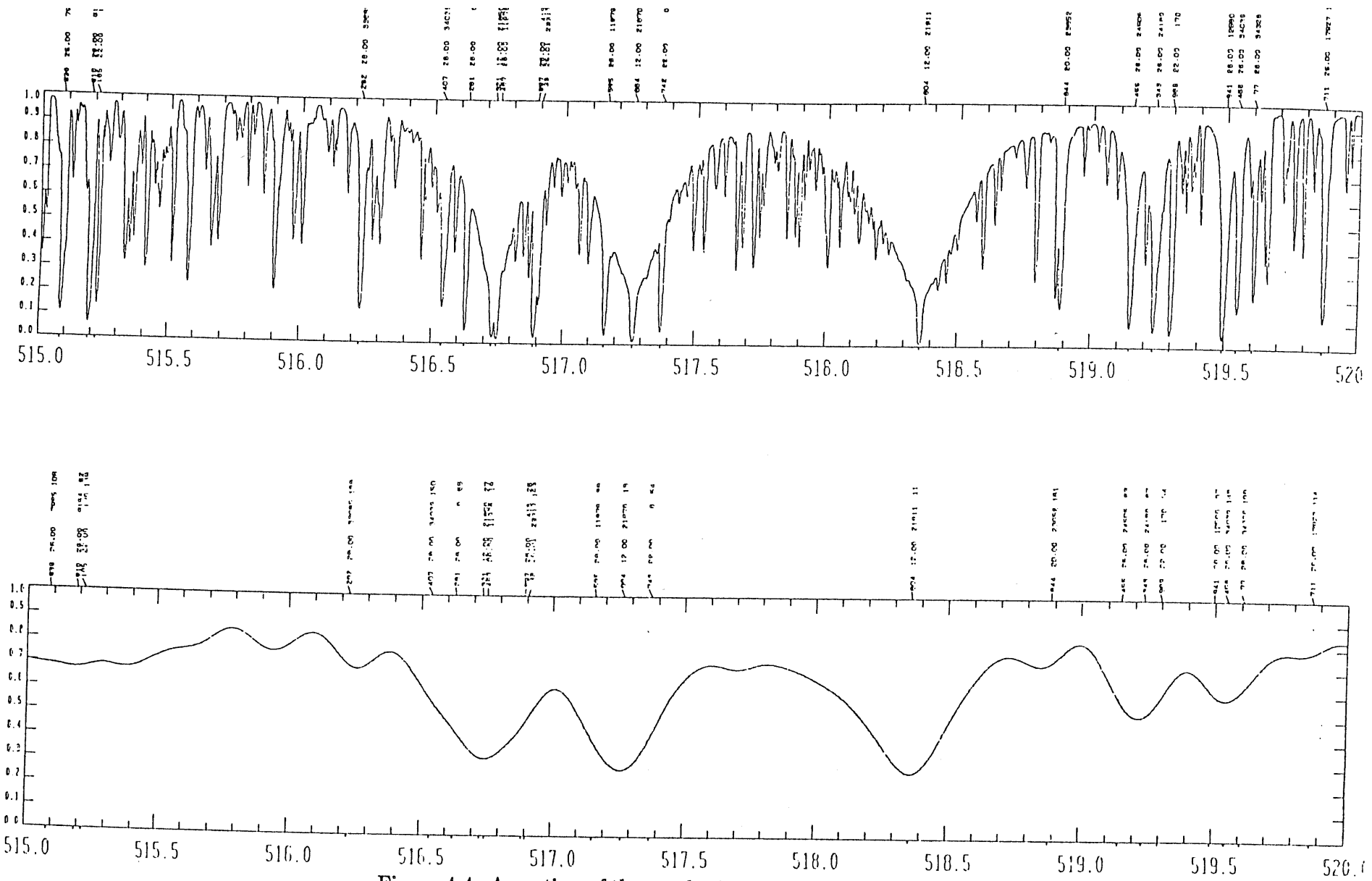

Figure 4.4: A portion of the synthetic spectra showing the effect of instrumental broadening for the K91 model (5000/4.5/0.0): a) without instrumental broadening (upper panel) b) with instrumental broadening due to gaussian profile of FWHM=1.65 A (lower panel).

Chapter 5

Theory vs. Observations

One of the great triumphs of modern astronomy and astrophysics has been the use of computed stellar atmospheric models and synthetic spectra for matching them, in detail, with the observed spectral features and to derive physical characteristic of stars. We have described before how we computed the grid of synthetic spectra for models representative of cool type stars. The next step is to examine the consistency of the grid which can be done by comparison with the observations.

In this chapter, we will deal with the steps involved in the process of comparing the synthetic spectra with the observations. We will investigate the dependence of strength of Mgb and MgH features, in the form of the Mg_2 index, on the atmospheric parameters. The last section is devoted to the implications of the index for study of galaxies and extragalactic objects.

5.1 Template synthetic spectra

In the process of comparing real stars with model atmospheres, we need to know the atmospheric parameters that govern the spectral energy distribution of stars so that the proper model can be computed. The main parameters that characterize the spectral energy distribution of stars are effective temperature, surface gravity and chemical composition.

A comprehensive review on the determination of effective temperature can be found in the review article written by Böhm-Vitense (1981). Also, while dealing with early type stars, we (Gulati *et al.*, 1989) have discussed the methods for estimating the effective temperatures and errors associated with them. In principle, the effective temperatures determined by the direct method, *i.e.* from the measurements of full energy distribution, should be the best ones. Unfortunately, only for a limited number of stars the full range of energy distribution is available. In most cases, this parameter is determined from color indices, or from Balmer lines profiles or from excitation equilibrium. Color indices such as $V-R, V-K$ and $R-I$ are generally used as temperature indicators for cool stars, since they vary rapidly with temperature, and can be measured for large stellar data bases. These colors can be transformed to effective temperatures via calibration, such as given by Blackwell *et al.* (1991).

As regards surface gravities, they can either be determined by spectroscopic means (Edvardsson, 1988) or from evolutionary tracks (Malagnini and Morossi, 1990).

The metal abundances are determined by indirect methods *i.e.* by comparing the equivalent widths or the line profiles of the observed spectra with the computed ones. In this case, a typical error on T_{eff} on the order of ± 100 K transforms in abundance an error on the order of ± 0.25 *dex* (Cayrel de Strobel, 1985).

We have collected atmospheric parameters from the compilation of Cayrel *et al.* (1985), who have gathered information on effective temperatures, surface gravities and chemical composition from different authors. For stars with more than one determinations of parameters, the average value is assumed. In this catalog, since the collection of parameters is from various sources, the error expected on the temperature is of the order of ± 200 K (Tripicco and Bell, 1990), ± 0.20 *dex* for log g, and ± 0.25 *dex* for [Fe/H]. As an intial step towards establishing the consistency of the library of synthetic spectra

Table 5.1: A list of reference stars and reference models used to compare the synthetic index

HD	T_{eff}	log g	[Fe/H]	Mg_2^{obs}	Mg_2^{syn}	T_{eff}	log g	[M/H]
	Literature values					Grid values		
1581	6000	4.50	-0.10	0.094	0.117	6000	4.5	0.0
1835	5793	4.45	0.05	0.149	0.150	5750	4.5	0.0
3443	5419	4.57	-0.16	0.173	0.195	5500	4.5	0.0
13611	5143	3.00	0.12	0.115	0.136	5250	3.0	0.0
14802	5929	4.40	0.00	0.089	0.117	6000	4.5	0.0
17925	5091	4.50	-0.15	0.304	0.361	5000	4.5	0.0
18322	4710	2.80	0.20	0.231	0.250	4750	3.0	0.0
20630	5663	4.45	0.08	0.177	0.150	5750	4.5	0.0
20766	5663	4.10	-0.06	0.131	0.106	5750	4.0	0.0
22049	5040	4.40	-0.23	0.316	0.361	5000	4.5	0.0
22484	6000	3.96	0.04	0.085	0.094	6000	4.0	0.0
30495	6000	4.50	0.10	0.119	0.117	6000	4.5	0.0
30562	5860	3.75	0.13	0.115	0.106	5750	4.0	0.0
37160	4941	2.57	-0.04	0.163	0.141	5000	2.5	0.0
39091	5663	3.94	0.00	0.098	0.106	5750	4.0	0.0
39523	4667	1.90	0.15	0.216	0.164	4750	2.0	0.0
46407	4990	2.55	0.03	0.147	0.141	5000	2.5	0.0
47205	4700	3.08	0.07	0.237	0.250	4750	3.0	0.0
65699	4846	1.50	-0.20	0.154	0.162	4750	1.5	0.0
69627	4308	1.87	-0.22	0.338	0.313	4250	2.0	0.0
76151	5600	4.40	-0.02	0.155	0.141	5500	4.0	0.0
88284	5040	2.86	0.10	0.190	0.166	5000	3.0	0.0
91805	4846	2.00	-0.10	0.151	0.164	4750	2.0	0.0
99491	5600	4.60	0.09	0.199	0.195	5500	4.5	0.0
100407	4846	2.2	-0.10	0.111	0.164	4750	2.0	0.0
102634	6072	4.30	0.12	0.093	0.117	6000	4.5	0.0
102870	6072	4.30	0.21	0.089	0.117	6000	4.5	0.0
111631	3907	4.50	0.10	0.657	0.666	4000	4.5	0.0
191408	4893	4.60	-0.07	0.310	0.361	5000	4.5	0.0
192310	4941	4.50	-0.08	0.339	0.361	5000	4.5	0.0
192947	4897	3.00	0.12	0.164	0.166	5000	3.0	0.0
211391	4941	2.80	-0.07	0.170	0.166	5000	3.0	0.0
212330	5793	4.20	0.00	0.114	0.106	5750	4.0	0.0
216437	5929	4.40	0.10	0.116	0.117	6000	4.5	0.0
216763	4893	2.5	-0.20	0.149	0.141	5000	2.5	0.0
219615	4800	2.42	-0.20	0.165	0.203	4750	2.5	0.0

with the observations, of the total observed sample we selected sub-sample of 36 stars with metallicity representative of solar chemical composition. We list them in Table 5.1 along with their atmospheric parameters in columns 2 to 4.

In order to compare synthetic spectra with the observed ones, we need to degrade the former to the resolution of the observations, which is measured as a full width at half maximum (FWHM) of one of the monochromatic lines in the spectra of standard lamp source taken with the same configuration (see section 4.2). An alternative way to determine the instrumental profile is to vary it in the synthetic spectrum of appropriate model until there is a good match between the synthetic and observed spectrum. Tests on this parameter has shown that the gaussian profile of full width at half maximum (FWHM) equal to 1.65 Å gives the best representation of the observed spectra. Therefore, to compare the synthetic spectra with the observed ones, each spectrum in the library was convolved with the gaussian profile of FWHM=1.65 Å.

The observed spectra in our sample were sampled at the wavelength step of 0.8 Å, whereas the grid of synthetic spectra was computed with resolution R = 250,000 corresponding to wavelength step of 0.02 Å. In order to perform mathematical operations on the observed and synthetic spectra, both were forced to match in the starting wavelength point and wavelength step, and thus in the number of wavelength points. In this way we prepared the grid of template synthetic spectra matching the observations. In total there are 661 wavelength points in the wavelength interval 4850.8–5378.8 Å at which we have both observed pixel counts and synthetic residual fluxes at the wavelength step of 0.8 Å.

5.1.1 Tracing of the continuum

On the theoretical side, we have the synthetic residual fluxes, *i.e.* the fluxes normalized to the continuum. On the other side, the observational data are given in the form of pixel counts which are not calibrated in absolute

fluxes. In order to compare pixel counts with synthetic residual fluxes, we normalized the observed data as follows.

For cool type stars, due to crowding and blending of atomic and molecular lines in the observational range, it is practically impossible to locate spectral regions free from lines, and to draw a continuum. We normalized the observed spectra by comparing them with template synthetic spectra based on grid of models with atmospheric parameters in columns 7 to 9 of Table 5.1. The choice of these parameters allows for the differences in literature and grid values of T_{eff}, log g and [M/H] on the order of $\pm$ 100 K, $\pm$0.20 *dex* and $\pm$0.23 *dex* respectively, which are within the uncertainties expected in the determinations reported in the literature values.

The procedure, which we adopted to derive the continuum, is as follows: At each wavelength point, the pixel count in the observed spectrum was divided by the normalized flux in its representative synthetic spectrum. We derived the second order polynomial fit through these data points following a least-squares procedure, with the constraint that the points lying farther than 3 times the root mean square error of this fit were automatically rejected during iterations. This polynomial is assumed to represent the "continuum" of the star, and will be referred to as "pseudo-continuum". For an illustration, in Figures 5.1, 5.2 we show for the star HD 30495:
a) the observed data in pixel counts (C_λ) (Figure 5.1a);
b) its template spectrum in the form of normalized flux (F_λ) (Figure 5.1b);
c) the ratio of the pixel counts to residual fluxes of the template spectrum (C_λ/F_λ) together with the proper pseudo-continuum (Figure 5.2a);
d) the normalized observed spectrum normalized to its pseudo-continuum together with its template spectrum (Figure 5.2b).

Following the above described procedure, each observed spectrum was normalized to its pseudo-continuum in the wavelength range 4850-5400 Å. In this way, we obtained a set of observed reference spectra normalized to pseudo-continuum which can be directly used for comparison with the syn-

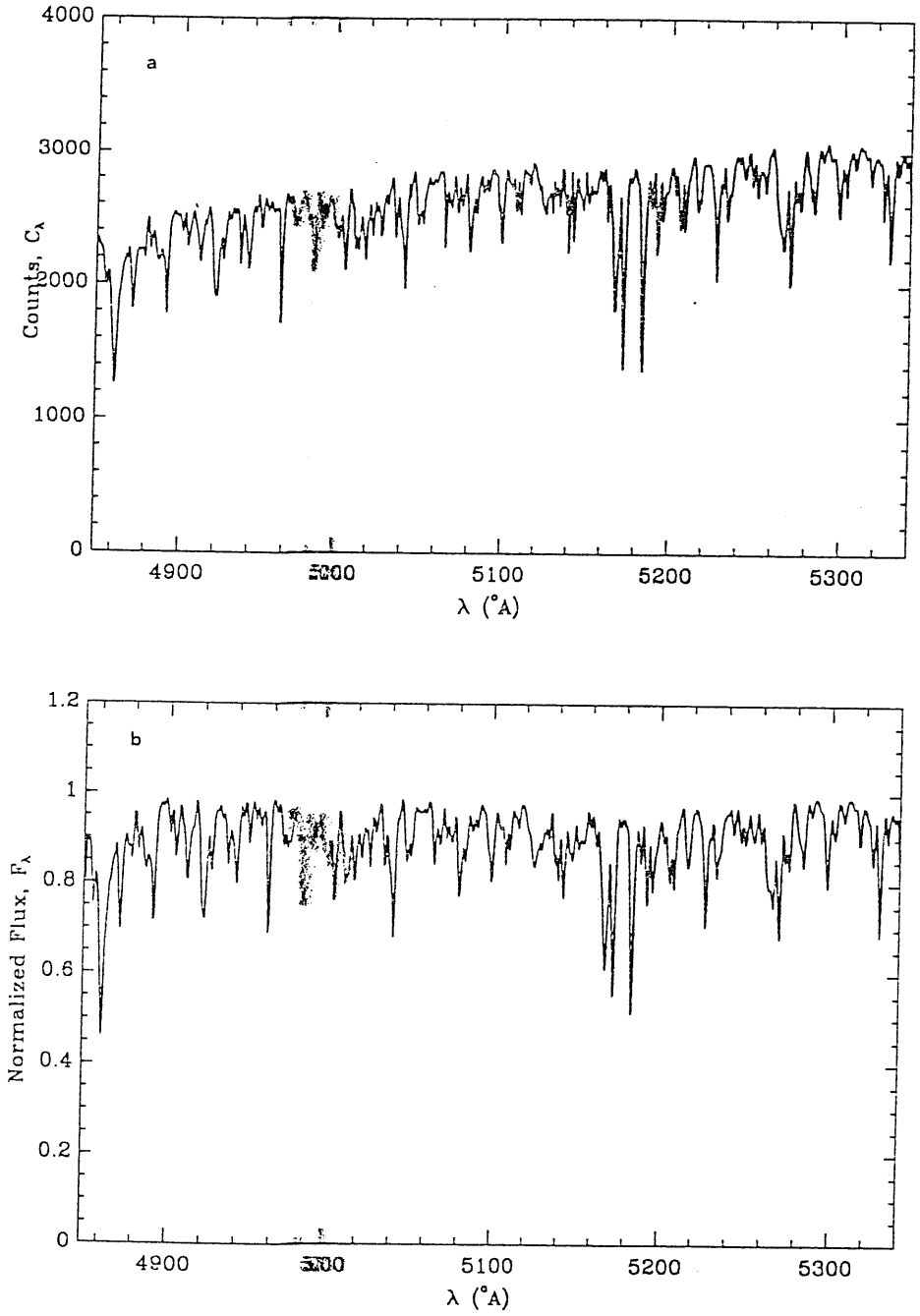

Figure 5.1: (a) Observed spectrum calibrated in wavelength for the star HD 30495; (b) Normalized synthetic spectrum representative of the observed star (HD 30495) with atmospheric parameter (6000/4.5/0.0).

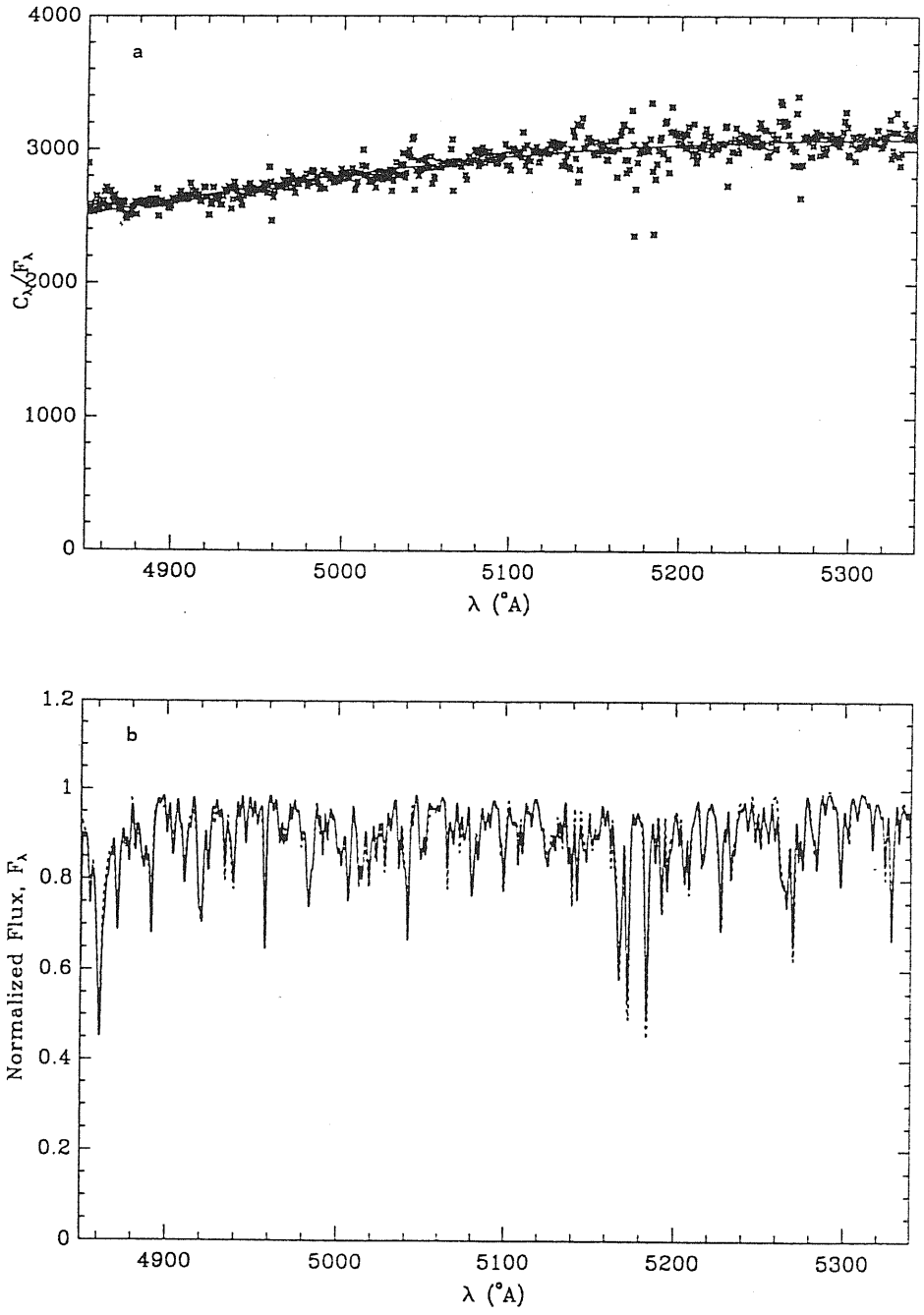

Figure 5.2: (a) Ratio of pixel counts of the observed spectrum of the star HD 30495 to the fluxes for synthetic spectrum (6000/4.5/0.0) as a function of wavelength. Solid line is the second order polynomial through ratio points (b) Comparison between normalized synthetic and observed spectra (Solid line: synthetic spectrum, Dashed line: the normalized observed spectrum.

thetic ones.

5.2 Qualitative comparison

At first sight, the comparison between the normalized observed spectrum of the star (HD 30495) and the one represented by the model (6000/4.5/0.0) shows, in general, a good agreement as far as the wavelength calibration and level of the continuum of these spectra are concerned (see Figure 5.2). As an example of the behaviour of the reference stars, we present the cases referring to three dwarfs and three giants of different temperatures. To illustrate the differences between the strength of synthetic and the observed spectral features, we show in Figures 5.3, 5.4 the plots of the ratio C_λ/F_λ vs. wavelength, arranged in order of decreasing temperature for three dwarfs and three giants, respectively, together with the appropriate pseudo-continuum. (Data are scaled to the range of [0–1], and there is a constant offset of 2 on the vertical axis.

Some general comments can be easily derived from these figures:
a. there is no systematic difference in the behaviour of C_λ/F_λ in the whole wavelength range, however, the discrepancies are more conspicuous in the central band than in side continua;
b. there is a trend in the scatter, in the sense that the scatter increases with the decrease of temperature both for dwarfs and giants;
c. the fluctuations of the C_λ/F_λ over the reference lines (pseudo-continuum) are generally small, and at the most they are within 5 %.

These figures can be directly compared with the ones presented in our previous investigation on the consistency of cool stars spectra using the GMM models and old line data. The similar trends were present there too, however, on comparing the stars in common with our previous studies, we can say that the discrepancies are reduced to large extent in the present case. The improvements in the discrepancies are due to K91 models that accounts for

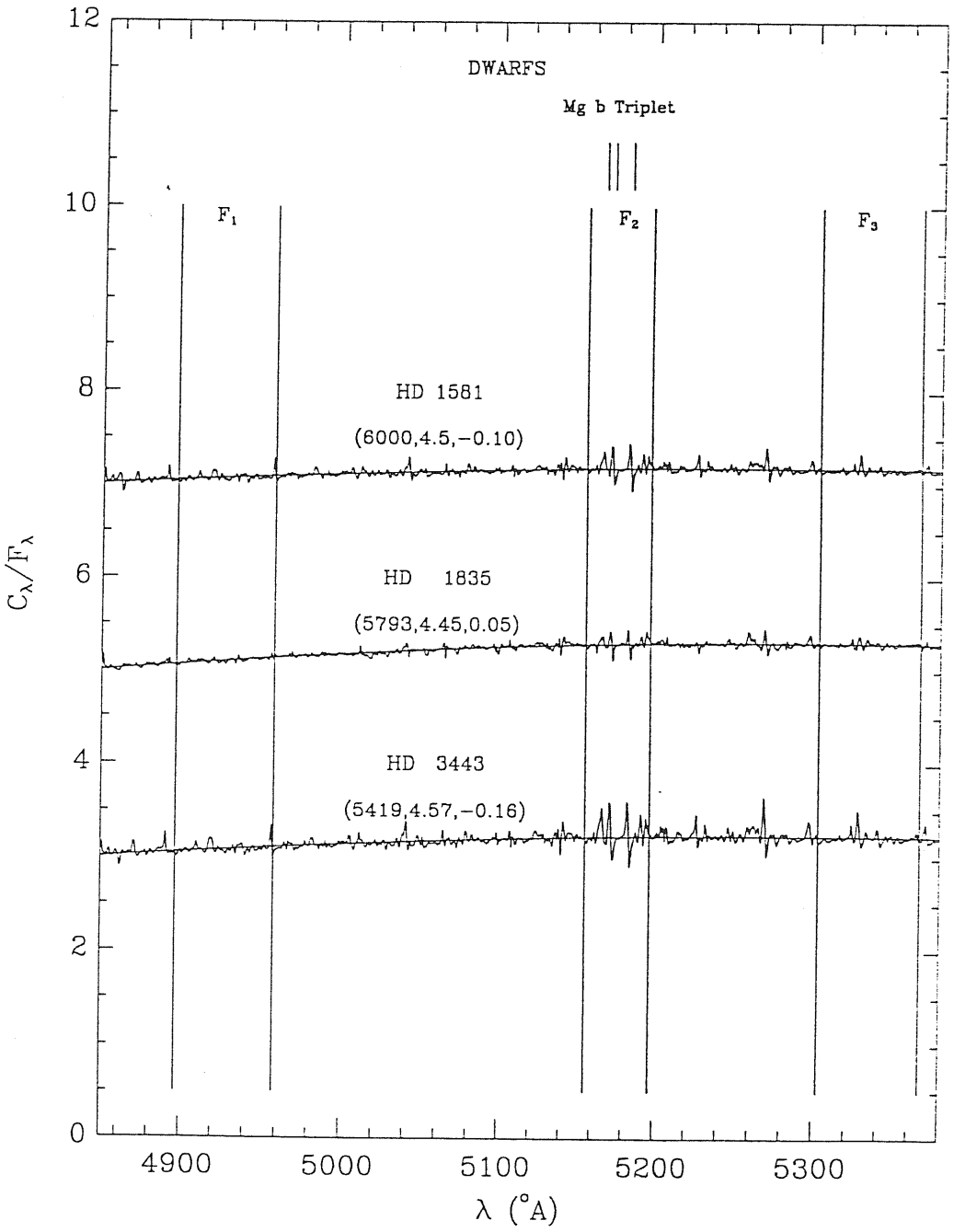

Figure 5.3: Reference fitted polynomial and ratio C_λ/F_λ, normalized to the first point of the polynomial for dwarfs. A constant offset of 2 is applied on the vertical axis. The position of the Mg b triplet (5167.321 Å, 5172.684 Å and 5183.604 Å) and of the three bandpass defining the Mg_2 index are marked.

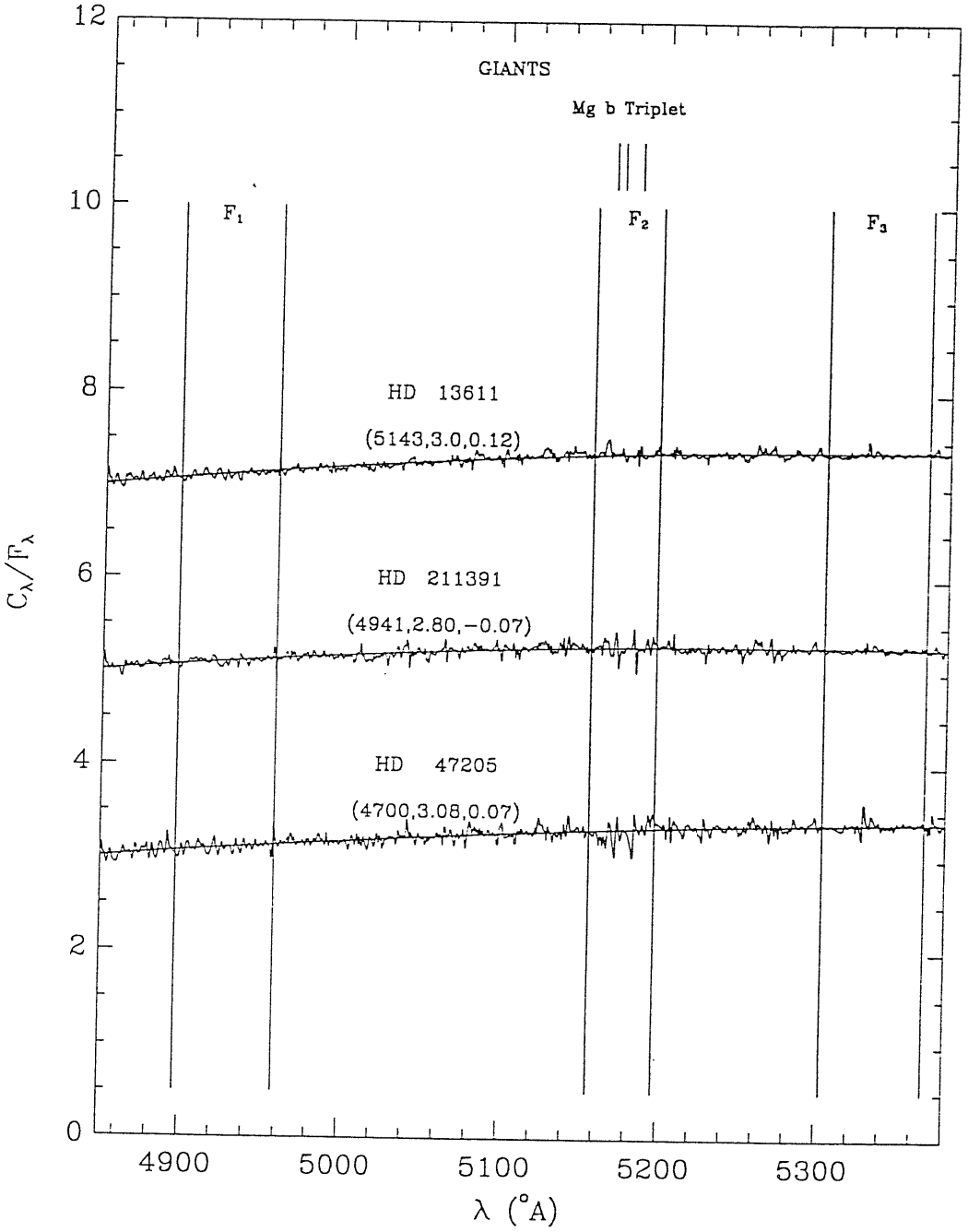

Figure 5.4: Same as in Figure 5.3, but for giants.

complete atomic as well molecular opacities important for cool stars and to the correction of line parameters involved in the synthesis of spectra.

In order to identify the differences in the spectral features, in particular in the central region, we zoomed this region of the synthetic stellar spectra and superimposed it on the normalized observed spectra. The plots for the complete sub-sample are presented in Appendix D. These spectra are arranged according to surface gravities values: a) log g $>$ 3 (dwarfs), b) 2.0 $\leq$ log g $\leq$ 3.0 (giants) and c) log g $<$ 2 (supergiants), in the decreasing order of temperatures. The general study of these figures suggest that the level of the continuum in the observations and theoretical predictions is in good agreement, however, in some cases minor differences between the observed and synthetic features can be seen.

In the case of dwarfs the agreement is generally good, since the theoretical predictions reproduce the observed spectral behaviour very well as far as the wings of the lines are concerned. The core of the predicted lines differ from the observed ones, but there is no systematic difference. These discrepancies could be attributed to a number of factors: on the observational side, the data might be affected by some bad pixel counts and on the theoretical side, the parameters of the template spectrum may be associated with large uncertainties.

In the case of giants, there are striking differences in the wavelength region of 5165 Å, where in some cases the observed features are stronger than the predicted ones and in others it is opposite. In order to identify these spectral features, we looked back to the solar atlas (Appendix A) where we did not find the presence of such asymmetric features around the wavelength 5165 Å. This result may be due to the physical conditions in the atmospheres of giants, which are different from that of solar atmosphere. Then we looked into the Arcturus atlas, which shows the contribution due to molecular band of MgH and C_2 also besides Fe lines. The input line data seem to be able to explain the discrepancy in some of the giants as the following argument

suggests: In our line data, the gf values are determined semi-empirically (see Section 2.2.3), *i.e.* they are determined by fitting the solar spectrum with the spectrum derived from the use of empirical solar model. Even though we include the lines present in the model of Arcturus, but their gf values have not been matched to the observed Arcturus spectrum. As seen from the comparison of model and observed Arcturus spectrum, the line strength predicted by the model is overestimated with respect to the observations (see Appendix C). The line data of these elements will be worth investigating when we will have high resolution Arcturus spectrum where we can resolve the contribution of one element from others.

Since our sample has only three supergiants, it is hard to reach any sound conclusion concerning the agreement between the observations and theoretical predictions. Moreover discrepancies between these stars and K91 models are not unexpected, since they are based on the assumptions of plane parallel geometry and LTE atmosphere while in supergiants, because of extended atmospheres and low gravity, these assumptions break down. According to Kurucz (1991b), for low gravity models due to the above reasons there still exists systematic errors. Therefore, we will not include this class of objects in the following analyses.

It is of our interest to investigate the behaviour of synthetic integrated fluxes with respect to observed ones, as a consequence the consistency of the synthetic Mg_2 index with the observed one. In the following section, we will quantify the distribution of spectral energy distributions in the regions contributing to the Mg_2 index.

5.3 Quantitative comparison

We have shown in section 5.2, the qualitative comparisons between the observed and synthetic spectra for the sub-sample of program stars, here we will quantify them by computing the integrated fluxes in the pseudo-continuum

bandpasses and the central bandpass involved in the definition of Mg_2 index.

5.3.1 Continuum bandpasses

Continuum bandpasses are located in the wavelength regions $\lambda\lambda$ 4897-4958.25 Å, referred to as blue bandpass (F_1) and $\lambda\lambda$ 5303-5366.75 Å, referred to as red bandpass (F_3). These wavelength regions are considered to be free from strong lines. In order to quantify the contribution of the spectral features in the blue and red bandpasses, we integrated the fluxes over the bandpasses for the template and the observed spectra. Figures 5.5, 5.6 show the comparison between integrated synthetic fluxes against those computed from the normalized observed spectra for the blue and red bands, respectively. To distinguish dwarfs, giants and supergiants, we mark them with different symbols: dwarfs are shown by filled squares, giants by filled triangles and supergiants by open triangles. In each plot we draw a line at 45° to look into the departure of synthetic flux values from the observed ones.

As we can see from these figures, dwarf, giants and supergiants do not form separate groups, except for two of the three supergiants which are lying below the line at 45° in the red bandpass. We exclude the supergiants in the following analyses, because of above said reasons. Furthermore, in the synthesis of old stellar systems this class of objects is not important. In general, the integrated synthetic fluxes in the blue and red band tend to be slightly higher than the observed values.

We looked into the systematic differences of synthetic and observed values quantitatively in the blue and red bandpasses by performing a linear least squares procedure on the sample of stars, excluding the supergiants, with the constraint that the points falling away from three times the root mean square error (σ) of the fit will be rejected automatically. This procedure resulted in rejection of no point in the red bandpass, whereas two stars were rejected in the blue bandpass, namely HD 13611 and HD 100407; the list of the fitting parameters along with their errors and σ is given in Table 5.2.

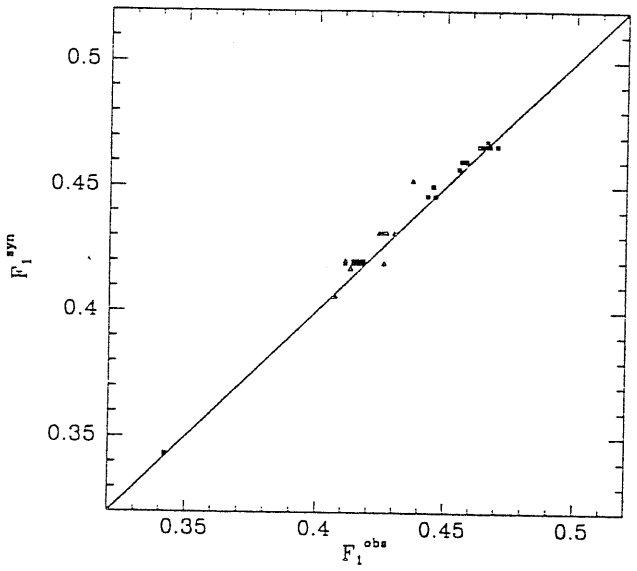

Figure 5.5: Comparison of synthetic vs. observed fluxes in the blue band.

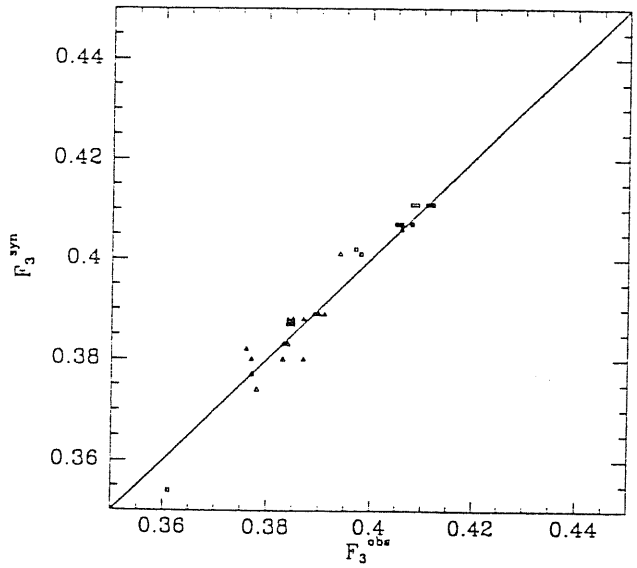

Figure 5.6: Comparison of synthetic vs. observed fluxes in the red band

Table 5.2: Coefficients a, b in the linear relationship between synthetic and observed quantities with their errors and RMSE

	a	σ_a	b	σ_b	RMSE
F_1	0.023	0.007	0.955	0.171	0.003
F_2	-0.007	0.008	1.013	0.022	0.005
F_3	-0.013	0.016	1.036	0.041	0.003
Mg_2	0.004	0.007	1.031	0.034	0.022

where a: intercept, and b: the slope of the linear relation

The percentage error on the average flux is on the order of 1 % at the 1-σ level, which is within the observational uncertainties.

5.3.2 Central bandpass

The central bandpass is an important contributor to the strength of the Mg_2 index and is situated in the wavelength region $\lambda\lambda$ 5156 – 5197.25 Å, referred to as F_2. To compare the synthetic with the observed fluxes in this bandpass we computed the integrated flux over the central bandpass for template and observed spectra. We plot them in Figure 5.7, where each luminosity class is distinguished following the symbols as mentioned in section 5.3.1. As we can see from this figure the agreement between synthetic and observed integrated fluxes is very good. There is no relevant systematic effect in the integrated fluxes contained in central bandpass. Following the same strategy as explained above, we quantify the correlation of synthetic fluxes with the observed ones by performing linear least squares procedure and the list of resulting fitting parameters is given in the Table 5.2 The iteration criteria do not find any star farther than 3σ. The percentage error on the average value is again on the order of 1% at the 1-σ level, which is well within the observational uncertainties.

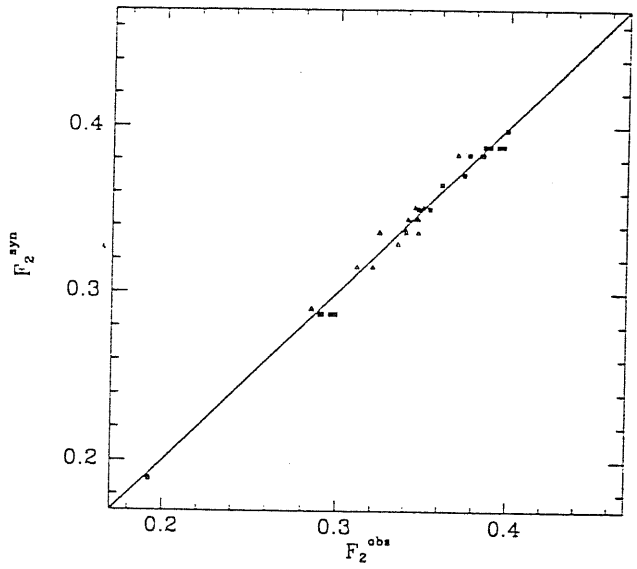

Figure 5.7: Comparison of synthetic vs. observed fluxes in the central band.

5.3.3 Comparison with previous results

The first phase of this project started three years ago, at that time Kurucz old grid of models was limited down to 5500 K and available opacity distribution functions accounted for contribution due to one million of atomic lines. We started extending this grid down to temperature 4000 K and built up a grid of models for solar chemical composition, from which synthetic spectra that include also the contribution of molecules in the region of our interest were computed. We made a comparative study on the integrated fluxes in the bands contributing to the Mg_2 index and the index itself with respect to a sample of observations representative of solar chemical composition stars. We found systematic discrepancies in the computed fluxes with respect to the observed ones not only in the continuum bandpasses, but also in the central bandpass. In particular, the synthetic integrated fluxes in the central band were found to be lower than the observed ones, while in the blue and red bands they were systematically higher than the observed ones.

One may argue how much we have gained by using K91 models ? The answer is that only minor differences in the red and blue bandpasses are present

and the central bandpass shows insignificant differences between predicted and observed fluxes. The tremendous improvement is in the central band, which is the most important one, where the dominant spectral features are well reproduced by synthetic spectra. The message we get through this work is that the K91 models that account for the sources of opacity important for cool stars are certainly better than any set of previous models.

5.3.4 Mg_2^{syn} vs. Mg_2^{obs} for the reference stars

To look into the consistency of the synthetic Mg_2 index with the observed one, we computed Mg_2 index for reference stars and their representative template synthetic spectra according to formula 3.1. We took into account the fractional contribution of fluxes at the edges of each bandpasses in the intervals of the Mg_2 index. In columns 5 and 6 of Table 5.1, we report the computed values of the index for the observed and synthetic reference spectra, respectively. To illustrate the comparison of synthetic and observed Mg_2 values, we plotted in Figure 5.8 the Mg_2^{syn} vs. Mg_2^{obs}. As seen before (sections 5.3.1 and 5.3.2) in the comparison of observed fluxes with the synthetic ones, the stars of different gravity classes do not form separate entities in the (Mg_2^{obs},Mg_2^{syn}) plane.

Since side continua bandpasses show slight systematic differences, we expect small differences in the combined effect of the three fluxes on the Mg_2 index in Figure 5.8. For reference, the straight line at 45^o is sketched to locate the synthetic Mg_2 values departing from the observations.

To quantify the discrepancies between the synthetic and the observed Mg_2 values, a linear least squares fit was performed through the data points with iteration strategy that any point farther than the 3σ were rejected automatically. It is worth reminding that we exclude supergiants while following fitting procedure (see sec. 5.3.1) The resulting fitting parameters along with their errors are given in the Table 5.2. The correlation between the synthetic and observed Mg_2 values is very good, the root mean square error of the fit

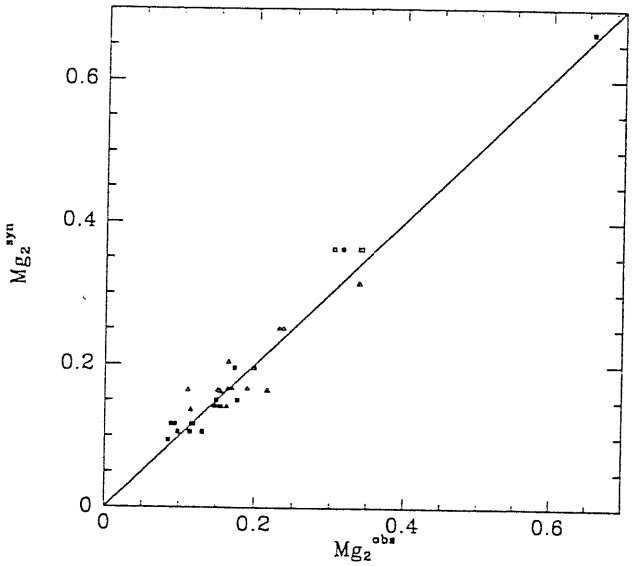

Figure 5.8: A comparison of synthetic Mg_2 vs. observed Mg_2.

is on the order of 0.02 *mag*.

As evident from Figure 5.8, the Mg_2^{syn} values are in generally good agreement with the Mg_2^{obs}, except in some cases the former values show minor discrepancies with respect to the observed ones. At the resolution of the observations, it is difficult to investigate the individual causes of discrepancies. The main source of error on Mg_2^{obs} values may be from the positioning of the continuum, which in our case is determined with respect to the template synthetic spectrum. On the other hand, the choice of stellar parameters from literature might affect both Mg_{obs} and Mg_2^{syn} determinations.

Previous study on the comparison of synthetic and observed Mg_2 values resulted in a systematic difference, in the sense that the Mg_2^{syn} were higher than the Mg_2^{obs} values. To conclude, we can say that the K91 models reproduce very well the Mg_2 index measured from the observations of dwarfs and giants.

5.3.5 Comparison of Mg_2^{syn} with empirical determinations

In order to provide the better base upon which to judge the consistency of our grid of Mg_2 index, we will compare our grid of Mg_2 index for solar chemical composition with empirical determination of Mg_2 values by Faber *et al.* (1985) and Buzzoni *et al.* (1991).

Faber *et al.* (1985) have measured the Mg_2 index for 110 K-giant stars from the spectra at 9 Å resolution. They have studied the dependence of the Mg_2 index on the basic atmospheric parameters empirically. As regards the collection of atmospheric parameters in their data, they chose $V-K$ color as a temperature indicator, since this color is relatively insensitive to blanketing and surface gravity. Most of the V-K colors were taken from different sources. The collection of iron abundance of their sample comes from low-resolution studies by Gottileb and Bell (1978), Gustafsson *et al.* (1974) and Hansen and Kjaergaard (1971). Faber (1991) has provided us privately with her data of K-giants stars including the surface gravity derived by comparing with evolutionary tracks for the cluster stars, and by an iterative procedure based on the Mg_2 line strengths for the field stars. In order to compare the grid with her data, we transformed $V-K$ colors of each star to effective temperatures using the calibration of Blackwell *et al.* (1991). The typical error in $V-K$ on the order of $\pm$ 0.05 *mag* corresponds to an uncertainty on T_{eff} on the order of 100 K.

In Figure 5.9 we plot the sub-sample of field K giants in FFBG data representative of solar chemical composition objects together with the proper grid of the Mg_2 index as a function of θ_{eff}. We have shown in Chapter 3 that the Mg_2 index values derived from our grid can be compared directly to values obtained from the spectra of 9 Å resolution, since the index computed at the resolution of our observations and FFBG observations results in the same values.

Different lines in the Figure 5.9 indicate the grid of the index for different

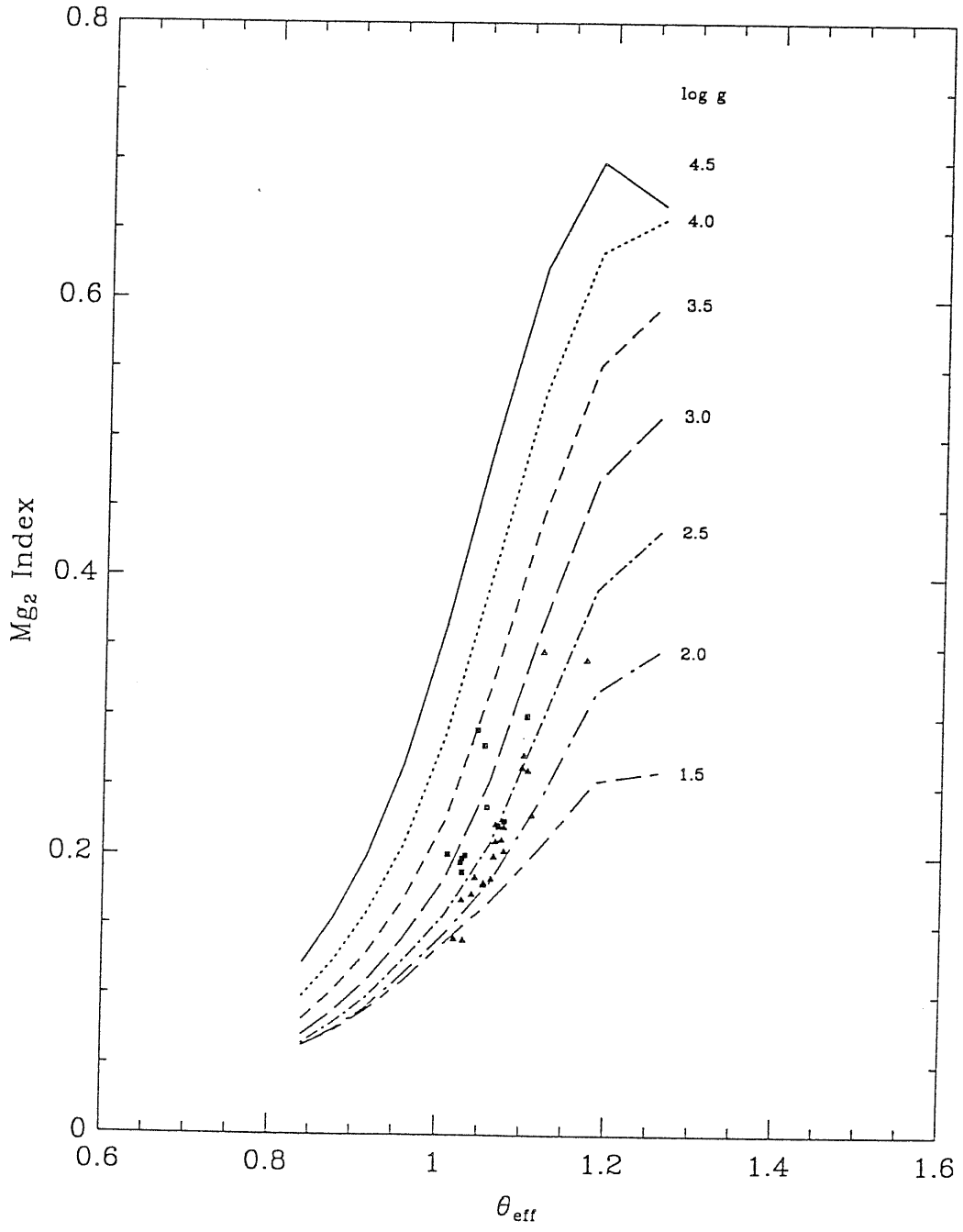

Figure 5.9: A grid of synthetic Mg_2 together with sub-sample of FFBG data.

gravity values. In order to differentiate FFBG sub-sample in terms of their gravity values on the (θ_{eff}, Mg_2) plane, we divided them into two groups: one with 2.0≤log g≤ 2.5, which comprised 19 stars and in Figure 5.9 we represent them with filled triangles, and others with 2.5 < log≤ 3.5 and this condition is fulfilled by 11 stars represented with filled squares. We deliberately excluded stars with log < 2, because of inadequacy of K91 models for low gravity stars. As evident from this figure, the behaviour of theoretical and observational Mg_2 index goes along *i.e.* there is a tendency of increase in the Mg_2 value with the decrease of temperature; there is a clear demarcation between two groups of gravity values in the sense that FFBG Mg_2 values are distributed on the theoretical grid in their proper gravity range, except for three stars namely HD 184406, HD 203349 and HD 219449 and two of them are placed near to their border value of gravity. The misplacement of these stars can be justified on the basis of errors associated with their determination of effective temperature, and surface gravity.

Recently Buzzoni *et al.* (1991) (hereafter referred to as BGM) have analysed the same sample of stars, part of which we have used for the current analyses, and have calibrated empirically the Mg_2 index with atmospheric parameters. To compare their Mg_2 values with the grid of synthetic Mg_2 for solar chemical composition, we selected stars with metallicity lying in the range -0.25 to 0.25 so that they can be treated as solar metallicity objects. In order to distinct gravity classes in Figure 5.10, we divided the sub-sample of BGM into two groups: one with 2 ≤ log g ≤ 3.0 which constitutes 16 stars and marked them with filled triangle and secondly with gravity 3 <log g≤ 4.5 (which composes 13 stars) they are marked with filled squares. As can be seen from the Figure 5.10, the theoretical behaviour of the index agrees completely with the observed one for most of the stars. The Mg_2 values for most of the stars are positioned well in their respective gravity ranges on the theoretical grid. Few cases lie little outside the grid, however, this may be due to errors in the tabulated temperatures and gravities of the stars and, on the other hand, to uncertainties affecting the determination of the index.

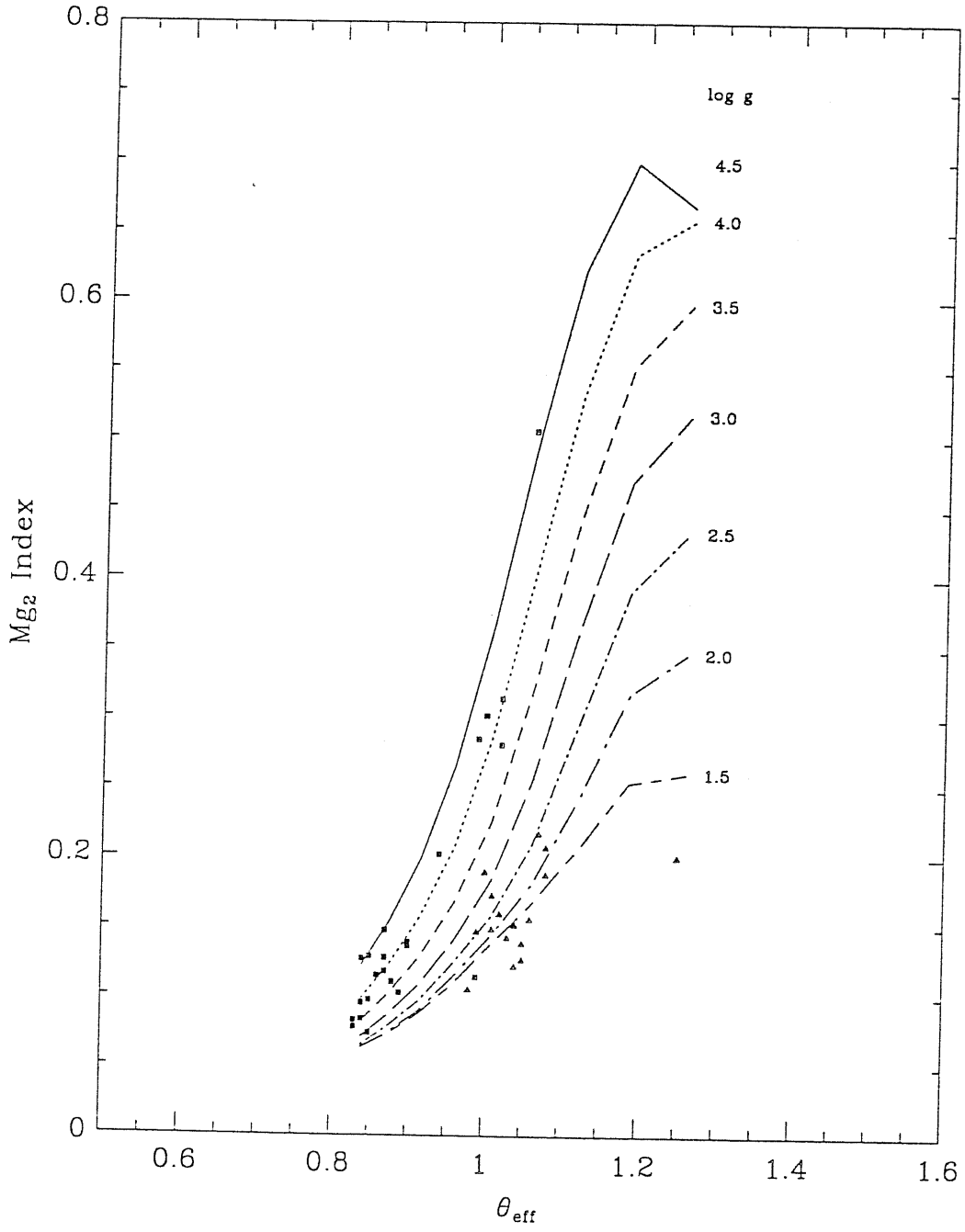

Figure 5.10: A grid of synthetic Mg_2 together with sub-sample of BGM data.

One star HD 95272 that breaks apart from the grid may reflect either large errors in the atmospheric parameters or noise in the pixel counts.

From the above discussion, we can draw the following conclusion: our theoretical grid of Mg_2 based on K91 models and new line data reproduces empirical determinations for cool dwarfs and giants of solar chemical composition. Having performed these investigations we now have specific guidelines over which the accurate Mg_2 index can be measured from the synthetic spectra, and thus we can gauge its utility in the integrated spectra of stellar systems. More observational data for reference stars covering wider range of T_{eff}, log g and [Fe/H] is needed to extend the comparison of Mg_2 index to non-solar chemical composition stars. On the theoretical side, self consistent models for cooler stars are required in order to extend the grid down to M stars since at present K91 grid is valid until K stars due to the absence triatomic molecules in the opacity calculations.

Summary and Conclusion

The main points of this investigations may be summarized as follows. Motivated by the availability of large set of measurements of Mg_2 index and its usefulness for stellar systems and individual field and stars in the nearby stellar systems, we have set up a library of synthetic spectra in the wavelength region 4850-5400 Å , following the spectrum synthesis technique. This library is based on the more recent K91 models which were chosen since they incorporate the opacities due to 58 million of atomic and molecular lines. The input line data parameters has been derived by matching the observed solar central intensity spectrum with the one produced by the solar empirical model. This library of synthetic spectra, which is also useful for deriving the basic stellar atmospheric parameters from comparison with observations, is available on the optical disk. It covers the effective temperature range from 4000-6000 K with step of 250 K, log g from 1.5 to 4.5 with step of 0.5, and metallicity [M/H] = -0.5, 0.0 and 0.5. The complete discussion of this library is given in Chapter two, where we have also investigated the behaviour of the synthetic spectra, in particular in the central bandpass of the Mg_2 index where the contribution of Mg b triplet and MgH molecules are dominant, with respect to the input parameters that control the behaviour of spectral energy distributions.

In Chapter three we have computed the synthetic Mg_2 index for this li-

brary of synthetic spectra and have investigated the effect of basic stellar atmospheric parameters on the Mg_2 index. As a consequence we found the biparametrical behaviour of the Mg_2 in the sense that it depends both on effective temperature and gravity for the different metallicity. We also provide the calibrations of the Mg_2 versus reciprocal of effective temperature, θ_{eff} for different values of gravity and metallicity. This calibration is an important step towards computing the integrated Mg_2 index for stellar systems in the context of population synthesis models.

In the last chapter, we have examined the consistency of the library of synthetic spectra in the light of observations described in fourth chapter for stars representative of solar chemical composition. The observational spectral behaviour is very well reproduced by template synthetic spectra for dwarfs, and most of giants; some giants show discrepancies at the wavelength 5165 Å which are attributed to the line parameters of molecular bands MgH and C_2.

The comparison of our grid of synthetic Mg_2 with empirical determinations of the index show in general good consistency for dwarfs and giants of solar chemical composition thus giving credibility to the grid of synthetic Mg_2 index. The empirical determinations of the index by other authors are in good agreement with the theoretical predictions.

At present, the grid is limited down to T_{eff} 4000 K because of lack of reliable TiO molecular data and of triatomic molecules, which are vital components of opacity for the coolest stars.

Further work is planned to apply the calibrations of the index to population synthesis models in order to derive the global Mg_2 index for stellar systems. The comparison of the integrated synthetic Mg_2 with the observations will facilitate in interpreting the underlying physical phenomenon in the stellar systems. The accomplishment of this project would hopefully provide the observational constraints both for astrophysical and cosmological theories.

Appendix A

Solar intensity spectrum

This appendix contains the plots of the observed solar central intensity spectrum together with one generated from the empirical solar model with line list corrected for line parameters in the wavelength regions of the Mg_2. In these plots, thick lines refer to the observed spectrum, and thin lines refer to the predicted spectrum and for detail see Chapter 2.

A.1 Spectrum in the blue bandpass

In this section, we present the portions of the predicted central intensity spectrum together with the observed one in the wavelength range $\lambda\lambda$ 489.0 – 496.1 nm.

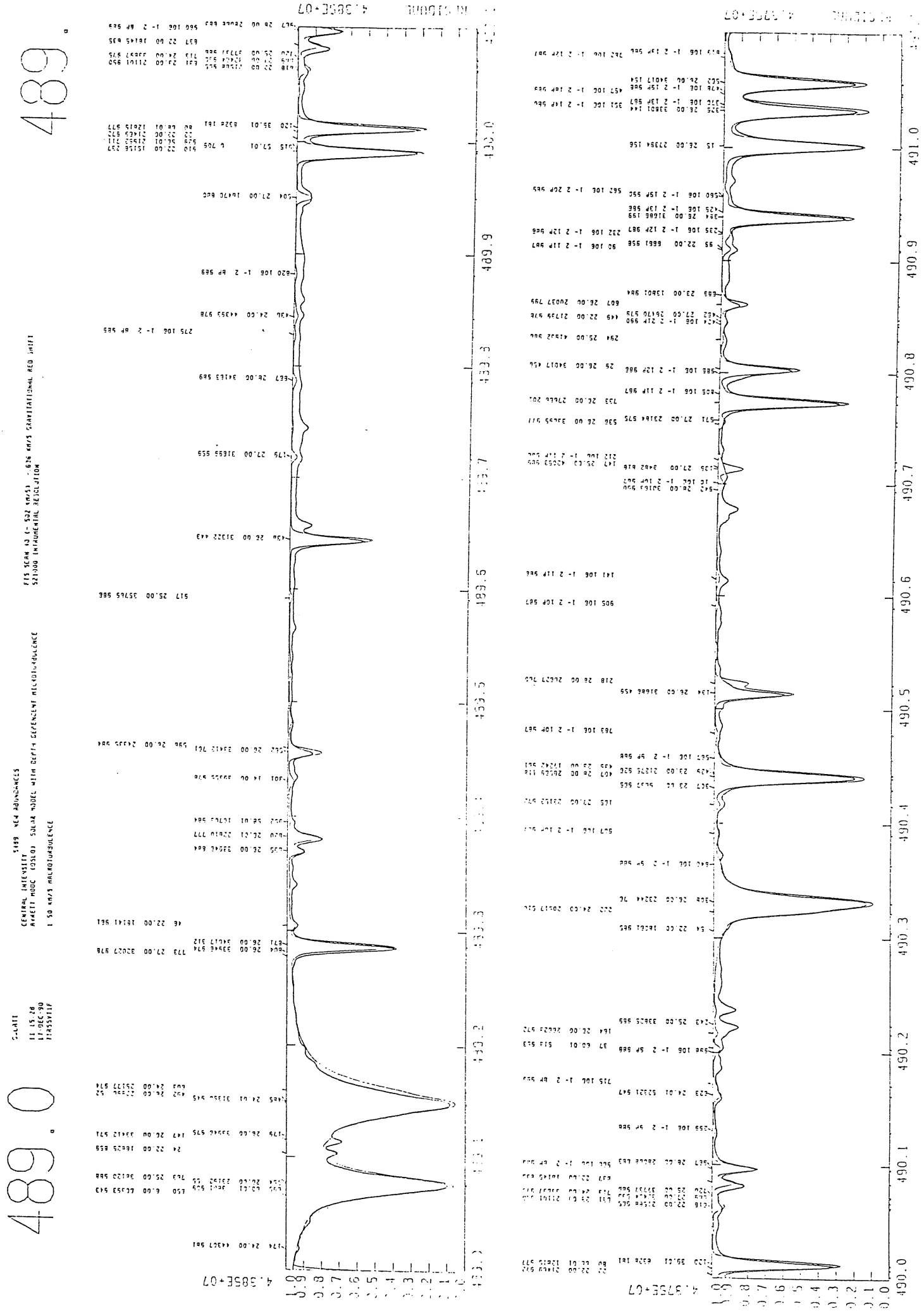
489.0
489.9
490.0
491.0
4.385E+07
4.375E+07
CENTRAL INTENSITY
ARGETT MODE (OSLO) SOLAR MODEL WITH DEPTH DEPENDENT MICRO-TURBULENCE
1 SO KM/S MACROTURBULENCE
FIS SCAN 43 (-502 KM/S) : 636 KM/S GRAVITATIONAL RED SHIFT
521000 INCREMENTAL RESOLUTION

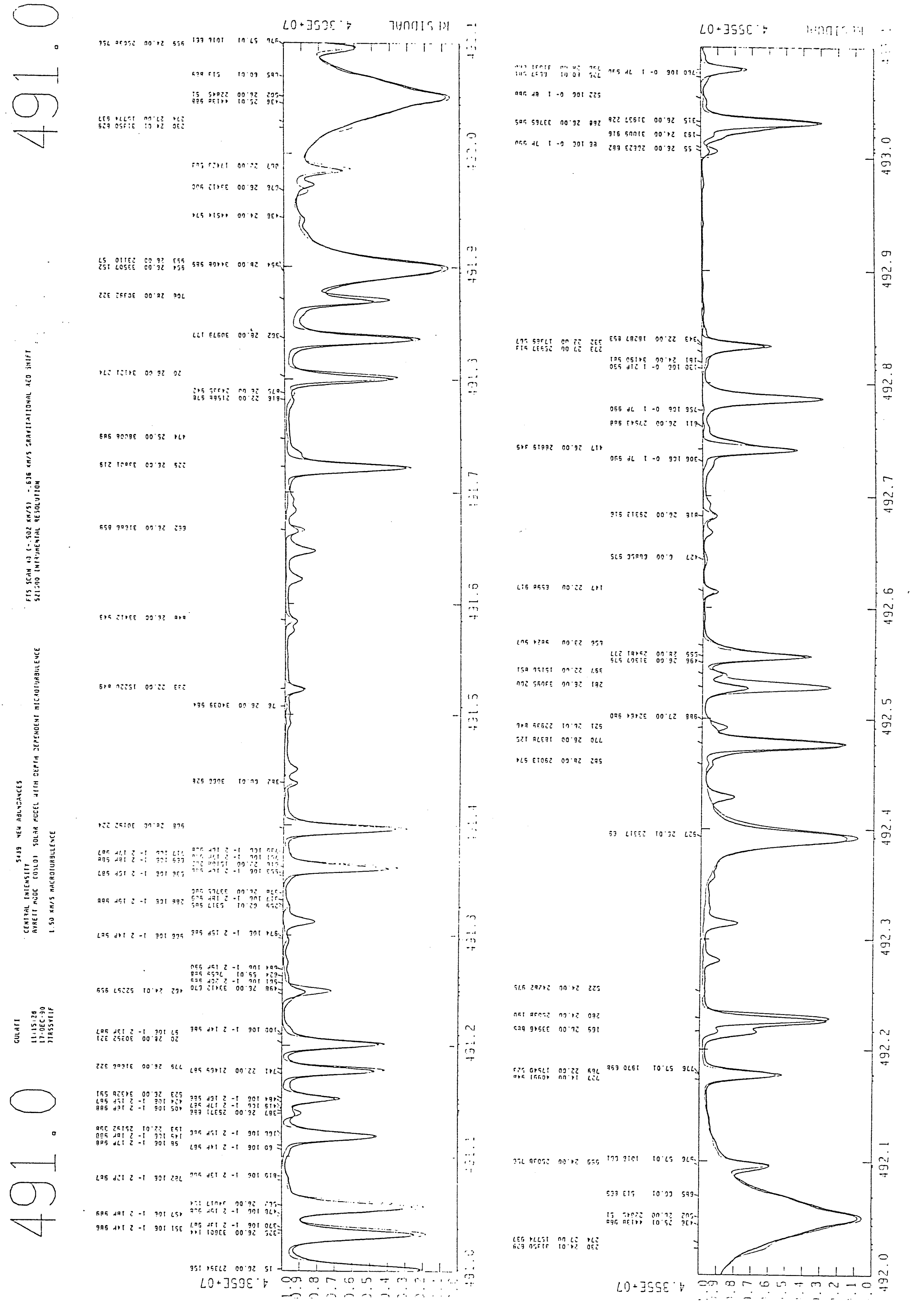
491.0
493.0
492.9
492.8
492.7
492.6
492.5
492.4
492.3
492.2
492.1
492.0

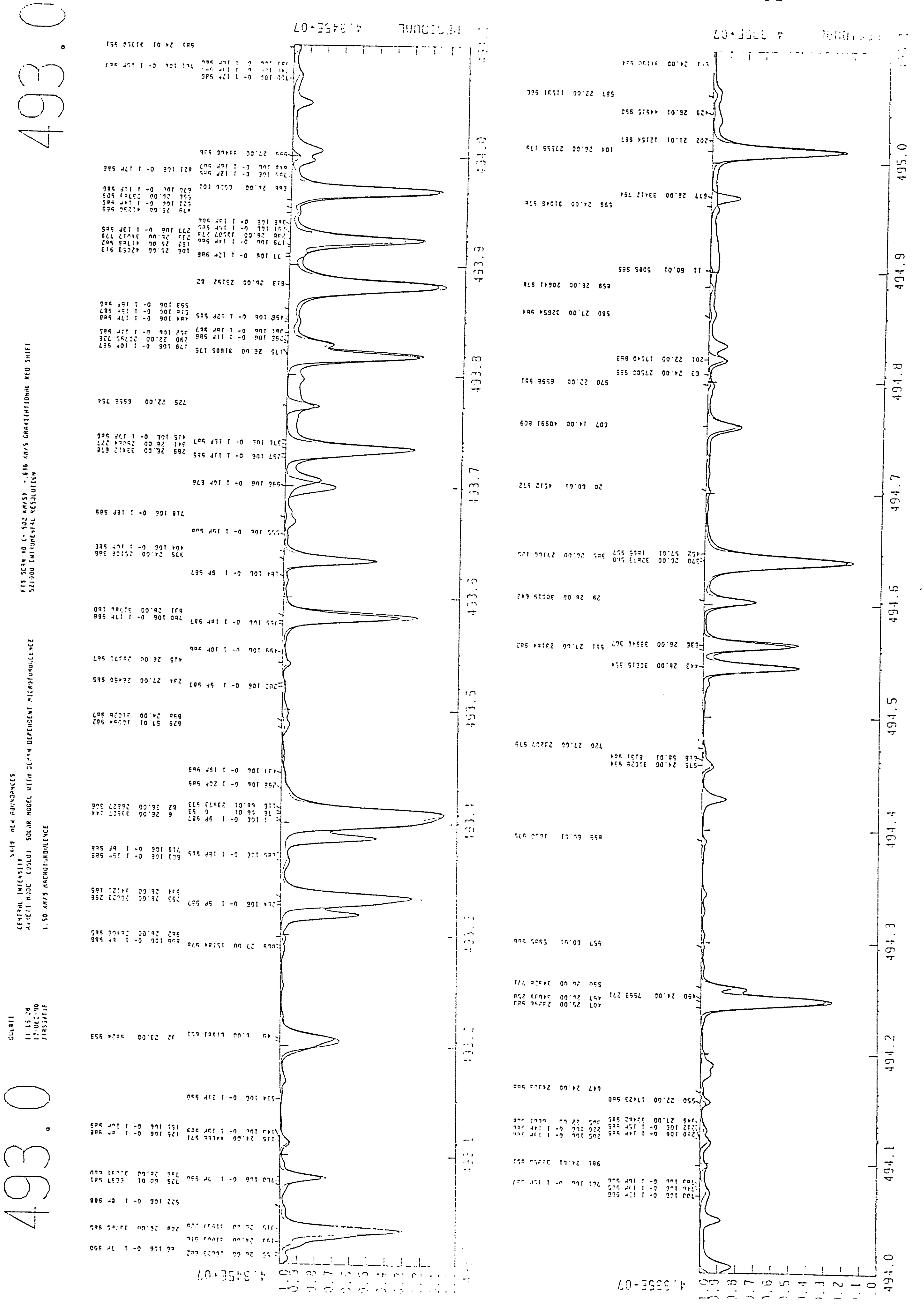
493.0
493.0
494.0
494.1
494.2
494.3
494.4
494.5
494.6
494.7
494.8
494.9
495.0

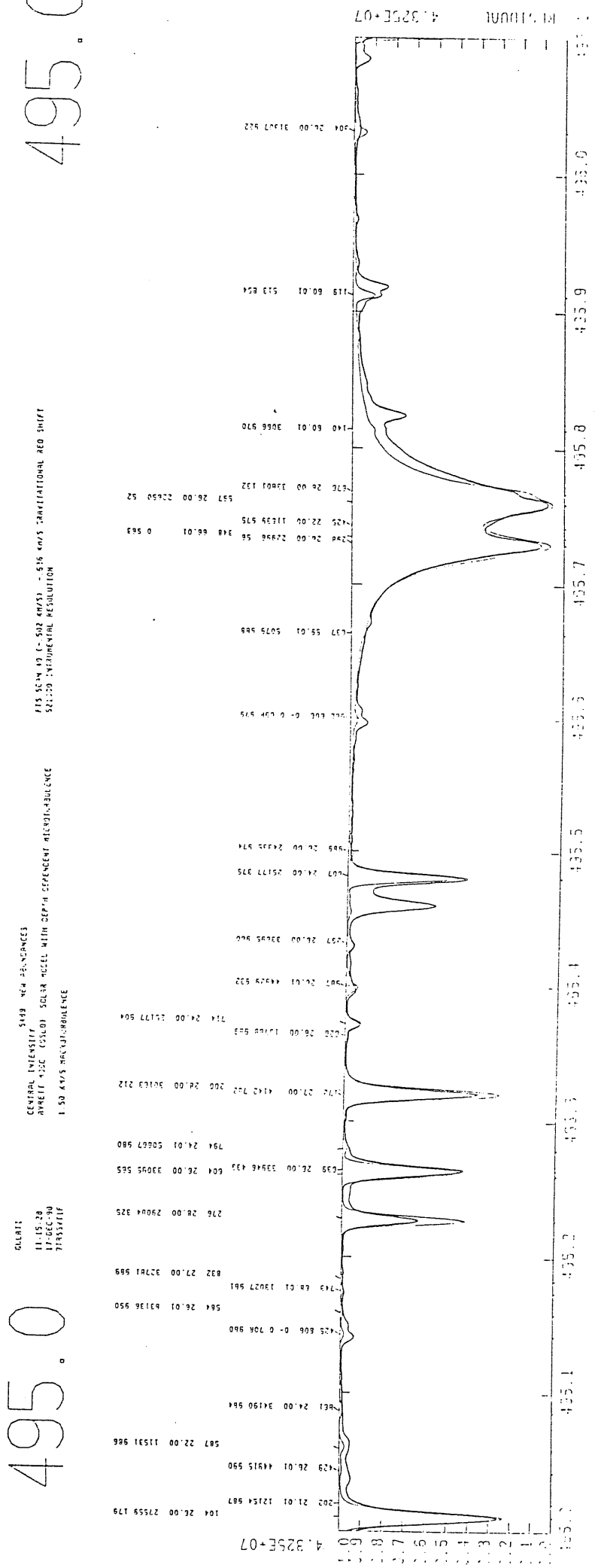
495.0
495.0
GALAXIE
11-15:28
17-DEC-90
CENTRAL INTENSITY
AVRETT+SEE (1981) SOLAR MODEL WITH DEPTH DEPENDENT MICROTURBULENCE
1.50 KM/S MACROTURBULENCE
FTS SCAN #3 (- 502 KM/S) - 516 KM/S GRAVITATIONAL RED SHIFT
SPECTRAL INSTRUMENTAL RESOLUTION
4.325E+07
435.9
435.8
435.7
435.6
435.5
435.4
435.3
435.2
435.1
RESIDUAL
4.325E+07
436.1
436.0

A.2 Spectrum in the central bandpass

In this section, we present the portions of the predicted central intensity spectrum together with the observed one in the wavelength range $\lambda\lambda$ 515.0 – –521.1 nm

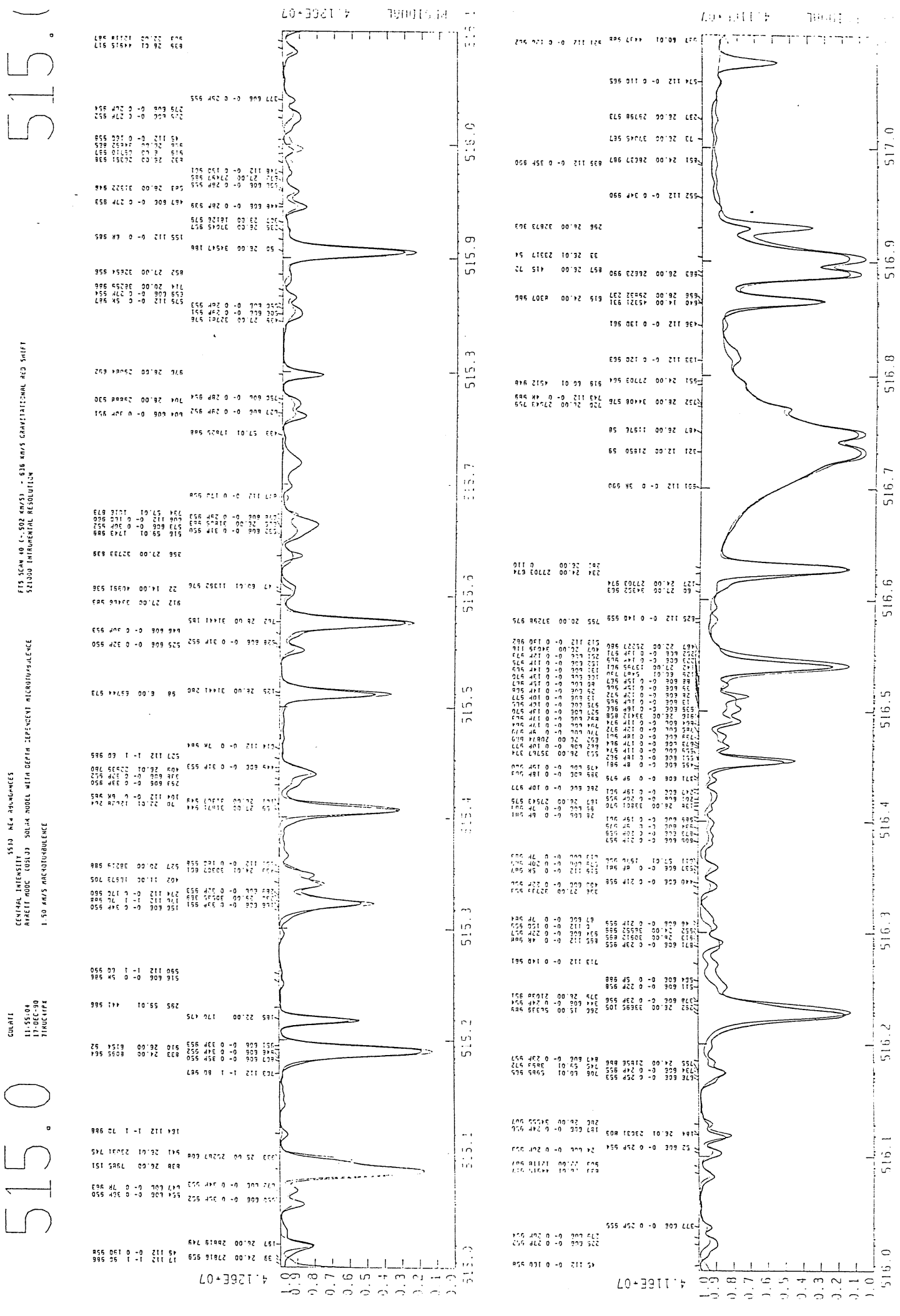
515.0
515.1
515.2
515.3
515.4
515.5
515.6
515.7
515.8
515.9
516.0
516.1
516.2
516.3
516.4
516.5
516.6
516.7
516.8
516.9
517.0
4.126E+07
4.116E+07
0.9
0.8
0.7
0.6
0.5
0.4
0.3
0.2
0.1
0.0
GOLAY
11-55.04
17-DEC-90
TRACHIPH
CENTRAL INTENSITY
ARNETT MODC (1981) SOLAR MODEL WITH DEPTH DEPENDENT MICROTURBULENCE
1.50 KM/S MACROTURBULENCE
FTS SCAN 40 (-.502 KM/S) - 636 KM/S GRAVITATIONAL RED SHIFT
521000 INSTRUMENTAL RESOLUTION

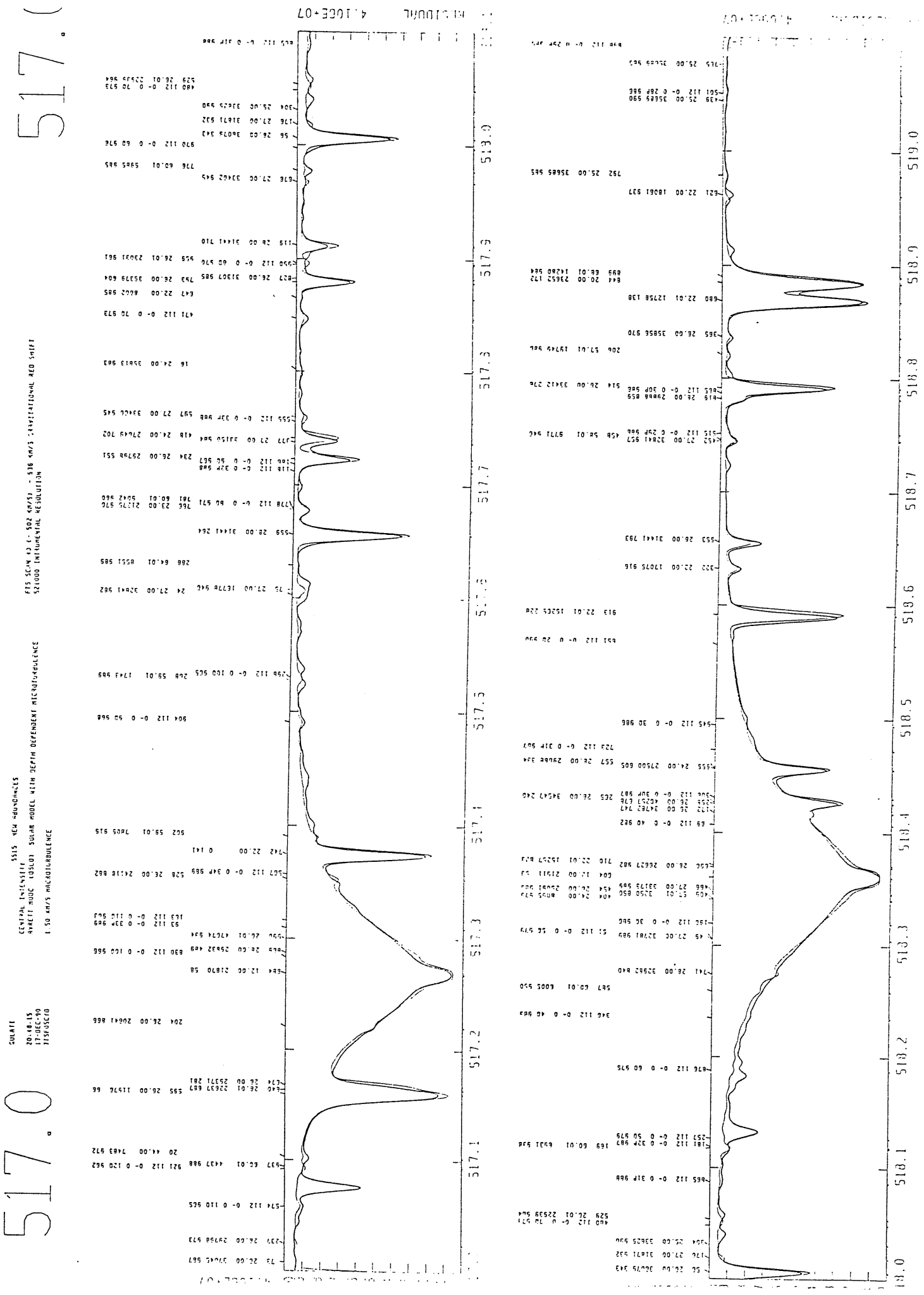
517.0
517.1
517.2
517.3
517.4
517.5
517.6
517.7
517.8
517.9
518.0
518.1
518.2
518.3
518.4
518.5
518.6
518.7
518.8
518.9
519.0
SOLAR
20:48:15
17-DEC-90
FTS SCAN 43 (- 502 KM/S) - 536 KM/S GRAVITATIONAL RED SHIFT
521000 INSTRUMENTAL RESOLUTION
CENTRAL INTENSITY 5515 NEW WAVENUMBERS
AVRETT MODEL (1981) SOLAR MODEL WITH DEPTH DEPENDENT MICROTURBULENCE
1.50 KM/S MACROTURBULENCE

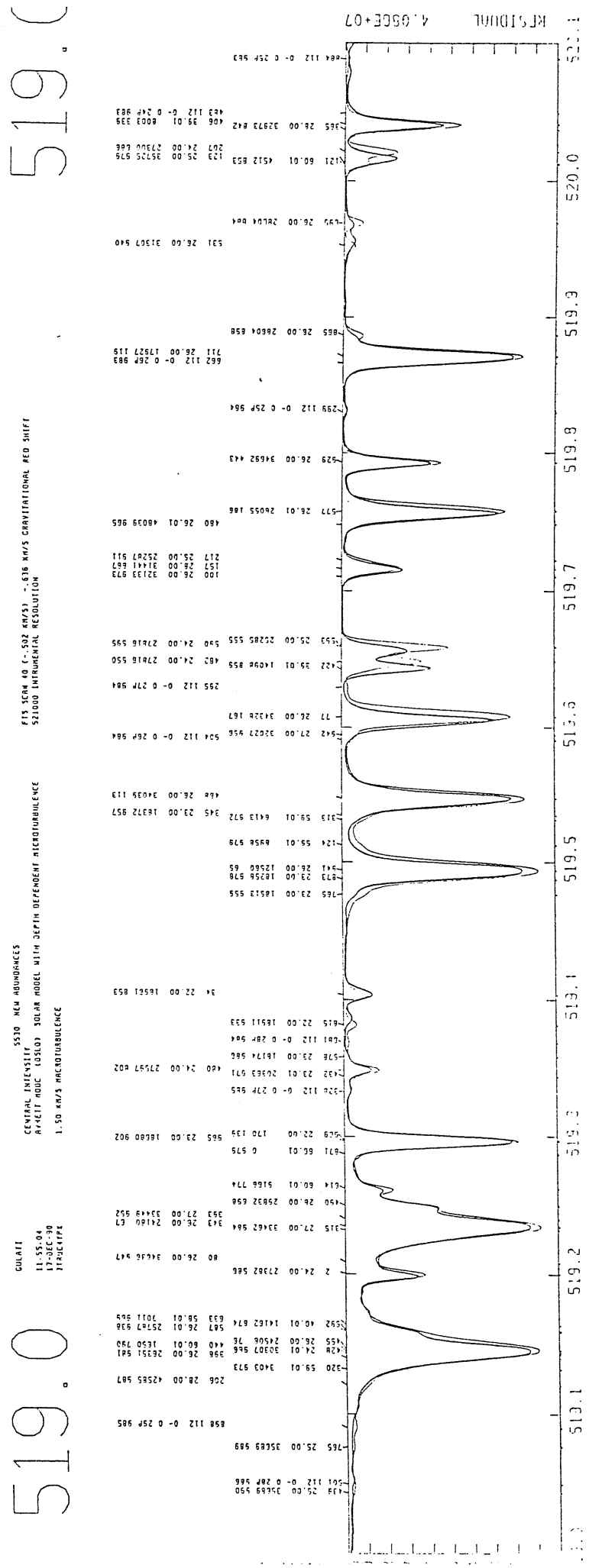
519.0
519.6
GULAIT
11-SS-04
17-DEC-90
ITRYCKTPX
SS30 NEW ABUNDANCES
CENTRAL INTENSITY
A+CKIT MODC (OSLO) SOLAR MODEL WITH DEPTH DEPENDENT MICROTURBULENCE
1.50 KM/S MACROTURBULENCE
FTS SCAN 40 (-.502 KM/S) -.636 KM/S GRAVITATIONAL RED SHIFT
521000 INTRUMENTAL RESOLUTION
4.0366+07
INTENSITY
519.1
519.2
519.3
519.5
519.6
519.7
519.8
519.9
520.0
4.0766+07
520.1
520.2
520.3
520.4
520.5
520.6
520.7
520.8
520.9
521.0

A.3 Spectrum in the red bandpass

In this section, we present the portions of the predicted central intensity spectrum together with the observed one in the wavelength range $\lambda\lambda$ 530.0 – 537.1 *nm*

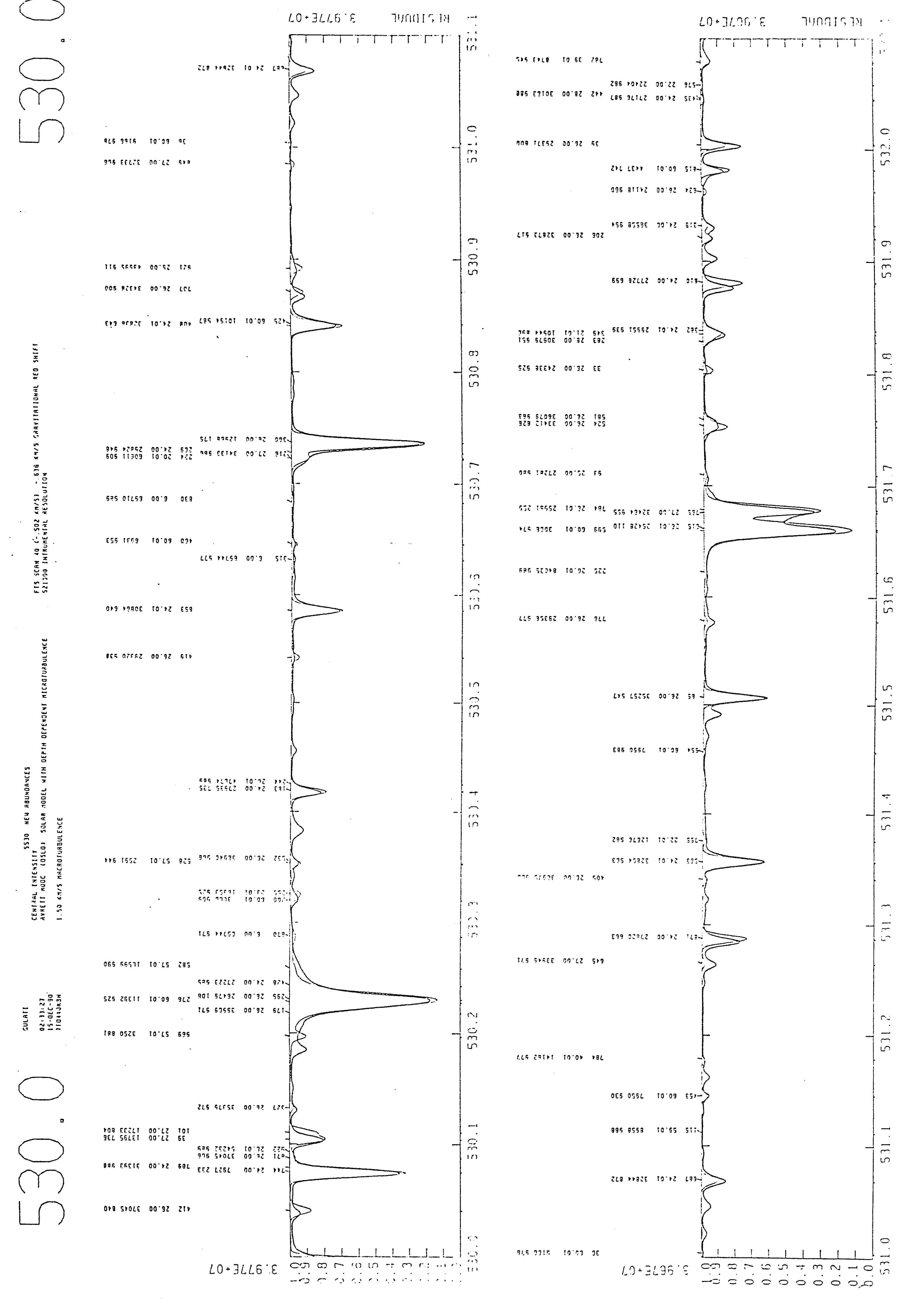
530.0
530.0
530.1
530.2
530.3
530.4
530.5
530.6
530.7
530.8
530.9
531.0
531.1
531.2
531.3
531.4
531.5
531.6
531.7
531.8
531.9
532.0
1.0 0.9 0.8 0.7 0.6 0.5 0.4 0.3 0.2 0.1 0.0
3.977E+07
3.967E+07

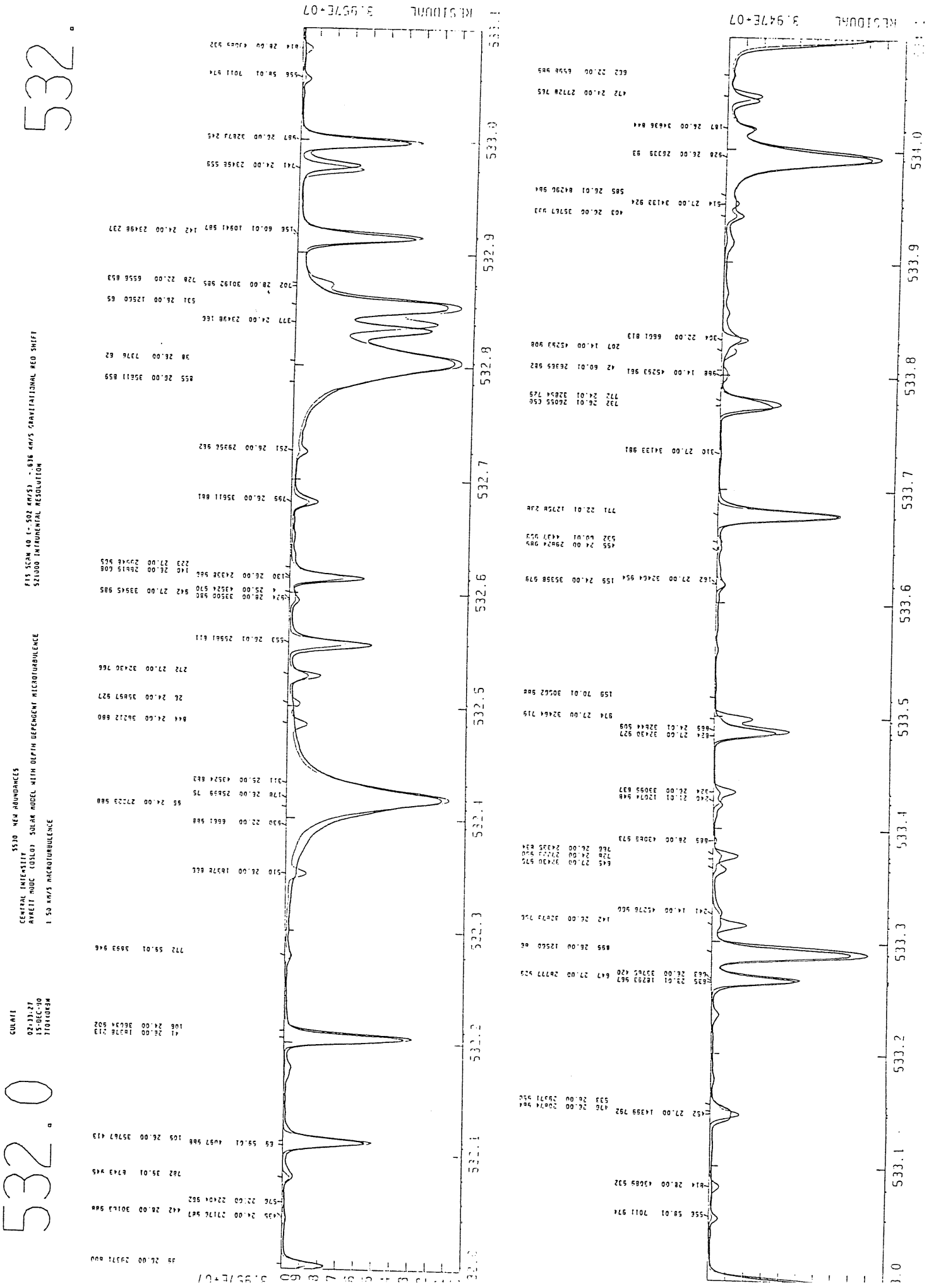
532.0
532.1
532.2
532.3
532.4
532.5
532.6
532.7
532.8
532.9
533.0
533.1
533.2
533.3
533.4
533.5
533.6
533.7
533.8
533.9
534.0
3.9576+07
3.9476+07
KL51DUNL
FTS SCAN 40 (-.502 KM/S) -.636 KM/S GRAVITATIONAL RED SHIFT
SZ1000 INTRUMENTAL RESOLUTION
CENTRAL INTENSITY 5530 NEW ABUNDANCES
AVRETT ADUC (DSLO3) SOLAR MODEL WITH DEPTH DEPENDENT MICROTURBULENCE
1.50 KM/S MACROTURBULENCE
GULATI
02:33:27
15-DEC-90

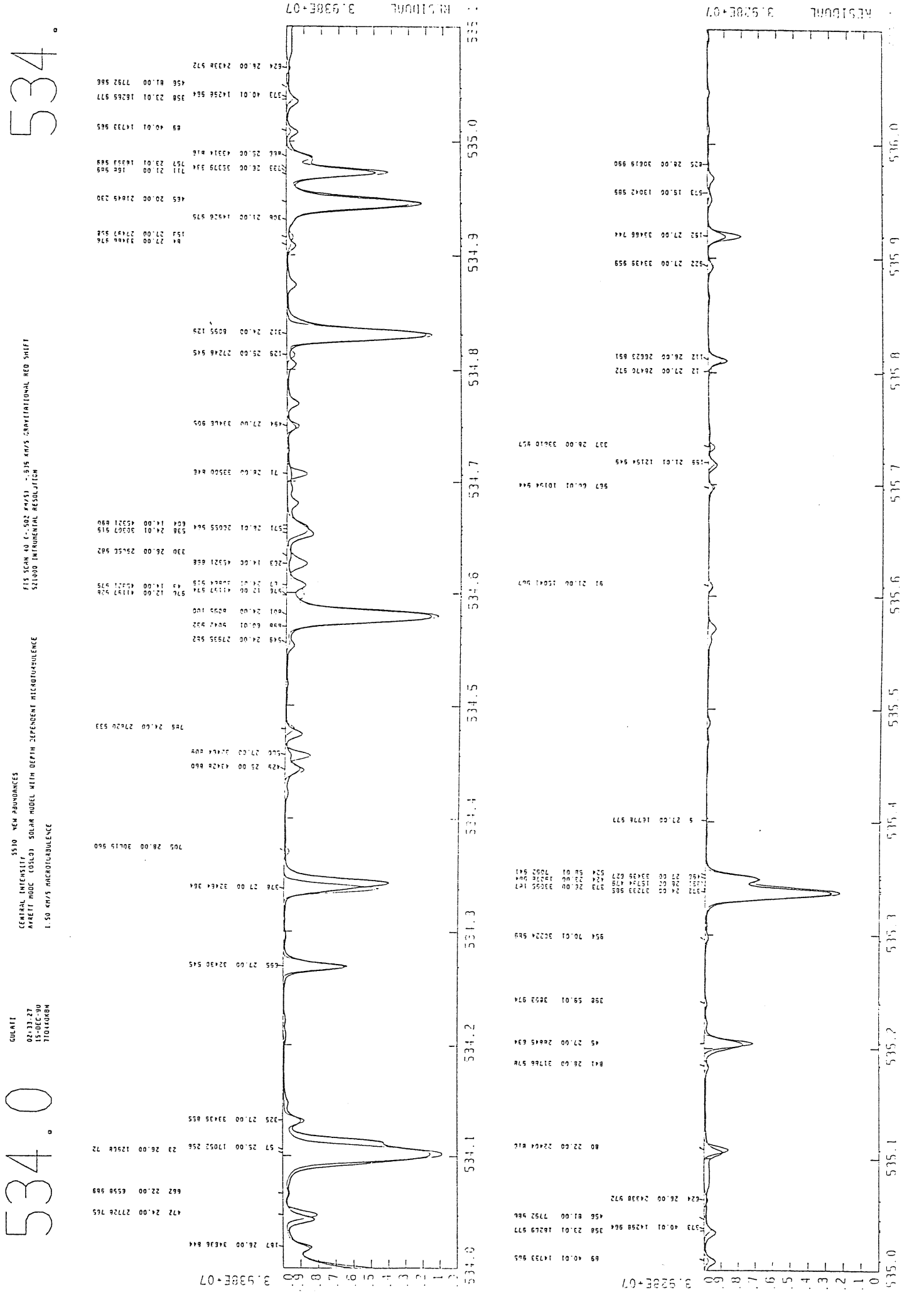
534.0
534.8
CENTRAL INTENSITY
AVRETT MODE (DSLG) SOLAR MODEL WITH DEPTH DEPENDENT MICROTURBULENCE
1.50 KM/S MACROTURBULENCE
FTS SCAN 40 (-.502 MA/S) -.635 KM/S GRAVITATIONAL RED SHIFT
S2000 INSTRUMENTAL RESOLUTION
3.938E+07
535.0
534.9
534.8
534.7
534.6
534.5
534.4
534.3
534.2
534.1
534.0
535.1
535.2
535.3
535.4
535.5
535.6
535.7
535.8
535.9
536.0

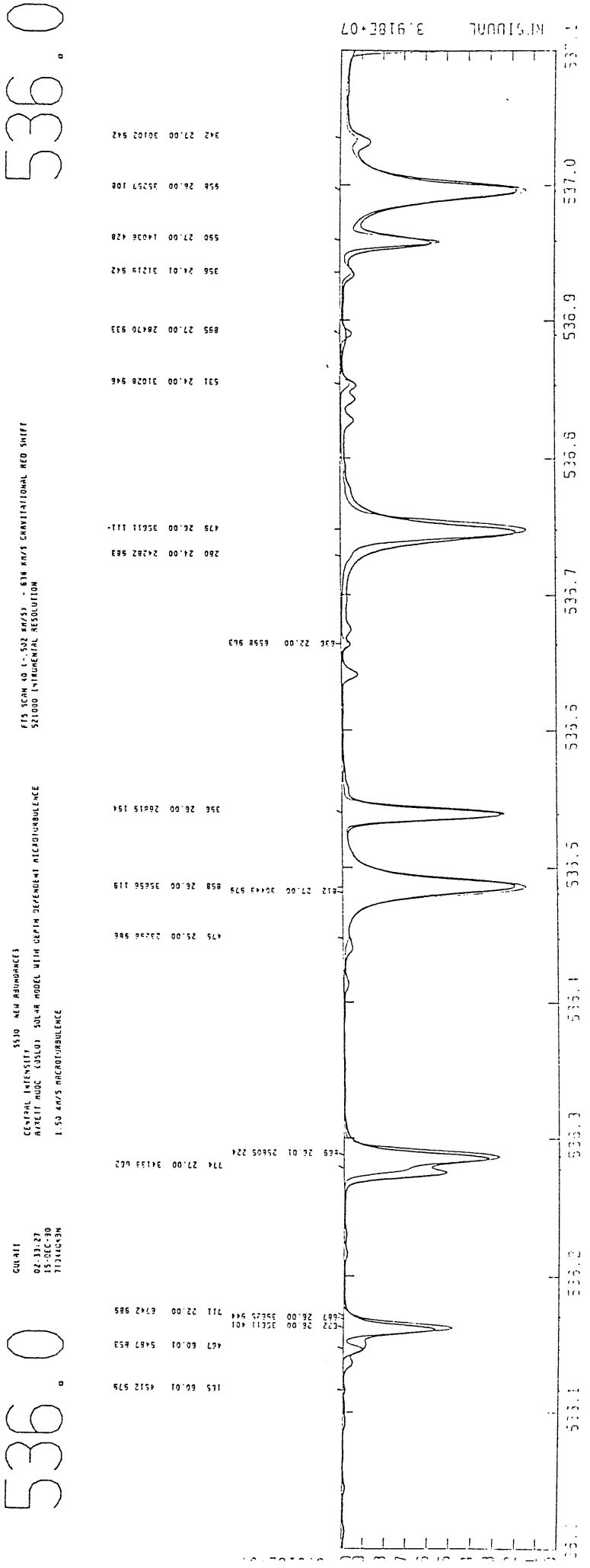
536.0
536.0
RESIDUAL 3.918E+07
537.1
537.0
536.9
536.8
536.7
536.6
536.5
536.4
536.3
536.2
536.1
536.0
FTS SCAN 40 (-.502 KM/S) - 638 KM/S GRAVITATIONAL RED SHIFT
521000 INSTRUMENTAL RESOLUTION
CENTRAL INTENSITY 5530 NEW ABUNDANCES
ARNETT MODEL (1981) SOLAR MODEL WITH DEPTH DEPENDENT MICROTURBULENCE
1.50 KM/S MACROTURBULENCE
GULATI
02:33:27
15-DEC-30

Appendix B

Solar flux spectrum

This appendix contains the plots of observed solar flux spectrum together with one generated using the solar empirical model and our line list. In all these spectra, thick lines refer to the observed solar flux spectra, and thin lines refer to those predicted with the model and they have been referred to in Chapter 2.

B.1 Spectrum in the blue bandpass

In this section, we present the portions of the predicted and the observed solar flux spectra in the wavelength range $\lambda\lambda 489.5 - -496.1\ nm$.

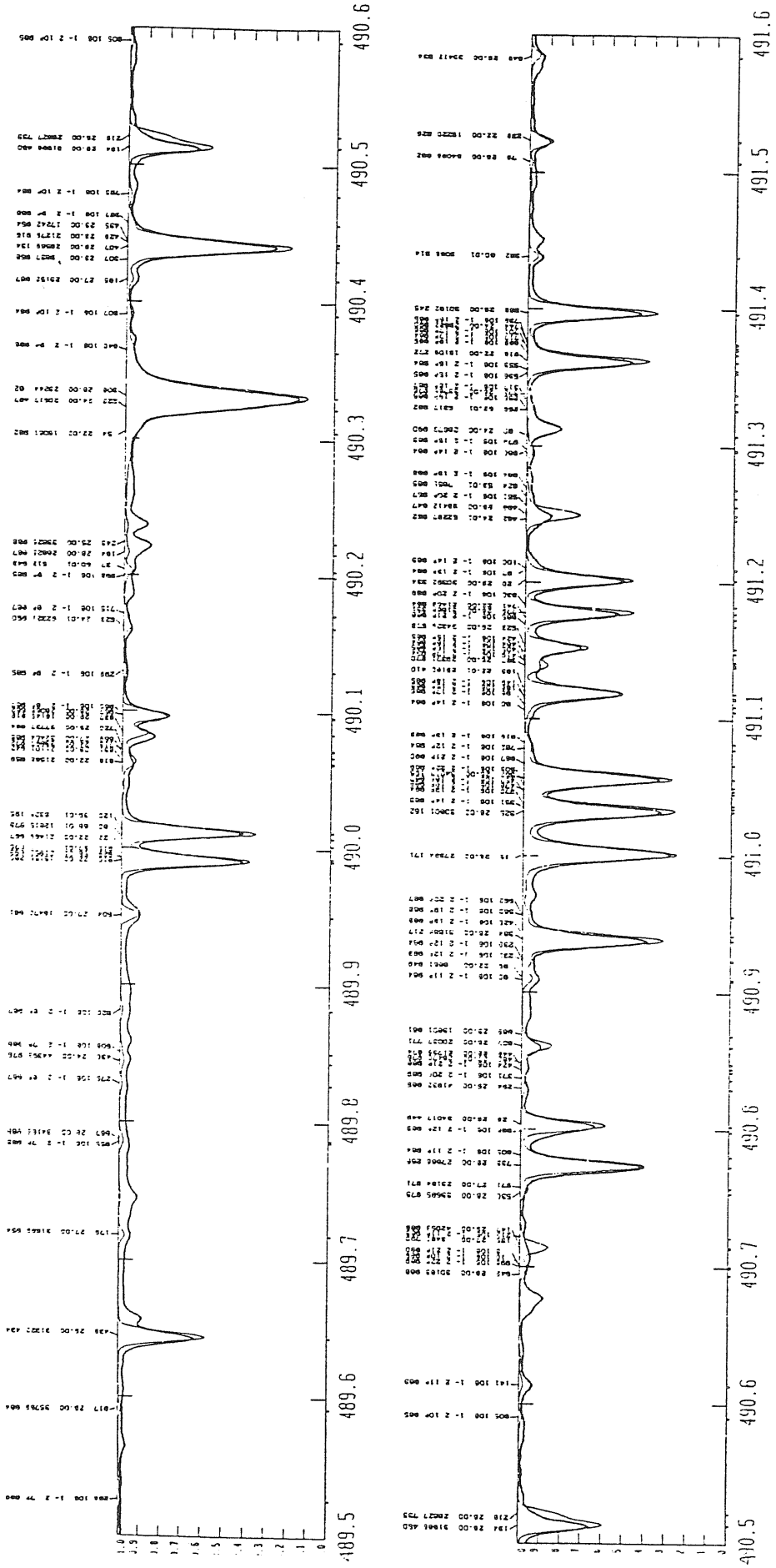
489.5
489.6
489.7
489.8
489.9
490.0
490.1
490.2
490.3
490.4
490.5
490.6
490.5
490.6
490.7
490.8
490.9
491.0
491.1
491.2
491.3
491.4
491.5
491.6

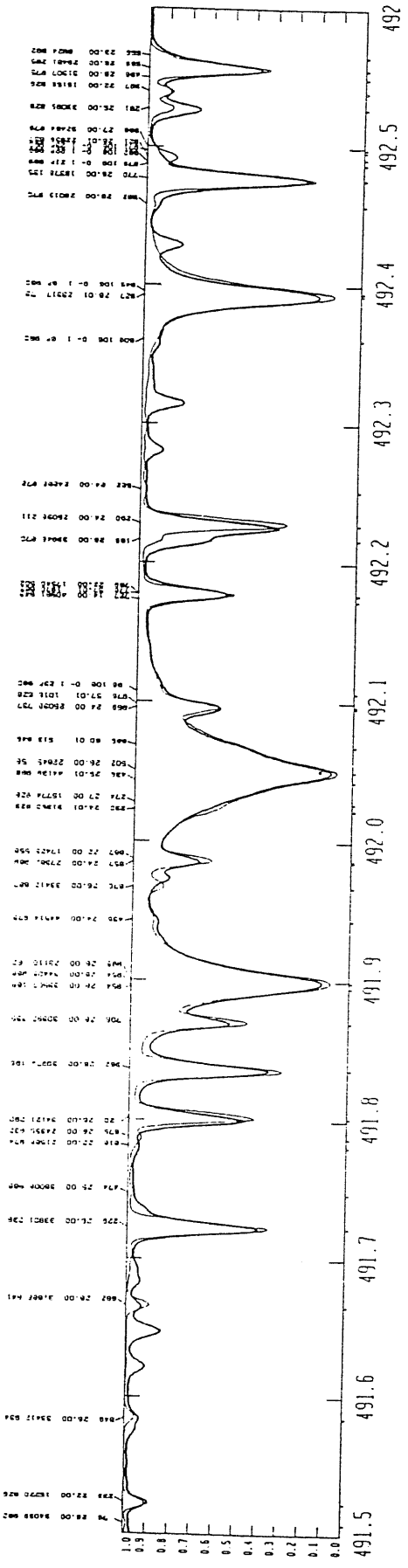
491.5
491.6
491.7
491.8
491.9
492.0
492.1
492.2
492.3
492.4
492.5
492
1.0
0.9
0.8
0.7
0.6
0.5
0.4
0.3
0.2
0.1
0.0

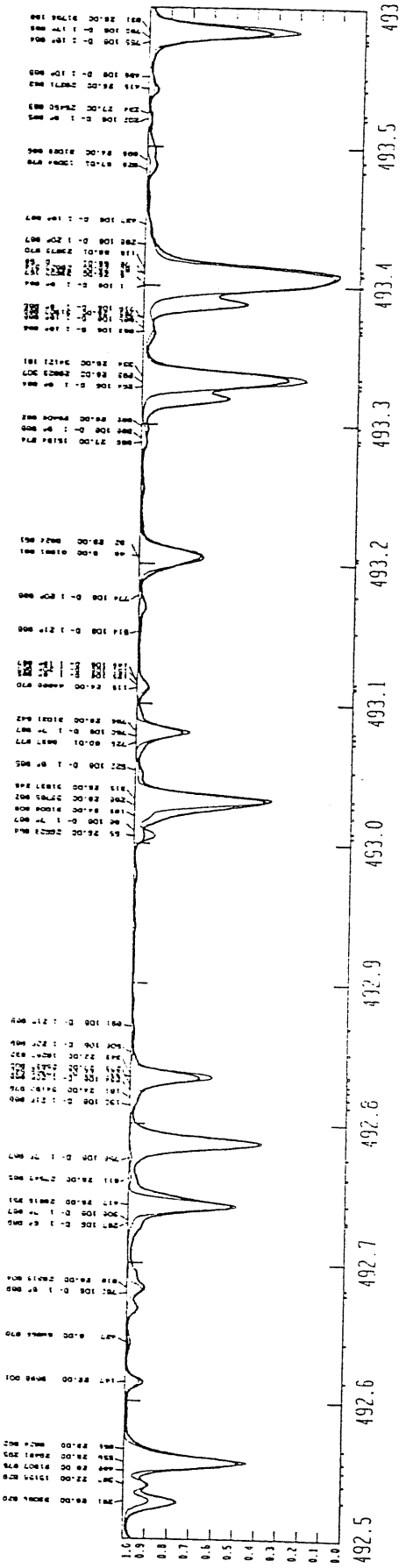
492.5
492.6
492.7
492.8
492.9
493.0
493.1
493.2
493.3
493.4
493.5
493
1.0
0.9
0.8
0.7
0.6
0.5
0.4
0.3
0.2
0.1
0.0

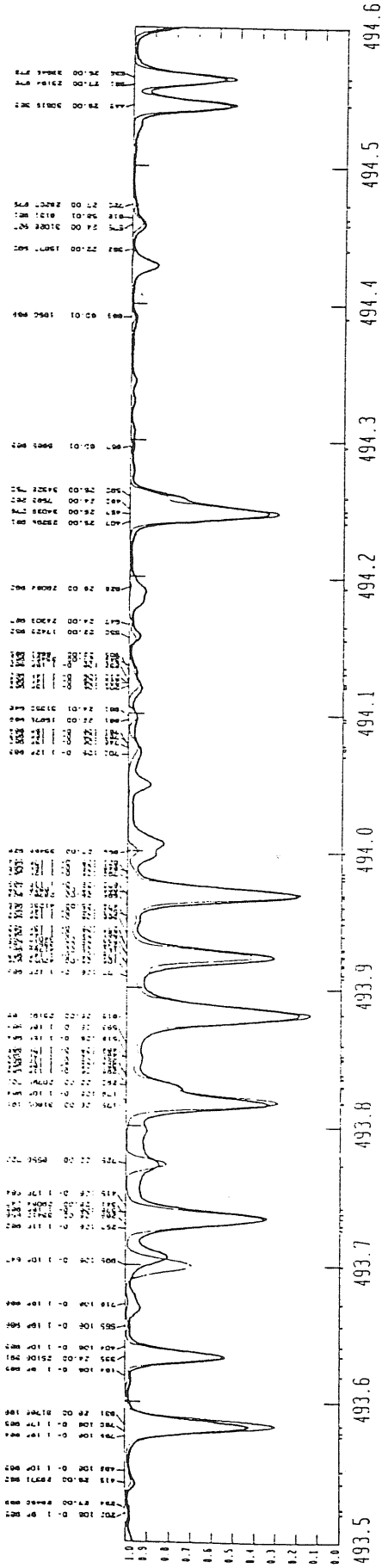
493.5
493.6
493.7
493.8
493.9
494.0
494.1
494.2
494.3
494.4
494.5
494.6

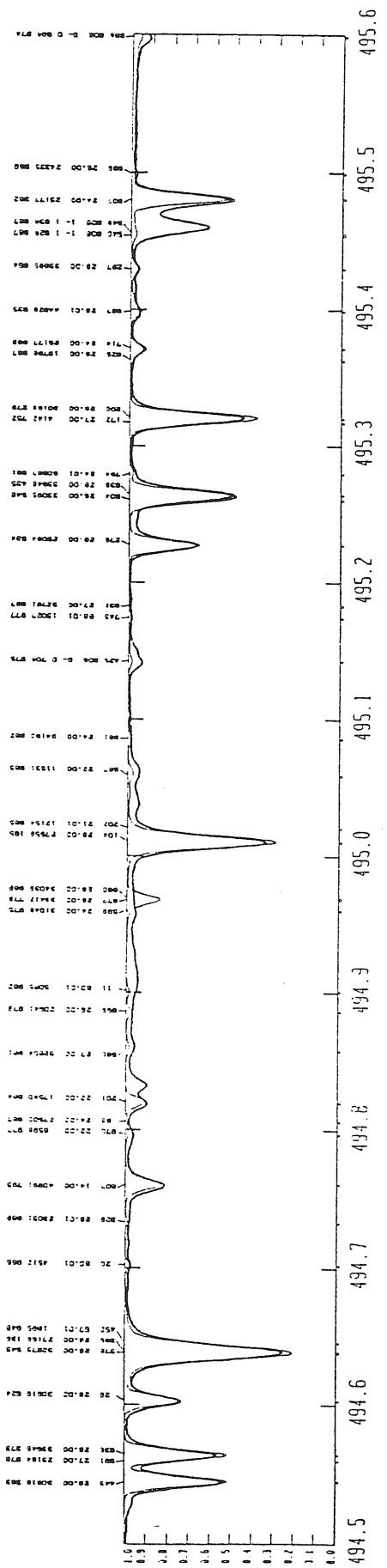
494.5
494.6
494.7
494.8
494.9
495.0
495.1
495.2
495.3
495.4
495.5
495.6

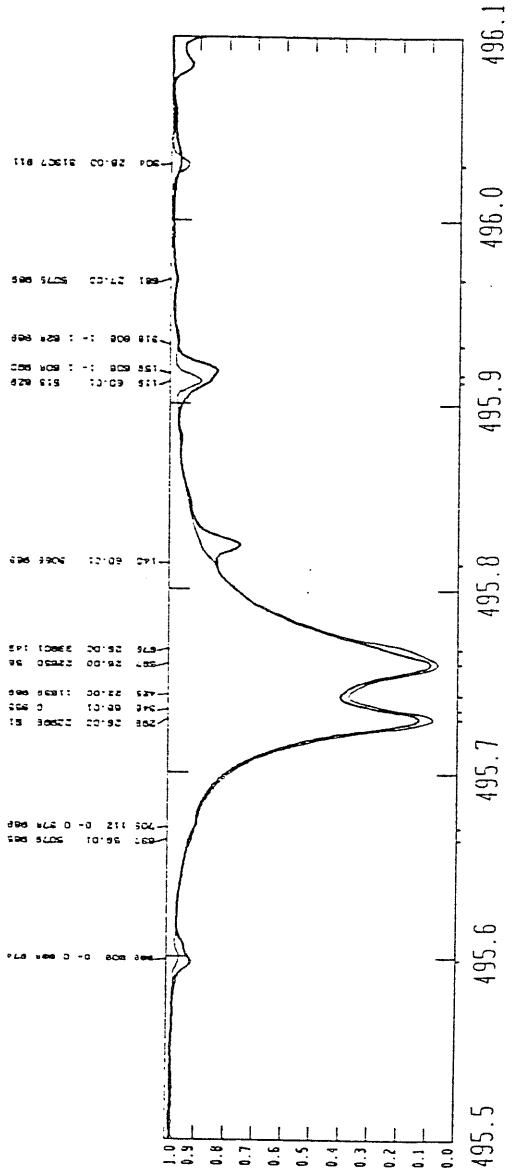
496.1
496.0
495.9
495.8
495.7
495.6
495.5
1.0
0.9
0.8
0.7
0.6
0.5
0.4
0.3
0.2
0.1
0.0

B.2 Spectrum in the central bandpass

In this section, we present the portions of the predicted and the observed solar flux spectra in the wavelength range of $\lambda\lambda 515.0 - -520.1\ nm$.

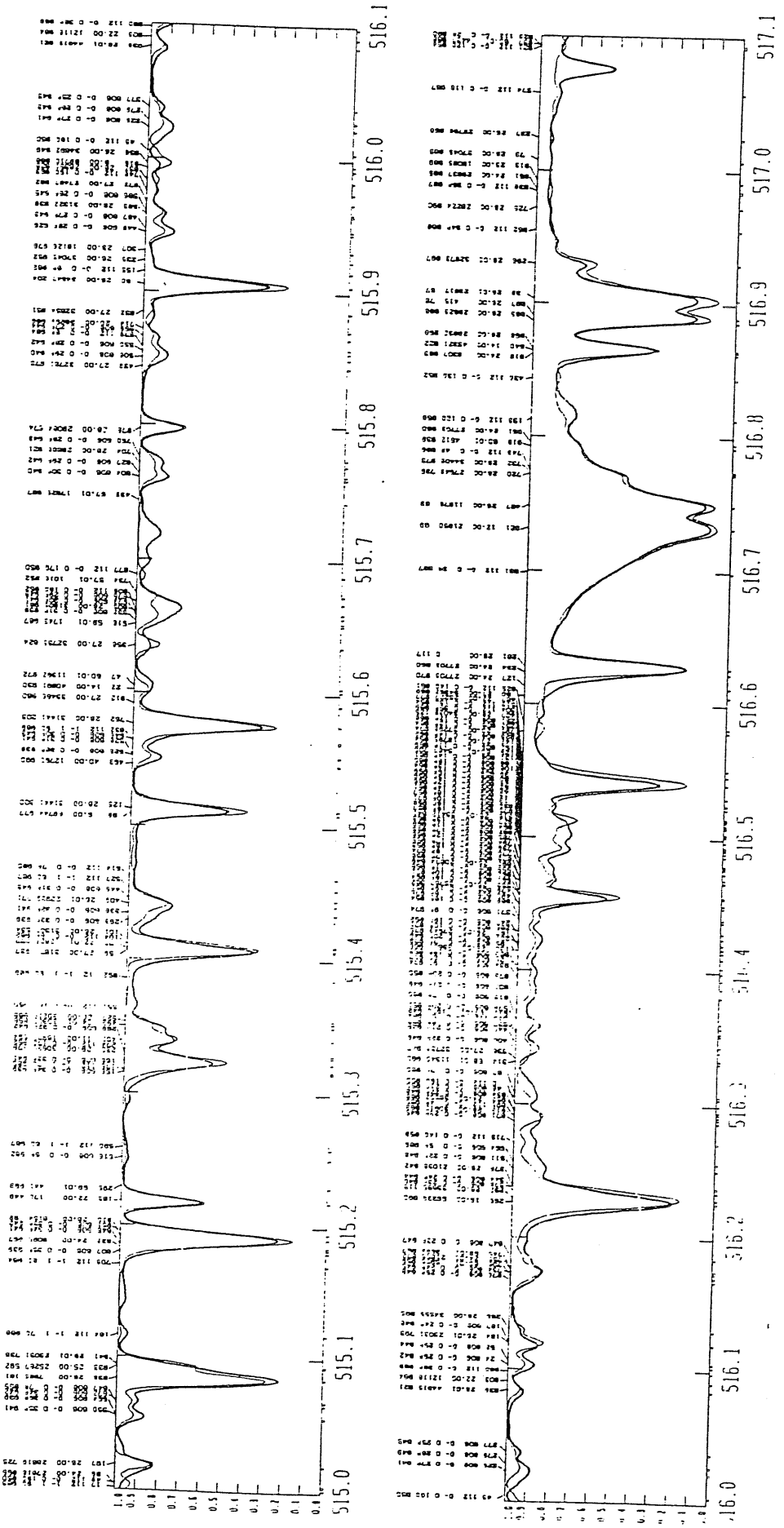
515.0
515.1
515.2
515.3
515.4
515.5
515.6
515.7
515.8
515.9
516.0
516.1
516.0
516.1
516.2
516.3
516.4
516.5
516.6
516.7
516.8
516.9
517.0
517.1

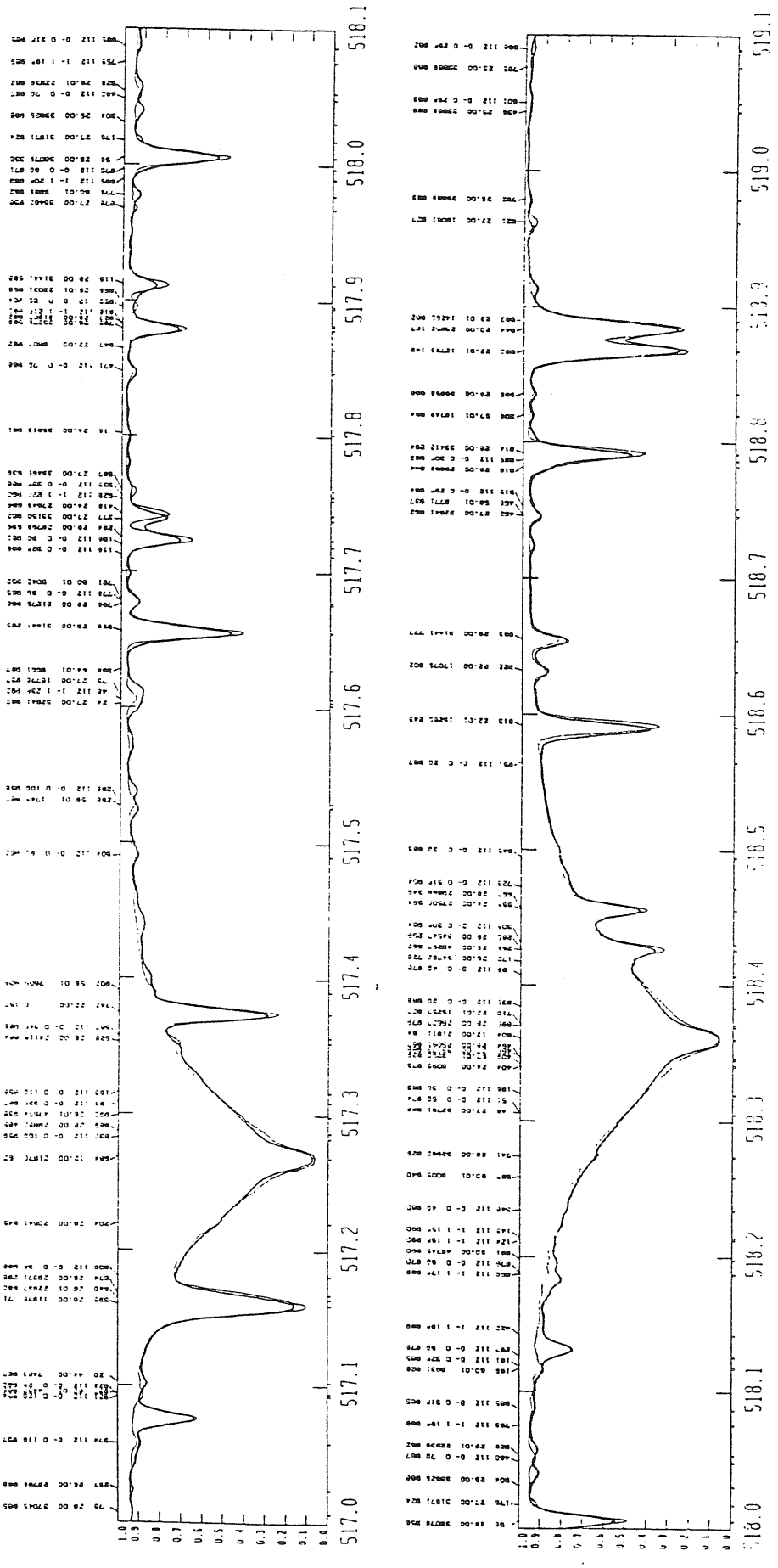
517.0
517.1
517.2
517.3
517.4
517.5
517.6
517.7
517.8
517.9
518.0
518.1
518.0
518.1
518.2
518.3
518.4
518.5
518.6
518.7
518.8
519.0
519.1

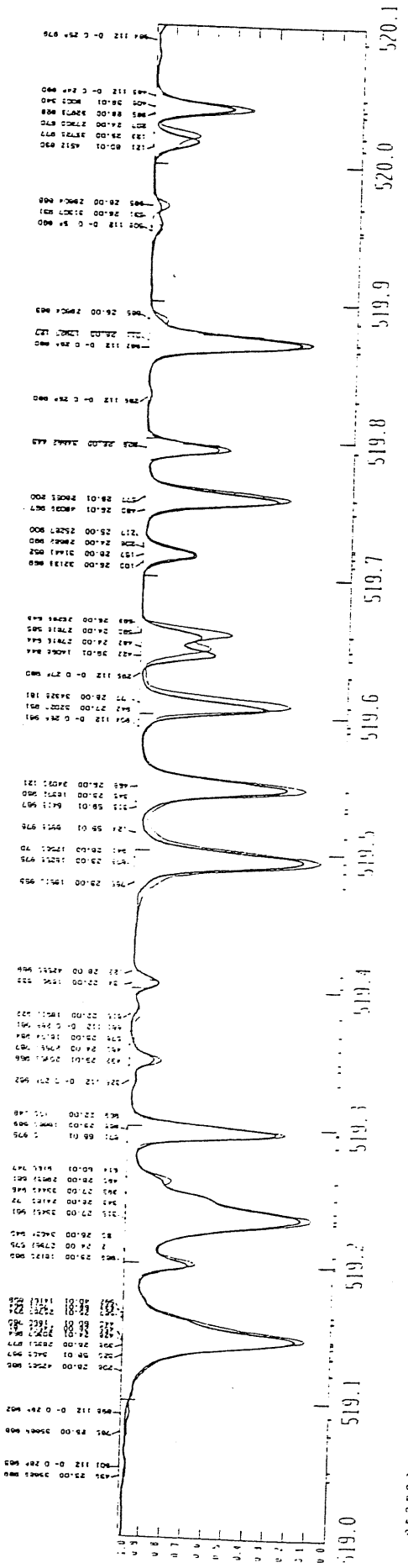
520.1
520.0
519.9
519.8
519.7
519.6
519.5
519.4
519.3
519.2
519.1
519.0

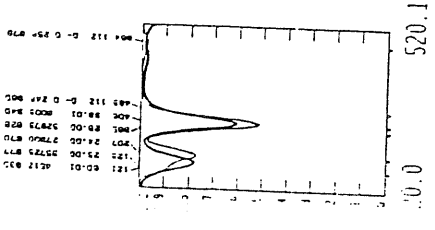
520.1
520.0

B.3 Spectrum in the red bandpass

In this section, we present the portions of the predicted and the observed solar flux spectra in the wavelength range of $\lambda\lambda 530.0 - -537.1\ nm$.

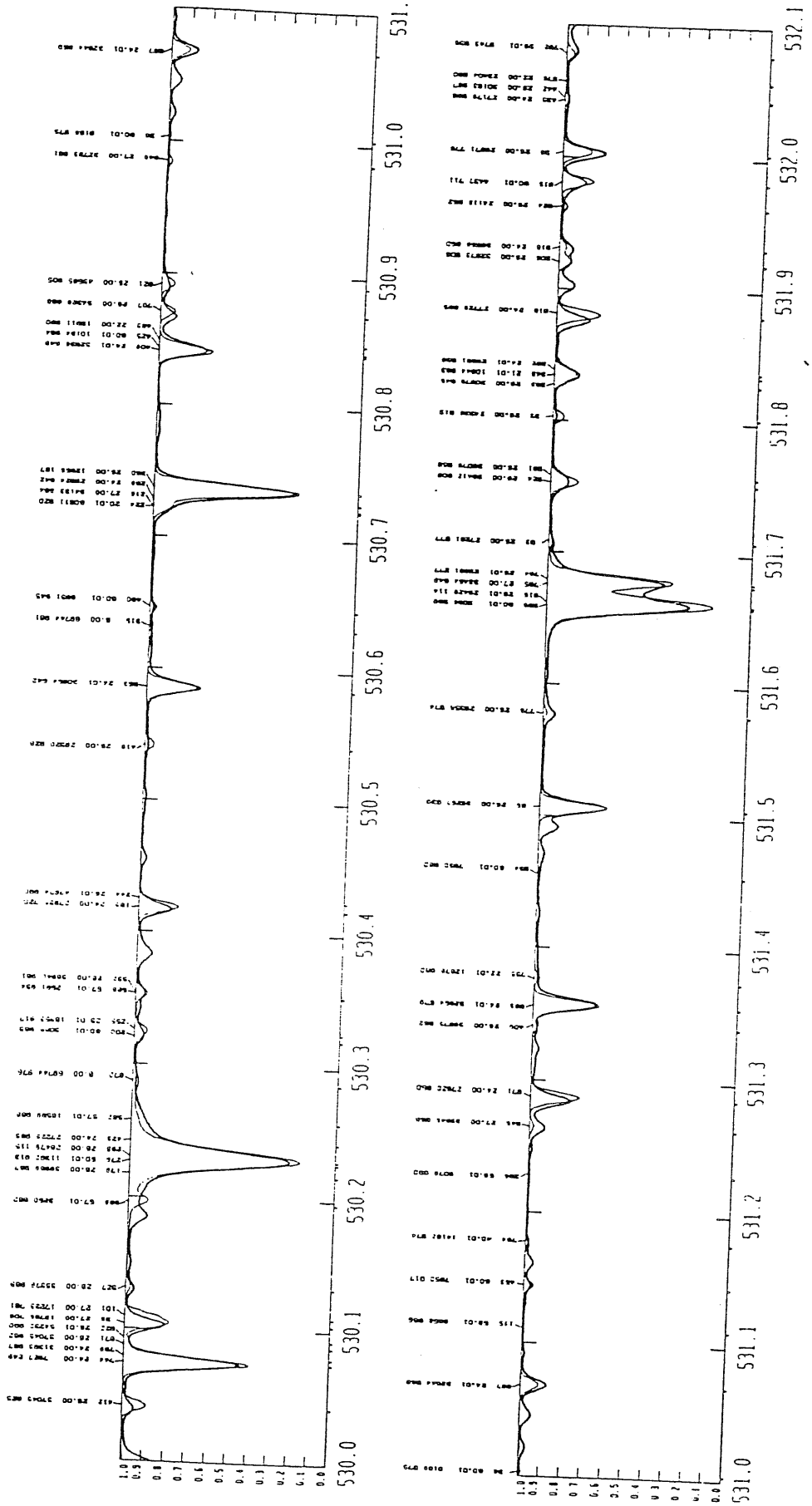
530.0
530.1
530.2
530.3
530.4
530.5
530.6
530.7
530.8
530.9
531.0
531.1
531.0
531.1
531.2
531.3
531.4
531.5
531.6
531.7
531.8
531.9
532.0
532.1

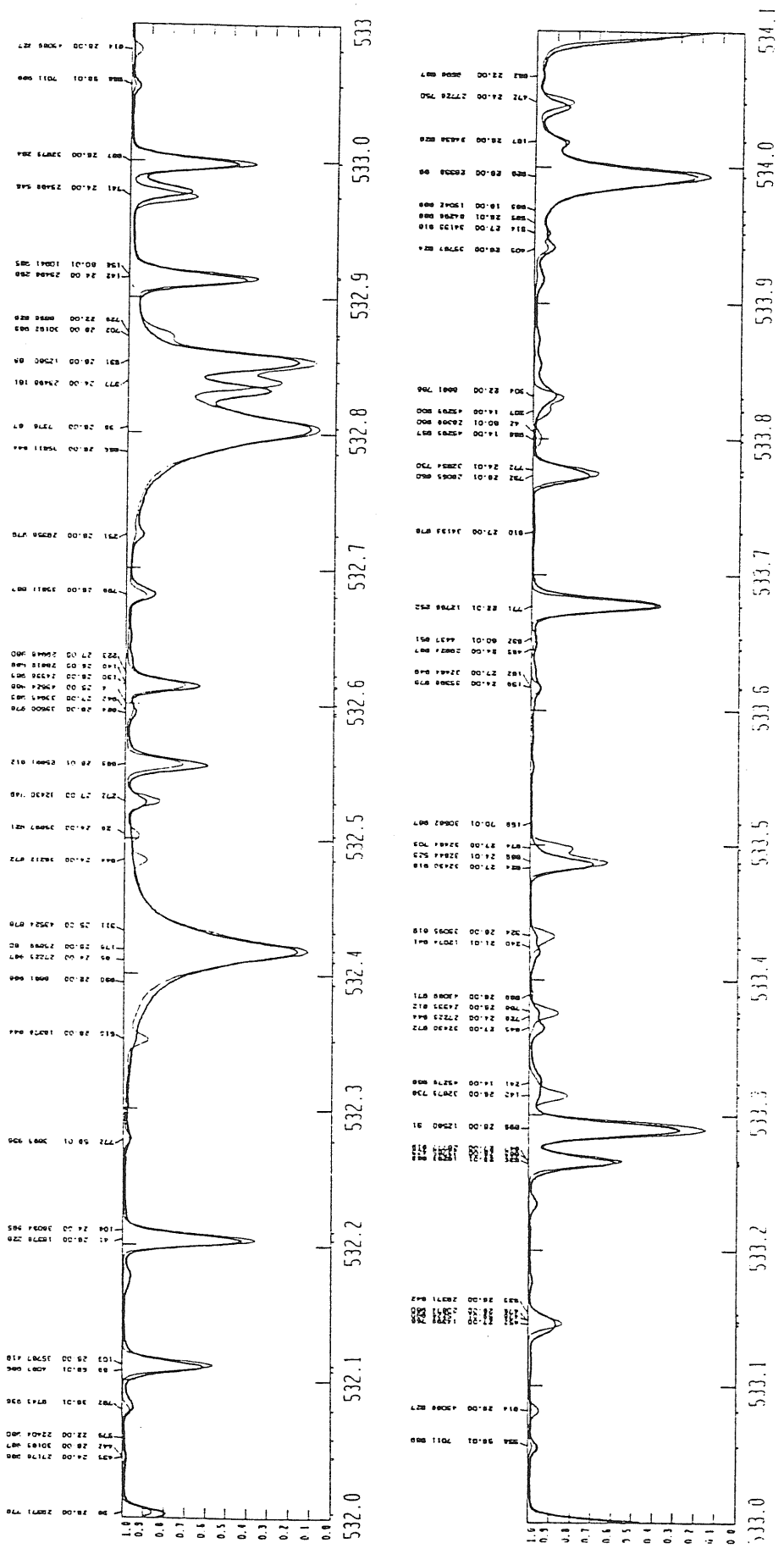
532.0
532.1
532.2
532.3
532.4
532.5
532.6
532.7
532.8
532.9
533.0
533
533.0
533.1
533.2
533.3
533.4
533.5
533.6
533.7
533.8
533.9
534.0
534.1

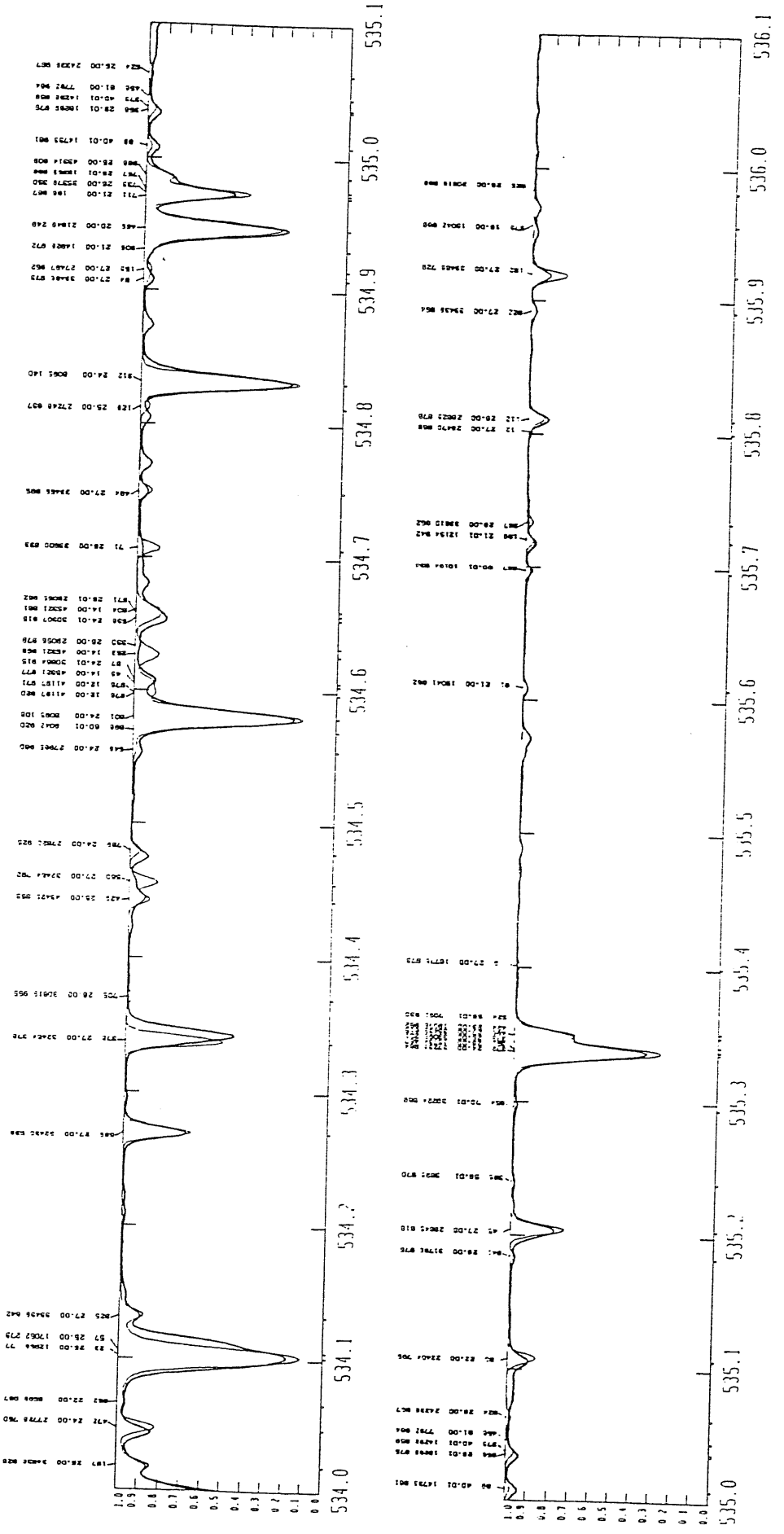
534.0
534.1
534.2
534.3
534.4
534.5
534.6
534.7
534.8
534.9
535.0
535.1
535.0
535.1
535.2
535.3
535.4
535.5
535.6
535.7
535.8
535.9
536.0
536.1

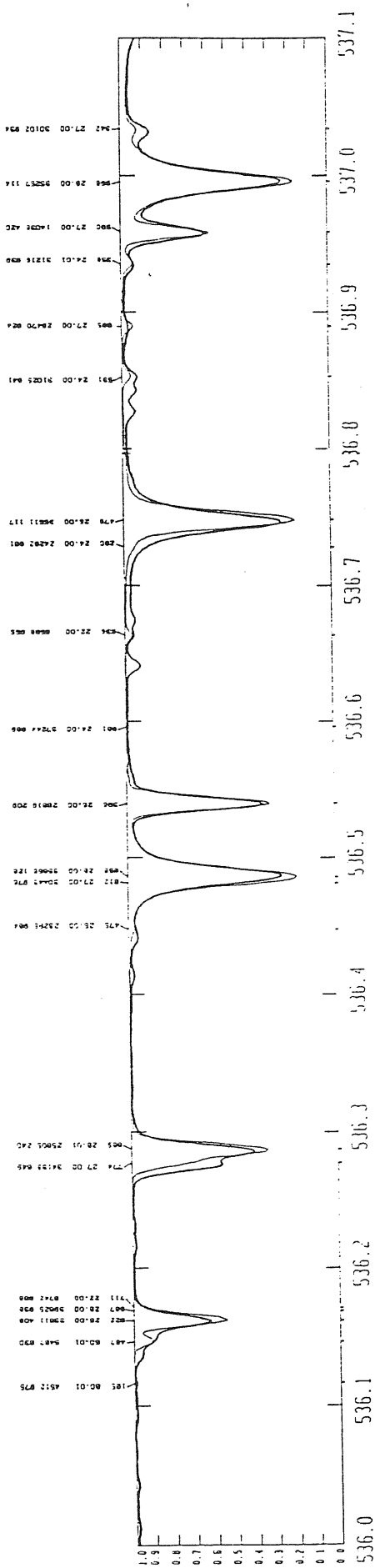
536.0
536.1
536.2
536.3
536.4
536.5
536.6
536.7
536.8
536.9
537.0
537.1

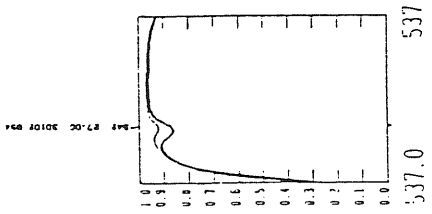
537.0
537.1

Appendix C

Arcturus spectrum

This appendix contains the plots of observed Arcturus spectra together with spectra generated from Peterson et al. (1991) Arcturus model and our line lists in the central bandpass of the Mg_2. The shaky lines represent the observed spectrum and thin smooth lines represent the predicted spectrum and they have been referred to in Chapter 2.

C.1 Spectrum in the central bandpass

Here we present the portions of predicted and observed spectrum of Arcturus in the wavelength range of $\lambda\lambda$ 514 – 520.1 nm.

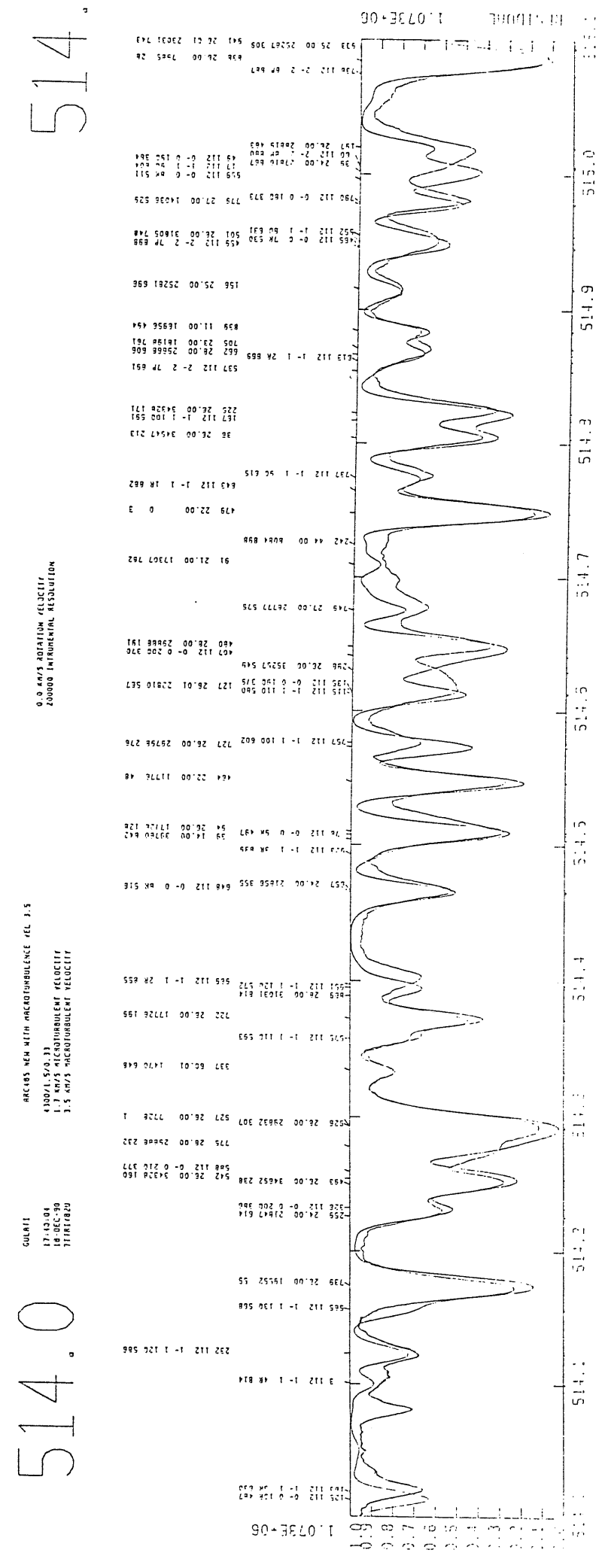
514.0
514.1
514.2
514.3
514.4
514.5
514.6
514.7
514.8
514.9
515.0
1.0736+06
ARC405 NEW WITH MACROTURBULENCE VEL 3.5
4100/1.5/0.33
1.7 KM/S MICROTURBULENT VELOCITY
3.5 KM/S MACROTURBULENT VELOCITY
GULATI
17:43:04
18-DEC-90
0.0 KM/S ROTATION VELOCITY
200000 INSTRUMENTAL RESOLUTION

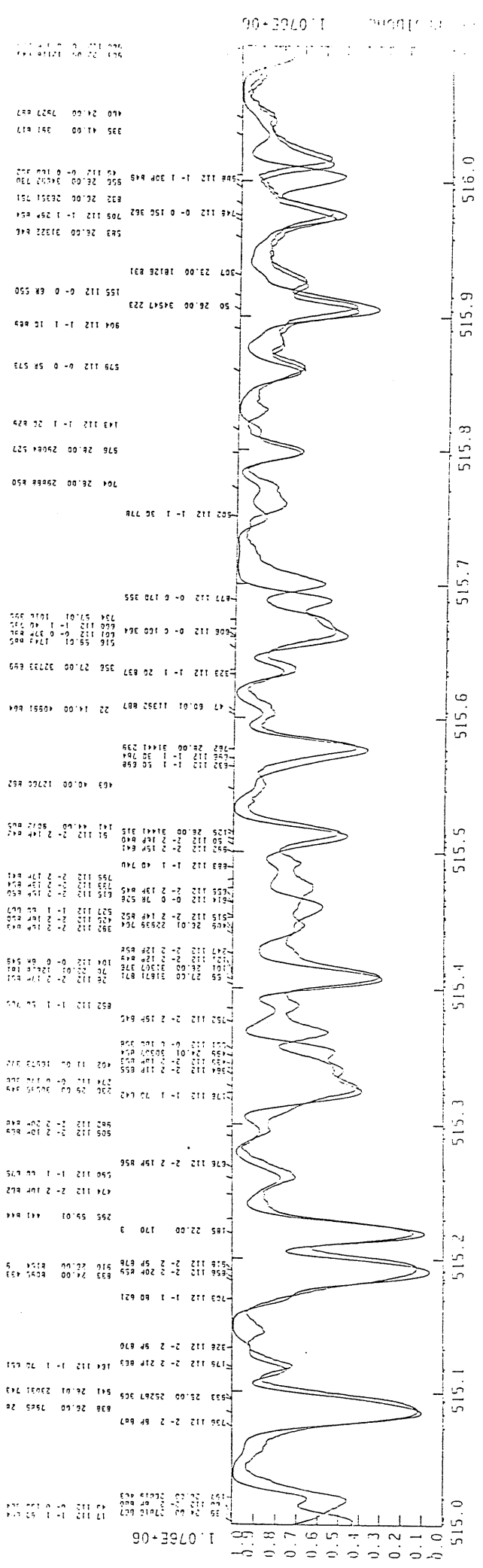
514.0
515.0
515.1
515.2
515.3
515.4
515.5
515.6
515.7
515.8
515.9
516.0
1.0736+06

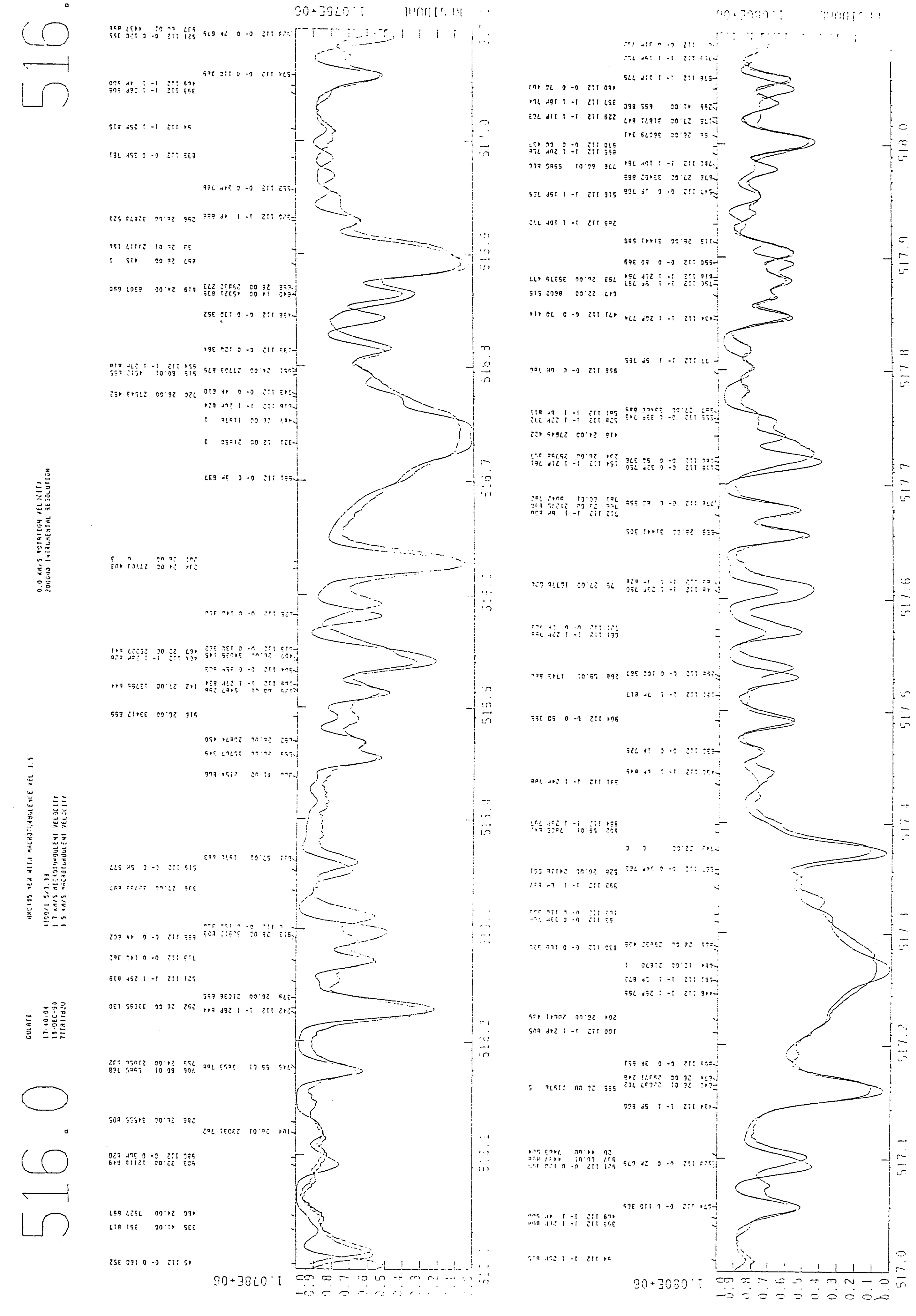
516.0

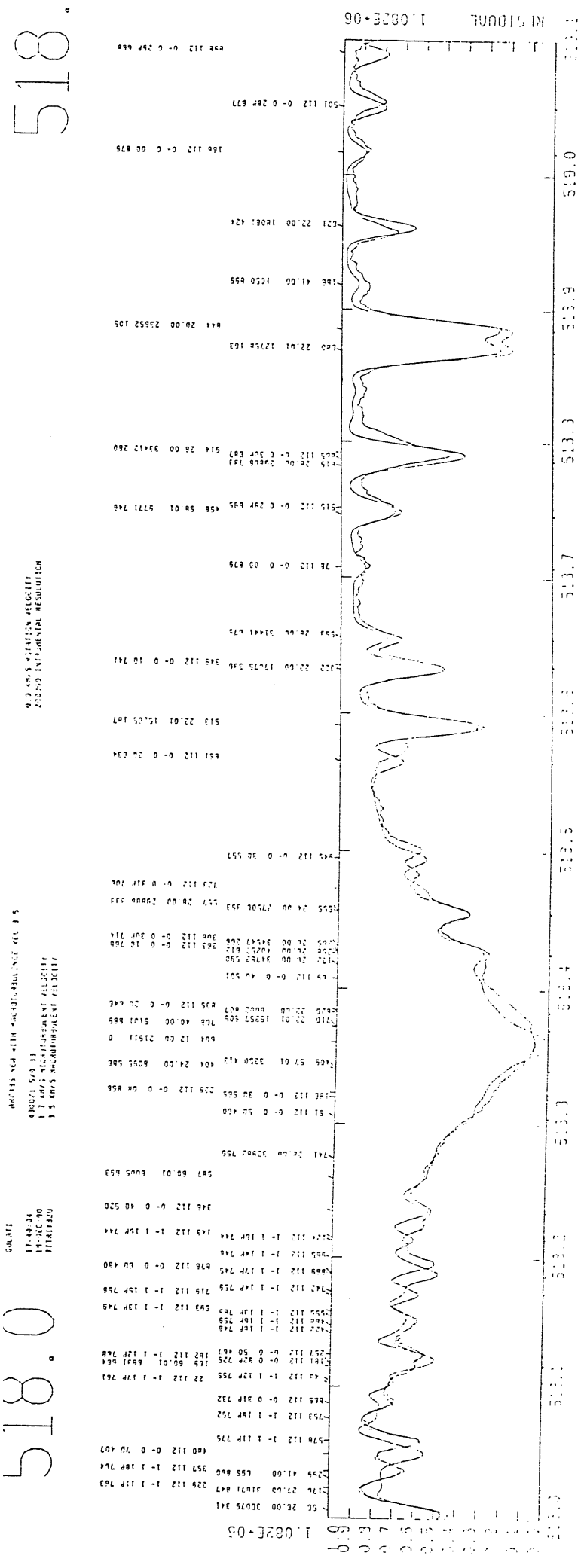
518.0
518.3
518.7
519.0
519.3
519.7
520.0

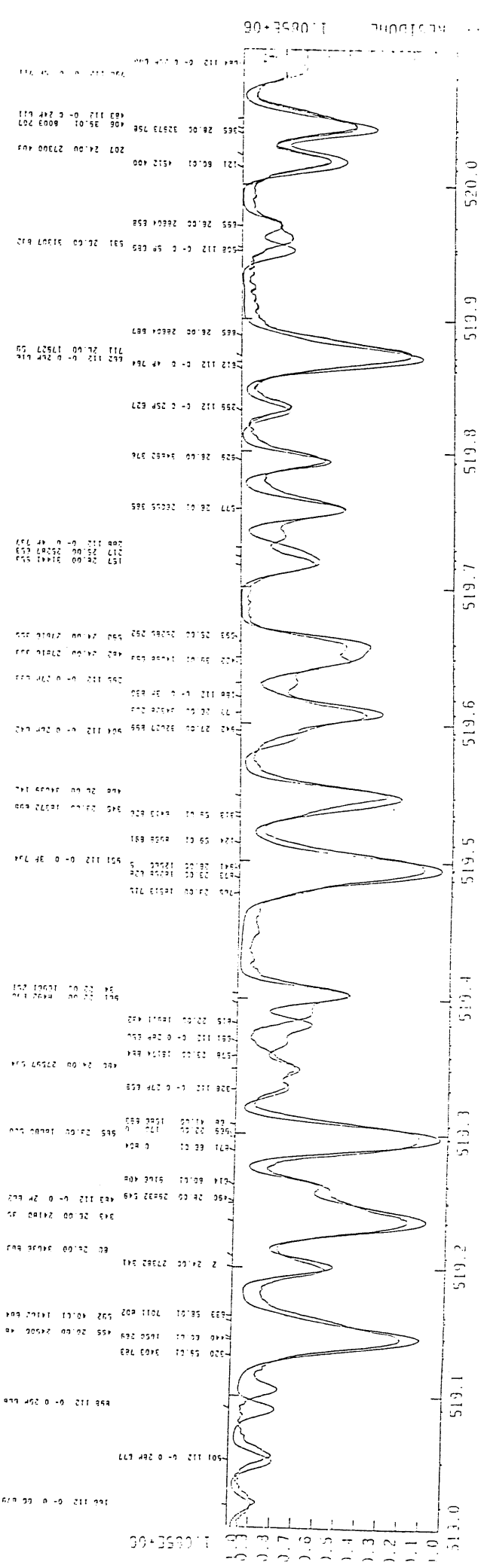
519.1
519.2
519.3
519.4
519.5
519.6
519.7
519.8
519.9
520.0

Appendix D

Observed and synthetic spectra

This appendix contains the residual flux spectra of reference stars used as a guide to establish the consistency of the library of synthetic spectra in the central bandpass of the Mg_2 index together with their template spectra. The spectra are arranged according to decreasing order of temperature for dwarfs, giants and supergiants classified in Chapter 4. In all these plots, thick lines refer to template synthetic spectra and dahsed lines refer to the normalized flux spectra of reference stars. The detailed description is given in Chapter 4.

D.1 Dwarfs

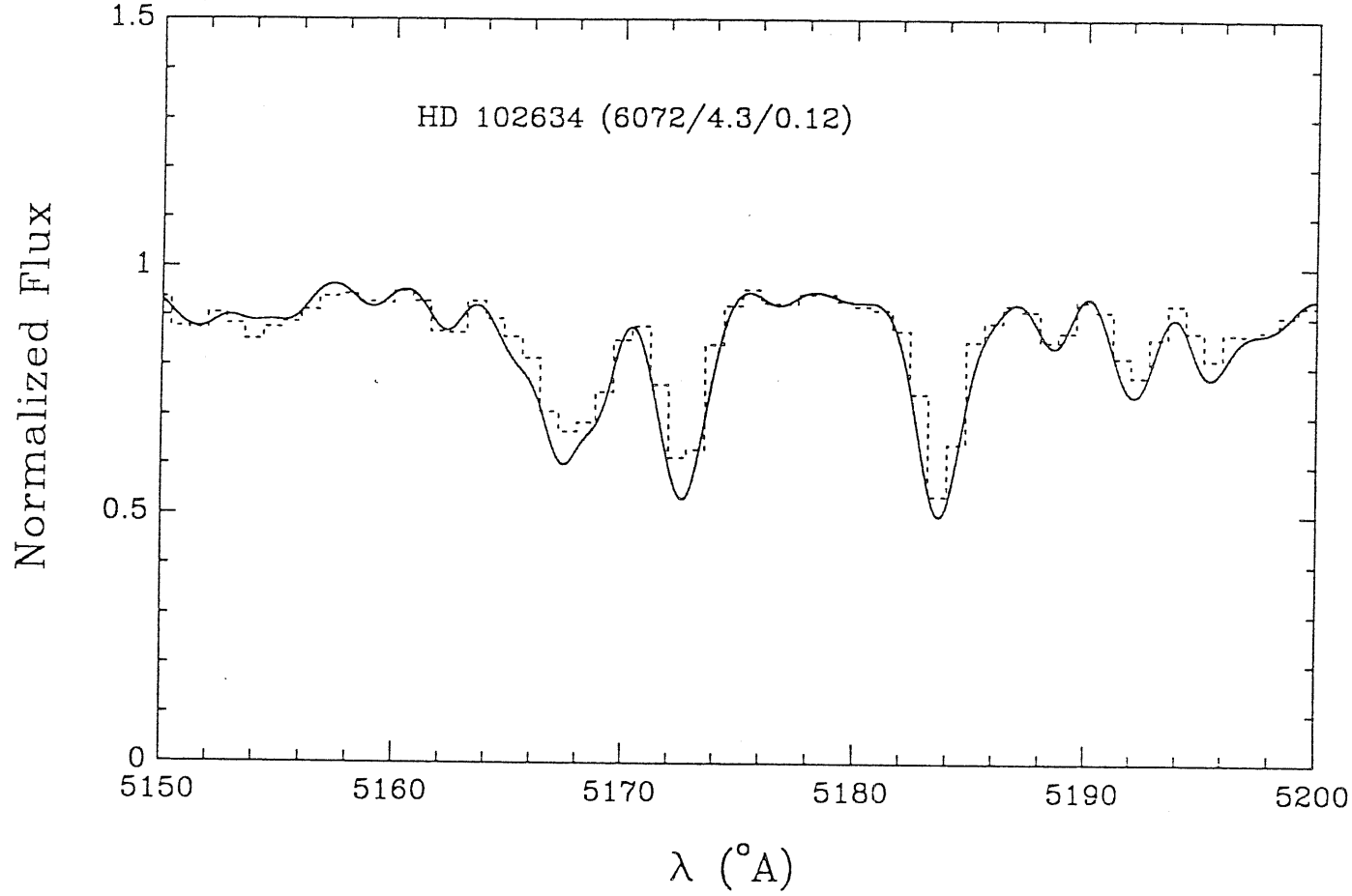
HD 102634 (6072/4.3/0.12)
Normalized Flux
1.5
1
0.5
0
5150
5160
5170
5180
5190
5200
λ (°A)

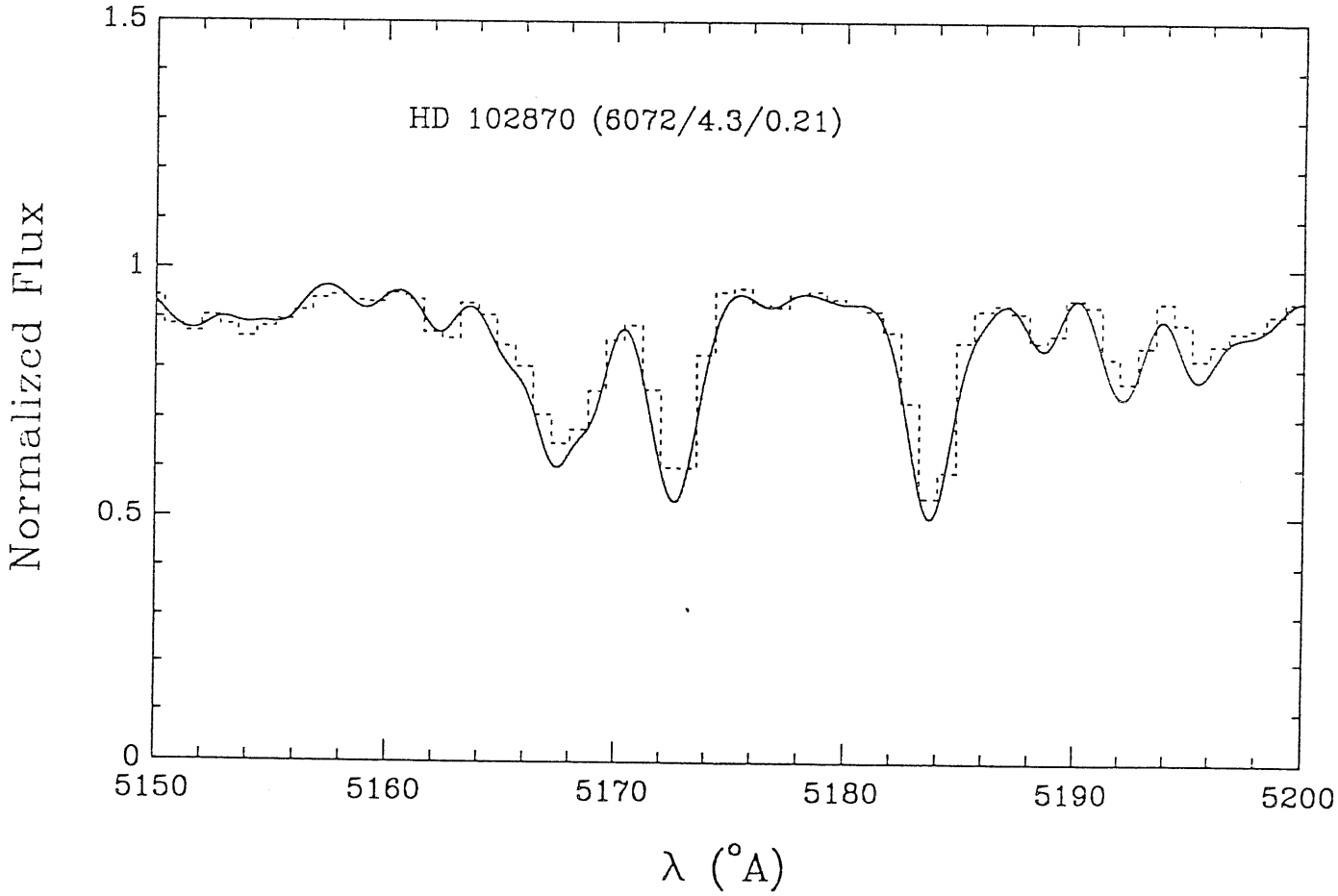
HD 102870 (6072/4.3/0.21)
Normalized Flux
1.5
1
0.5
0
5150
5160
5170
5180
5190
5200
λ (°A)

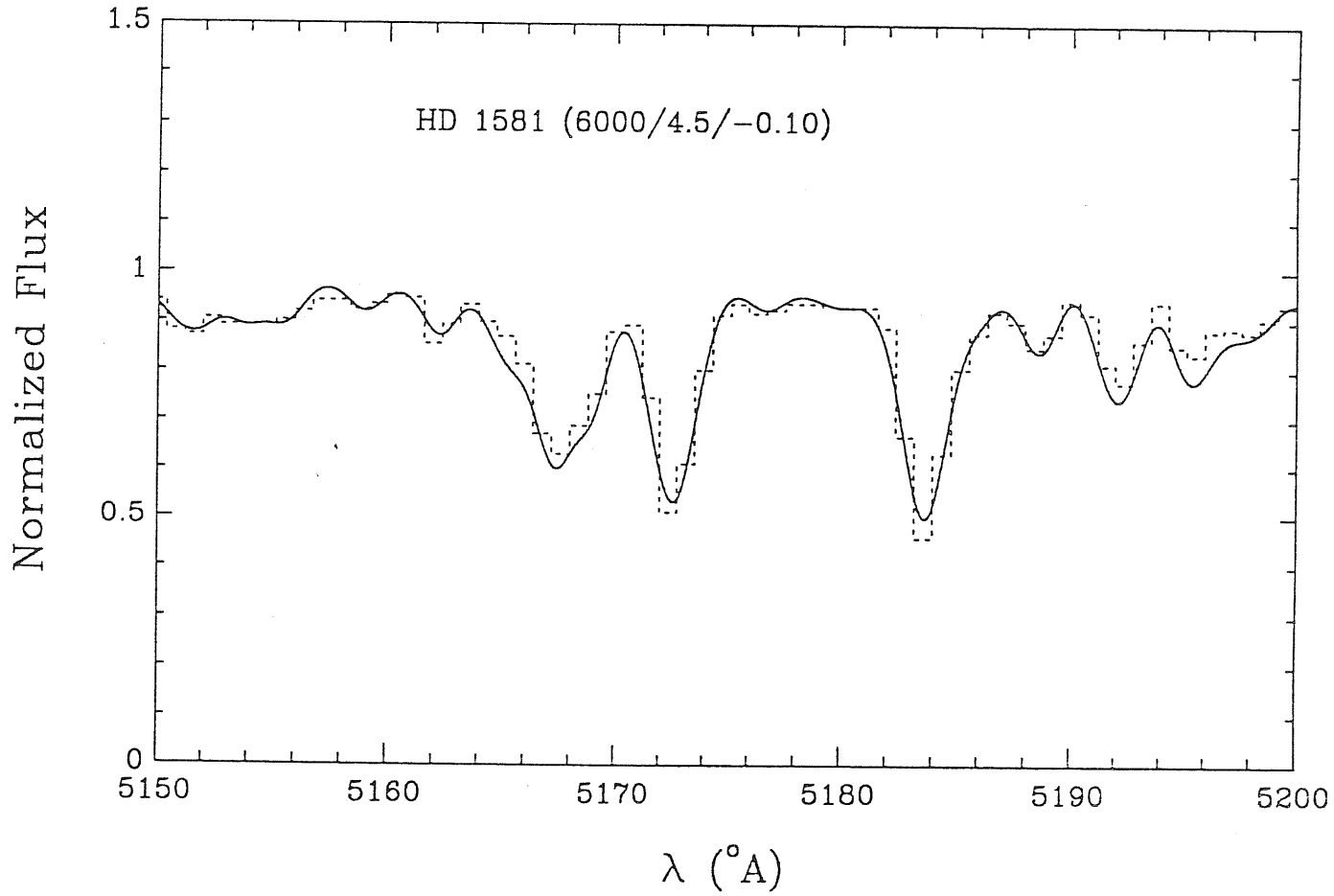
HD 1581 (6000/4.5/−0.10)
Normalized Flux
1.5
1
0.5
0
5150
5160
5170
5180
5190
5200
λ (°A)

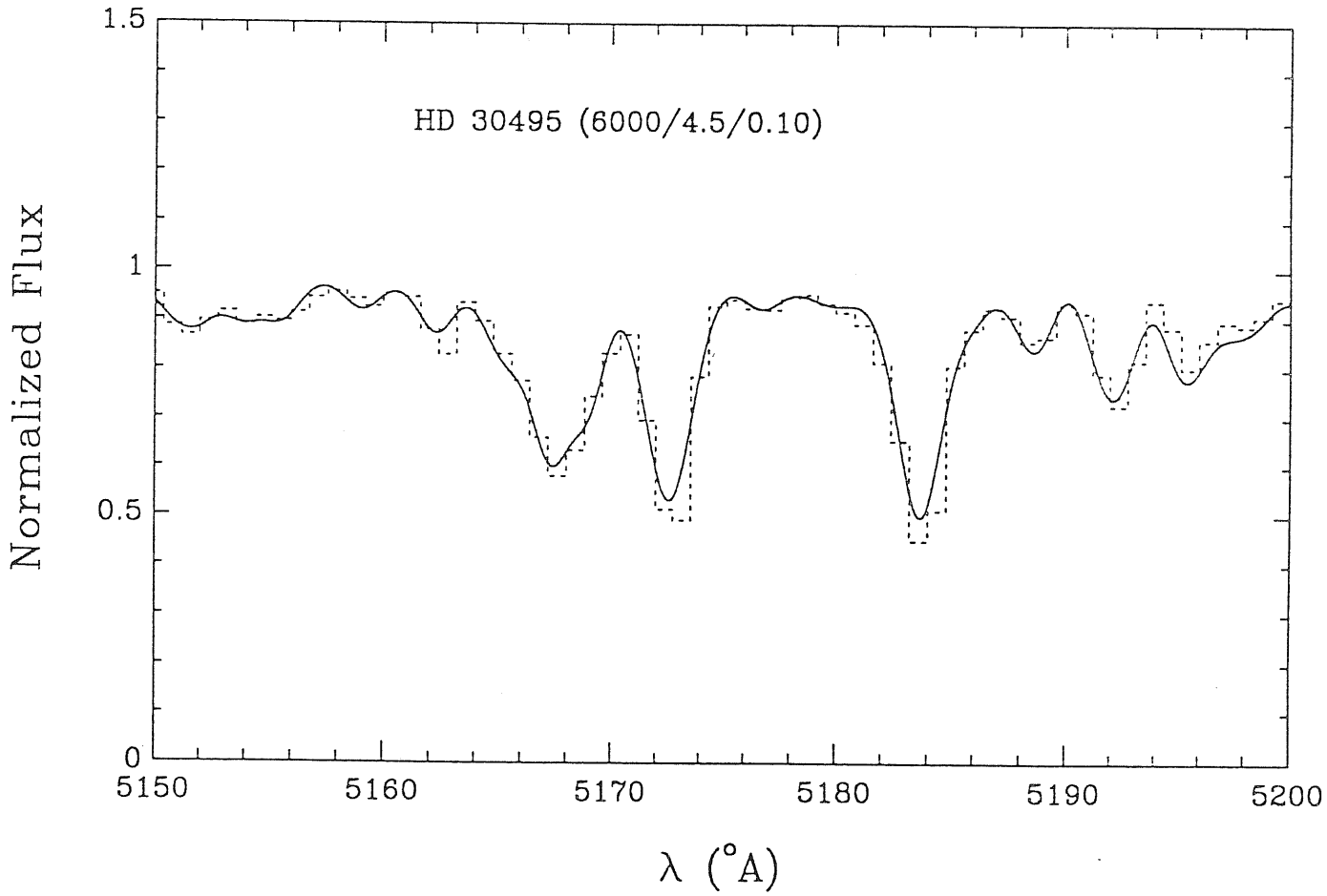
HD 30495 (6000/4.5/0.10)
Normalized Flux
1.5
1
0.5
0
5150
5160
5170
5180
5190
5200
λ (°A)

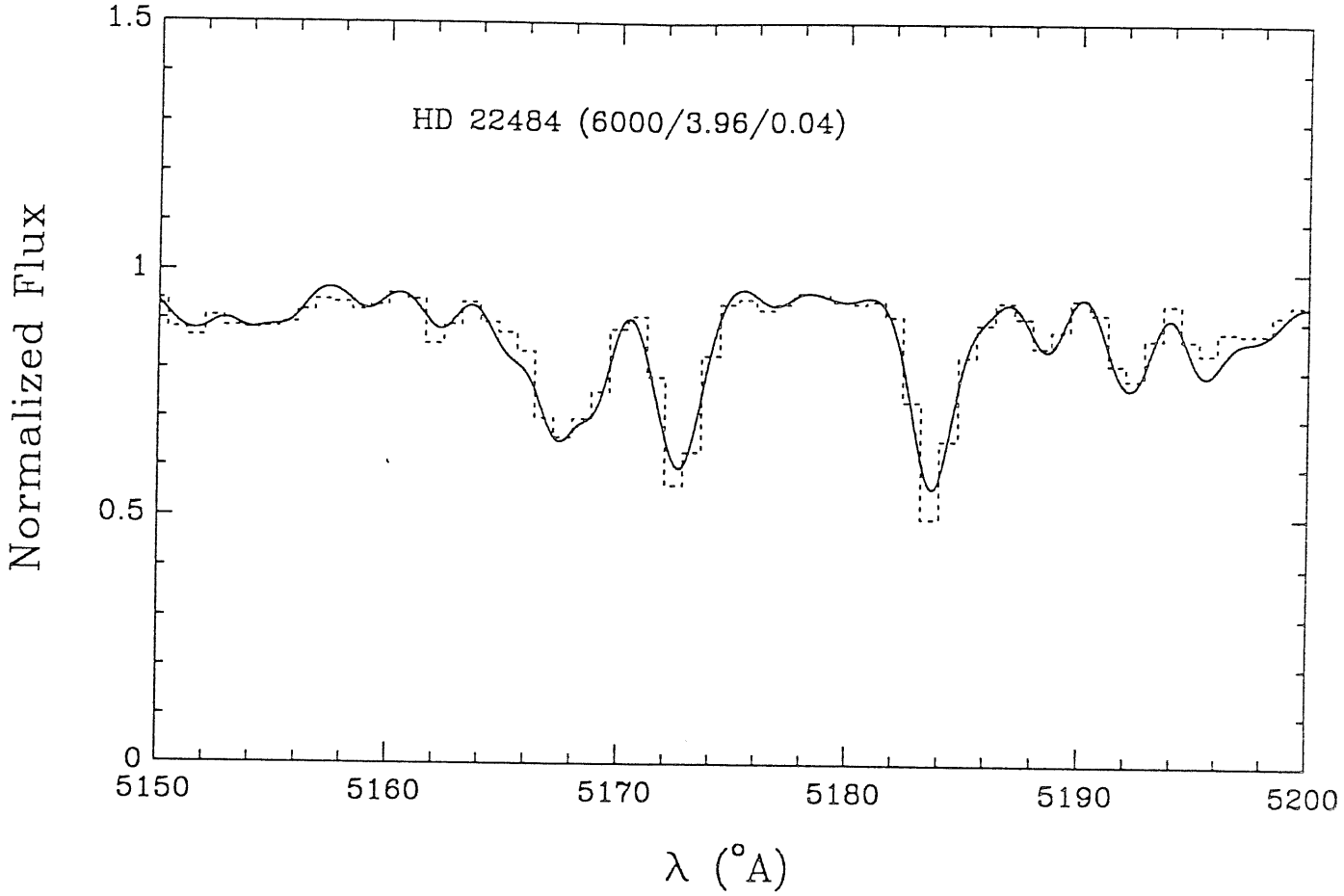
HD 22484 (6000/3.96/0.04)
Normalized Flux
1.5
1
0.5
0
5150
5160
5170
5180
5190
5200
λ (°A)

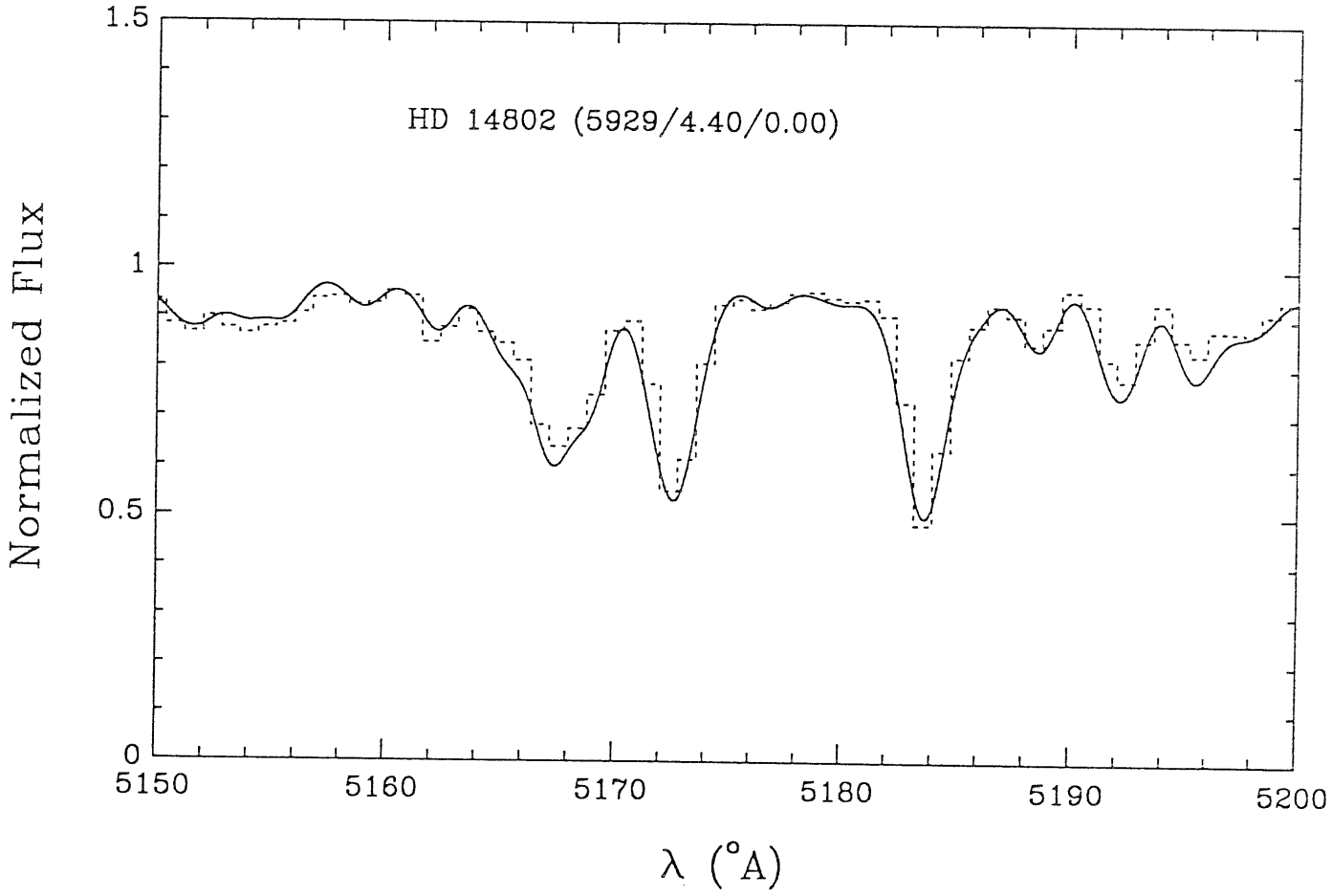
HD 14802 (5929/4.40/0.00)
Normalized Flux
1.5
1
0.5
0
5150
5160
5170
5180
5190
5200
λ (°A)

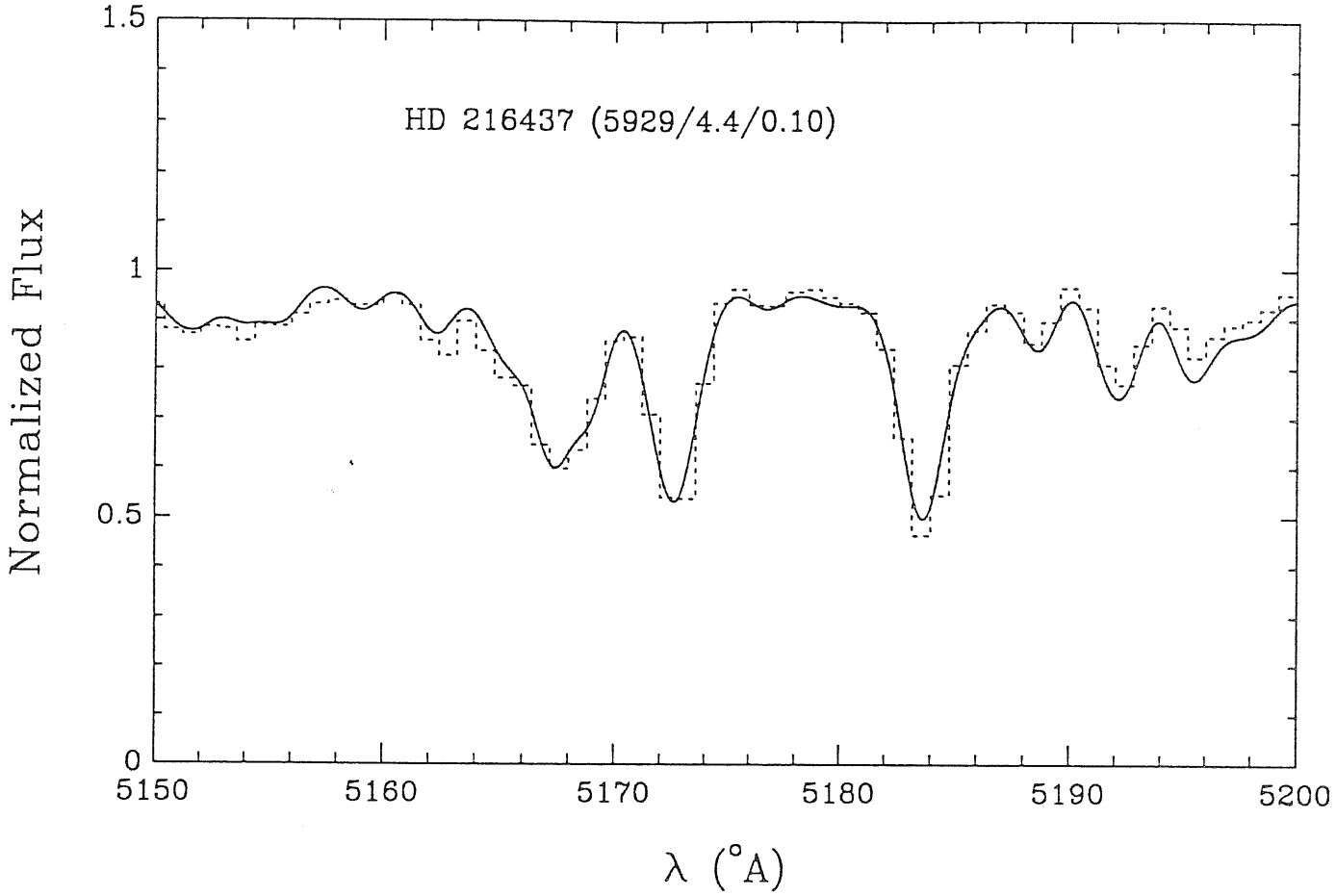
HD 216437 (5929/4.4/0.10)
Normalized Flux
1.5
1
0.5
0
5150
5160
5170
5180
5190
5200
λ (°A)

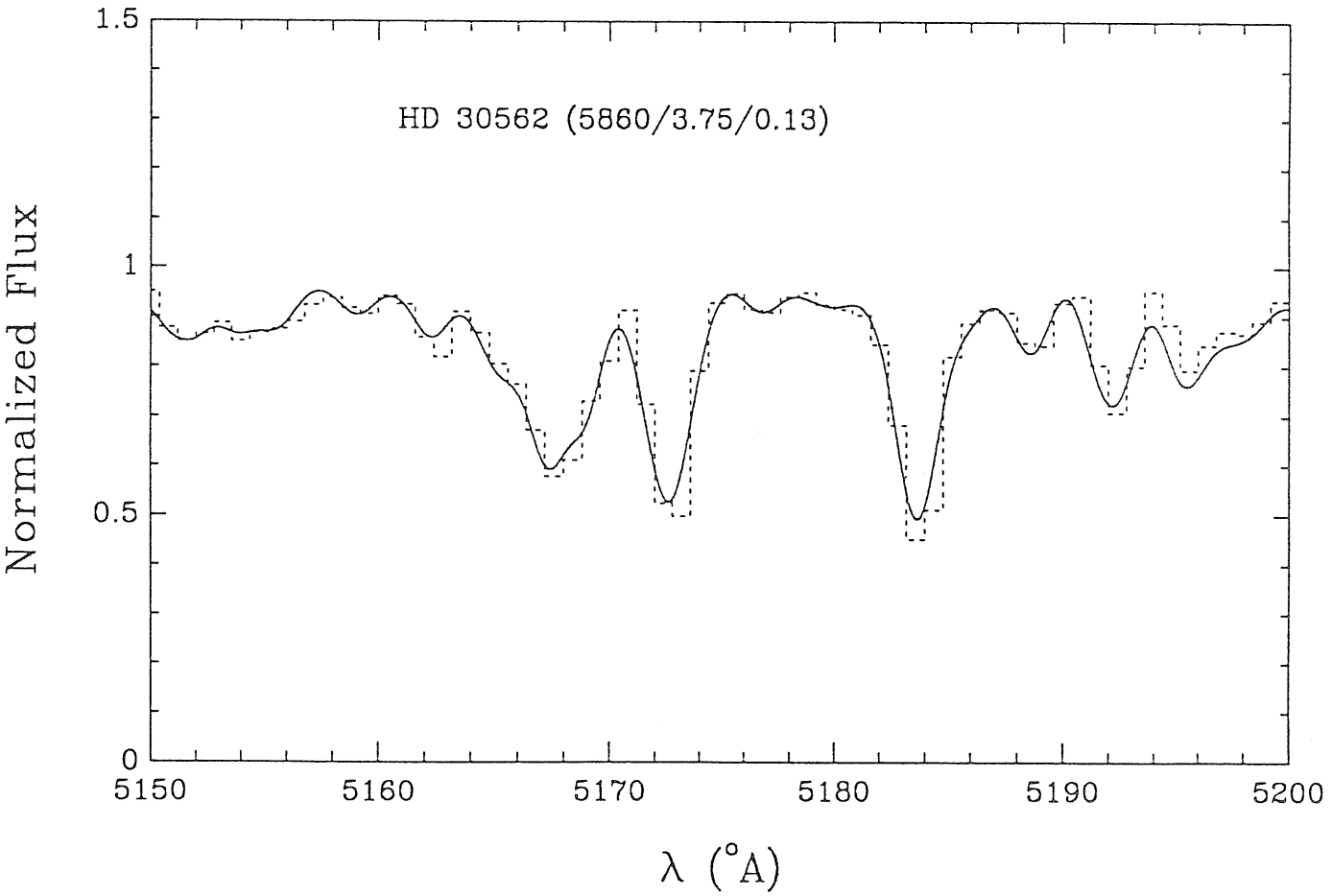
HD 30562 (5860/3.75/0.13)
Normalized Flux
1.5
1
0.5
0
5150
5160
5170
5180
5190
5200
λ (°A)

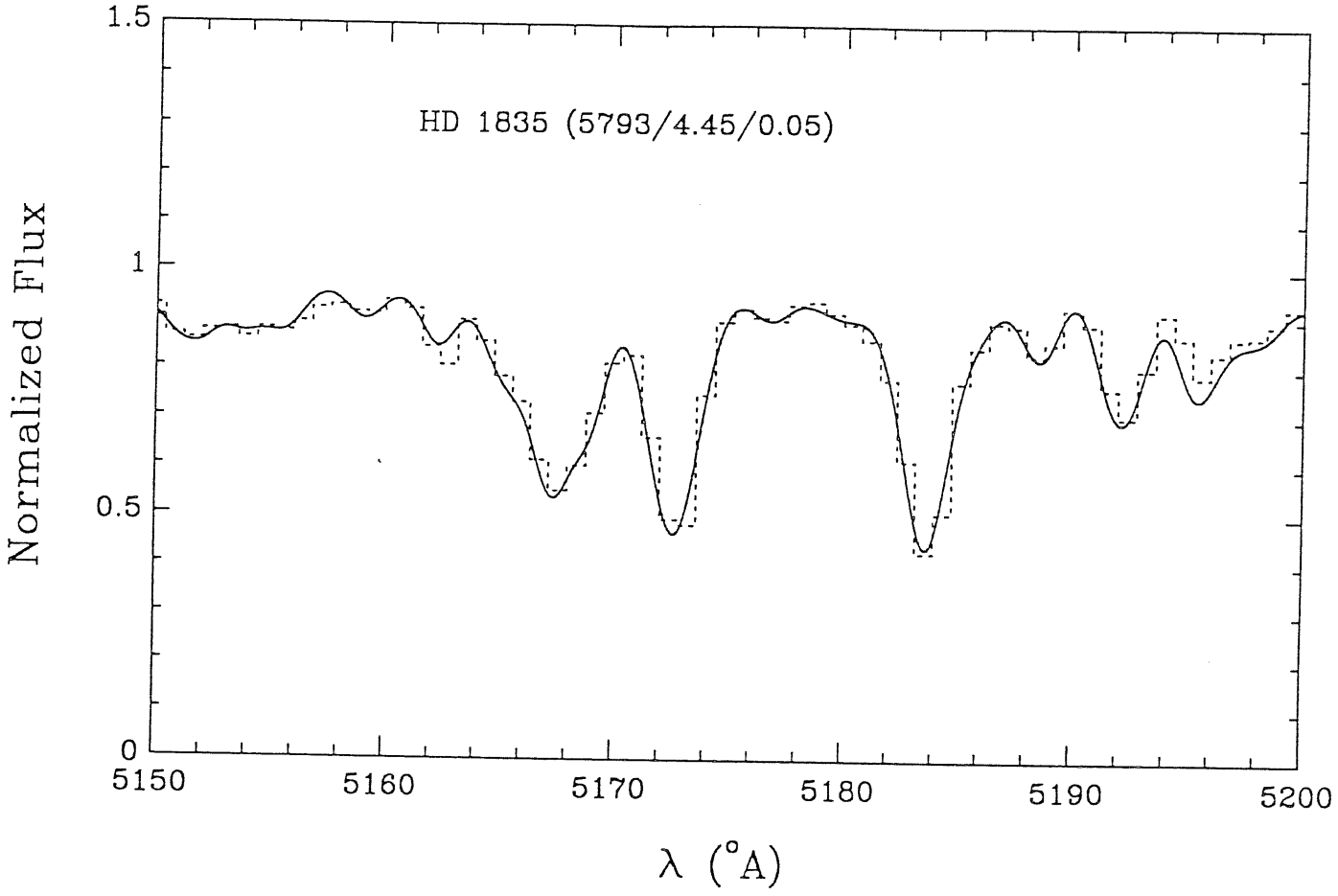
HD 1835 (5793/4.45/0.05)
Normalized Flux
1.5
1
0.5
0
5150
5160
5170
5180
5190
5200
λ (°A)

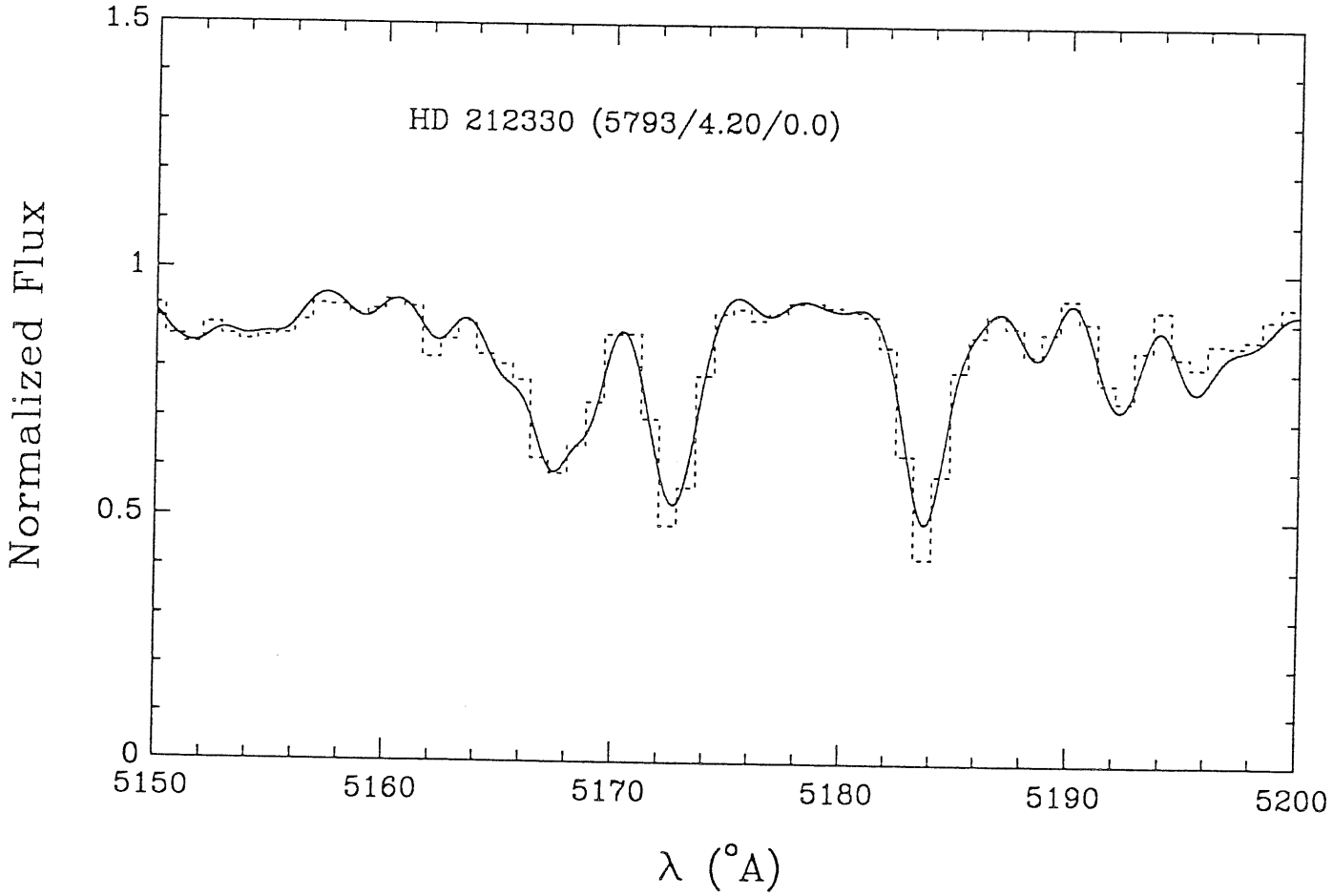
HD 212330 (5793/4.20/0.0)
Normalized Flux
1.5
1
0.5
0
5150
5160
5170
5180
5190
5200
λ (°A)

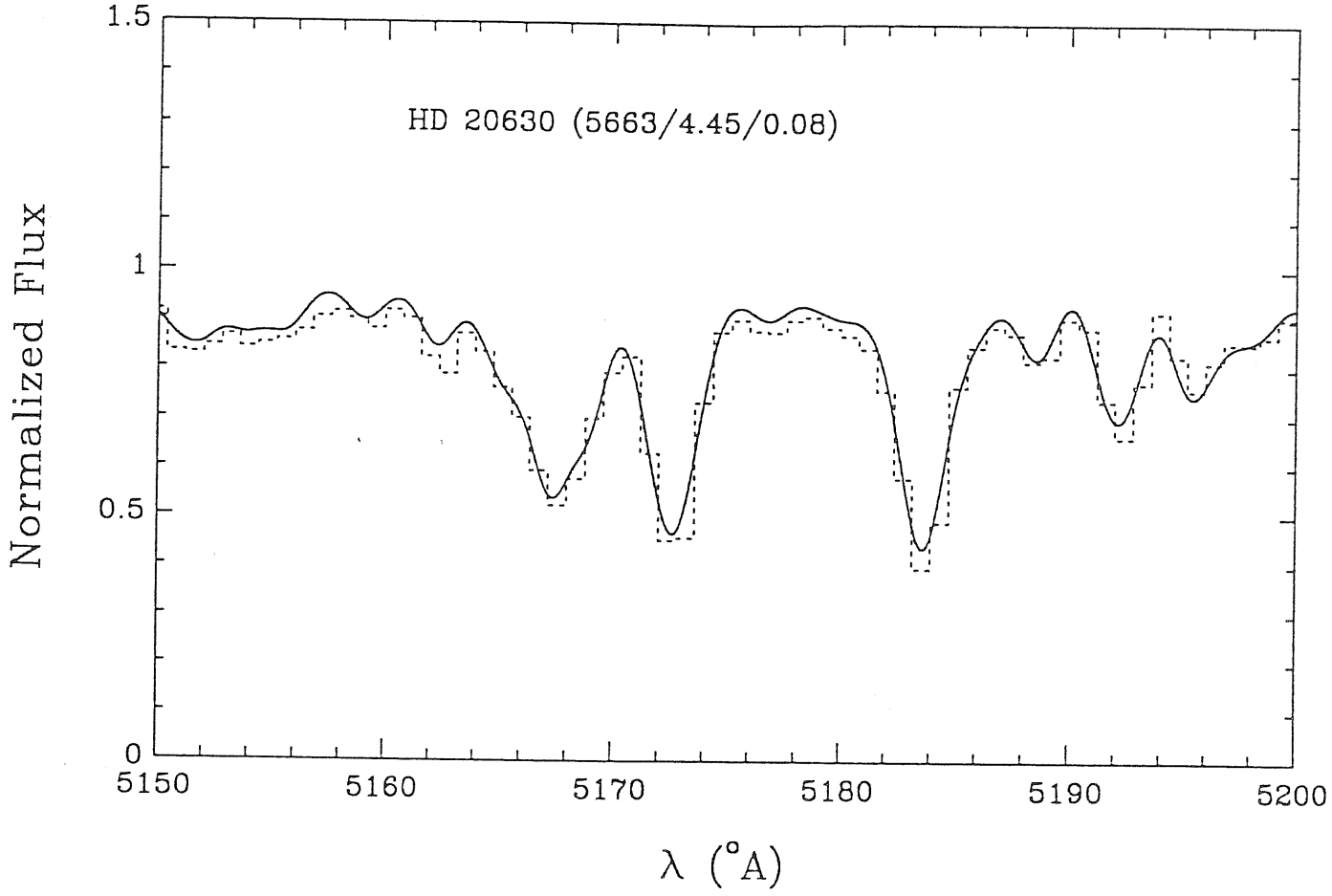
HD 20630 (5663/4.45/0.08)
Normalized Flux
1.5
1
0.5
0
5150
5160
5170
5180
5190
5200
λ (°A)

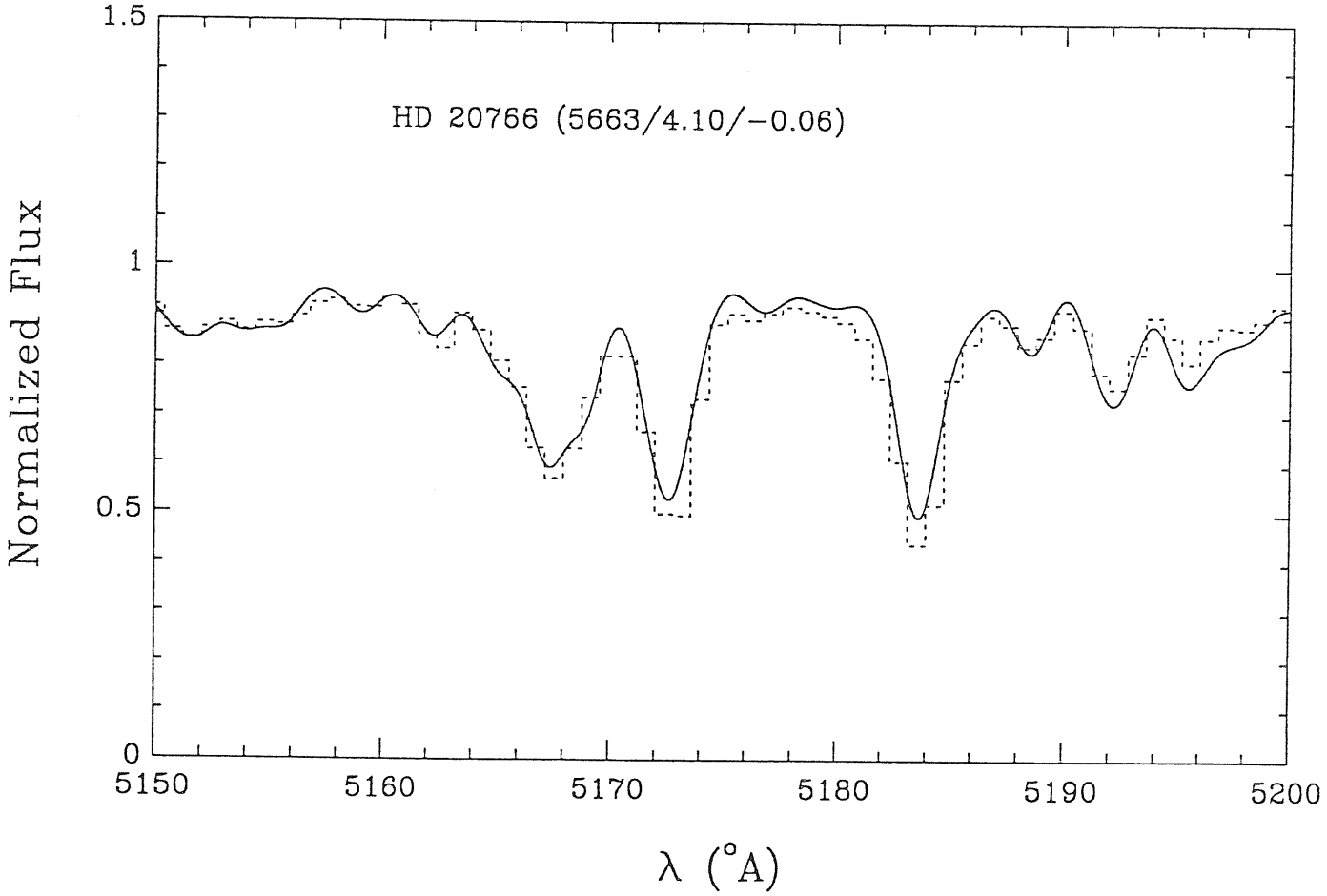
HD 20766 (5663/4.10/−0.06)
Normalized Flux
1.5
1
0.5
0
5150
5160
5170
5180
5190
5200
λ (°A)

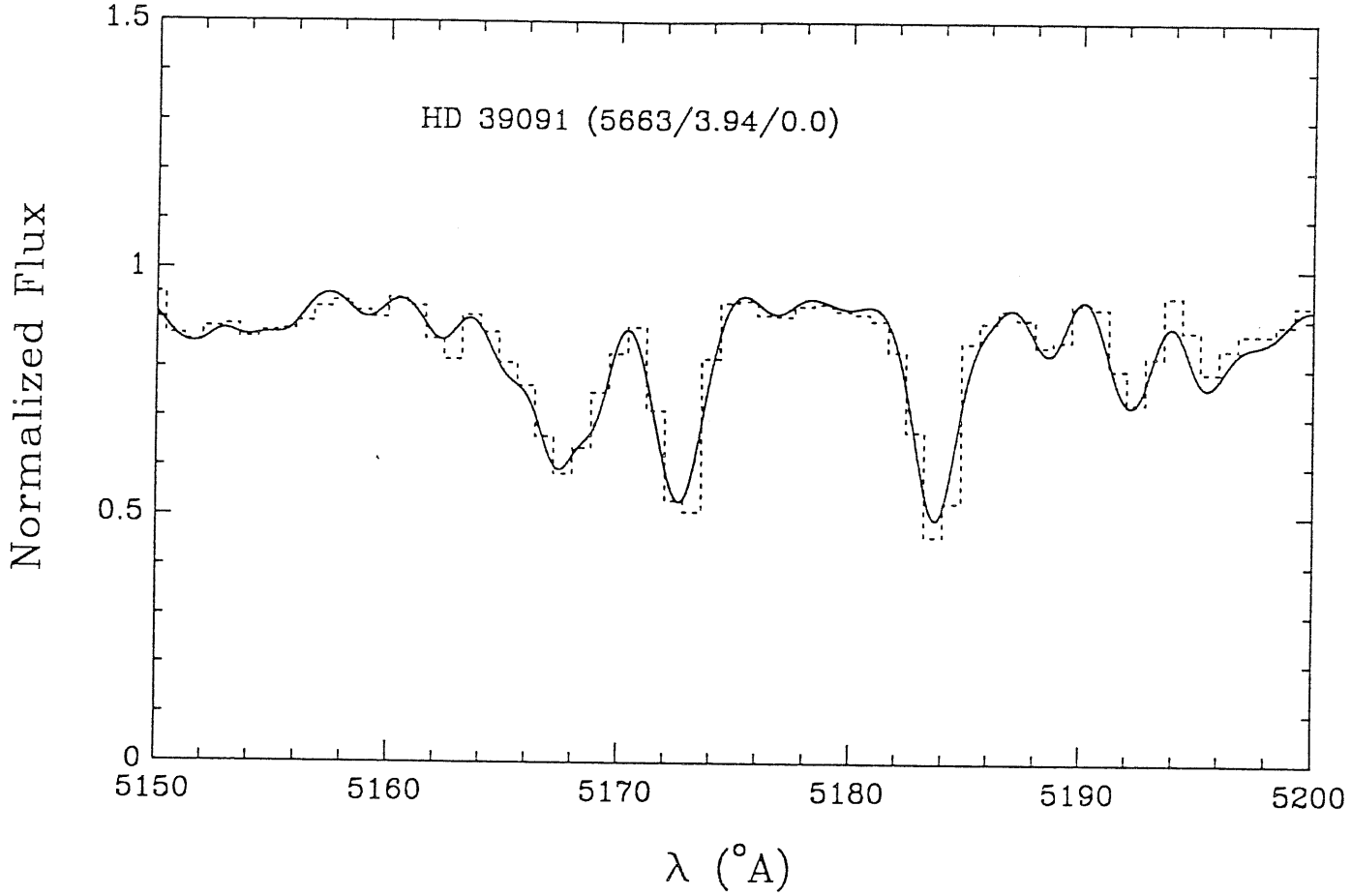
HD 39091 (5663/3.94/0.0)
Normalized Flux
1.5
1
0.5
0
5150
5160
5170
5180
5190
5200
λ (°A)

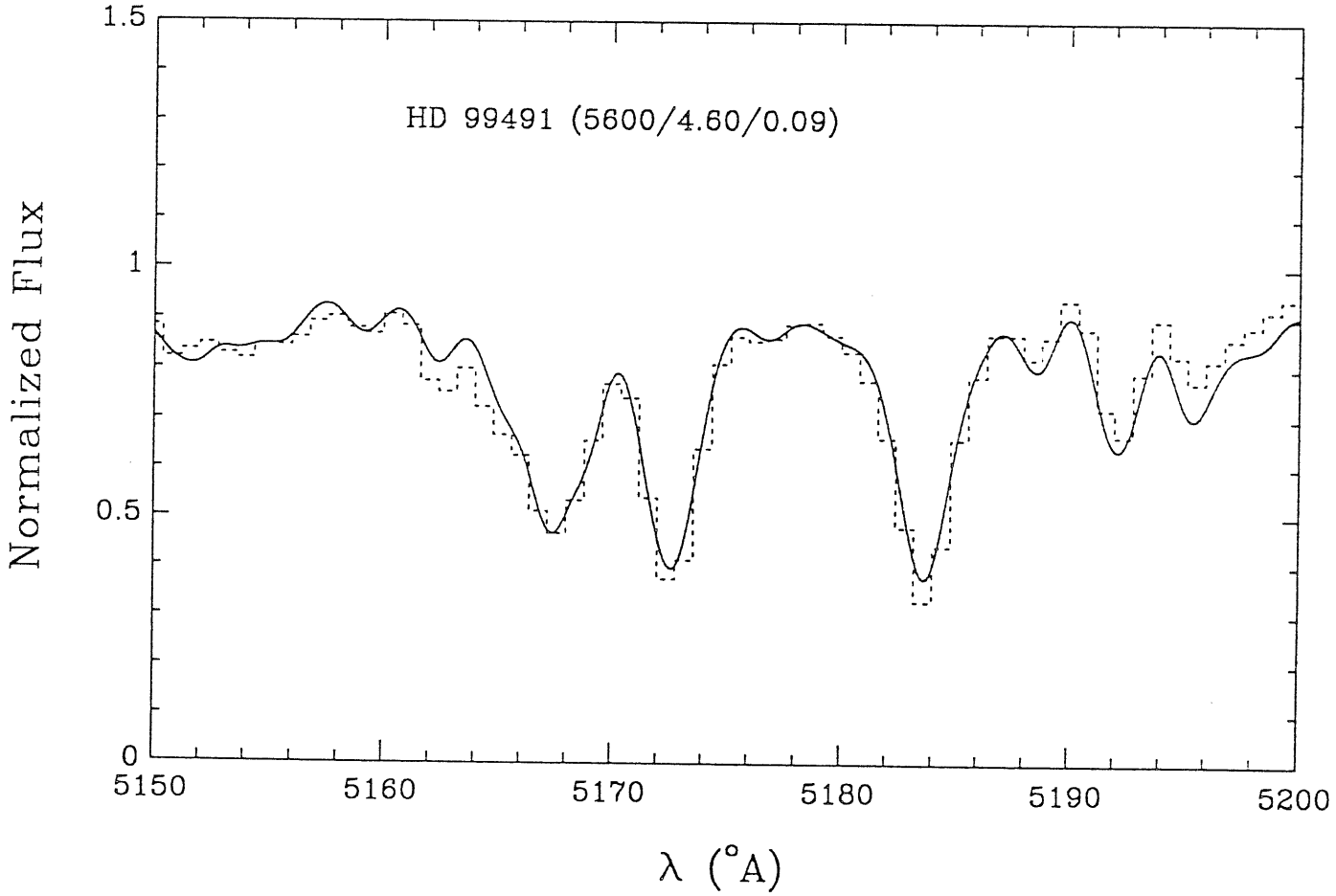
HD 99491 (5600/4.60/0.09)
Normalized Flux
1.5
1
0.5
0
5150
5160
5170
5180
5190
5200
λ (°A)

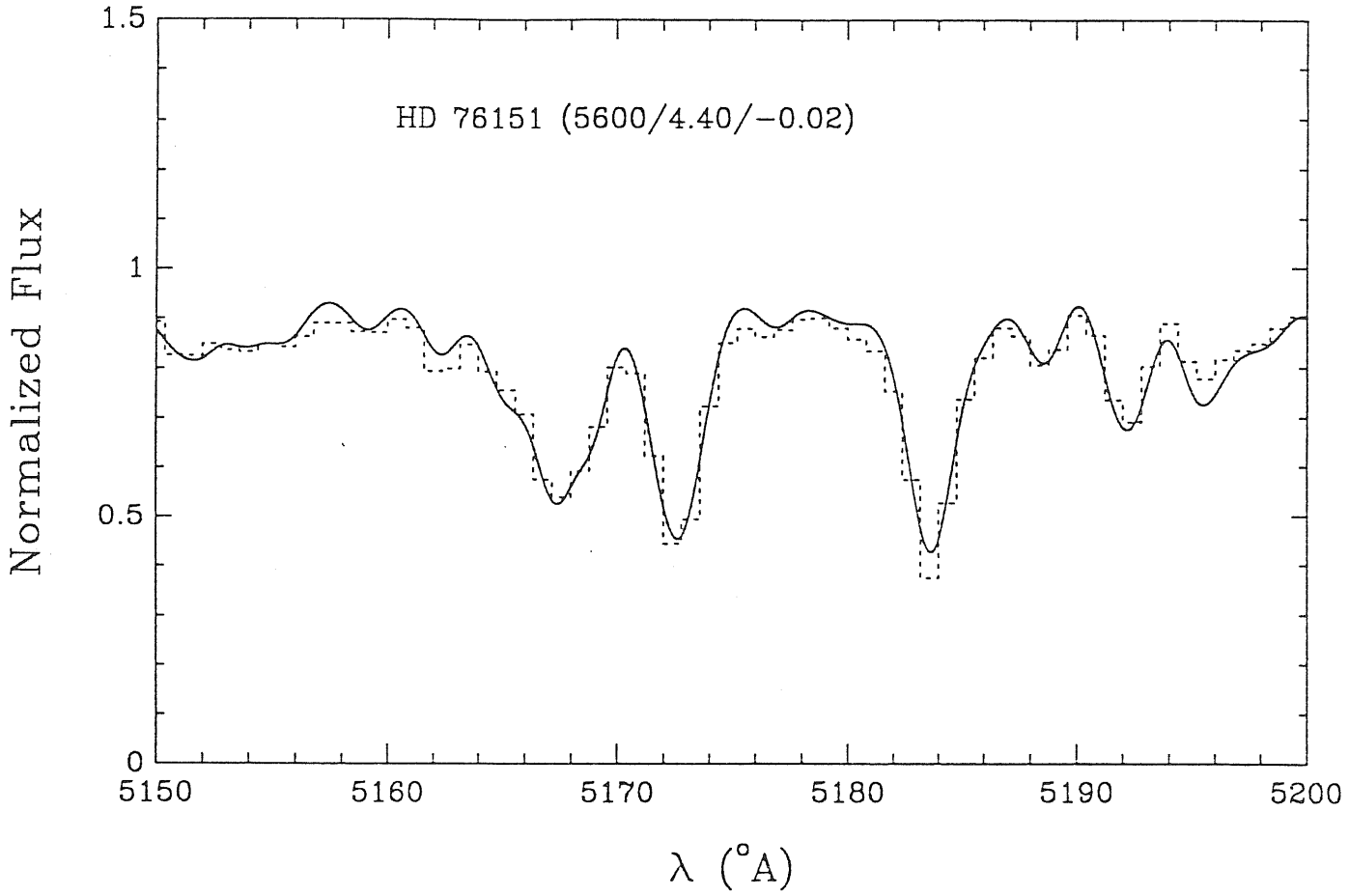
HD 76151 (5600/4.40/−0.02)
Normalized Flux
1.5
1
0.5
0
5150
5160
5170
5180
5190
5200
λ (°A)

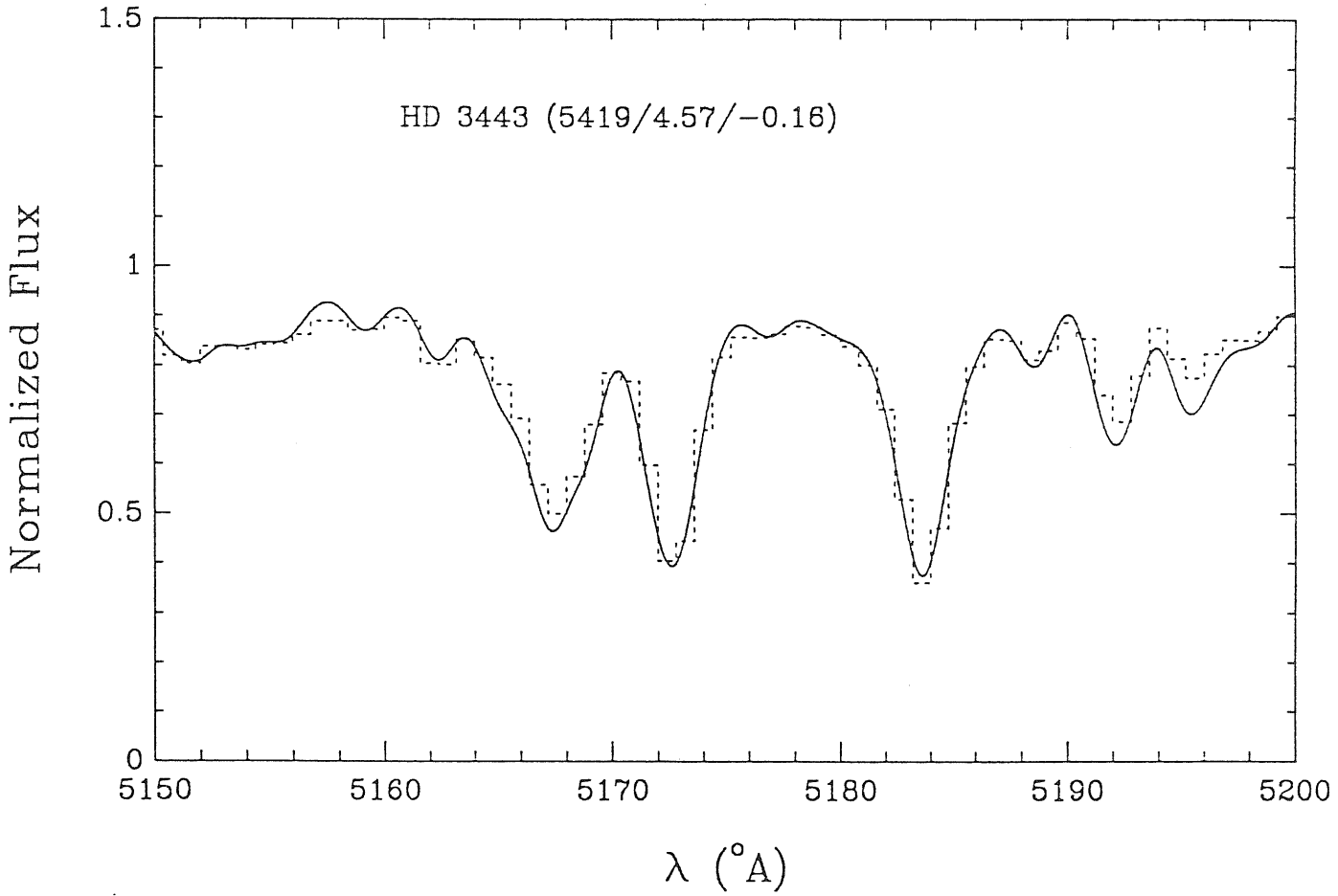
HD 3443 (5419/4.57/−0.16)
Normalized Flux
1.5
1
0.5
0
5150
5160
5170
5180
5190
5200
λ (°A)

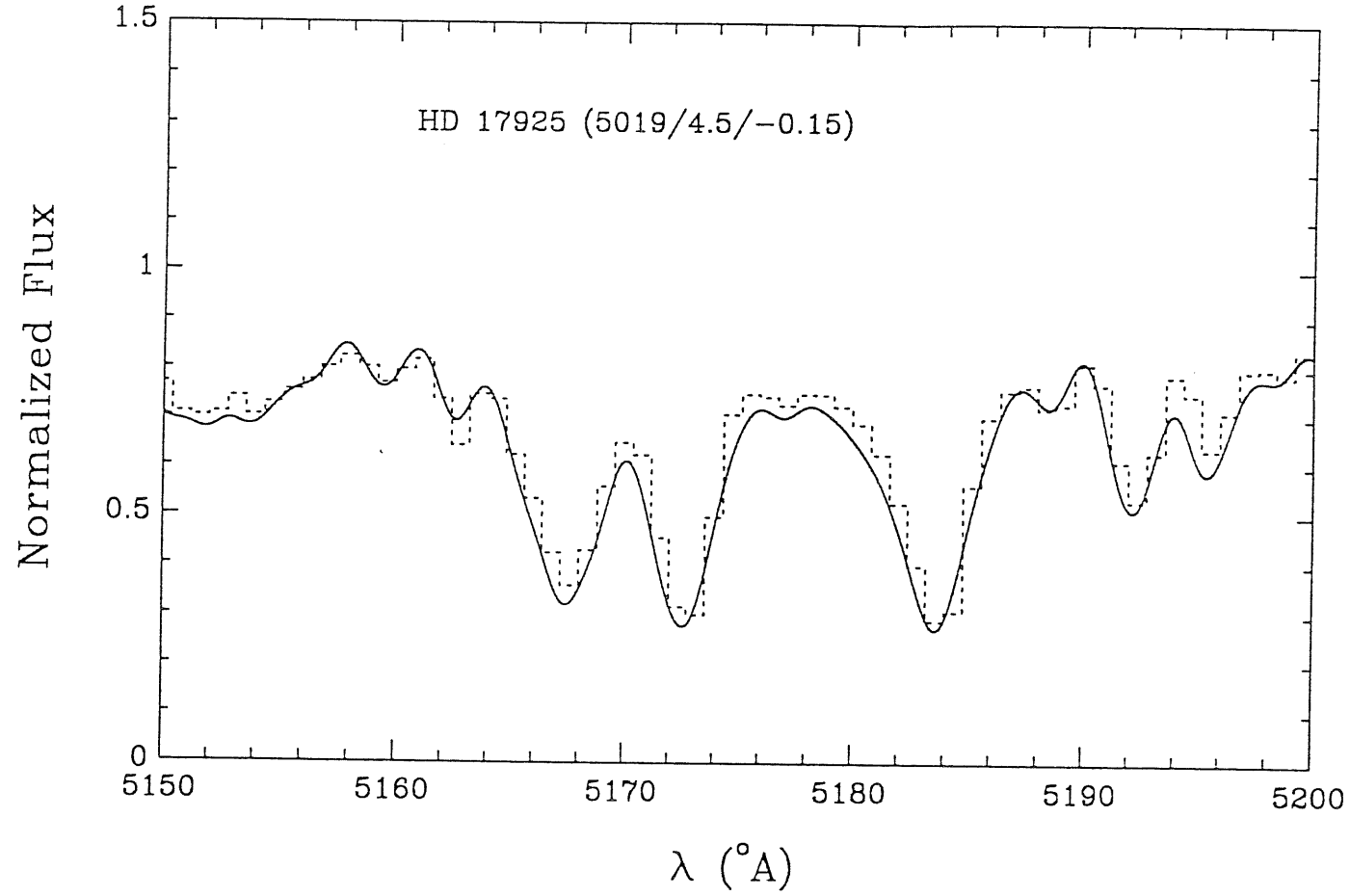
HD 17925 (5019/4.5/−0.15)
Normalized Flux
1.5
1
0.5
0
5150
5160
5170
5180
5190
5200
λ (°A)

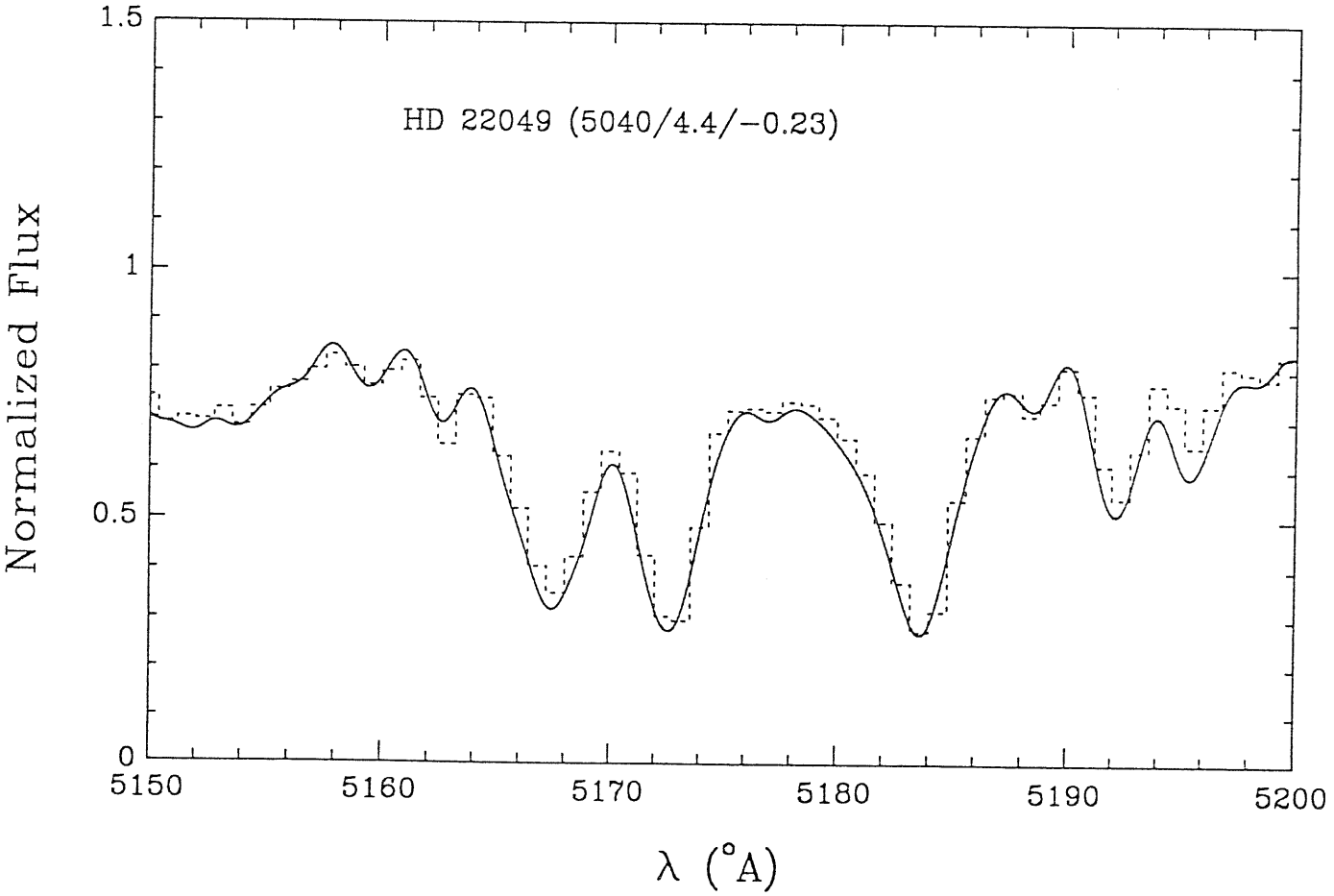
HD 22049 (5040/4.4/−0.23)
Normalized Flux
1.5
1
0.5
0
5150
5160
5170
5180
5190
5200
λ (°A)

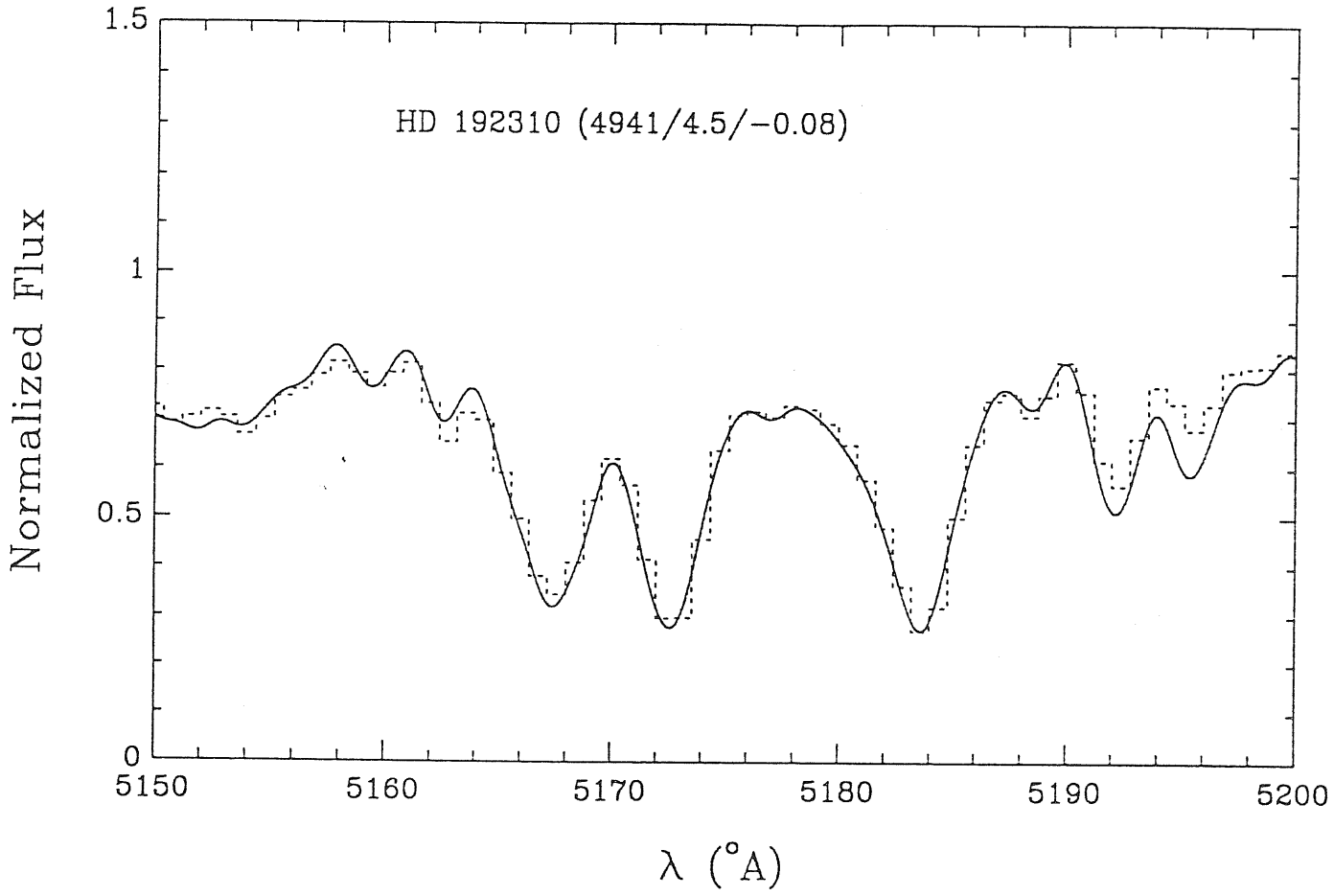
HD 192310 (4941/4.5/−0.08)
Normalized Flux
1.5
1
0.5
0
5150
5160
5170
5180
5190
5200
λ (°A)

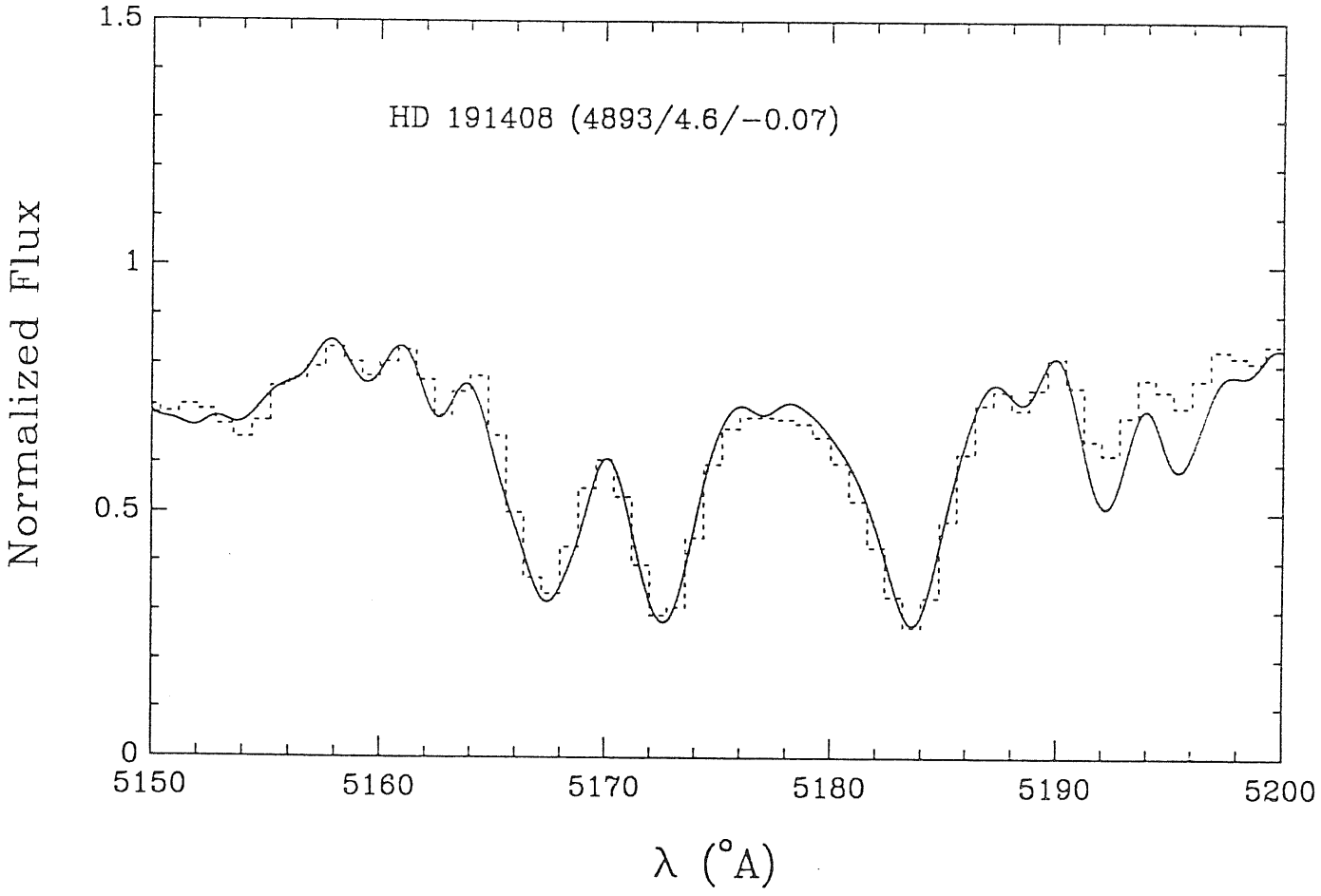
HD 191408 (4893/4.6/−0.07)
Normalized Flux
1.5
1
0.5
0
5150
5160
5170
5180
5190
5200
λ (°A)

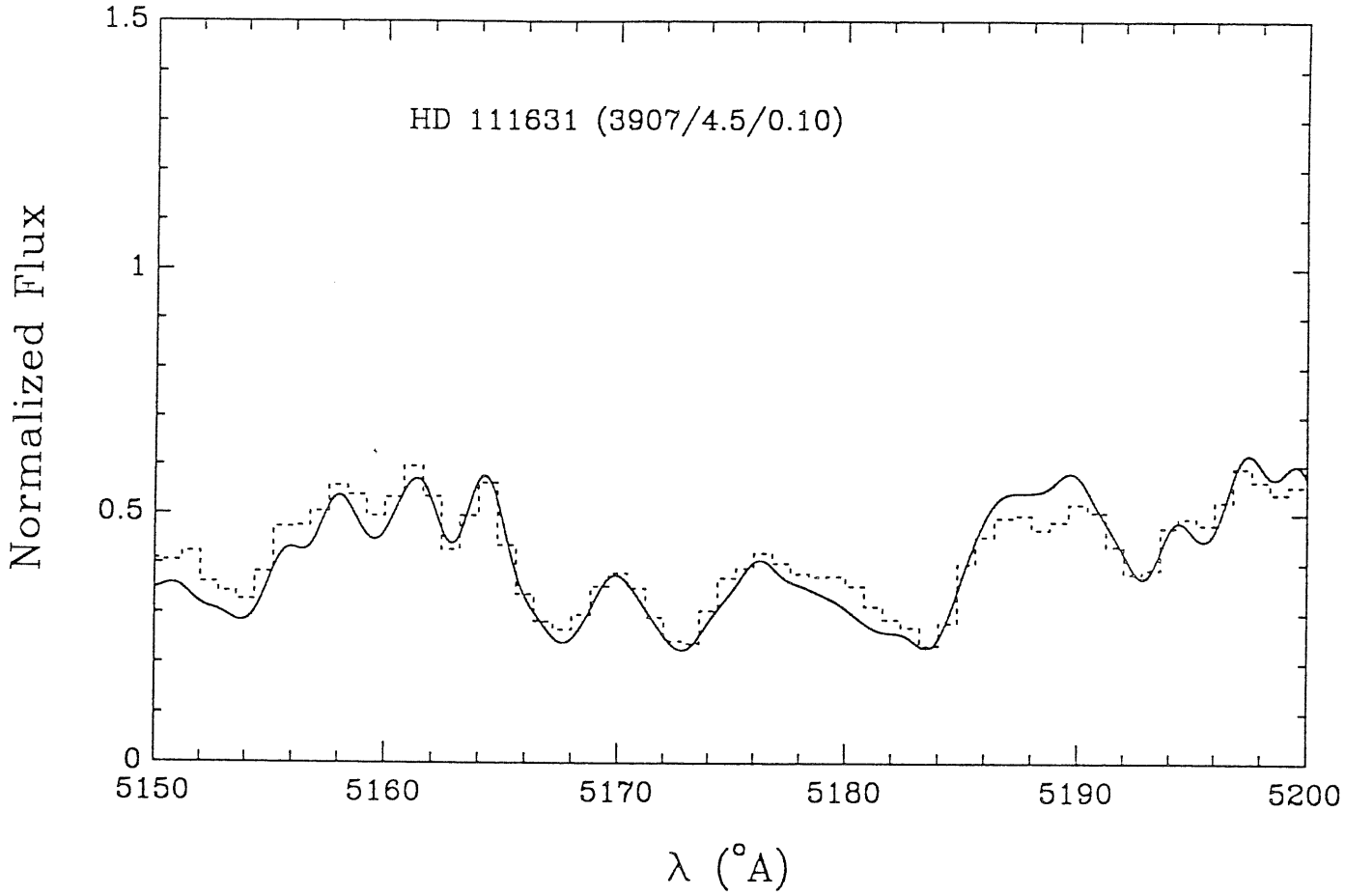
HD 111631 (3907/4.5/0.10)
Normalized Flux
1.5
1
0.5
0
5150
5160
5170
5180
5190
5200
λ (°A)

D.2 Giants

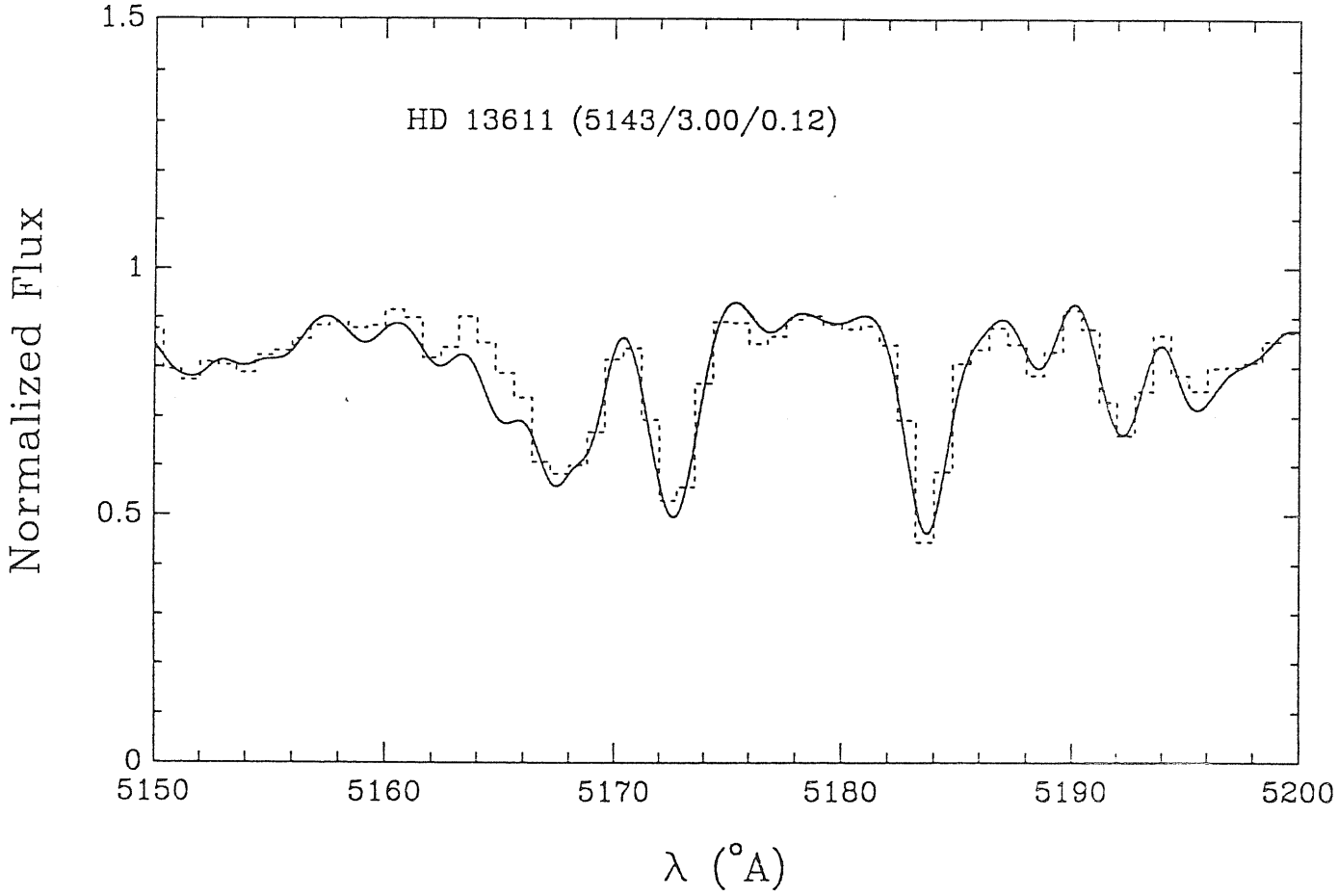
HD 13611 (5143/3.00/0.12)
Normalized Flux
1.5
1
0.5
0
5150
5160
5170
5180
5190
5200
λ (°A)

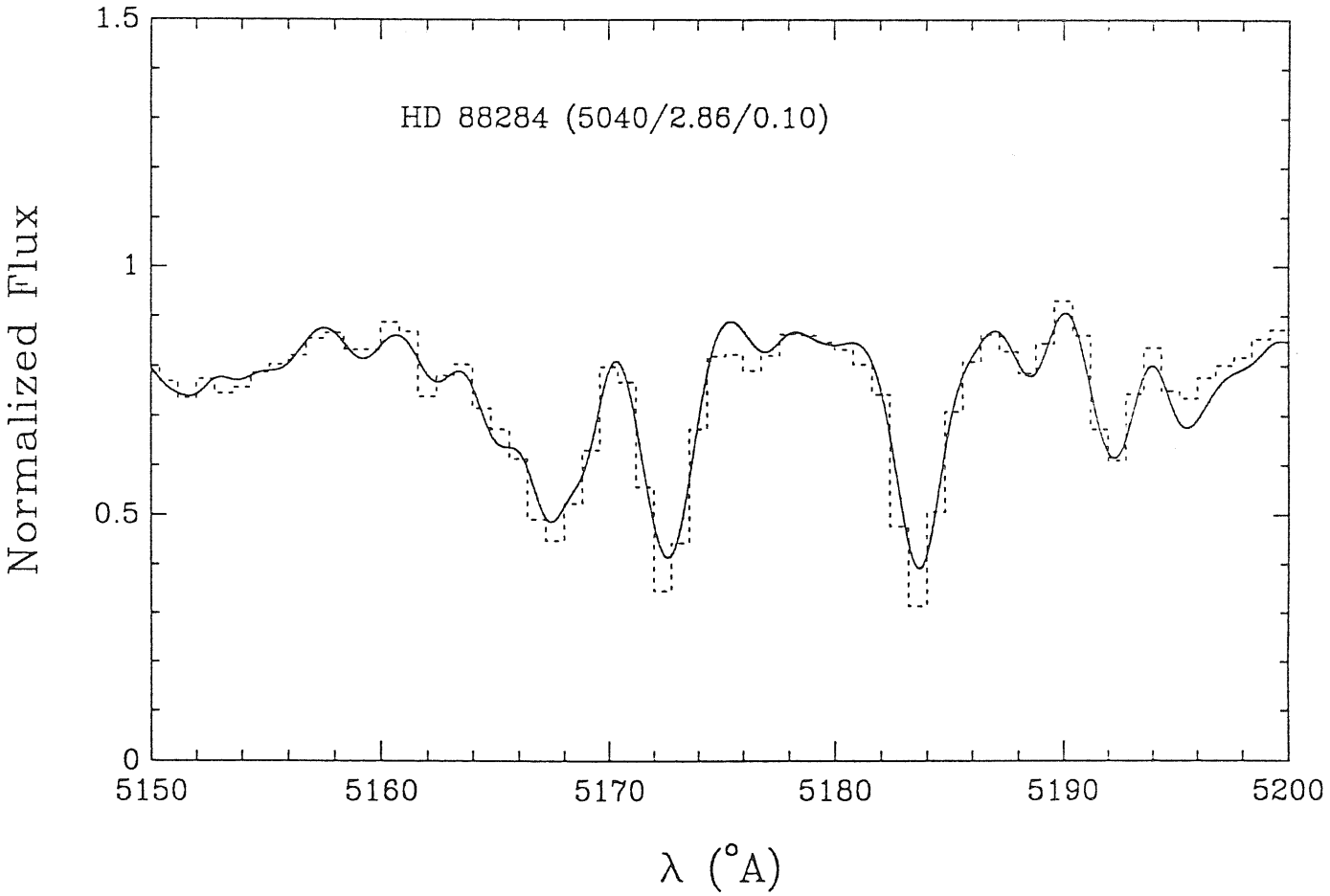
HD 88284 (5040/2.86/0.10)
Normalized Flux
1.5
1
0.5
0
5150
5160
5170
5180
5190
5200
λ (°A)

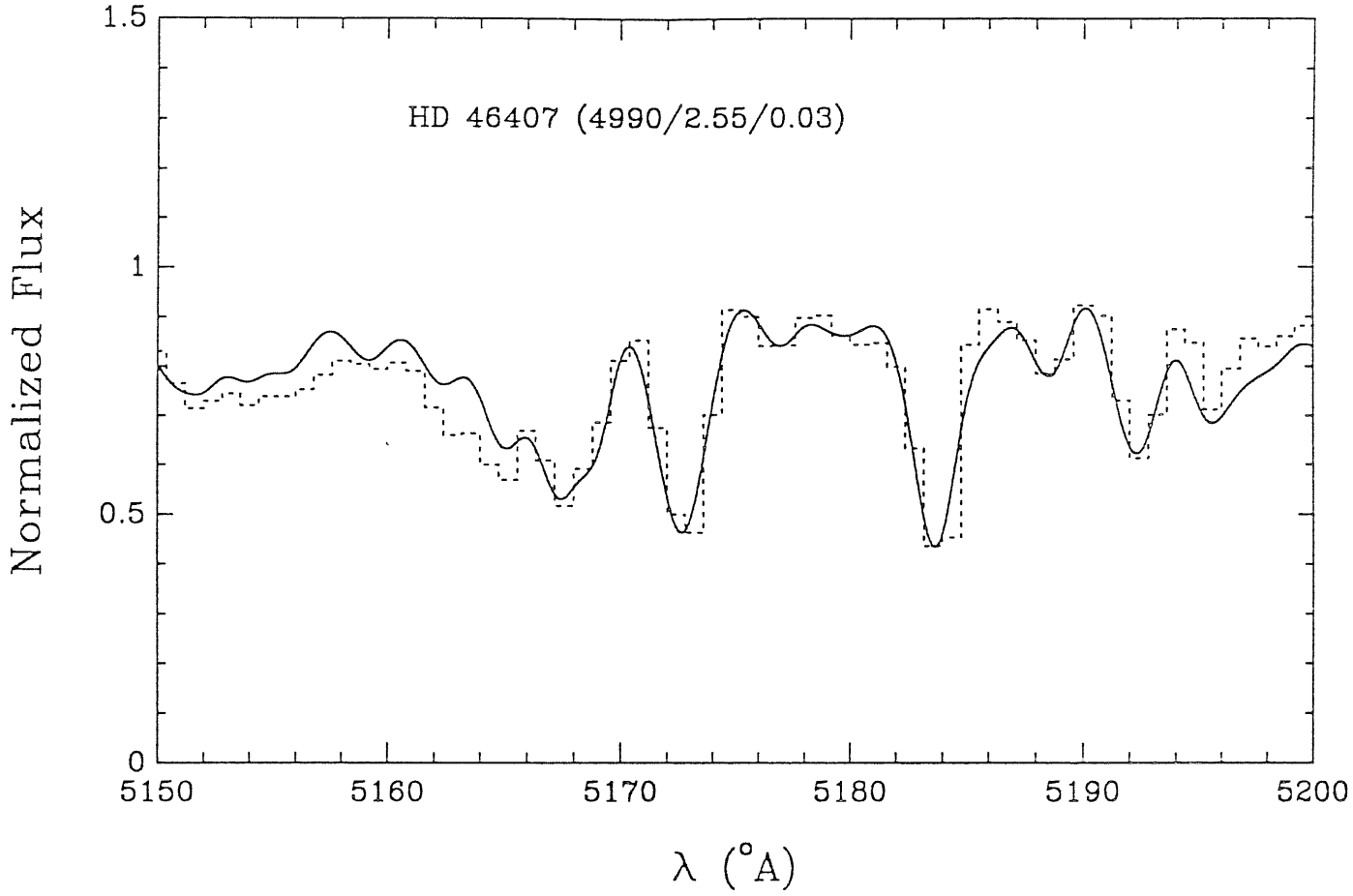
HD 46407 (4990/2.55/0.03)
Normalized Flux
1.5
1
0.5
0
5150
5160
5170
5180
5190
5200
λ (°A)

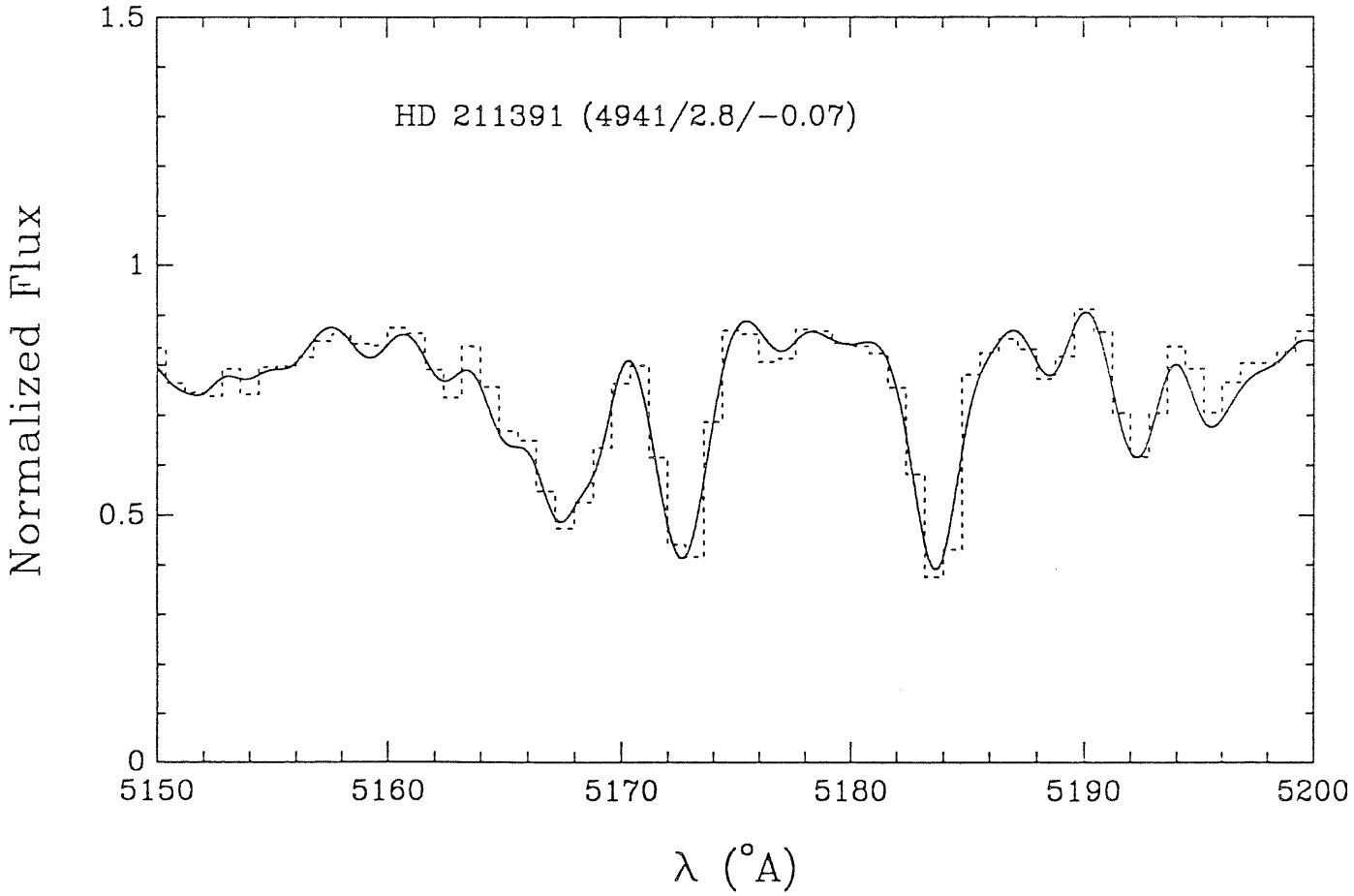
HD 211391 (4941/2.8/−0.07)
Normalized Flux
1.5
1
0.5
0
5150
5160
5170
5180
5190
5200
λ (°A)

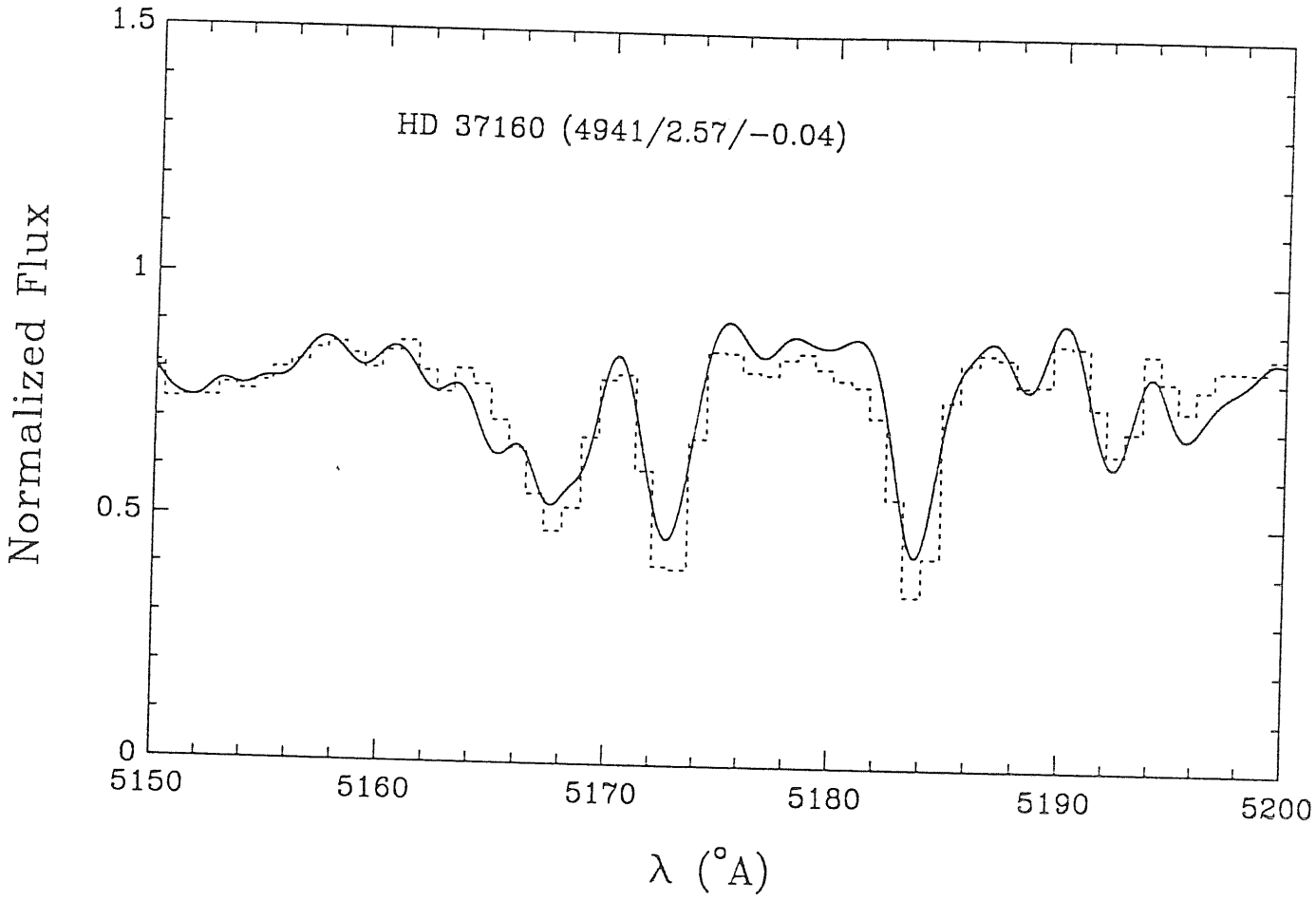
HD 37160 (4941/2.57/−0.04)
Normalized Flux
1.5
1
0.5
0
5150
5160
5170
5180
5190
5200
λ (°A)

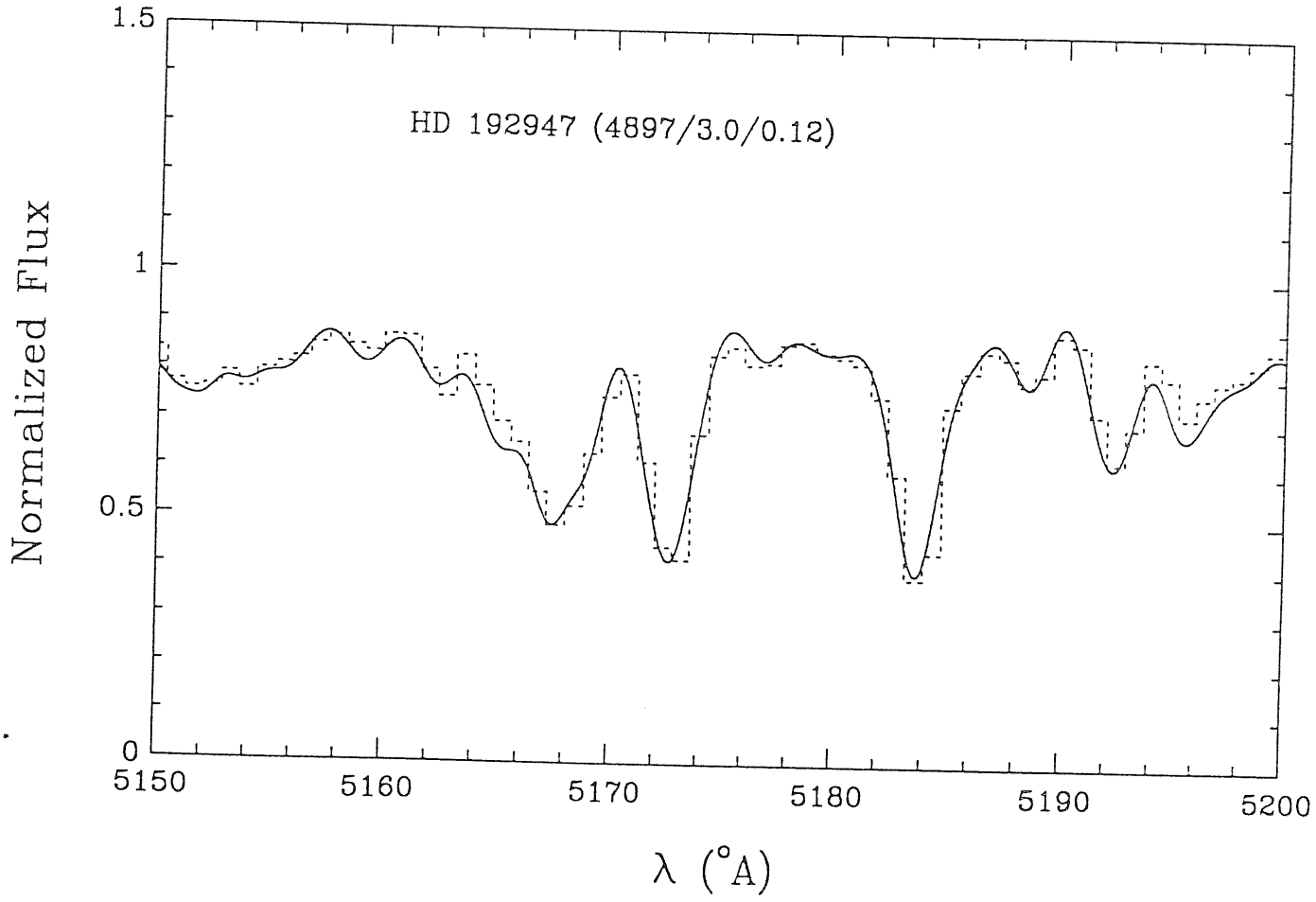
HD 192947 (4897/3.0/0.12)
Normalized Flux
1.5
1
0.5
0
5150
5160
5170
5180
5190
5200
λ (°A)

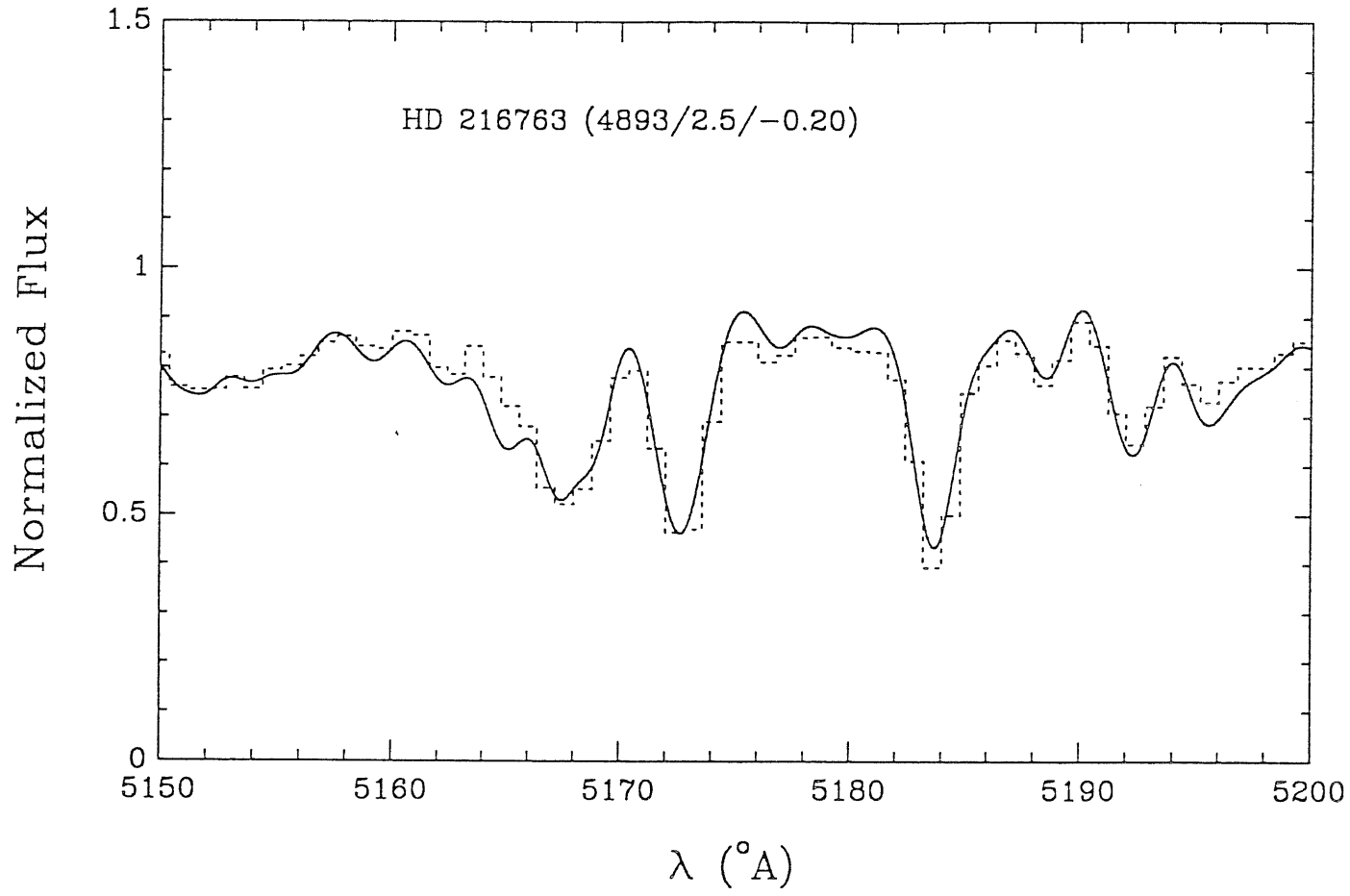
HD 216763 (4893/2.5/−0.20)
Normalized Flux
1.5
1
0.5
0
5150
5160
5170
5180
5190
5200
λ (°A)

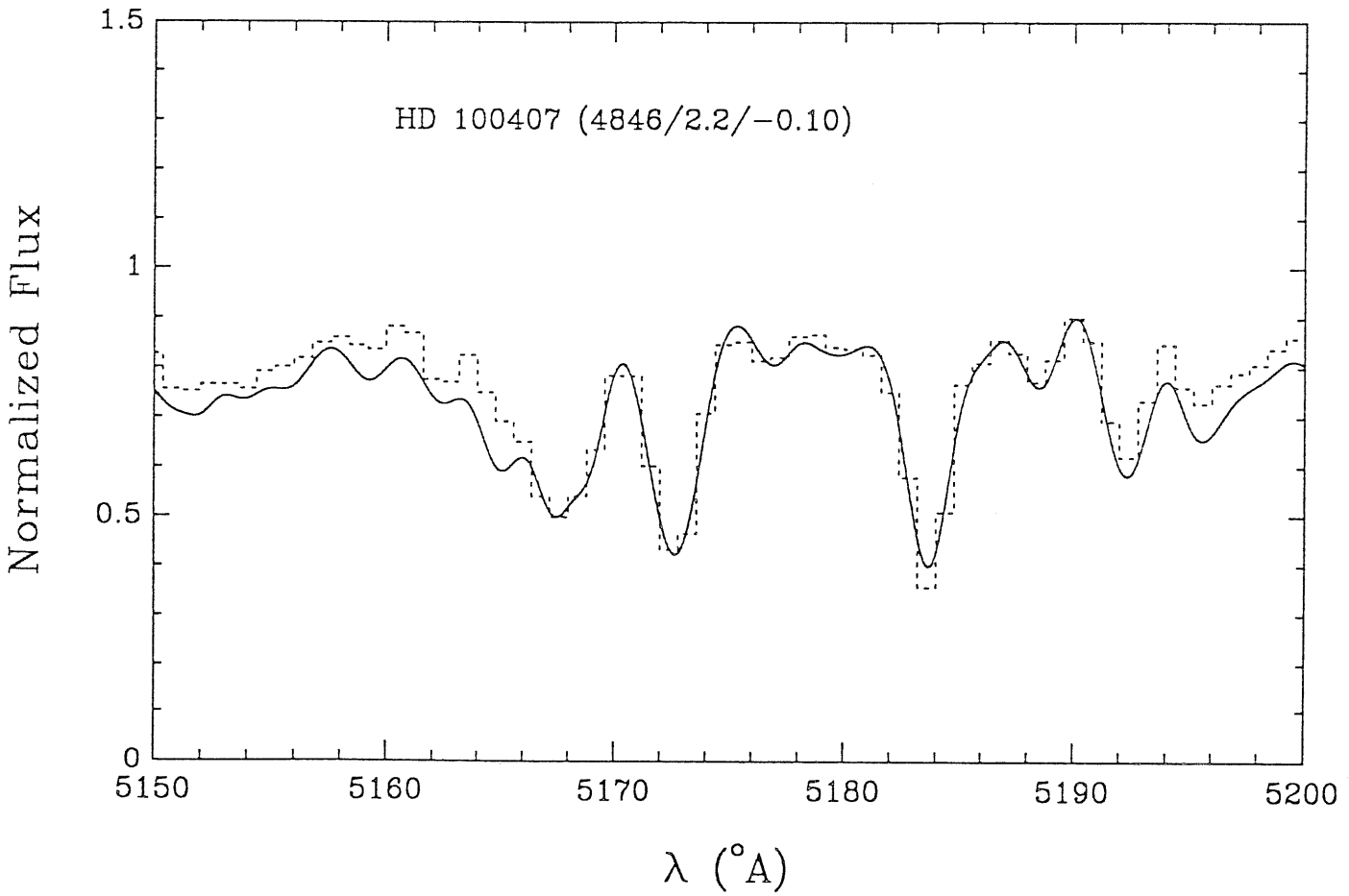
HD 100407 (4846/2.2/−0.10)
Normalized Flux
1.5
1
0.5
0
5150
5160
5170
5180
5190
5200
λ (°A)

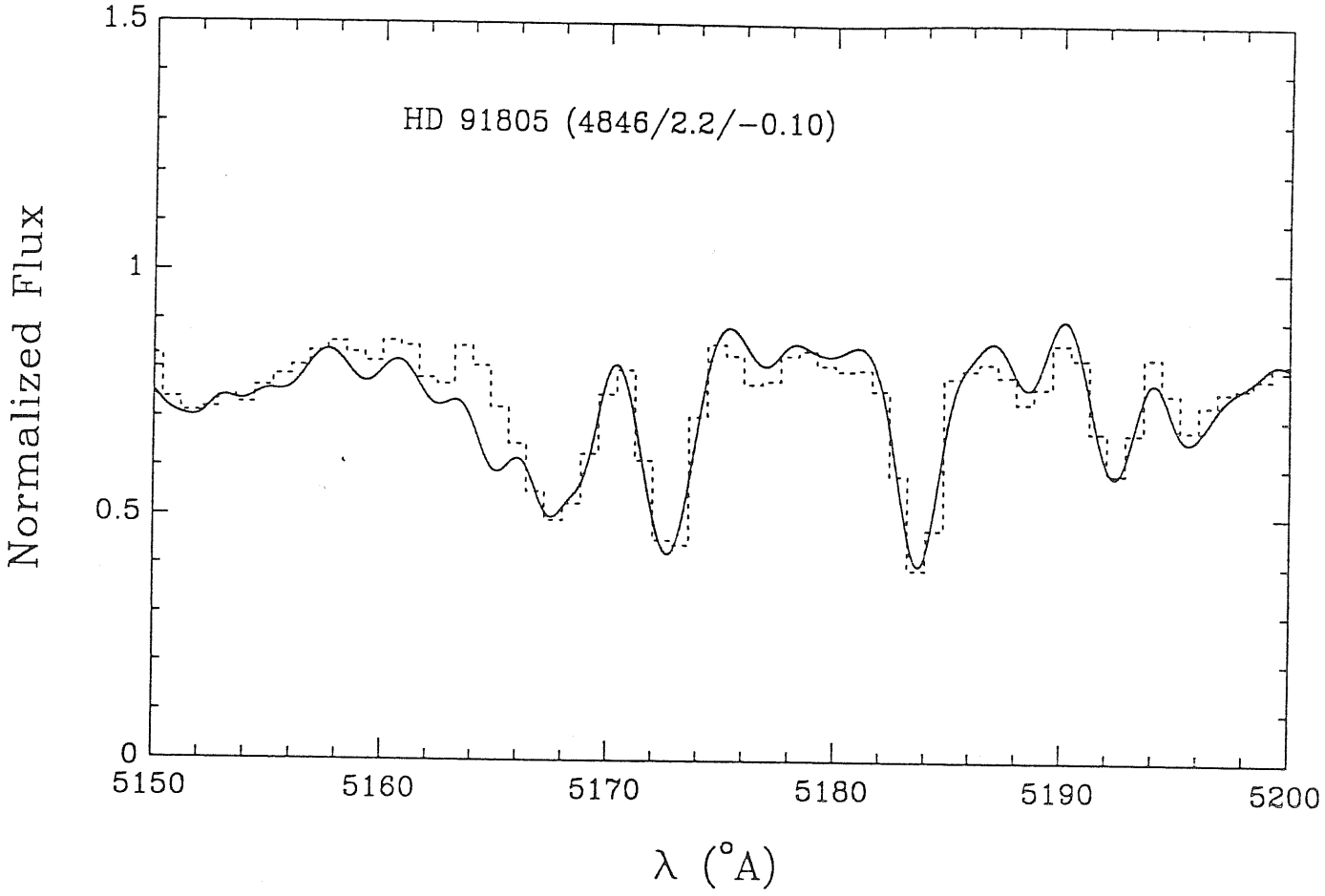
HD 91805 (4846/2.2/−0.10)
Normalized Flux
1.5
1
0.5
0
5150
5160
5170
5180
5190
5200
λ (°A)

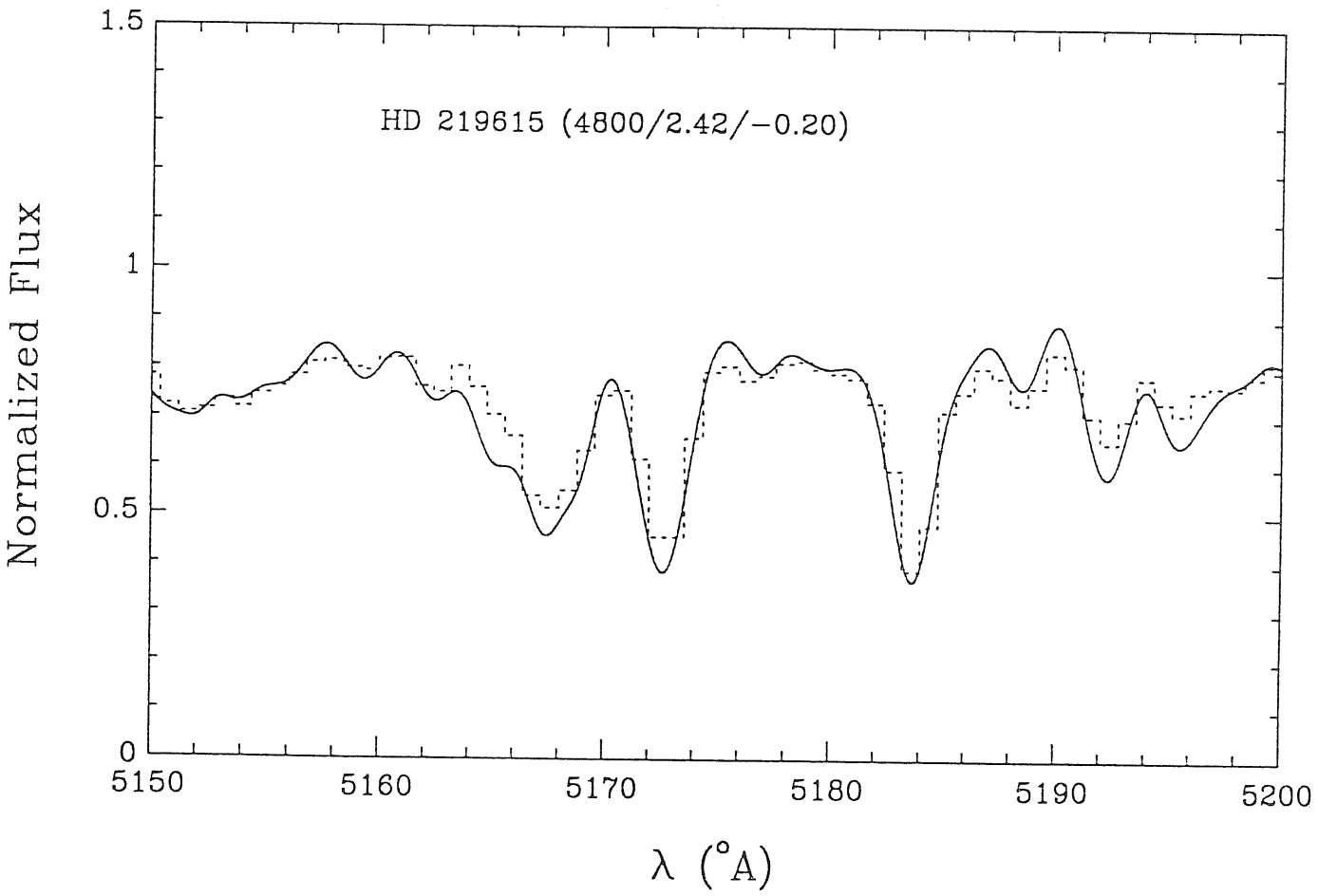
HD 219615 (4800/2.42/−0.20)
Normalized Flux
1.5
1
0.5
0
5150
5160
5170
5180
5190
5200
λ (°A)

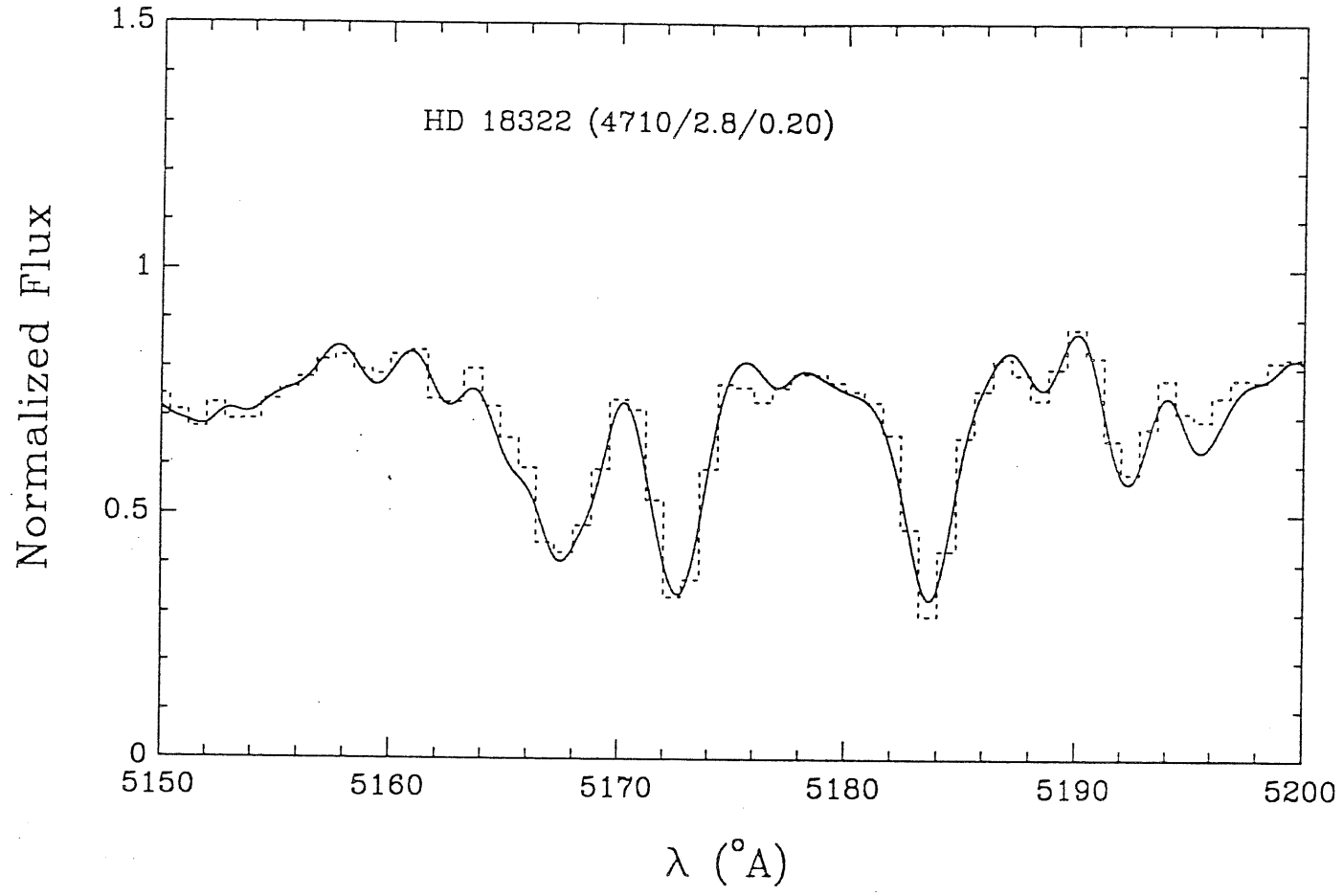
HD 18322 (4710/2.8/0.20)
Normalized Flux
1.5
1
0.5
0
5150
5160
5170
5180
5190
5200
λ (°A)

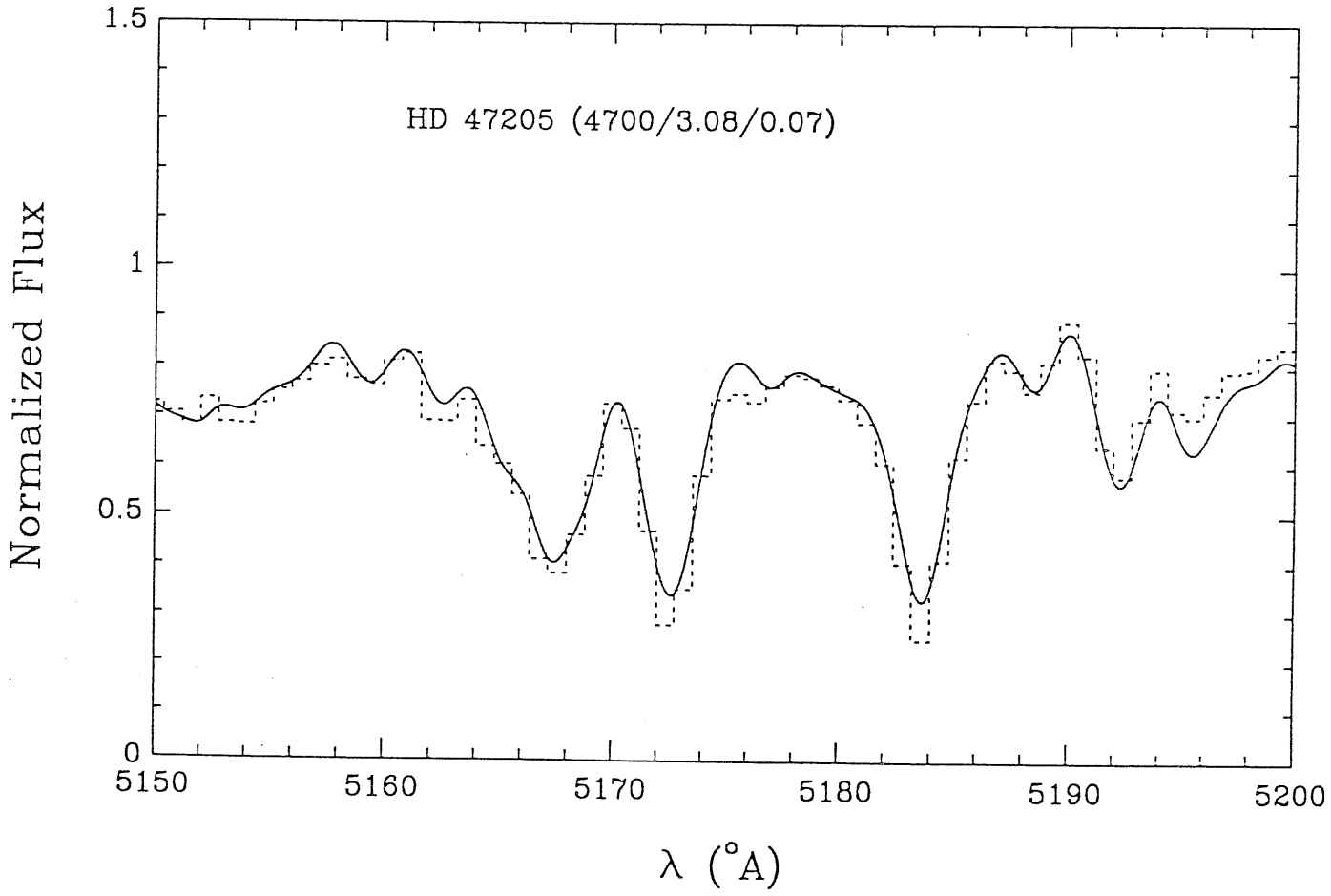
HD 47205 (4700/3.08/0.07)
Normalized Flux
1.5
1
0.5
0
5150
5160
5170
5180
5190
5200
λ (°A)

D.3 Supergiants

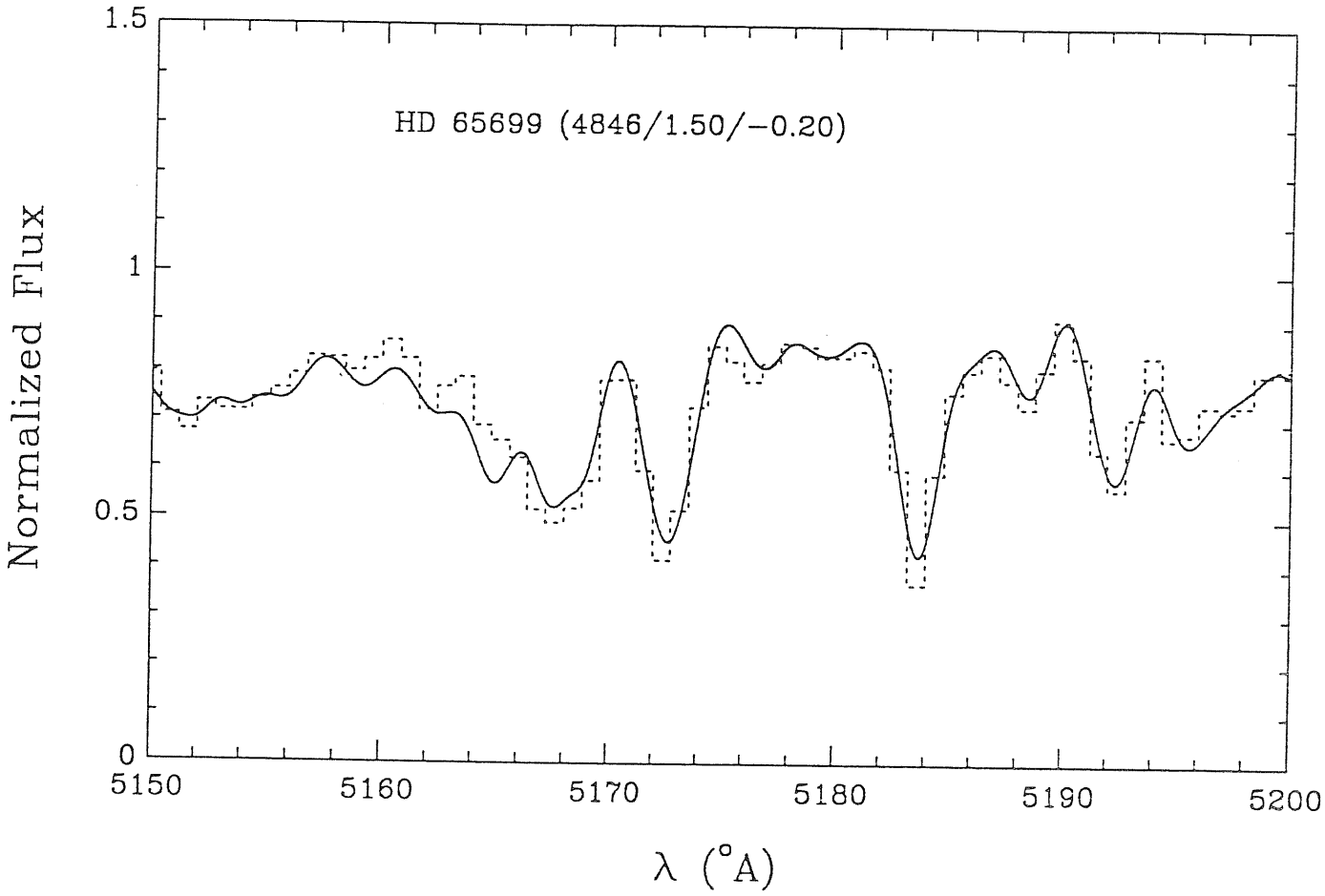

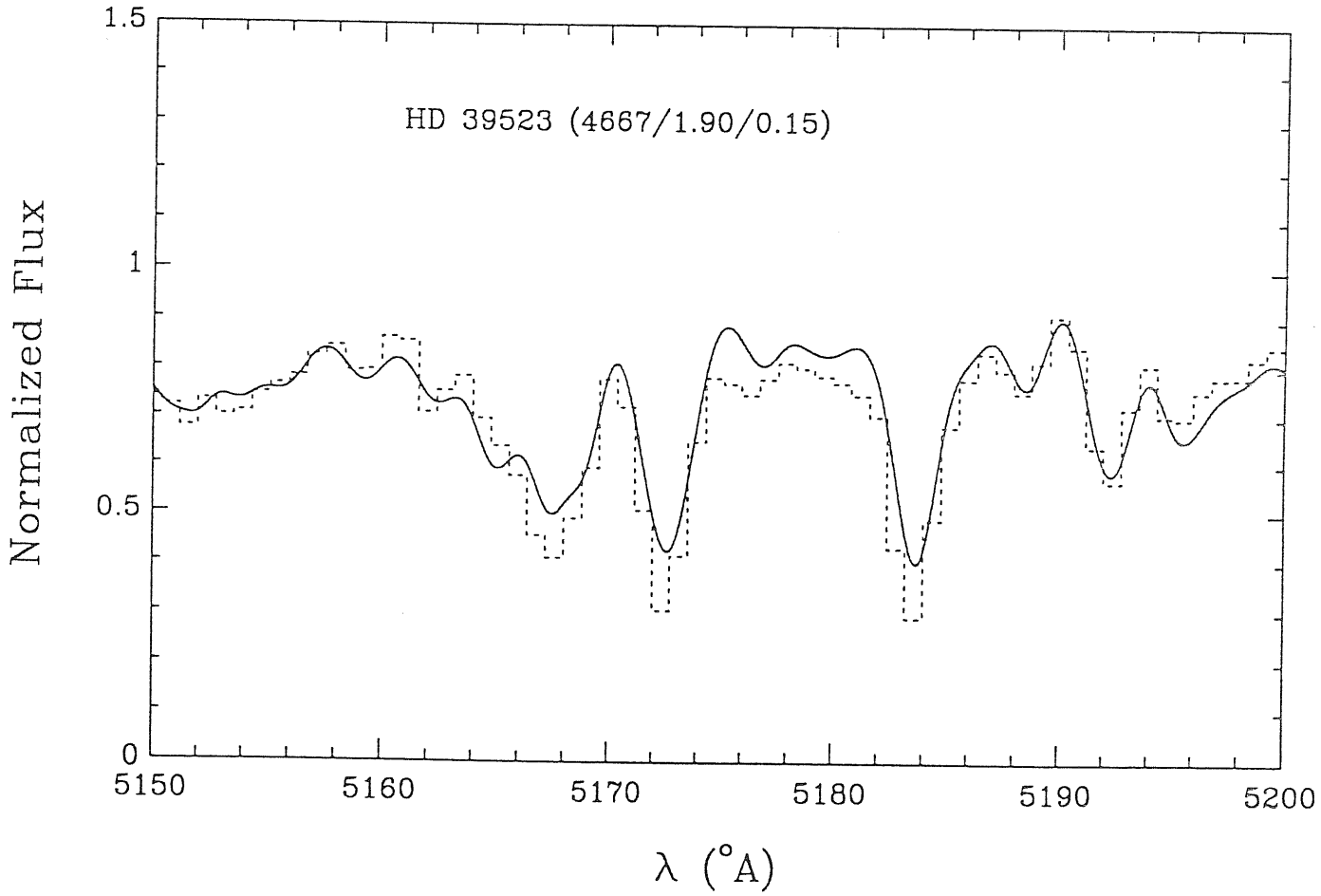

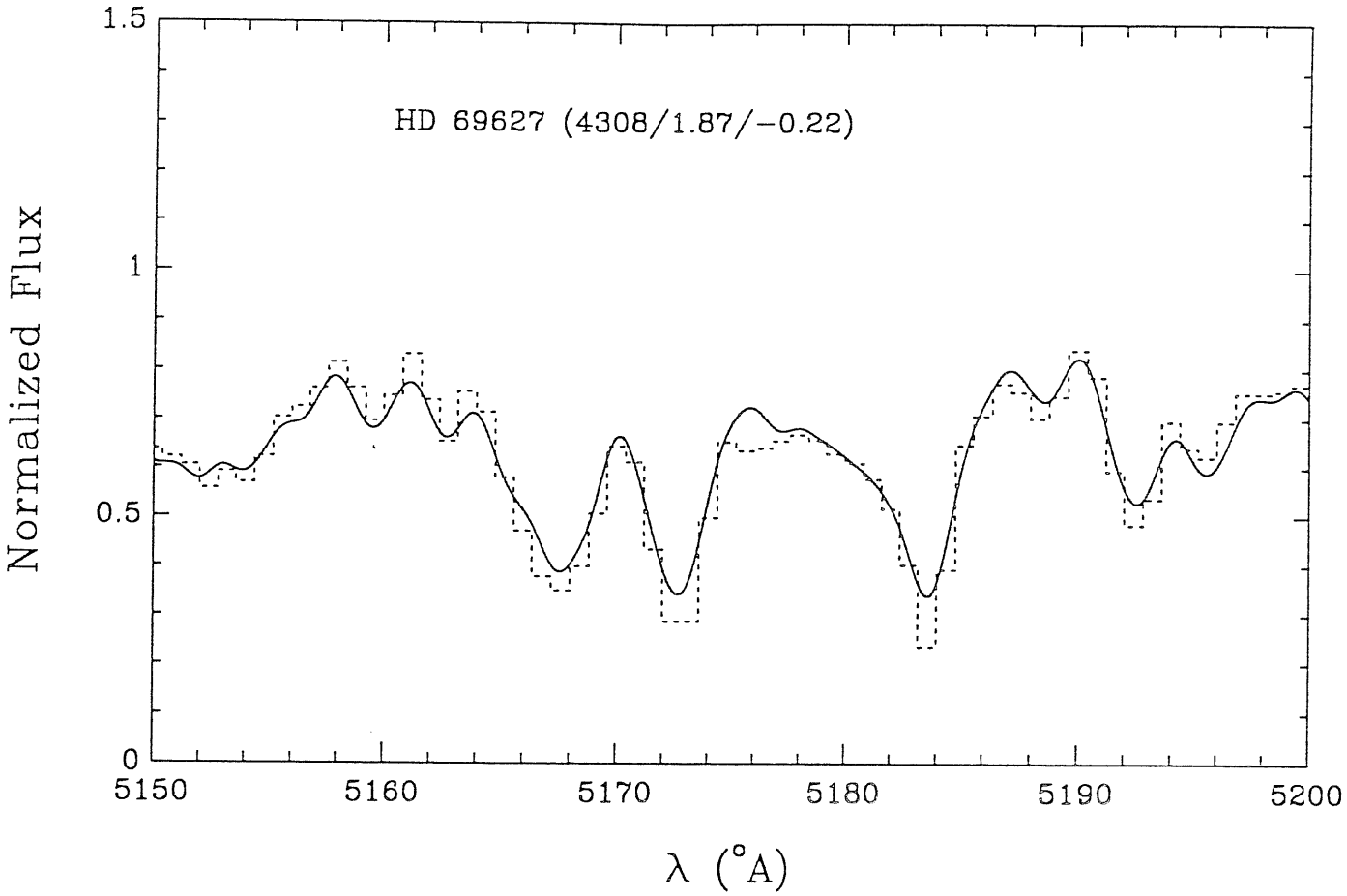
HD 69627 (4308/1.87/−0.22)
Normalized Flux
1.5
1
0.5
0
5150
5160
5170
5180
5190
5200
λ (°A)

Bibliography

[1] Anders, A., Grévesse, N. : 1989, *Geochem. Cosmochim. Acta* **53**, 197.

[2] Arimoto, N., Yoshi, Y. : 1986, *Astron. Astrophys.* **164**, 260.

[3] Artru, M.C., Lanz, T. : 1987, *Astron. Astrophys.* **182**, 273.

[4] Barbaro, G., Olivi, F.M. : 1986, in *Erice Workshop, Spectral Evolution of Galaxies*, eds. C.Chiosi and A. Renzini (Dordrecht:Reidel), p. 283.

[5] Barbuy, B. : 1989, *Astrophys. Space Sc.* **157**, 111.

[6] Barbuy, B., Erdelyi-Mendes, M., Milone, A. : 1991, *submitted to Astron. Astrophys. Suppl. Ser.*

[7] Bell, R.A., Edvardsson, B., Gustafsson, B. : 1985, *Mon. Not. R. Astron. Soc.* **212**, 497.

[8] Blackwell, D.E., Lynas-Gray, A.E., Petford, A.D. : 1991, *Astron. Astrophys.* **245**, 567.

[9] Böhm-Vitense, E. : 1981, *Ann. Rev. Ast. & Astrophys.* **19**, 295.

[10] Brodie, J.P., Huchra, J.P. : 1990, *Astrophys. J.* **362** , 503.

[11] Brodie, J.P., Huchra, J.P. : 1991, in *Astronomical Soc. of Pacific Conference Ser. Vol. 13 on The Formation and Evolution of Star Clusters*, ed. Keneth Janes p.495.

[12] Burstein, D. : 1985, *Pub. Astron. Soc. Pacific* **97**, 89.

[13] Burstein, D., Faber, S.M., Gaskell, C.M., Krumm, N. : 1984, *Astrophys. J.* **287**, 586.

[14] Buzzoni, A. : 1989, *Astrophys. J. Suppl. Ser.* **71**, 817.

[15] Buzzoni, A., Gariboldi, G., Mantegazza, L. : 1991, *Preprint*

[16] Castelli, F. : 1988, *Pubbl. Osservatorio Astronomico di Trieste*, N. **1164**.

[17] Cayrel de Strobel, G. : 1985, *Calibration of Fundamental Stellar Quantities* **IAU Sym. 111**, 137.

[18] Cayrel de Strobel, G., Bentolila, C., Hauck, B., and Duquennoy : 1985, *Astron. Astrophys. Suppl. Ser.* **59**, 145.

[19] Cayrel, R., Perrin, M.N., Barbuy, B., Buser, R. : 1991, *Astron. Astrophys.* **247**, 108.

[20] Charlot, S., Bruzual, A.G. : 1983, *Astrophys. J.* **367**, 126.

[21] Davis, R.L, Burstein, D., Dressler, A., Faber, S.M., Lynden-Bell, D., Terlevich, R.J., Wegner, G. : 1987, *Astrophys. J. Suppl. Ser.* **59**, 145.

[22] Deeming, T.J. : 1960, *Mon. Not. R. Astron. Soc.* **121**, 52.

[23] Edvardsson, B. : 1988, *Astron. Astrophys.*, **190**, 148.

[24] Faber, S.M. : 1973, *Astrophys. J.* **179**, 731.

[25] Faber, S.M. : 1991, *private communication.*

[26] Faber, S.M., Burstein, D., Dressler, A. : 1977, *Astron. J.* **82**, 941.

[27] Faber, S.M., Friel, E.D., Burstein, D., Gaskell, C.M. : 1985, *Astrophys. J. Suppl. Ser.* **57**, 711.

[28] Fano, U. : 1961, *Phys. Rev.* **124**,1866.

[29] Frogel, J.A., Whitford, A.E. : 1987, *Astrophys. J.* **320**, 199.

[30] Gorgas, J., Efstanthiou G., Aragón Salamanca, A. : 1990, *Mon. Not. R. Astron. Soc.* **245** 217.

[31] Gottileb, D.J., Bell, R.A. : 1978, *Astron. Astrophys.* **19**, 434.

[32] Green, E.M, Demarque, P., King, C.R. : 1987, *The Revised Yale Isochrones and Luminosity Functions*, (Yale Univ. Obs., New Haven).

[33] Griffin, R.F. : 1968, *A Photometric Atlas of the Spectrum of Arcturus* ed. Cambridge Philosophical Society.

[34] Guinan, E.F., Smith, G. H. : 1984, *Pub. Astron. Soc. Pacific* **96**, 354.

[35] Gulati R.K. : 1989, *M.Phil Thesis.* SISSA.

[36] Gulati R.K., Malagnini, M.L., Morossi, C. : 1989, *Astron. Astrophys. Suppl. Ser.* **80**, 73.

[37] Gulati R.K., Malagnini, M.L., Morossi, C. : 1991, *Astron. Astrophys.* **247**, 447.

[38] Gustafsson, B. : 1991, *private communication.*

[39] Gustafsson, B., Bell, R.A. : 1979, *Astron. Astrophys.* **74**, 313.

[40] Gustafsson, B., Kjaergaard, P., Anderson, S. : 1974, *Astron. Astrophys.* **34**, 99.

[41] Gustafsson, B., Bell, R.A., Eriksson, K., Nordlund, A. : 1975, *Astron. Astrophys.* **42**, 407.

[42] Hansen, L., Kjaergaard, P. : 1971, *Astron. Astrophys.* **15**, 123.

[43] Huchra, J.P. : 1977, *Astrophys. J.* **217**, 928.

[44] Jaschek, C., Jaschek, M. : 1990, in *The Classification of Stars* ed. Cambridge University Press.

[45] Kepple, P., Griem, H. R. : 1968, *Phys. Rev.* **173**, 317.

[46] Kurucz, R.L. : 1970, *Smithson. Ap. Obs. Spec.* Rep. **309**.

[47] Kurucz, R.L. : 1979a, *Astrophys. J. Suppl.* **40**, 1.

[48] Kurucz, R.L. : 1979b, *Dudley Obs. Report* **14**, 363.

[49] Kurucz, R.L. : 1981, *Smithsonian Astrophys. Obs. Spec. Rep.* **390**, 391.

[50] Kurucz, R.L. : 1987, in *The Second Conference on Fiant Blue Stars, IAU Colloquium No. 95*, A. G. Davis Philip, D. S. Hayes, and J. W. Leibert eds., p. 129.

[51] Kurucz, R.L. : 1988, *line list on magnetic tapes.*

[52] Kurucz, R.L. : 1990a, *Harvard-Smithsonian Preprint Series* **No. 3060**.

[53] Kurucz, R.L. : 1990b, *Molecular data on magnetic tapes.*

[54] Kurucz, R.L. : 1991a, *private communications.*

[55] Kurucz, R.L.: 1991b, in *Precision Photometry Astrophysics of the Galaxies*, A. G. Davis Philip, Arthur R. Upgreen and Kenneth A. Janes eds.

[56] Kurucz, R.L., Avrett, E.H. : 1981, *Smithson. Astrophys. Obs. Special Rep.* **391**.

[57] Kurucz, R.L., Peytremann, E. : 1975, *Smithson. Astrophys. Obs. Special Rep.* **362**.

[58] Kurucz, R.L., Furenlid, I., Brault, J., Testerman, L. : 1984, *Solar Flux Atlas from 296 to 1300 nm.* National Solar Obs. Sunspot, 240.

[59] Lester, J. : 1990, *Pub. Astron. Soc. Pacific* **102** , 1039.

[60] Malagnini, M.L., Morossi, C. : 1983, in *Statistical Methods in Astronomy*, ESA SP-**201**, 27.

[61] Malagnini, M.L., Morossi, C. : 1988, in *New Direction in spectrophotometry*, A. G. Davis Philip, D.S. Hayes and S.J. Adelman eds.

[62] Malagnini, M.L., Morossi, C. : 1990, *Astron. Astrophys. Suppl* **85**, 1015.

[63] Maltby, P., Avrett, E.H., Carlsson, M., Kjelaseth-Moe, O., Kurucz, R.L., Loeser, R. : 1986, *Astrophys. J.* **306**, 284.

[64] Mould, J. : 1978, *Astrophys. J.* **220**, 434.

[65] Ohman, Y. : 1936, *Stockholm Obs. Ann.* **12**, No. 18.

[66] O'Connell, R.W. : 1973, *Astron. J.* **78**, 1074.

[67] O'Connell, R.W. : 1980, *Astrophys. J.* **236**, 430.

[68] Peterson, R., Dalle Ore, C., Kurucz, R.L. : 1991, *private communication.*

[69] Pickles, A.J. : 1985, *Astrophys. J. Suppl Ser.* **59**, 33.

[70] Pritchet, C., van den Berg, S. : 1977, *Astrophys. J. Suppl Ser.* **34**, 101.

[71] Price, M. J. : 1966, *Mon. Not. R. Astron. Soc.* **134**, 135.

[72] Renzini, A., Buzzoni, A. : 1986, in *Erice Workshop, Spectral Evolution of Galaxies*, eds. C.Chiosi and A. Renzini (Dordrecht:Reidel) , p.195.

[73] Rocca-Volmerange, B., Lequeux, J., Maucherat-Joubert, M. : 1981, *Astron. Astrophys.* **104**, 177.

[74] Rose, J.A. : 1984, *Astron. J.* **89**, 1238.

[75] Ross, J., Aller, L. : 1968, *Astrophys. J.* **153**, 235.

[76] Spinrad, H., Taylor, B.J. : 1969, *Astrophys. J.* **157**, 1279.

[77] Spinrad, H., Taylor, B.J. : 1971, *Astrophys. J. Suppl.* **22**, 445.

[78] Spinrad, H., Wood, D.B. : 1965, *Astrophys. J.* **141**, 109.

[79] Thackeray, A.D. : 1939, *Mon. Not. R. Astron. Soc.* **99**, 492.

[80] Thackeray, A.D. : 1949, *Mon. Not. R. Astron. Soc.* **109**, 436.

[81] Thévnin, F., Foy, R. : 1983, *Astron. Astrophys.* **122**, 261.

[82] Tinsley, B.M. : 1972, *Astron. Astrophys.* **20**, 383.

[83] Tinsley, B.M. : 1975, *Mem. Soc. Astron. It.* **46**, 3.

[84] Tripicco, M.J., Bell, R.A. : 1990, *Astron. J.* **99**, 691.

[85] VandenBerg, D.A. : 1985, *Astrophys. J. Suppl.* **58**, 711.

[86] Veeder, G.J. : 1975, *Astrophys. J.* **79**, 1056.

[87] Vidal, C.R., Cooper, J., Smith, E.W. : 1970, *J. Quant. Spectro. Radiative Transfer* **10**, 1011.

[88] Vidal, C.R., Cooper, J., Smith, E.W. : 1973, *Astrophys. J. Suppl. Ser.* **25**, 136.

[89] Whipple, F.L. : 1935, *Harvard College Obs. Circ.* 404, 1.

J. Astrophys. Astr. (1987) 8, 315–329

$E(B-V)$ Determination from an UV-Visual Two-Colour Diagram: O and B Stars in the Catalogue of Stellar Ultraviolet Fluxes

R. K. Gulati *International Centre for Theoretical Physics, Strada Costiera 11, I-34100 Trieste, Italy* and *Dipartimento di Astronomia, Università degli Studi di Trieste, Via Tiepolo 11, I-34131 Trieste, Italy*

M. L. Malagnini *Dipartimento di Astronomia, Università degli Studi di Trieste, Via Tiepolo 11, I-34131 Trieste, Italy*

C. Morossi *Osservatorio Astronomico, P.O. Box Succursale Trieste 5, Via Tiepolo 11, I-34131 Trieste, Italy*

Received 1987 July 5; accepted 1987 September 15

Abstract. We present here, for the O and B type stars in the Catalogue of Stellar Ultraviolet Fluxes, an approach which does not require a precise knowledge of spectral type and luminosity class for deriving $E(B-V)$ colour excesses. The method is based on the use of an UV-visual two-colour diagram; galactic variations in the interstellar extinction law are analyzed and fully taken into account. Our results have been compared with those derived by using the differences between observed and intrinsic colours for stars with known spectral classification. The very good agreement in a large number of cases (94 per cent) demonstrates that our approach permits the derivation of reliable colour excess values for early-type stars even if only a rough spectral classification is available.

Key words: interstellar medium, extinction—stars, colours of—ultraviolet observations.

1. Introduction

The HR diagram is a fundamental tool in the comparison of stellar evolutionary models with observations. In particular, an accurate positioning of early-type field stars, O and B, on the theoretical HR diagram would permit astronomers to test different hypotheses of models for massive stars, to complete the upper main sequence for the solar neighbourhood, to support the determination of the initial mass function in the form derived from clusters and associations (Lequeux 1985; Scalo 1986). However, since theory provides quantities such as absolute luminosities and effective temperatures, while observations provide apparent magnitudes or fluxes and/or spectral classifications, links between these different sets of data must be carefully investigated. In fact, the tests sought by the theory may require not only accuracy on the observational side, but also uniqueness in the relationships between 'observables' and physical quantities.

Along this line, the most relevant difficulties to be expected are due to the following problems:

1. derivation, for a star, of actual apparent magnitude values from the observed one (or from the fluxes) through correction for interstellar extinction;
2. derivation of effective temperature from photometric or spectroscopic data and/or spectral classification;
3. determination of absolute luminosities or bolometric magnitudes from 'observables', different kind of measurements, distance determinations, and, in general, bolometric corrections.

In previous works devoted to the determination of effective temperatures and bolometric corrections, Malagnini *et al.* (1986, and references therein), resorted to the use of intrinsic colours for dereddening the stellar fluxes. This choice was not particularly critical because they were dealing with bright stars slightly reddened, and spectral classification could be carefully checked individually, due to the limited number of objects under study. On the other hand, the application of such a method to very large data bases becomes impractical because it is almost impossible to check spectral classifications and to guarantee their overall consistency and homogeneity, especially for poorly studied stars. We faced this problem when analyzing the data of Thompson *et al.* (1978, hereafter Thompson Catalogue), for the project of deriving the HR diagram for early-type field stars. Interstellar extinction can not be ignored since, due to the absolute high brightness of O and B stars, very highly reddened objects are expected to be present in the Thompson Catalogue which contains also stars with $V > 9$ mag.

In fact, the knowledge of interstellar extinction is of paramount importance for many different applications, such as distance determination, derivation of flux distribution, calibration of photometric data as a function of stellar physical parameters, comparison between theoretical and observed fluxes. Interstellar extinction depends on both the characteristics and the column density of interstellar matter lying in between the star and the observational apparatus.

It is usual to give a global measure of extinction at a specific wavelength, A_λ, as the product between a dimensionless wavelength-dependent term, k_λ, and a sort of reference scale factor, the colour excess $E(B-V) = A_B - A_V$(mag). While the same set of k_λ's, which represents the interstellar reddening law, may hold valid for different objects, the $E(B-V)$ value has to be estimated for every object under study.

Among the different methods devised in order to determine $E(B-V)$, the following are most widely applied:

1. computing the difference between the observed colour, $(B-V)$, and the intrinsic colour, $(B-V)_0$;
2. making use of two-colour diagrams, like $(U-B)$ versus $(B-V)$;
3. comparing star-to-star;
4. ironing out of the 2200 Å bump.

In the first case, intrinsic colours are obtained from compilations such as that of FitzGerald (1970), once spectral classification has been assessed. Obviously, reliable classification and accurate photometry are needed in order to avoid large errors in $E(B-V)$.

The second method requires the knowledge of the loci of sequences of unreddened stars and of the slope of the reddening line in the two-colour diagram. If the reference sequence results are different for different luminosity classes, then reliable spectral classification, in addition to accurate photometry, is also required.

In the third case, magnitude differences between nearby and distant stars of the same type are measured in a set of spectral bands. $E(B-V)$ can be obtained, once the galactic interstellar reddening law is assumed. Mismatch error in spectral type and/or luminosity class must be carefully checked.

Eventually, $E(B-V)$ can be derived by applying a mean extinction law, such as that by Nandy *et al.* (1975), to the spectral flux energy distribution with varying values of $E(B-V)$ until the bump at 2200 Å due to interstellar absorption is ironed out. In this case we should be certain about the exactness of the applied extinction law.

We present here, for the O and B stars in the Thompson Catalogue, a particular two-colour diagram devised for the purpose of obtaining the $E(B-V)$ colour excesses without an accurate *a priori* knowledge of their spectral classification.

The input data are described in section 2; the two-colour diagrams with reference sequences and reddening line slopes are presented in section 3 for twelve different regions in the galaxy; results and comparison with determinations of colour excess by the intrinsic colour method are given in section 4.

2. The input data

The Catalogue of Stellar Ultraviolet Fluxes (Thompson *et al.* 1978) contains the amplest collection of stellar absolute ultraviolet fluxes collected by the S2/68 ultraviolet sky survey telescope aboard the ESRO TD-1 satellite. The magnetic tape version of this catalogue, prepared by United Kingdom Science Research Council, is the result of merging the Thompson Catalogue with a consistent set of catalogues (see Carnochan 1982) providing information on other relevant stellar quantities. It was prepared at University College London (UCL) and provided to us by the NASA World Data Center. It contains the absolute fluxes and their one-sigma errors in four UV passbands, centred on 1565 Å, 1965 Å, 2365 Å, and 2740 Å for 31290 stars; the broadband fluxes have been calculated by combining the individual data points, obtained with a resolution of about 20 Å, which fall within the bandwidth of 330 Å.

The stars have been selected with the constraint that the signal-to-noise ratio (S/N) should be at least 10.0 in any one of the passbands.

The following complementary ground-based information, if available, is also provided on the magnetic tape: (i) HD number, DM number, SAO number, Bright Star number and the name of the star; (ii) right ascension (RA) and declination (Dec); (iii) proper motion in RA and Dec; (iv) UBV photometry; (v) Strömgren parameters; (vi) Spectral classification; (vii) peculiarity; (viii) radial and rotational velocities.

It is worth remembering that the entry referring to spectral classification, if present, may come from different sources, and represents either the only determination found in the literature, or the average of more than one determination, or the result of Carnochan's choice in the case of stars classified in very different ways by different researchers.

All the UV fluxes and errors were transformed into magnitudes by using the Hayes & Latham (1975) absolute calibration of Vega.

From the Thompson catalogue we have selected the magnitude at 1965 Å wavelength to define a new colour, i.e. $(m_{1965} - V)$. This colour should be more appropriate than the classical Johnson $(U - B)$ colour in analyzing especially O and B type stars. In fact the $(m_{1965} - V)$ colour permits us to extend the wavelength coverage of the star's energy distribution to the ultraviolet region where most of the flux is emitted by early-type stars. Moreover, the $(U - B)$ colour includes residual atmospheric extinction (Johnson 1963) which introduces uncertainties and inaccuracies in the $(U - B)$ versus $(B - V)$ two-colour diagram.

Among the four UV bands we have preferred the magnitude at 1965 Å due to the following reasons: (1) the absolute calibration of the 1965 Å band of TD-1 satellite is in good agreement with that of the IUE satellite, which is considered the most accurate and reliable. In fact, in its wavelength region the correction factors needed to convert individual TD-1 fluxes to the IUE absolute scale are very close to 1 and only slightly dependent on wavelength (see Table 2 in Bohlin & Holm 1984); (2) the 2740 Å band is very likely to be affected by calibration errors which cannot be easily corrected for by introducing a constant scale factor (Faraggiana & Malagnini 1984). Therefore the colour excesses obtained by using two-colour diagrams based on the 2740 Å fluxes, as for instance the one presented in the Thompson Catalogue (page XVI), may be affected by unpredictable and non-negligible errors; (3) over the 2365 Å band the correction factors needed to convert individual TD-1 fluxes to the IUE absolute scale depend significantly on wavelength (see Table 2 in Bohlin & Holm 1984); moreover, this band includes the maximum of the 2200 Å bump due to interstellar extinction that causes heavily reddened stars to have very low signal-to-noise ratios. The situation is obviously better in the 1965 Å band, even if it is affected by the interstellar bump, because here the intrinsic fluxes for O and B type stars are expected to be higher; (4) the 1565 Å band includes strong resonance lines such as those due to C IV and Si IV which are critically sensitive to luminosity and mass loss effects.

Galactic coordinates (l^{II}, b^{II}) have been computed for each star starting from right ascension and declination and the whole sample was divided into twelve different regions (see Table 1) analogously to the regions defined by Meyer & Savage (1981, hereafter MS) in order to compare our results with theirs. Region A includes stars in the Scorpius-Ophiuchus; regions B, E, F, G, and H include stars along the galactic plane whereas region K includes stars from Orion region. The other regions are included so as to cover the rest of the sky.

3. Two-colour diagram

Instead of preparing an $(m_{1965} - V)$ versus $(B - V)$ colour diagram we decided to use, by analogy with the Johnson colour factor Q, a reddening-free quantity defined as

$$Q_{UV} = (m_{1965} - V) - (k_{1965} - R)\,(B - V)$$

where k_{1965} is the coefficient of interstellar extinction at 1965 Å band, $A_{1965}/E(B - V)$, and R is $A_V/E(B - V)$.

Since the interstellar extinction is different in different regions of our galaxy (see for example Koorneef 1978; MS; Carnochan 1986) the proper extinction coefficient $(k_{1965} - R)$, hereafter denoted as c, was derived in each region. To derive c values, plots of $E(1965 - V)$ versus $E(B - V)$ have been prepared for stars with available

Table 1. The extinction coefficients and intrinsic colour line parameters for the twelve regions of the sky used in this paper.

Name	l^{II}, b^{II}	No.	c	2σ	a	2σ	b	2σ
A	90 to 30 6 to 90	38	4.94	0.14	0.176	0.005	0.086	0.007
B	330 to 30 −6 to 6	22	5.04	0.17	0.179	0.005	0.088	0.008
C	280 to 30 −90 to −6	28	5.33	0.10	0.190	0.006	0.094	0.008
D	30 to 60 −90 to −6	31	4.57	0.22	0.166	0.005	0.082	0.007
E	60 to 90 −6 to 6	28	4.44	0.28	0.162	0.004	0.080	0.007
F	90 to 160 −6 to 6	22	5.08	0.17	0.180	0.005	0.088	0.008
G	160 to 230 −6 to 6	47	5.36	0.30	0.191	0.006	0.095	0.008
H	230 to 330 −6 to 6	54	4.78	0.17	0.171	0.005	0.085	0.007
J	230 to 280 −90 to −6	49	4.56	0.39	0.165	0.005	0.082	0.007
K	185 to 230 −90 to −6	50	5.22	0.25	0.185	0.006	0.090	0.008
L	60 to 185 −90 to −6	59	5.32	0.10	0.189	0.006	0.094	0.008
M	60 to 290 6 to 90	31	5.37	0.10	0.191	0.006	0.095	0.008

No. = number of stars, $c = (k_{1965} - R)$, $(B-V)_0 = a \times Q_{UV} + b$.

spectral classification. The intrinsic colours used to compute $E(1965-V)$ and $E(B-V)$ are from Carnochan (1982); the following selection criteria were adopted to arrive at the appropriate c values for each region. According to Bless & Savage (1972) O and early B type stars with the same spectral type and intrinsic visual colours exhibit similar relative flux distributions in the UV while this does not hold valid for later spectral types. In fact the UV flux decreases steeply with decreasing temperature, and the spread in temperature for different stars of the same spectral subclass causes significant differences in the UV colours for late B and A stars, thus preventing well-defined intrinsic $(m_{1965}-V)_0$ values. To overcome this problem related to the coarseness of the spectral type classification, only stars classified as B3 or earlier were selected to arrive at c values. The stars with very blue $E(1965-V)$ were omitted and only stars having S/N more than 10 in the 1965 Å band were retained.

The linear least-squares fits through the data were performed with an iterative procedure such that points away from the linear relation by more than 2 times the root-mean-square error of the fit were rejected. A first check on the values of the intercepts was performed and, since in all the cases intercepts were not significantly different from zero, the slopes derived with the above-described method have been accepted as reliable estimates of the extinction coefficients. They were actually found to be significantly different for different regions by using a Student t-test, thus confirming the variation of the interstellar extinction along different directions of

observation in our Galaxy in good agreement with the MS determinations at ANS wavelengths (see Fig. 1). In fact, in each region, the extinction coefficient at 1965 Å band lies in between the two values derived by MS from the ANS bands at 1800 and 2200 Å, respectively, if the two-sigma error bars are taken into account. These results are shown in Table 1 and, for an illustration, the data and the linear least-squares fit for one of the regions is shown in Fig. 2.

For each of the twelve regions defined in Table 1, the proper c extinction coefficient has been used together with intrinsic colours from Carnochan's (1982) Tables 3 and 29, to prepare the twelve intrinsic two-colour diagrams, namely one Q_{UV} versus $(B-V)_0$ diagram for each region (see Fig. 3 as an example). In all the plots, referring to the different galactic regions, the points corresponding to the eleven different

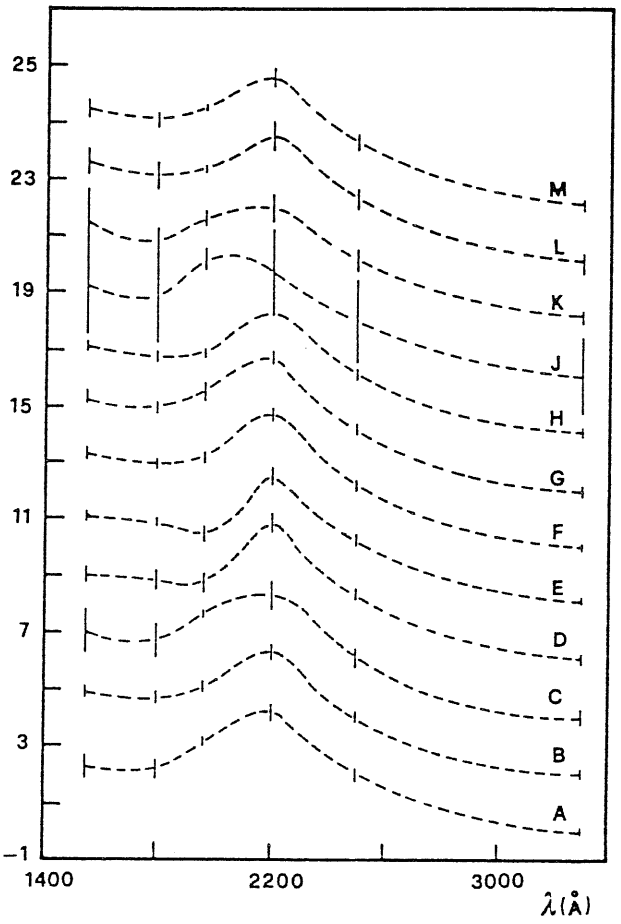

Figure 1. Extinction coefficients (c) at 1965 Å and two-sigma error bars are plotted for the twelve regions given in Table 1 together with the extinction coefficients for the ANS passbands at 1550, 1800, 2200, 2500, and 3300 Å from Table 3 in Meyer & Savage (1981). The extinction coefficients for the ith region have been shifted by putting the value at 3300 Å equal to $(i-1) \times 2$. Smooth dashed lines through the points have been drawn by hand just to make the figure more readable.

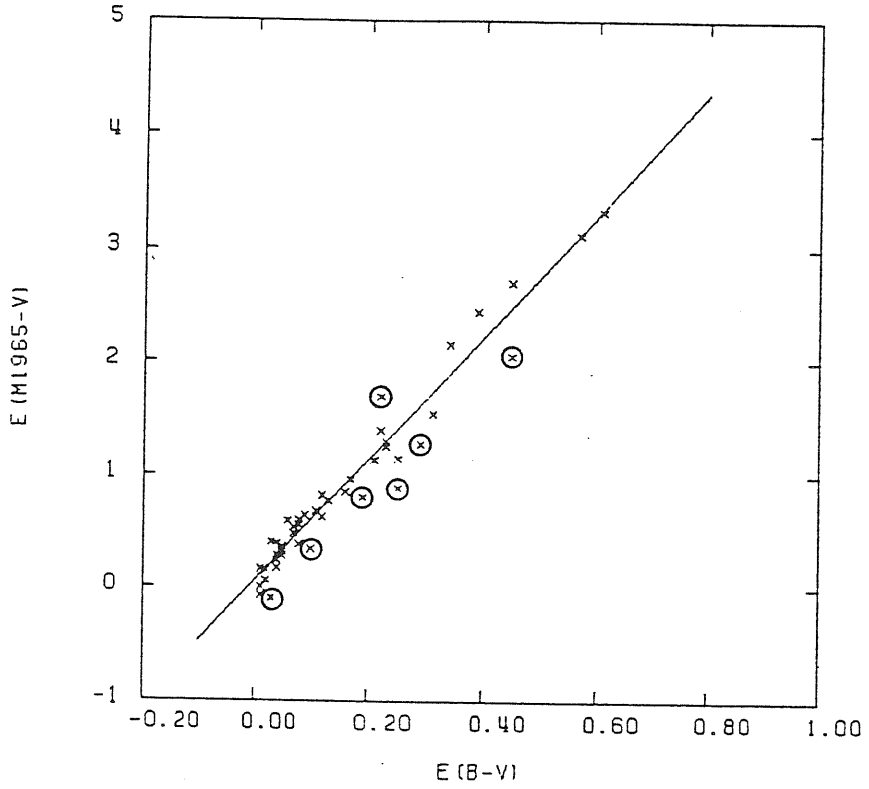

Figure 2. Correlation between $E(1965-V)$ and $E(B-V)$ for stars in region M. The encircled points have not been used in deriving the slope of the L.M.S. straight line (see text) which is also shown. As expected the L.M.S. line passes very close to the origin.

luminosity classes (*i.e.* V, IV–V, IV, III–IV, III, II–III, II, Ib–II, Ib, Iab, Ia) listed in Carnochan (1982), do not build up clearly separated sequences but are mixed together. Only three points fall away from the main bulk of data; they correspond to the intrinsic colours for the spectral classes B9 II, B9.5 II and A0 II, and have been obtained by Carnochan (1982) by interpolating the data for the very few luminosity class II stars at his disposal. It is very likely that their anomalous positions in the two-colour diagrams are due to the poor statistics for this luminosity class and do not reflect intrinsic properties. For these reasons, we decided to ignore them in the following analysis.

We can see that, for spectral types earlier than B8.5 ($Q_{UV} < -0.80$), at any fixed Q_{UV} value the spread in the corresponding intrinsic colours $(B-V)_0$'s due to the presence of different luminosity classes is always less than 0.04 mag. This figure is equivalent to twice the actual uncertainty on $(B-V)_0$, therefore an unique mean relationship between the two colours can be adopted without introducing significant systematic additional errors. By fitting a least-squares straight line through the points in each of the twelve diagrams, we found the mean relations, $(B-V)_0$ versus Q_{UV}, which permit us to give an estimation of $(B-V)_0$ starting from a Q_{UV} value. This estimate is independent of spectral type and luminosity class, and is affected by an uncertainty of ± 0.02 mag, which is comparable to the figure given in FitzGerald's (1967) Table 6.

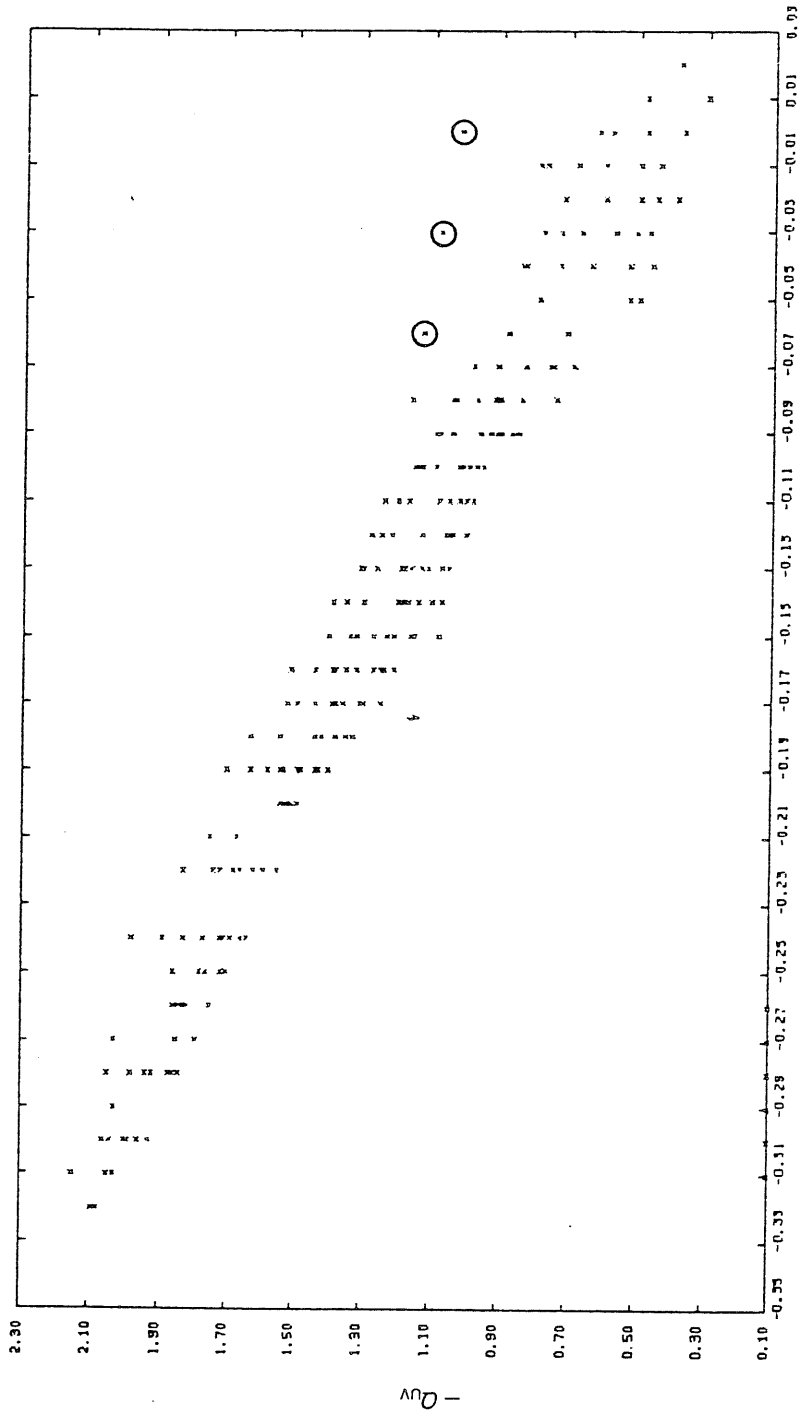

Figure 3. An example of intrinsic two-colour diagrams, $-Q_{UV}$ versus $(B-V)_0$. The interstellar extinction coefficient for region M, and Carnochan's (1982, Tables 3 and 29) intrinsic colours $(m_{1965}-V)$ and $(B-V)_0$ have been used. The encircled points, corresponding to spectral classes B9 II, B9.5 II and A0 II, have not been used in deriving the values of the parameters a and b given in Table 1 (see text).

For each region the parameters a and b (slopes and intercepts) of the linear relations between $(B-V)_0$ and Q_{UV} are given in Table 1, together with their uncertainties. It is now possible to use these relationships to assign intrinsic $(B-V)_0$ colours to actual stars: from the observed values of $(B-V)$ and $(m_{1965}-V)$ we derive Q_{UV}, taking into account the position of the star in the sky so that the appropriate value for the extinction coefficient c can be used. Finally, the following relation is used to derive $E(B-V)$:

$$E(B-V) = (B-V) - (B-V)_i \tag{1}$$

where

$$(B-V)_i = a \times Q_{UV} + b$$

and

$$Q_{UV} = (m_{1965}-V) - c \times (B-V).$$

In order to estimate the accuracy of our determinations of $E(B-V)$, we took into account the following sources of uncertainties:

(a) photometric errors in the observed $(B-V)$ and V, which are on the order of 0.02 and 0.05 mag, respectively (see Blanco *et al.* 1968);
(b) photometric errors in m_{1965} from the Thompson Catalogue;
(c) uncertainties in the parameters a and b, and in the interstellar extinction coefficient c as given in Table 1.

Hence the final error in $E(B-V)$ was derived by using the standard propagation of errors:

$$\begin{aligned}\sigma^2(E(B-V)) = {} & (1+c\times a)^2 \times \sigma^2(B-V) \\ & + ((m_{1965}-V) - c \times (B-V))^2 \times \sigma^2(a) \\ & + a^2 \times \sigma^2(m_{1965}) + a^2 \times \sigma^2(V) \\ & + (a \times (B-V))^2 \times \sigma^2(c) + \sigma^2(b).\end{aligned} \tag{2}$$

It is worth noting that the main contributions to the actual errors on $E(B-V)$ are the photometric errors on $(B-V)$ and m_{1965}. The 0.02 mag uncertainty on $(B-V)$ causes an uncertainty on $E(B-V)$ of 0.04 mag, while the errors on m_{1965} start to be important only when the signal-to-noise ratio in this band is lower than 7.

4. Results and discussion

We applied formulae 1 and 2, for each region separately, to the 1155 O and B type stars (the values obtained are available on request) whose spectral classifications are given in the Thompson Catalogue. This figure of 1155 stars comes from the full set of 31290 stars contained in the magnetic tape version of such a catalogue by adopting the following selection criteria based on the information contained in the catalogue itself:

(1) no indication of peculiarity, variability and/or duplicity;
(2) presence of both spectral type and luminosity class;
(3) positive values for both the flux and the corresponding error at 1965 Å band;
(4) presence of $(B-V)$ colour and V magnitude;

(5) computed Q_{UV} value smaller than -0.80 (to reject stars for which the spread in the intrinsic two-colour diagrams, due to luminosity effect, is larger than the observational uncertainties in the photometric quantities).

The fulfillment of the criterion 2 for these 1155 stars permitted us to compare our results, EBV, with those, EBVF, obtained from the difference of observed colour, $(B-V)$, and intrinsic colour, $(B-V)_0$, taken from FitzGerald (1970) according to the listed spectral classification. There is a very good agreement between the EBV's and EBVF's values in most of the cases (see for example in Fig. 4 the plot of EBV versus EBVF referring to the stars in region M).

In order to identify the discordant cases, we defined a 'diagonal distance', D, which is related to the uncertainties on EBV and EBVF, namely

$$D = [\sigma^2(\mathrm{EBV}) + \sigma^2(\mathrm{EBVF})]^{1/2};$$

here σ(EBVF) was assumed to be 0.04 mag because of uncertainty of 0.02 mag in both $(B-V)$ and $(B-V)_0$.

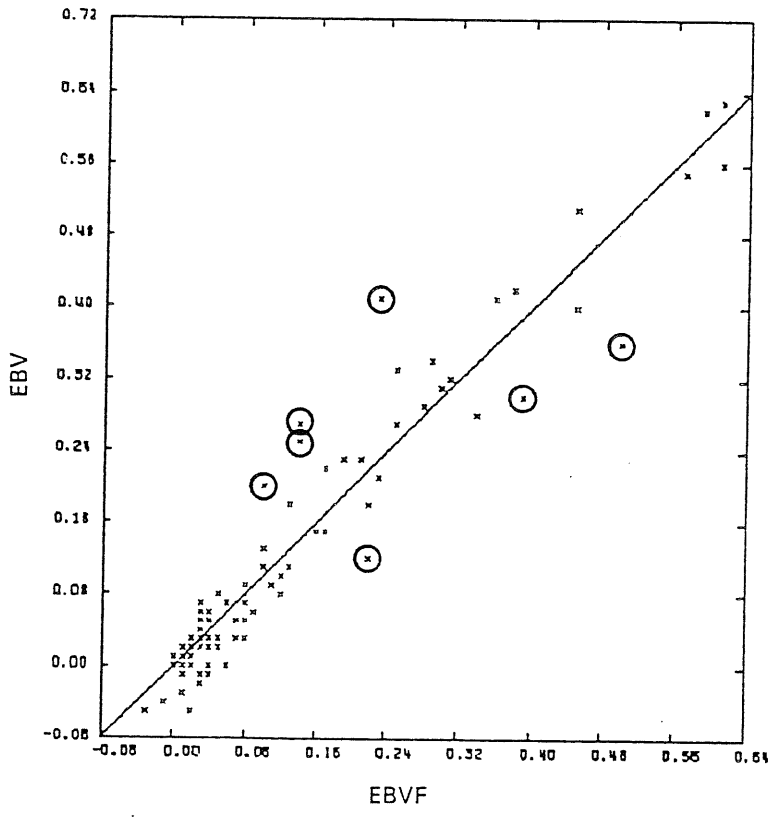

Figure 4. Comparison of $E(B-V)$ derived in this paper with those obtained by using FitzGerald's intrinsic $(B-V)_0$ for the stars in region M. Points with significant discrepancy in the two colour excess determinations are encircled and the line at 45 degrees is also plotted.

A check on the ratio of actual distance (d) from the line at 45 degrees to the diagonal distance (D) was made. We found 67 cases (6 per cent of the total) for which the ratios d/D are larger than 1 and the list of the corresponding stars is given in Table 2 with some remarks. Out of 67 stars, one star has d/D greater than 3, five stars have ratios between 2 and 3 and the rest of the stars have ratios between 1 and 2. These too large d/D values can be attributed to one or more of the following reasons: (i) wrong spectral classification: it causes a mistake in the EBVF estimation; (ii) anomalous photometric data reported in the Thompson Catalogue which will effect both EBV and EBVF determinations; (iii) underestimation of errors on EBV and EBVF values: it will effect the ratio between the actual and diagonal distance; (iv) peculiar extinction for the stars, which effects the c value used in the EBV determination; (v) presence of binary stars or multi-component systems; (vi) stellar peculiarity and/or variability.

Investigating the first possibility, thirty-two out of the 67 stars are found to have some classifications in the literature different from that given in the Thompson Catalogue. By choosing properly one of these, a good agreement between EBV and EBVF determinations can be achieved in twenty-three cases. If we add the fact that we could not check the reliability of spectral classification for those stars with only one determination, we can be confident that the inaccuracy of spectral classification will attribute most of the cases in Table 2 to wrong EBVF estimates. Therefore the advantage of our method, which does not require accurate knowledge of the stellar spectral type and luminosity class, is clearly confirmed and particularly evident.

The second and third possibilities seem to be less important. We have found no large differences between all the UBV photometric values given in the literature and those reported in the Thompson Catalogue. Therefore, both our estimates of Q_{UV} and D should be correct. But we have to recall that in some of the cases only one set of UBV photometric data has been found, thus preventing any check on their reliability.

Massa, Savage & Fitzpatrick (1983) and Carnochan (1986) have deeply analyzed individual stars to study deviations from the mean extinction law and they concluded that some of the stars have actually peculiar extinction. Comparing their list of peculiar extinction stars with Table 2, we found five stars in common with Carnochan and one star in common with Massa, Savage & Fitzpatrick (1983). Hence the fourth possibility cannot be excluded.

As far as possibilities (v) and (vi) are concerned, we looked in the literature for any indication of variability, duplicity and/or peculiarity of all the stars listed in Table 2 even if they are classified as single normal stars in the Thompson Catalogue. Actually we found three binaries, one Be-shell, two variables and two chemically peculiar stars. It is possible that the use of non-simultaneous observations in the UV and in the visible produce spurious results for these kinds of objects (probably with the exception of chemically peculiar stars): in general, results for undetected variables or binaries may be unpredictable.

In conclusion, we can say not only that our method of estimating $E(B-V)$ gives reliable results as compared to those from the standard intrinsic colour method but also that, if for some stars discrepancies arise, this can be considered as a good indication that these objects are worth deeper analysis.

The main advantage of this method is that it makes it possible to estimate the colour excess for a much larger number of objects than usual, since it requires only a very rough indication of spectral type.

Table 2. List of stars for which the colour excess value computed in the present paper (EBV) differs significantly from the value obtained by using FitzGerald's intrinsic colour calibration (EBVF).

HD	EBVF	EBV	σ	D	d	d/D	Sp.	Remarks
9695	0.17	0.29	0.05	0.07	0.09	1.29	B9 III	A0, B8 III
14220	0.21	0.12	0.05	0.06	0.03	1.06	B2 V	
20961	0.13	0.25	0.05	0.07	0.09	1.30	A0 V	A1 V, B9.5 V
24129	0.17	0.33	0.05	0.07	0.11	1.74	B9.5 II–III	B9 II, B9 III, A0 III, B8 III
33189	0.20	0.33	0.05	0.06	0.09	1.48	B9 V	
34792	0.35	0.50	0.05	0.06	0.11	1.67	B9 V	
35329	0.41	0.61	0.05	0.07	0.14	2.12	B9 V	
37366	0.34	0.47	0.05	0.06	0.09	1.54	B1.5 V	B3, O9.5 V
38087	0.31	0.45	0.04	0.06	0.10	1.68	B4 V	B3, pec. extinction
38658	0.37	0.51	0.05	0.07	0.10	1.52	B3 II	
41831	0.36	0.52	0.05	0.06	0.11	1.80	B3 V	
42966	0.27	0.46	0.05	0.06	0.14	2.19	B9 V	
43025	0.13	0.22	0.05	0.06	0.06	1.01	B9 V	
43836	0.51	0.75	0.06	0.07	0.17	2.45	B9.5 II	A0 II, B9 II
43954	0.35	0.66	0.05	0.07	0.22	3.25	A0 V	
44290	0.38	0.61	0.05	0.06	0.16	2.56	B9 V	Ap, B9 V Cr Eu
45337	0.14	0.25	0.05	0.06	0.08	1.29	B5 V	
46592	0.23	0.41	0.05	0.06	0.13	2.10	B5 V	
48038	0.29	0.15	0.04	0.06	0.10	1.74	B1 V	
48282	0.50	0.61	0.06	0.07	0.08	1.11	B3 III	Be and shell
52382	0.38	0.47	0.05	0.06	0.06	1.06	B1.5 Ib	B2, B1 Ib
52533	0.20	0.29	0.04	0.06	0.06	1.09	B0.5 V	B6, O8.5 V, O9 V
52559	0.22	0.11	0.04	0.06	0.08	1.33	B2 IV–V	pec. extinction
57109	0.10	0.20	0.05	0.06	0.07	1.11	B9 V	
69253	0.16	0.27	0.04	0.06	0.08	1.42	B4 V	B3 V, B5 V

71609	0.39	0.28	0.04	0.06	0.08	1.33	B0 V	B2/3 II, B3 II
86606	0.11	0.20	0.05	0.06	0.06	1.06	B1 Ib	B0, B0.5 III/IV, B2 Ib
96261	0.35	0.48	0.06	0.07	0.09	1.33	B1 Ib–II	B0.5 III
112481	0.20	0.35	0.05	0.07	0.11	1.63	B2 Ib	B2 II/III
117856	0.46	0.56	0.04	0.06	0.07	1.20	B0 Ib	B0/1 III, B0 II, O9.5 III
124471	0.12	0.23	0.04	0.06	0.08	1.42	B2 Ib–II	B2 III/IV, B1.5 III, B2 III
137569	0.40	0.56	0.05	0.06	0.11	1.80	B5 III	
151310	0.19	0.31	0.05	0.06	0.09	1.40	B5 V	B8, B2 V, B3 V
151865	0.28	0.40	0.06	0.07	0.09	1.24	B8.5 V	B9, B8 V
155217	0.21	0.33	0.05	0.06	0.09	1.42	B3 V	B5, B2 II/III, B1 V, B1.5 III
155506	0.14	0.24	0.04	0.06	0.07	1.23	B3 V	B5, B2 V, B1 V, B1.5 V
156004	0.21	0.31	0.04	0.06	0.07	1.23	B3.5 V	B5, B2 II, B2 V, B1 V, B0.5 III
159831	0.14	0.27	0.05	0.06	0.09	1.43	A0 V	
166192	0.44	0.55	0.05	0.06	0.08	1.29	B2 V	
166787	0.68	0.82	0.06	0.07	0.10	1.35	B1 Ib	B3, B0.5 Ib-II
168302	0.36	0.47	0.05	0.07	0.08	1.18	B5 V	
170580	0.34	0.26	0.04	0.06	0.06	1.03	B2 V	binary, pec. extinction
170650	0.08	0.00	0.04	0.05	0.06	1.05	B4 IV–V	B6 IV
174403	0.44	0.58	0.05	0.06	0.10	1.62	B6 IV	variable
175156	0.34	0.25	0.04	0.06	0.06	1.11	B4.5 III	B5 II, He abnormal
176254	0.28	0.20	0.04	0.06	0.06	1.03	B2 IV	
183561	0.41	0.30	0.04	0.06	0.08	1.37	B2 III	pec. extinction
186536	0.27	0.18	0.04	0.06	0.06	1.13	B2 V	
187879	0.22	0.12	0.04	0.06	0.07	1.23	B1 III–IV	B2 II, variable, sp. binary (?)
188504	0.20	0.30	0.05	0.06	0.07	1.18	B9 III	B7 III, A4 Ia, binary (?)
191201	0.43	0.29	0.05	0.06	0.10	1.64	B0 III–IV	O9.5 IV, B2 V
191423	0.47	0.38	0.04	0.06	0.06	1.11	O9 V	O9 III, A9 V:
191456	0.29	0.21	0.04	0.06	0.06	1.03	B1.5 III	B0.5 III, B3, B0.5 IV, B0.5 II–III, pec. e
191746	0.25	0.15	0.04	0.05	0.07	1.31	B2 IV	
192517	0.14	0.03	0.04	0.05	0.08	1.44	B0.5 V	
192539	0.36	0.24	0.04	0.06	0.09	1.53	B2 III	
195556	0.15	0.05	0.04	0.05	0.07	1.32	B2 V	
197511	0.14	0.06	0.04	0.05	0.06	1.06	B2 V	
198784	0.30	0.19	0.04	0.06	0.08	1.42	B2 V	
200804	0.52	0.63	0.05	0.06	0.08	1.29	B3 IV	B2 II

Table 2. Continued

HD	EBVF	EBV	σ	D	d	d/D	Sp.	Remarks
205139	0.39	0.30	0.04	0.06	0.06	1.08	B0.5 II	B0, B1 II
206636	0.28	0.43	0.05	0.06	0.11	1.77	B7 V	
208218	0.50	0.36	0.05	0.07	0.10	1.52	B1 III	
213322	0.22	0.09	0.05	0.06	0.09	1.48	B2 IV	
250310	0.40	0.54	0.05	0.06	0.10	1.54	B3 V	
256413	0.51	0.67	0.06	0.07	0.11	1.54	B5 III	
290385	0.13	0.24	0.05	0.06	0.08	1.27	B8 V	

d = distance of the star's position in the EBV versus EBVF plot from the 45 degrees line;
$D = (\sigma^2(\text{EBV}) + \sigma^2(\text{EBVF}))^{1/2}$;
Sp = Spectral classification given in Thompson Catalogue.
Spectral types in the remarks are from Blanco *et al.* (1968), Buscombe (1968, 1977, 1980, 1981, 1984), Kennedy & Buscombe (1974), Houk (1978, 1982), Houk & Cowley (1975), Jaschek & Egret (1982).
By using the spectral types underlined, the new d/D ratios are lower than 1.

Acknowledgements

The facilities of the Astronet Center of Trieste on the Vax 11/750 were used for the computations. The NASA World Data Center is acknowledged for providing the UCL Ultraviolet Star Catalogue on magnetic tape through the Astronomical Data Center. Partial supports from a CNR-GNA grant, from the Universitá degli Studi di Trieste (MPI 60 per cent grant), and from ICTP are acknowledged. R.K.G. appreciates the hospitality given to him by the Osservatorio Astronomico di Trieste during his stay in Trieste while working on the present project. We are grateful to Prof. M. Hack of the Astronomy Department of Trieste University for critically going through the manuscript, for helpful comments and suggestions.

References

Blanco, V. M., Demers, S., Douglass, G. G., FitzGerald, M. P. 1968, *Photoelectric Catalogue*, Publ. U.S. Naval Obs., **21**.
Bless, R. C., Savage, B. D. 1972, *Astrophys. J.*, **171**, 293.
Bohlin, R. C., Holm, A. V. 1984, *NASA IUE Newsletter*, No. 24, p. 74
Buscombe, W. 1968, *MK Spectral Classification*, Northwestern Univ., Evanston.
Buscombe, W. 1977, *MK Spectral Classification*, Vol. 3, Northwestern Univ., Evanston.
Buscombe, W. 1980, *MK Spectral Classification*, Vol. 4, Northwestern Univ., Evanston.
Buscombe, W. 1981, *MK Spectral Classification*, Vol. 5, Northwestern Univ., Evanston.
Buscombe, W. 1984, *MK Spectral Classification*, Vol. 6, Northwestern Univ., Evanston.
Carnochan, D. J. 1982, *Mon. Not. R. Astr. Soc.*, **201**, 1139.
Carnochan, D. J. 1986, *Mon. Not. R. Astr. Soc.*, **219**, 903.
Faraggiana, R., Malagnini, M. L. 1984, *Astr. Astrophys.*, **137**, 149.
FitzGerald, M. P. 1967, *Doctoral Thesis*, Case Inst. Tech.
FitzGerald, M. P. 1970, *Astr. Astrophys.*, **4**, 234.
Hayes, D. S., Latham, D. W. 1975, *Astrophys. J.*, **197**, 593.
Houk, N. 1978, *Michigan Spectral Catalogue*, Vol. 2, Univ. Michigan.
Houk, N. 1982, *Michigan Spectral Catalogue*, Vol. 3, Univ. Michigan.
Houk, N., Cowley, A. P. 1975, *Michigan Spectral Catalogue*, Vol. 1, Univ. Michigan.
Jaschek, M., Egret, D. 1982, Catalog of Stellar Groups, Part one: The earlier groups, Centre Donnèes Stellaires, Strasbourg.
Johnson, H. L. 1963, in *Basic Astronomical Data*, Ed. K. Aa. Strand, Univ. Chicago Press, p. 204.
Kennedy, P. M., Buscombe, W. 1974, *MK Spectral Classification*, Northwestern Univ., Evanston.
Koorneef, J. 1978, *Astr. Astrophys.*, **68**, 139.
Lequeux, J. 1985, in *Birth and Infancy of Stars*, Ed. R. Lucas, A. Omont & R. Stora, North-Holland, Amsterdam, p. 3.
Malagnini, M. L., Morossi, C., Rossi, L., Kurucz, R. L. 1986, *Astr. Astrophys.*, **162**, 140.
Massa, D., Savage, B. D., Fitzpatrick, E. L. 1983, *Astrophys. J.*, **266**, 662.
Meyer, D. M., Savage, B. D. 1981, *Astrophys. J.*, **248**, 545.
Nandy, K., Thompson, G. I., Jamar, C., Monfils, A., Wilson, R. 1975, *Astr. Astrophys.*, **44**, 195.
Scalo, J. M. 1986, *Fund. Cosmic Phys.*, **11**, 1.
Thompson, G. I., Nandy, K., Jamar, C., Monfils, A., Houziaux, L., Carnochan, D. J., Wilson, R. 1978, *Catalogue of Stellar Ultraviolet Fluxes*, UK Science Research Council (for the magnetic tape version).

ASTRONOMY & ASTROPHYSICS
SUPPLEMENT SERIES

Astron. Astrophys. Suppl. Ser. **80**, 73-88 (1989)

Empirical temperature calibrations for early-type stars

R. K. Gulati ([1]), M. L. Malagnini ([2]) and C. Morossi ([3])

([1]) International School for Advanced Studies, Strada Costiera 11, 34100 Trieste, Italy
([2]) Dipartimento di Astronomia, Universita' degli Studi di Trieste, Via Tiepolo 11, I-34131 Trieste, Italy
([3]) Osservatorio Astronomico, P.O. Box Succursale Trieste 5, Via Tiepolo 11, I-34131 Trieste, Italy

Received January 19, accepted April 28, 1989

Summary. — Three temperature calibrations of suitable photometric quantities have been derived for O and B stars. A sample of 120 stars with reliable $T_{\rm eff}$ determinations has been used for establishing each calibration. The different calibrations have been critically discussed and compared. Temperature determinations for 1009 program stars have been obtained with an accuracy of the order of 10 % .

Key words: stars : early-type — temperature — colors.

1. Introduction.

Most of our knowledge about stellar populations comes from basic physical parameters for individual stars, particularly in the form of the HR diagram. This is certainly a powerful technique, whose scope is being expanded as more sophisticated instrumentation is brought into use.

The accurate location of early-type stars, in particular of O and B stars, on the theoretical HR diagram would permit us, for instance, to derive the initial mass function from star count analysis, by comparing the theoretical models with the observations (Scalo, 1986). However, there are many problems involved with this. On the theoretical side, we are provided with the effective temperatures and absolute luminosities, whereas the observations provide photometric and/or spectrophotometric measurements.

In order to convert photometric parameters, such as the apparent magnitude, into absolute values, we need to know the distance and the interstellar extinction for stars. Then the bolometric correction is applied to the derived absolute magnitude to obtain the bolometric magnitude. For early-type stars, the bolometric correction is somewhat uncertain and varies considerably with intrinsic colors, in particular with $(B-V)_0$; also in practice other information derived from the observations, as for instance the spectral classification, is needed in order to convert the absolute magnitude into the bolometric magnitude.

Send offprint requests to : M. L. Malagnini.

The direct determination of the effective temperature for O and B stars is in itself a difficult task, which is becoming more feasible with improved techniques both in modeling and in observations. A comprehensive review of this subject has been made by Underhill and Doazan (1982) and by Böhm-Vitense (1981). Böhm-vitense has classified the $T_{\rm eff}$ determinations into direct, semidirect and indirect methods.

In principle, the effective temperature of a star is derived from the integration of flux per unit of stellar surface over the infinite wavelength range. As early-type stars emit most of their flux in the ultraviolet region, which is inaccessible to ground-based observations, this important part of the flux was measured only after the advent of space observatories. Nonetheless, due to a lack of data that cover the whole wavelength range, the fluxes from stellar atmosphere models have to be combined with the observed ultraviolet and visible fluxes to determine reliable effective temperature values. This approach can be applied only to the small samples of stars for which absolute spectrophotometric data, both in the ultraviolet and in the visible ranges, are available.

Code *et al.* (1976) have determined the effective temperature of 32 stars on the basis of their spectral energy distributions in as large a wavelength range as possible, so that the approximations made to compute the flux in the

unobservable regions of the spectrum are not particularly critical. This method is known as the "direct method", since the absolute fluxes per unit of stellar surface are computed starting from the observational data by using the directly observed apparent angular diameters. In fact, this is the best method, since it fits in very well with the definition of effective temperature, but, on the other hand, it has a practical limitation due to the small number of stars for which observed apparent angular diameters are available.

The approach adopted by Underhill *et al.* (1979) and Malagnini *et al.* (1986) to determine the effective temperature is also based on the integration of the spectral energy distribution in as large a wavelength range as possible, but the apparent angular diameters are not measured directly ; rather they are estimated by indirect, model-dependent, methods. This approach is not limited in the same way as the direct method in its application, but it is more strongly affected by any inadequacy in the models used. This kind of approach is regarded as a "semidirect method".

Besides these, other, indirect methods are used to determine the effective temperature, such as the comparison of energy distributions in the visible and/or in the UV with model energy distributions (see, for instance, Morossi and Malagnini, 1985), or the analysis, in high resolution spectra, of the relative strengths of temperature-sensitive lines of the same element (see for instance Adelman, 1978).

For very large samples of stars, the application of the above-mentioned methods may be impossible because of insufficient data ; therefore, two other approaches are generally used. The first one utilizes spectral types as indicators of temperature, thus overlooking the fact that spectral classification was not designed for $T_{\rm eff}$ determination. Moreover, a reliable spectral classification of complete samples is still lacking, except for stars in the solar neighborhood. The second approach is based on the calibration of suitable intrinsic colors, thus involving the careful removal of interstellar reddening effects from the observations or else recourse to reddening-free indices. For O and B stars, visual colors or color factors, such as $(B-V)_0$ and Q, vary only slightly with $T_{\rm eff}$, and it is highly desirable to have information extended to the ultraviolet range in order to obtain accurate temperatures and to locate the early-type stars on the theoretical HR diagram.

With these problems in mind, we planned to investigate the possibility of deriving $T_{\rm eff}$ calibrations by using selected UV photometric data available for large samples of early-type stars. In this paper, we shall present calibrations of $T_{\rm eff}$ for O and B type stars for which ultraviolet fluxes, measured in the 1965 Å band, are given in the Catalogue of Stellar Ultraviolet Fluxes (Thompson *et al.*, 1978, hereafter S2/68 catalogue).

The input data are described in section 2 ; the methods used to estimate $T_{\rm eff}$ from colors are presented in section 3 ; a general discussion is given in section 4, and section 5 contains the results for the program stars.

2. The input data.

The Catalogue of Stellar Ultraviolet Fluxes, which has the largest collection of absolute stellar ultraviolet fluxes, is the main source of input data for our present research work. It consists of fluxes and their one sigma errors at four passbands, centered on 1565 Å, 1965 Å, 2365 Å and 2740 Å, for 31 290 stars (magnetic tape version of the catalogue). The stars referred to in this paper are those extracted, by using information contained in the catalogue itself, according to the following selection criteria : 1) no indication of peculiarity, variability, and/or duplicity ; 2) the presence of both spectral type and luminosity class (stars earlier than B8.5 are considered) ; 3) positive values for both the flux and the corresponding error at the 1965 Å band ; 4) the presence of $(B-V)$ color and V magnitude.

A total of 1155 stars fulfilled the above criteria. Then, for these stars, we derived the color excesses, $E(B-V)'$s, by the method described in Gulati *et al.* (1987, hereafter referred to as Paper I). Among the 1155 stars, we found 26 stars with $E(B-V)'$s lower than -0.02 mag : in the following analyses, we decided to exclude these stars, since too negative a derived $E(B-V)$ value may indicate anomalies in the star itself and/or in its photometric data. However, the few stars with $E(B-V)'$s between 0.0 and -0.02 mag were retained, because this range is on the same order as the uncertainties expected for the observed $(B-V)$ and for the derived $E(B-V)$. For these stars we assume that the observed $(B-V)$ is equal to the intrinsic $(B-V)_0$, so that the color excesses in these cases are set at zero.

Consequently, we obtained a list of 1129 stars : out of this set, there are 120 stars for which $T_{\rm eff}$, determined by either direct, semidirect or indirect methods, is available in the literature. The list of these stars is given in table I ; in columns 1 to 3 we report the HD number, the location in the sky as defined in table II, and the spectral type from Jaschek (1978), respectively.

We used these 120 stars as reference stars for our purposes, i.e. to establish the $T_{\rm eff}$ calibrations of suitable colors and/or color factors and to estimate the $T_{\rm eff}$ values for the remaining sample of 1009 stars.

The determinations of $T_{\rm eff}$ taken from the literature were grouped, according to the methods used by the different authors, in the following order :

1) the temperature is determined from the integration of the flux in a very large wavelength range, as in Code *et al.* (1976), Underhill *et al.* (1979), and Malagnini *et al.* (1986) ;

2) the temperature is obtained from the comparison of the observed flux in the visible region or in the ultraviolet with the predictions from model atmospheres (see, for example, Morossi and Malagnini, 1985) ;

3) the temperature is derived from high resolution spectra analysis (see, for example, Adelman, 1978).

If there is more than one determination for the same

star obtained by different methods, we chose the "best" determination, following the group order given above. In some cases, when more than one determination was available and obtained by using the same method, mean values of the effective temperatures were computed.

In general, the errors on $T_{\rm eff}$ are not given in the original papers ; therefore, we have given a percent error value for each group code on the basis of the few available data.

We assume the error on the $T_{\rm eff}$'s to be equal to 3 % for the first group and to 5 % for the others. In columns 4, 5, and 6 of table I we report the adopted Log $T_{\rm eff}$, the group code, and the sources, respectively.

3. Method

In this section we discuss the method used to derive the empirical relationships between the $T'_{\rm eff}$s of the 120 reference stars and three suitable photometric parameters : a) a reddening free color factor, b) an UV-visual color, and c) a visual color. The photometric parameters which we consider here are :

a) the reddening-free color factor, QUV, which is a combination of the $(m1965 - V)$ and $(B - V)$ colors, and is defined as :

$$\mathrm{QUV} = (m1965 - V) - c\,(B - V)\ ; \quad c = k1965 - R \quad (1)$$

where $k1965$ is the extinction coefficient at the 1965 Å band and R is the ratio of extinction at the V band to $E\,(B - V)$. The coefficient c depends upon the interstellar reddening law, and its variations from region to region in the sky have been discussed in paper I. Table II reports the twelve regions in the sky that were studied to arrive at proper c values in paper I ;

b) the intrinsic color $(m1965 - V)_0$;

c) the classical color $(B - V)_0$.

The $E\,(B - V)$'s needed to derive these photometric parameters come from paper I, while, as described in section 2, the effective temperatures for the 120 reference stars have been taken from the literature. We recall that the errors on $T_{\rm eff}$ are assigned according to the code given in table I.

In order to illustrate the dependency of $T_{\rm eff}$ on these photometric parameters, we plotted Log $T_{\rm eff}$ against each of them. Different interpolation curves, in particular represented by algebraic polynomials or by hyperbolic functions, have been fitted through the data points using as our constraint the condition that points lying farther away than three times the root mean square error of the fit would be automatically rejected by an iterative procedure. The procedure takes into account errors both on $T_{\rm eff}$ and on the photometric parameters. Errors on $T_{\rm eff}$ come from the percent errors already mentioned ; errors on the photometric parameters are computed from the individual terms involved in their definition by using the standard propagation error theory.

In all the cases, only one star was rejected during the iterations, and precisely HD 137569 : this fact reflects either very large errors in photometric determinations or some peculiarities in the star itself.

Careful analyses of the residuals and of the errors on the coefficients of the least mean squares fits, led us to exclude all the interpolation functions except the linear and the hyperbolic ones. Even if the hyperbolic curve takes into account the saturation of the photometric parameters towards high temperatures, our final choice was to reject it for the following reasons : a) we lack data at both extrema for high and low temperatures, so that extrapolations are expected to be unreliable in this case : b) owing to the propagation of errors, the uncertainty in the photometric parameters led to rather large uncertainties in the derived temperatures.

Each of the three photometric parameter calibrations will now be described in detail.

3.1 Relationship between Log $T_{\rm eff}$ and QUV.

The use of the color factor, QUV, for the calibration of the effective temperature has the advantage of being a reddening-free parameter, but on the other hand this color factor depends directly on the extinction coefficient, c, which varies from region to region in the galaxy. Therefore, we need as many calibrations as there are regions reported in table II.

In principle it is better to have, in each of the twelve regions, a sufficient number of reference stars to establish the correlations we are interested in. Unfortunately, we do not have enough reference stars for each region, so we devised the following procedure in order to overcome the problem.

We made all reference stars belong to each of the twelve regions by performing these steps :

step (a) : suppose that star $A\,(i)$ is present in region i with its observed color $\mathrm{QUV}\,(i) = \mathrm{QUV}_0\,(i)$;

step (b) : compute separately the ingredients of $\mathrm{QUV}_0\,(i)$, $(m1965 - V)_0$ and $(B - V)_0$; they should obviously be the same for $A\,(i)$ in any region of the sky ;

step (c) : derive $\mathrm{QUV}\,(j) = \mathrm{QUV}_0\,(j)$, by using the proper extinction coefficient corresponding to region j, and the intrinsic colors derived in step (b).

In this way, for each star, we derived twelve QUV values ; therefore, we could derive twelve calibrations, each one based on the complete set of the 120 reference stars.

For each region in the sky, Log $T'_{\rm eff}$s were plotted against QUV's, and the linear least squares fit was performed. As an example, in figure 1a, the plot between Log $T_{\rm eff}$ and QUV, with the best fitted line, is shown for the region labelled M in table II.

The set of the fitting parameters, i.e. intercepts and slopes, together with their errors, is given in columns 5-8 of table II.

The general expression for the fitted line is :

$$\mathrm{Log}\,T_{\rm eff} = a\,(i) + b\,(i)\ \ \mathrm{QUV}\,(i)\,, \quad i = 1, 12 \quad (2)$$

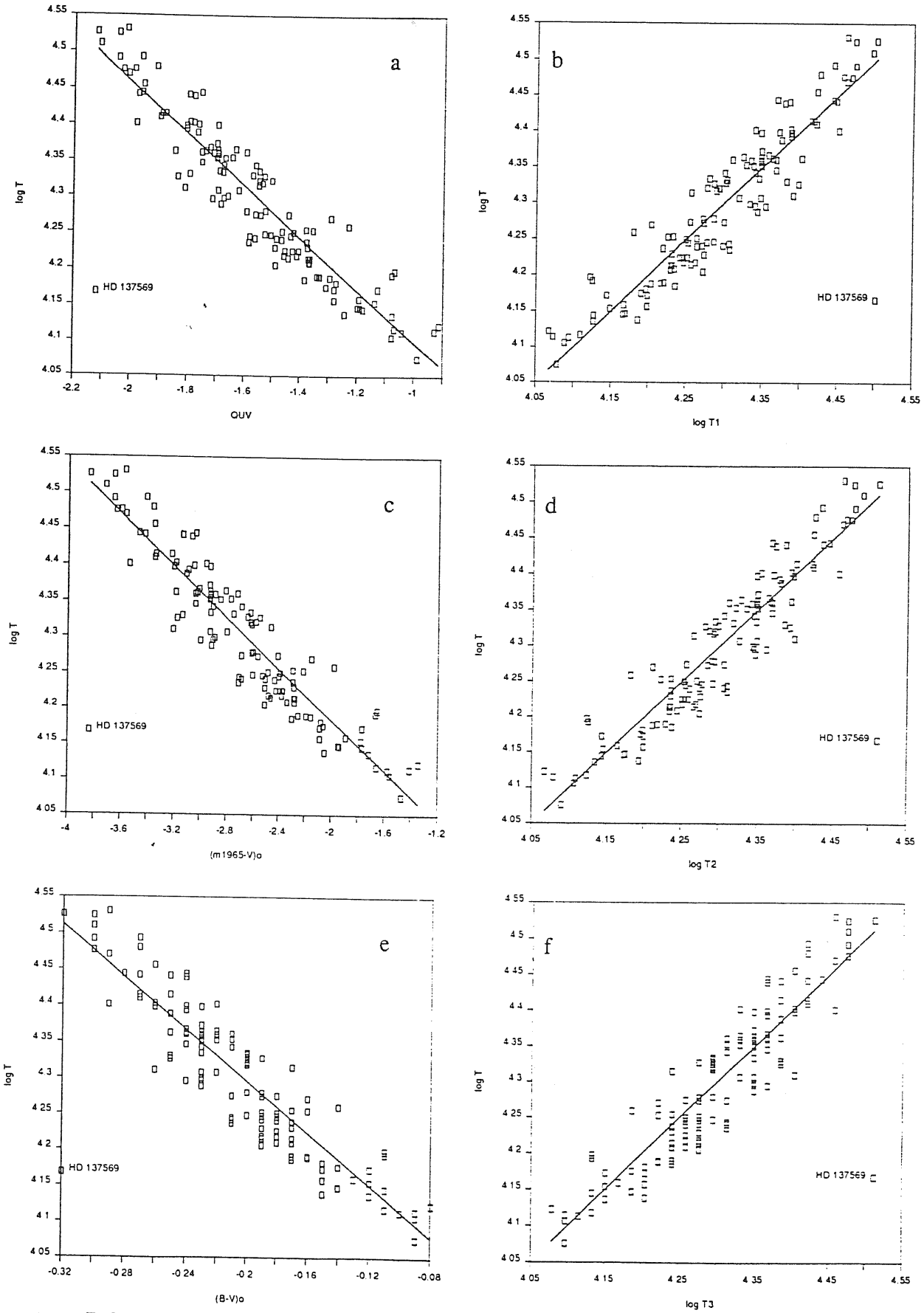

FIGURE 1. — Reference stars : Temperature calibrations. Correlations between Log $T_{\rm eff}$ and QUV (a), $(m1965 - V)_0$ (c), and $(B - V)_0$ (e). Comparisons between reference Log $T'_{\rm eff}$s and Log $T_{\rm eff}$ values computed from QUV (b), $(m1965 - V)_0$ (d), and $(B - V)_0$ (1f) ; HD 137569 is indicated.

where $a(i)$ and $b(i)$ are the fitting parameters.

In all cases the root mean square error is 8 %.

3.2 RELATIONSHIP BETWEEN LOG $T_{\rm eff}$ AND $(m1965 - V)_0$. — In order to determine the intrinsic color, $(m1965 - V)_0$, from the observed color, we used the proper extinction coefficient and color excess as derived in paper I.

This color should be a very good indicator of the effective temperature for early-type stars, since it includes the contribution from the ultraviolet, where these stars exhibit the overwhelming part of their radiation.

Again we plotted Log $T_{\rm eff}$ against $(m1965 - V)_0$ for the reference stars, and derived the linear least squares fit through the data points, with the strategy of iterations described above. Figures 1c shows this plot, together with the best fitted line.

We obtained the following linear relationship with 9 % as the root mean square error :

$$\begin{array}{ll} \text{Log } T_{\rm eff} & = a + b\,(m1965 - V)_0 \\ \text{where } a & = 3.828 \pm 0.017 \\ \text{and } \quad b & = -0.178 \pm 0.006 \end{array} \qquad (3)$$

3.3 RELATIONSHIP BETWEEN $T_{\rm eff}$ AND $(B - V)_0$. — The use of $(B - V)_0$ in this paper is mainly intended for comparison with existing calibrations. Although the low sensitivity of this color of temperature for early-type stars is well known, $(B - V)_0$ is widely used as a temperature indicator. We derived this intrinsic color by using the method outlined and applied in paper I. We prefered this approach because, unlike most of the other approaches, it does not require precise *a priori* knowledge of the spectral type and luminosity class, so it can be applied to stars lacking a spectral classification or with discrepant classifications. In figure 1e, we plot Log $T_{\rm eff}$ *versus* $(B - V)_0$, together with the best fitted line.

We derived the following linear relationship, with 9 % as the root mean square error :

$$\begin{array}{ll} \text{Log } T_{\rm eff} & = a + b\,(B - V)_0 \\ \text{where } a & = 3.933 \pm 0.015 \\ \text{and } \quad b & = -1.809 \pm 0.070 \end{array} \qquad (4)$$

4. Results and discussion.

To test the validity of the calibrations obtained, we applied relationships (2), (3) and (4) to the reference stars and compared the computed temperatures Log T_1, Log T_2 and Log T_3, respectively, with the values reported in table I. As an illustration, the plots between adopted Log $T_{\rm eff}$ and Log T_1, Log T_2, Log T_3, together with the 45-degree straight lines, are shown in figures 1b, 1d and 1f, respectively. It is evident from these plots that the star HD 137569, which was rejected during the least squares fit, always falls far away from the main bulk of the data.

In figures 2a, 2b and 2c, we present the three frequency distributions of the percent differences between $T_{\rm eff}$ and T_1, T_2 and T_3, respectively. The histograms are well described by Gaussian curves with a 0.0 mean and dispersions equal to the computed RMSE's (8 % , 9 % and 9 %). The 95 % confidence intervals are (−15 %, +16 %), (−15 %, +16 %), (−16 %, +17 %), which are very close to those expected from the normal distribution, namely, (−16 %, +16 %), (−17 %, +17 %), and (−18 %, +18 %), respectively.

As far as the errors on T's are concerned, we computed them by taking into account the contributions from different terms, according to the standard propagation theory of errors :

$$\Delta \text{ Log } T_i = \left(\Delta^2 a_i + c_i^2\,\Delta^2 b_i + b_i^2\,\Delta^2 c_i\right)^{1/2} \qquad i = 1,\ 2,\ 3 \qquad (5)$$

where the subscript i refers to the photometric parameter used to calibrate the temperatures.

In all cases, the term dominating the error on temperatures is the third, which contains the slope of the regression line and the errors on the photometric measurements. In general, the expected error on the derived temperatures is on the order of 10 % , which is in good agreement with the dispersion of the percent difference between the computed and the adopted temperatures as discussed above. We can conclude that the three calibrations do not differ significantly in quality from one another.

Still, the advantage of using one calibration rather than another can be explored by looking in detail into the quality of each photometric quantity contained in the term which contributes most of the error involved in deriving Log T's.

As regards the color factor QUV, used for the first calibration, the sources of errors are :

1) error on $m1965$;

2) error on V, which can be assumed to be generally equal to 0.05 mag ;

3) error on the extinction coefficient c given in column 4, table II ;

4) error on $(B - V)$, which can be assumed to be equal to 0.02 mag.

For stars with good-quality data in the UV band, the leading error terms are due to the error on the extinction coefficient, and to the error on $(B - V)$; thus, at least 0.1 mag of uncertainty can be expected.

The main advantage of using this calibration is that the color factor, QUV, is reddening-free. This approach allows one to derive the $T_{\rm eff}$ for stars, without requiring any knowledge of their color excesses. Furthermore, the advantage of using QUV over the classical Q color factor is that QUV takes into account a band in the UV region where the early-type stars emit most of their flux.

As regards $(m1965 - V)_0$, used in the second calibration, the sources of error are :

1-3) as in the previous case ;

4) error on $E(B - V)$ which is at least 0.02 mag.

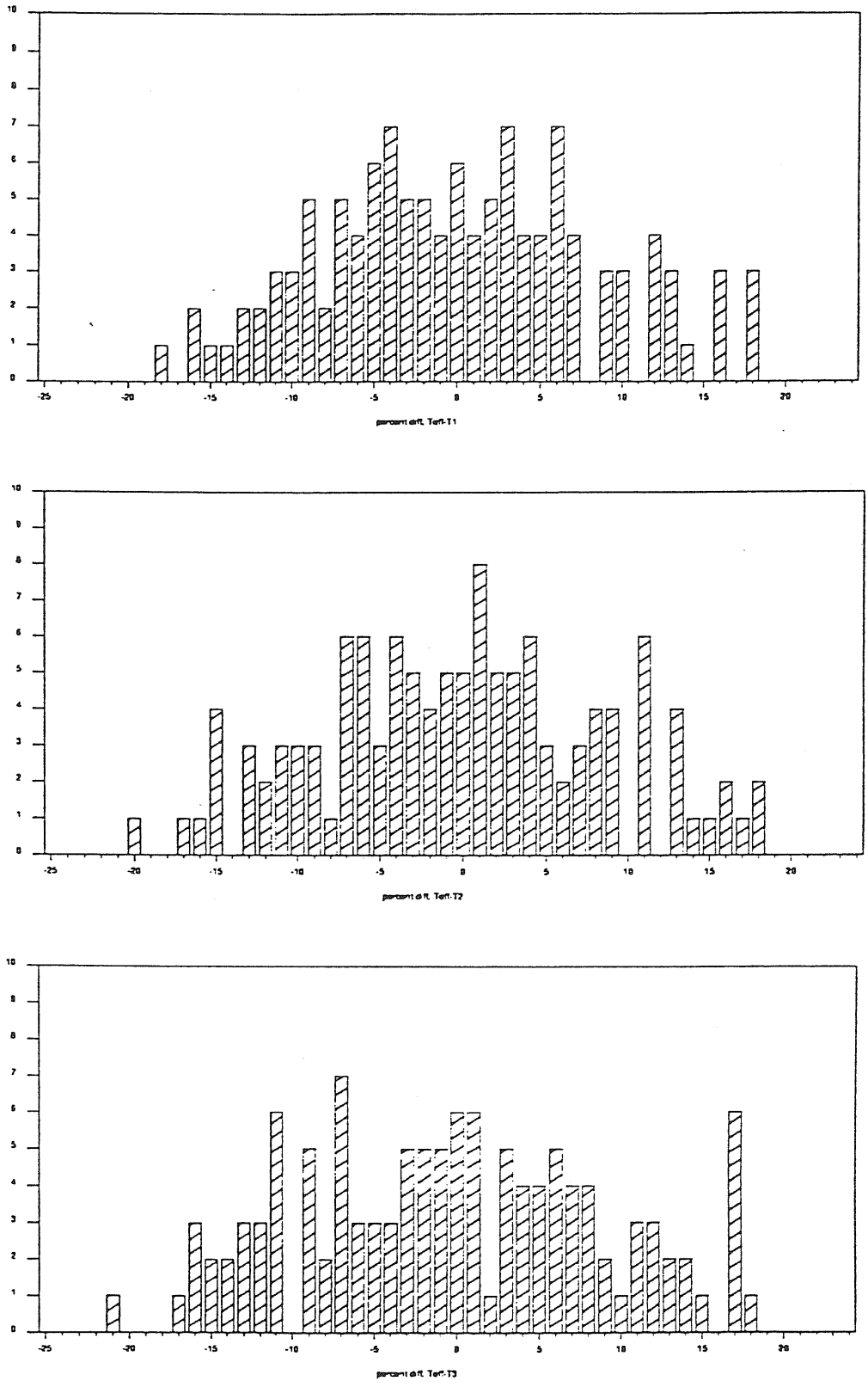

FIGURE 2. — Reference stars : Frequency distributions of percent difference between reference $T'_{\rm eff}$s and computed T_1 (a), T_2 (b) and T_3 (c) ; HD 137569 is not included.

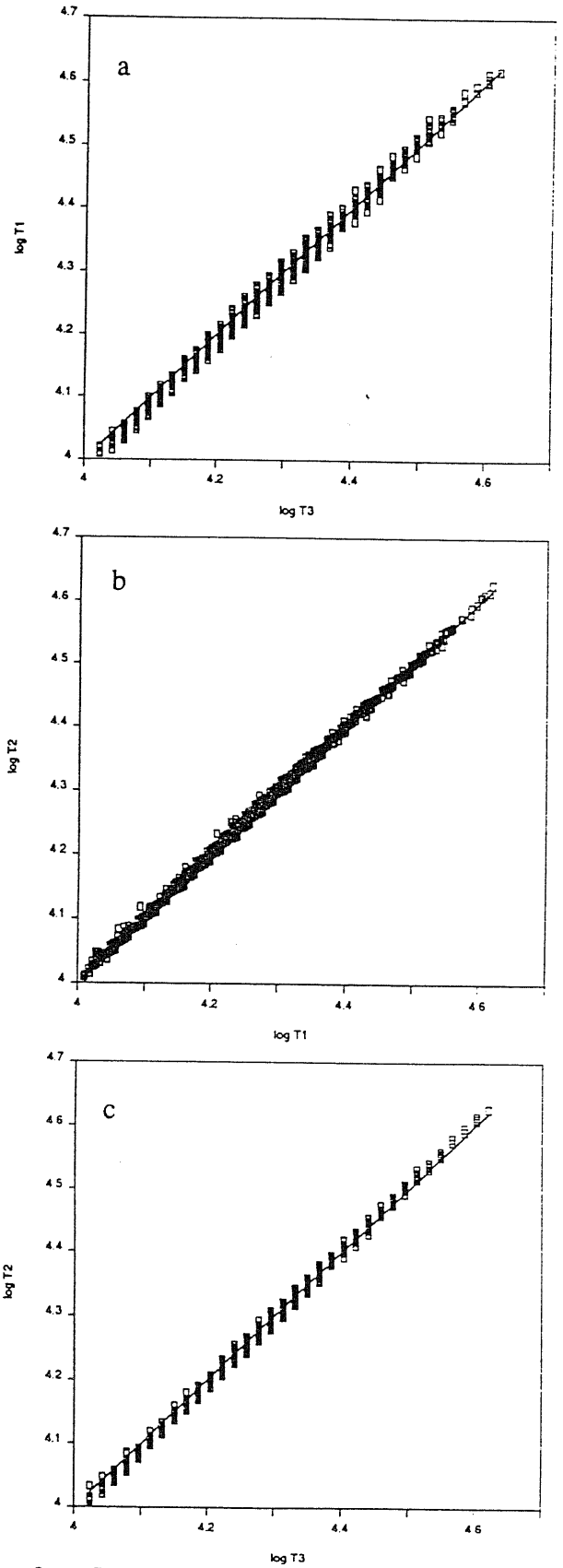

FIGURE 3. — Program stars : comparisons of temperatures derived from the three different calibrations (T_1, T_2, and T_3 refer to temperatures derived from QUV, $(m1965 - V)_0$, and $(B - V)_0$, respectively).

In the case of good-quality data in the UV band, the main contribution to the error comes from terms including c and $E(B-V)$, which vanish if $E(B-V)$ is negligible. In the other cases, a minimum of 0.1 mag of uncertainty is expected, owing to the product of c times the error on the color excess.

The $(m1965 - V)_0$ color is a good indicator of $T_{\rm eff}$ for early-type stars (for example, Malagnini *et al.*, 1984, presented a calibration of $\theta_{\rm eff} = 5040/T_{\rm eff}$ *versus* Log $(F1965/F5445)$). Unlike the classical $(U-B)_0$, this color is not contaminated by atmospheric extinction ; moreover, it comprises a band in the UV not accessible from ground based instrumentation, i.e. in a wavelength region which is important for early-type stars. On the other hand, the interstellar extinction law is more variable in the 1965 Å band than in the U band. Therefore, the accuracy of the derived intrinsic colors depends upon the goodness of the corrections for the atmospheric extinction in one case and the interstellar reddening in the other.

The advantage of using the $(m1965 - V)_0$ color over the $(U-B)_0$ for estimating the $T_{\rm eff}$ for stars earlier than B 8.5, is that the $(m1965 - V)_0$ is not so strongly dependent on the luminosity class as the $(U-V)_0$ color. Therefore, estimates of $T_{\rm eff}$ accurate to within 10 % can be achieved even without the determination of the stellar luminosity class.

The linear relationship obtained here is consistent with the calibration, found by Lesh (1976), between $T_{\rm eff}$ and the $(1910 - V)_0$ color obtained by using 12 stars earlier than A2 and luminosity classes III to V. The flux at the 1910 A band was taken from OAO-2 data (from the Space Astronomy Laboratory of the University of Wisconsin) and $T_{\rm eff}$ values came from Code *et al.* (1976).

The error on $(B-V)_0$, used in the third calibration, depends on the way the color was derived and amounts to at least 0.02 mag.

This calibration is particularly suitable for comparing our results with analogous ones present in the literature. In table III, we present a comparison of Böhm-Vitense's (1981) and Underhill and Doazan's (1982) results, reported in columns 2 and 3 respectively, with the present calibration. These results appear to be in good agreement, if we take into account the expected uncertainty of 10 % on the temperature derived in the present paper, and the dispersions given for $T_{\rm eff}$ by the above-mentioned authors.

In conclusion, we want to stress that, with respect to calibration 3, calibration 2 is more sensitive to $T_{\rm eff}$ and will make it possible to obtain very accurate temperatures, provided that precise UV photometry is available. In theory the first calibration is less accurate because of the various parameters involved in computing QUV, but it is the only one that can be safely used if the color excess $E(B-V)$ is affected by large errors or even unknown.

5. Program stars.

We applied the three calibrations to the 1009 program stars selected from the S2/68 catalogue as described in section

2. In table IV, we present, for each star, identified by its HD number, the temperatures and errors obtained by the three calibrations (a colon indicates temperatures obtained from photometric quantities outside the range available for the calibration). We here recall that the $(B-V)_0$ and the $E(B-V)$ correction have been derived as described in paper I and that their relative uncertainties, used to compute the Log T errors, were computed accordingly. In figure 3 we compare the Log T's derived from the three calibrations for the 1009 program stars. The plots show that all the determinations are closely correlated and that no systematic differences are present.

Acknowledgements.

The facilities of the Astronet Pole of Trieste, partly supported by the MPI40 % "Progetto Nazionale ASTRONET" grant were used for the computations.

The NASA WORLD DATA CENTER kindly provided the UCL Ultraviolet Star Catalogue on magnetic tape through the Astronomical Data Center.
R.K.G. thanks the Osservatorio Astronomico di Trieste for hospitality extended to him while working on the present project.

References

ADELMAN S. J. : 1978, *Astrophys. J.* **222**, 547.
ADELMAN S. J., PYPER D. M., WHITE R. E.. : 1980, *Astrophys. J. Suppl. Ser.* **43**, 491.
ADELMAN S. J., PYPER D. M. : 1983, *Astrophys. J.* **266**, 732.
BÖHM-VITENSE E. : 1981, *Ann. Rev. Astron. Astrophys.* **19**, 295.
CODE A. D., DAVIS J., BLESS R. C., HANBURY BROWN R. : 1976, *Astrophys. J.* **203**, 417.
CONTI P.S. : 1973, *Astrophys. J.* **179**, 161.
GLUSHNEVA I. N. : 1983, *Sov. Astron.* **27**, 326.
GLUSHNEVA I. N. : 1985, *Sov. Astron.* **29**, 659.
GULATI R. K., MALAGNINI M. L., MOROSSI C. : 1987, *J. Astrophys. Astron.* **8**, 315.
JASCHEK M. : 1978, Catalogue of Selected Spectral Types in the MK System (Strasbourg : Centre de Données Stellaires).
LECKRONE D. S. : 1971, *Astron. Astrophys.* **11**, 387.
LESH J. R. : 1976, *Astrophys. J.* **208**, 135.
MALAGNINI M. L., FARAGGIANA R., MOROSSI C. : 1983, *Astron. Astrophys.* **128**, 375.
MALAGNINI M. L., FARAGGIANA R., MOROSSI C. : 1984, in "The MK Process and Stellar Classification" Ed. R. F. Garrison (David Dunlap Obs., Toronto, Canada) p. 321.
MALAGNINI M. L., MOROSSI C., ROSSI L., KURUCZ R. L. : 1985, *Astron. Astrophys.* **152**, 117.
MALAGNINI M. L., MOROSSI C., ROSSI L., KURUCZ R. L. : 1986, *Astron. Astrophys.* **162**, 140.
MOROSSI C., CRIVELLARI L. : 1980, *Astron. Astrophys. Suppl. Ser.* **41**, 299.
MOROSSI C., MALAGNINI M. L. : 1985, *Astron. Astrophys. Suppl. Ser.* **60**, 365.
REMIE H., LAMERS H. J. G. L. M. : 1982, *Astron. Astrophys.* **105**, 85.
SCALO J. M. : 1986, *Fund. Cosmic Phys.* **11**, 1.
THEODOSSIOU E. : 1985, *Mon. Not. R. Astron. Soc.* **214**, 327.
THOMPSON G. I., NANDY K., JAMAR C., MONFILS A., HOUZIAUX L., CARNOCHAN D. J., WILSON R. : 1978, Catalogue of Stellar Ultraviolet Fluxes (UK Science Research Council, for the magnetic tape version).
UNDERHILL A. B. : 1981, *Astrophys. J.* **244**, 963.
UNDERHILL A. B., DIVAN L., PREVOT-BURNICHON L., DOAZAN V. : 1979, *Mon. Not. R. Astron. Soc.* **189**, 601 and Microfiche MN 189/1.
UNDERHILL A. B., DOAZAN V. : 1982, B stars with and without emission lines, NASA SP-456.

TABLE I — *Reference stars (see text).*

HD	REG	SP	LOG TEFF	CODE	SOURCES
886	L	B2 IV	4.334	2	b
3360	L	B2 IV	4.387	1	m
14228	J	B8 IV-V	4.117	2	g
16582	L	B2 IV	4.372	1	e
16908	L	B3 V	4.229	2	g
17769	L	B7 V	4.138	2	b
20365	L	B3 V	4.215	2	g
22203	K	B8 V + B9V	4.106	2	g
22928	F	B5 III SB	4.144	1	f,h
23408	L	B8 III	4.122	2	c
23466	L	B3 V	4.218	2	g
24398	L	B1 IB	4.299	1	e,k
25558	K	B3 V	4.240	2	g
26912	L	B3 IV	4.214	2	g
27396	F	B4 IV	4.225	1	q
29248	K	B2 III	4.353	1	e,o
30211	K	B5 IV	4.175	1	e,h
30836	K	B2 III SB	4.327	1	e,o
31237	K	B2 III SB	4.314	1	e
32249	K	B3 V	4.328	1	e
32630	G	B3 V	4.245	1	f
34503	K	B5 III	4.154	1	e,h
34759	G	B5 V	4.185	3	b
34816	K	B0.5 IV	4.456	1	f,o
35468	K	B2 III	4.332	1	a,e,o
35708	L	B2.5 IV	4.295	2	g
35715	K	B2 IV	4.362	2	g
36512	K	B0 V	4.510	3	l
36591	K	B1 IV	4.415	2	c
36779	K	B2.5 V	4.352	1	q
36819	G	B2.5 IV	4.247	2	g
36822	K	B0 IV SB	4.493	2	g
37356	K	B2 IV-V	4.326	2	g
37742	K	O9.5 IB SB	4.442	1	a,e
38771	K	B0.5 IV V	4.393	1	a
40111	G	B1 IB	4.330	1	o
40494	J	B2.5 IV	4.237	2	g
41692	K	B5 IV	4.159	2	h
41753	G	B3 IV	4.241	1	e
42560	G	B3 IV	4.250	1	q
44402	J	B2.5 IV	4.342	1	e
44743	K	B1 II-III	4.402	1	a,e,o
45813	J	B4 V	4.209	2	g
50707	J	B1 IV	4.403	1	e
51309	K	B3 II	4.172	1	e
52089	J	B2 II	4.334	1	a,e,o
52266	G	O9 V	4.525	3	p
57682	G	O9 V	4.531	1	n
57821	H	B7 IV	4.114	1	q
63922	J	B0 III	4.477	1	f,k
67797	M	B5 IV	4.189	1	e
74280	M	B3 V SB	4.274	1	e
74575	H	B1.5 III	4.364	1	e,o
76728	J	B8 III	4.075	1	e
81188	H	B2 IV	4.317	2	g
88206	H	B3 IV	4.270	2	g
90994	M	B6 V	4.146	1	f
91316	M	B1 IB SB	4.307	1	f
93549	H	B7 IV	4.157	2	g
99264	C	B2 IV-V1	4.310	2	g
99556	H	B3 IV	4.214	2	g
105937	A	B3 V	4.244	2	g
106490	H	B2 IV	4.360	1	e
109026	C	B5 V	4.190	1	e
111123	H	B0.5 III	4.441	1	a
113703	A	B5 V	4.205	2	g
115823	A	B6 V	4.181	2	g
120315	M	B3 V SB	4.225	1	d,f
121743	A	B2 IV	4.363	2	g
122980	A	B2 V	4.307	2	g
123335	H	B5 IV	4.225	2	g
132058	A	B2 III	4.367	1	e,o
132200	A	B2 IV	4.360	1	e
132955	A	B3 V	4.274	2	g
136298	A	B1.5 V	4.388	1	e,o
137569	A	B5 III:	4.167	2	g
139365	A	B2.5 V	4.320	1	e
142096	A	B2.5 V	4.342	1	q
142669	A	B2 IV-V	4.358	1	e
142883	A	B3 V	4.218	1	
143118	A	B2.5 IV	4.346	1	e
143275	A	B0.5 IV	4.480	1	a,e
144470	A	B1 V	4.410	1	f,e
147165	A	B1 III SB,V	4.470	1	e,k
147394	M	B5 IV	4.188	1	f,h
148703	A	B2 III	4.362	2	g
149038	B	B0 IA	4.444	2	g
149438	A	B0 V	4.476	1	o
155763	M	B6 III	4.113	1	e,h
157056	A	B2 IV	4.359	1	e
158408	B	B2 IV	4.359	1	e
158926	B	B1.5 IV	4.444	1	e,o
160578	B	B1.5 III	4.399	1	e
160762	M	B3 V SB	4.251	1	e
165024	C	B2 IB	4.236	1	q
169467	C	B3 IV	4.279	1	e
170465	C	B6 IV	4.136	2	g
172910	C	B2.5 V	4.296	2	g
175191	C	B3 IV	4.278	1	e
178475	M	B6 IV	4.146	2	i
180163	M	B2.5 IV	4.254	1	e
182568	M	B3 IV	4.288	1	e
188209	M	O9.5 IA	4.442	1	o
188892	E	B5 IV	4.192	1	e
190993	E	B3 V	4.241	1	f
192685	E	B3 V	4.246	1	f
193924	C	B2 IV	4.273	1	a
195556	E	B2.5 IV	4.259	1	e
198820	L	B3 III	4.208	2	g
204172	L	B0 IB *	4.401	1	e
204403	L	B3 IV *	4.230	2	g
205021	M	B1 III *	4.415	1	e,o
206165	M	B2 III SB,V	4.197	1	e
206672	F	B3 IV	4.253	1	e
212120	L	B6 V	4.172	2	h
212978	L	B2 V	4.398	1	k
213420	L	B2 IV	4.321	1	e,k
214680	L	O9 V	4.526	1	f
215191	L	B1 IV	4.398	1	k
218376	M	B0.5 IV	4.439	1	e

Note: (*) spectral type from S2/68 Catalogue
Sources:
a) Code et al. (1976); b) Adelman (1978); c)Adelman et al. (1980); d) Adelman & Pyper (1983); e) Underhill et al. (1979) ; f) Malagnini et al. (1986); g) Morossi and Malagnini (1985); h) Malagnini et al. (1985); i) Malagnini et al. (1983); j) Morossi and Crivellari (1980); k) Theodossiou (1985); l) Leckrone (1971); m) Glushneva (1985); n) Underhill (1981); o) Remie and Lamers (1982); p) Conti (1973) ;q) Glushneva (1983).

TABLE II. — *The extinction coefficients and fitting parameters with their errors used to derive temperatures from QUV for the twelve regions of the sky.*

Name	l", b"	c	er(c)	a	er(a)	b	er(b)
A	90 to 30 6 to 90	4.94	0.07	3.751	0.019	-0.333	0.011
B	330 to 30 -6 to 6	5.04	0.09	3.748	0.019	-0.339	0.012
C	280 to 30 -90 to -6	5.33	0.05	3.739	0.019	-0.358	0.012
D	30 to 60 -90 to -6	4.57	0.11	3.761	0.019	-0.313	0.011
E	60 to 90 -6 to 6	4.44	0.14	3.764	0.018	-0.306	0.012
F	90 to 160 -6 to 6	5.08	0.09	3.747	0.019	-0.342	0.012
G	160 to 230 -6 to 6	5.36	0.15	3.738	0.019	-0.359	0.011
H	230 to 330 -6 to 6	4.78	0.09	3.755	0.019	-0.324	0.011
J	230 to 280 -90 to -6	4.56	0.20	3.762	0.018	-0.312	0.012
K	185 to 230 -90 to -6	5.22	0.13	3.743	0.019	-0.350	0.012
L	60 to 185 -90 to -6	5.32	0.05	3.739	0.019	-0.357	0.012
M	60 to 290 6 to 90	5.37	0.05	3.738	0.019	-0.360	0.012

c = (k1965-R), Log T1 = a + b*QUV .

TABLE III. — *Log T_{eff} as a function of $(B-V)_0$ from three different sources.*

(B-V)o	Log Teff (a)	Log Teff (b)	Log Teff (this paper)
-0.32	4.562		4.512
-0.31	4.516		4.494
-0.30	4.484	4.488	4.478
-0.29	4.458		4.458
-0.28	4.435	4.466	4.439
-0.27	4.410		4.421
-0.26	4.389	4.430	4.403
-0.25		4.410	4.385
-0.24	4.342	4.358	4.367
-0.22	4.297	4.309	4.331
-0.20	4.248	4.268	4.295
-0.18	4.199	4.213	4.259
-0.16	4.161	4.181	4.222
-0.14	4.127	4.138	4.186
-0.13		4.113	4.168
-0.12	4.097		4.150
-0.10	4.072	4.075	4.114
-0.08	4.045		4.078
-0.07		4.038	4.060
-0.06	4.029		4.041
-0.04	4.009	4.009	4.005
-0.02	3.991		3.969

(a) Böhm-Vitense(1981) for luminosity classes II-V;
(b) Underhill, Doazan(1982) for luminosity classes IV-V.

TABLE IV. — *Temperatures and their errors for the 1009 program stars (T_1, T_2, and T_3 are derived from QUV, $(m1965-V)_0$, and $(B-V)_0$, respectively).*

HD	Log T1	ERT1	Log T2	ERT2	Log T3	ERT3
73	4.399	0.049	4.403	0.039	4.403	0.043
560	4.038:	0.044	4.043:	0.034	4.060:	0.039
593	4.445	0.050	4.445	0.040	4.440	0.044
829	4.325	0.047	4.329	0.037	4.331	0.042
1279	4.071:	0.044	4.079	0.034	4.096	0.040
1334	4.353	0.052	4.351	0.039	4.349	0.042
1383	4.486	0.070	4.484	0.052	4.476	0.060
1606	4.218	0.046	4.218	0.036	4.222	0.041
1810	4.508	0.070	4.504	0.052	4.494	0.060
1976	4.190	0.045	4.195	0.035	4.204	0.040
1999	4.149	0.052	4.155	0.043	4.168	0.057
2083	4.502	0.052	4.502	0.041	4.494	0.045
2329	4.272	0.051	4.273	0.038	4.277	0.041
2654	4.389	0.047	4.388	0.035	4.385	0.043
3264	4.358	0.050	4.364	0.038	4.367	0.043
3369	4.191	0.045	4.195	0.035	4.204	0.040
3379	4.326	0.047	4.329	0.037	4.331	0.042
3901	4.241	0.046	4.248	0.036	4.259	0.041
4142	4.222	0.046	4.230	0.036	4.241	0.041
4727	4.200	0.045	4.209	0.035	4.222	0.041
6118	4.038:	0.044	4.043:	0.034	4.060:	0.039
6226	4.232	0.048	4.235	0.036	4.241	0.041
6300	4.251	0.046	4.254	0.036	4.259	0.041
6417	4.281	0.055	4.278	0.045	4.277	0.058
6675	4.496	0.062	4.499	0.049	4.494	0.060
6811	4.070:	0.044	4.078	0.034	4.096	0.040
6882	4.169	0.045	4.174	0.035	4.186	0.040
7374	4.138	0.045	4.141	0.035	4.150	0.040
8965	4.425	0.064	4.425	0.049	4.421	0.059
9695	4.293	0.065	4.293	0.048	4.295	0.058
9878	4.023:	0.047	4.026:	0.035	4.042:	0.039
10205	4.096	0.044	4.101	0.034	4.114	0.040
10362	4.062:	0.047	4.064:	0.035	4.078	0.039
10747	4.360	0.049	4.364	0.038	4.367	0.043
11241	4.404	0.049	4.406	0.039	4.403	0.043
11529	4.101	0.045	4.103	0.034	4.114	0.040
11857	4.091	0.049	4.089	0.036	4.096	0.040
11860	4.023:	0.065	4.026:	0.047	4.042:	0.056
11917	4.224	0.082	4.231	0.059	4.241	0.075
12303	4.026:	0.045	4.047:	0.034	4.042:	0.039

TABLE IV (*continued*).

HD	Log T1	ERT1	Log T2	ERT2	Log T3	ERT3
12707	4.275	0.063	4.275	0.047	4.277	0.058
14220	4.196	0.053	4.198	0.044	4.204	0.057
14372	4.162	0.045	4.171	0.035	4.186	0.040
15640	4.087	0.061	4.086	0.045	4.096	0.057
17543	4.171	0.045	4.176	0.035	4.186	0.040
18352	4.324	0.054	4.318	0.045	4.313	0.058
18604	4.122	0.045	4.132	0.034	4.132	0.040
18883	4.181	0.045	4.190	0.035	4.204	0.040
19341	4.250	0.075	4.243	0.057	4.241	0.075
19356	4.155	0.045	4.158	0.035	4.168	0.040
19374	4.368	0.048	4.369	0.038	4.367	0.043
19805	4.070:	0.081	4.078	0.058	4.096	0.074
19893	4.047:	0.052	4.048:	0.042	4.060:	0.056
19968	4.153	0.069	4.148	0.054	4.150	0.074
20315	4.107	0.045	4.116	0.034	4.132	0.040
20340	4.258	0.046	4.248	0.036	4.241	0.041
20418	4.221	0.046	4.229	0.036	4.241	0.041
20809	4.213	0.046	4.216	0.035	4.222	0.041
20863	4.116	0.048	4.120	0.035	4.132	0.040
20961	4.149	0.060	4.156	0.045	4.168	0.057
21071	4.197	0.046	4.199	0.035	4.204	0.040
21091	4.075	0.057	4.080	0.044	4.096	0.057
21279	4.112	0.053	4.118	0.043	4.132	0.057
21398	4.044:	0.052	4.046:	0.042	4.060:	0.056
21428	4.254	0.043	4.255	0.035	4.259	0.041
21455	4.165	0.047	4.173	0.036	4.186	0.040
21483	4.325	0.054	4.329	0.045	4.331	0.058
21672	4.085	0.048	4.086	0.035	4.096	0.040
21803	4.292	0.047	4.293	0.037	4.295	0.041
21856	4.413	0.048	4.420	0.039	4.421	0.043
21933	4.047:	0.044	4.058:	0.034	4.060:	0.039
22252	4.047:	0.045	4.047:	0.034	4.060:	0.039
22401	4.058:	0.059	4.063:	0.044	4.078	0.056
22586	4.269	0.042	4.279	0.034	4.295	0.041
22951	4.462	0.049	4.463	0.040	4.458	0.044
23180	4.359	0.047	4.364	0.038	4.367	0.043
23324	4.106	0.044	4.115	0.034	4.132	0.040
23478	4.322	0.047	4.327	0.037	4.331	0.042
23625	4.407	0.049	4.417	0.039	4.421	0.043
23675	4.313	0.072	4.313	0.056	4.313	0.075
23793	4.256	0.046	4.266	0.036	4.277	0.041
23800	4.399	0.064	4.393	0.049	4.385	0.059
24129	4.304	0.062	4.299	0.047	4.295	0.058
24131	4.453	0.049	4.459	0.040	4.458	0.044
24263	4.205	0.046	4.212	0.035	4.222	0.041
24432	4.381	0.078	4.375	0.059	4.367	0.076
24504	4.183	0.042	4.181	0.034	4.186	0.040
24587	4.202	0.044	4.201	0.035	4.204	0.040
24640	4.432	0.049	4.439	0.039	4.440	0.044
24757	4.192	0.039	4.195	0.033	4.204	0.040
24760	4.411	0.048	4.419	0.039	4.421	0.043
25132	4.261	0.049	4.258	0.037	4.259	0.041
25330	4.245	0.046	4.251	0.036	4.259	0.041
25443	4.336	0.075	4.344	0.058	4.349	0.076
25539	4.333	0.048	4.342	0.037	4.349	0.042
25787	4.312	0.049	4.312	0.038	4.313	0.042
25799	4.298	0.048	4.306	0.037	4.313	0.042
26171	4.089	0.045	4.097	0.034	4.114	0.040
26326	4.221	0.045	4.220	0.035	4.222	0.041
26356	4.225	0.046	4.231	0.036	4.241	0.041
26739	4.241	0.045	4.239	0.035	4.241	0.041
27192	4.355	0.045	4.353	0.037	4.349	0.042
28114	4.185	0.044	4.183	0.035	4.186	0.040
28149	4.206	0.046	4.212	0.035	4.222	0.041
28217	4.077	0.045	4.082	0.034	4.096	0.040
28375	4.239	0.045	4.238	0.035	4.241	0.041
28436	4.134	0.070	4.139	0.055	4.150	0.074
29180	4.355	0.066	4.352	0.049	4.349	0.058
29309	4.332	0.052	4.342	0.039	4.349	0.042
29335	4.156	0.044	4.159	0.034	4.150	0.040
29376	4.277	0.046	4.267	0.036	4.259	0.041
29487	4.131	0.063	4.138	0.047	4.150	0.057
30112	4.310	0.046	4.302	0.036	4.295	0.041
30409	4.095	0.073	4.101	0.056	4.114	0.074
30675	4.299	0.059	4.306	0.046	4.313	0.058
31069	4.033:	0.045	4.041:	0.034	4.060:	0.039
31195	4.152	0.060	4.157	0.045	4.168	0.057
31327	4.314	0.055	4.314	0.047	4.313	0.058
31331	4.213	0.045	4.207	0.035	4.204	0.040
31726	4.384	0.048	4.377	0.038	4.367	0.043
31894	4.436	0.057	4.441	0.048	4.440	0.060
32328	4.106	0.047	4.106	0.035	4.114	0.040
32330	4.296	0.074	4.305	0.058	4.313	0.075
32612	4.341	0.047	4.337	0.037	4.331	0.042
32672	4.388	0.055	4.389	0.047	4.385	0.059
32686	4.232	0.045	4.225	0.035	4.222	0.041
32816	4.052:	0.051	4.050:	0.042	4.060:	0.056
32867	4.239	0.046	4.229	0.036	4.222	0.041
32884	4.056:	0.051	4.052:	0.042	4.060	0.056
32964	4.025:	0.042	4.027:	0.033	4.042:	0.039
32989	4.353	0.056	4.362	0.046	4.367	0.059
32990	4.281	0.046	4.288	0.036	4.295	0.041
33189	4.313	0.056	4.304	0.045	4.295	0.058
33190	4.105	0.048	4.105	0.035	4.114	0.040
33403	4.151	0.056	4.147	0.044	4.150	0.057
33483	4.044:	0.065	4.037:	0.046	4.042:	0.056
33547	4.206	0.051	4.203	0.037	4.204	0.040
33949	4.068:	0.043	4.086	0.034	4.078	0.039
34078	4.614:	0.061	4.615:	0.052	4.602:	0.062
34179	4.171	0.048	4.167	0.036	4.168	0.040
34233	4.239	0.047	4.238	0.036	4.241	0.041
34251	4.289	0.046	4.282	0.037	4.277	0.041
34447	4.308	0.046	4.301	0.036	4.295	0.041
34511	4.291	0.046	4.283	0.036	4.277	0.041
34576	4.287	0.052	4.291	0.038	4.295	0.041
34792	4.353	0.059	4.342	0.047	4.331	0.058
34989	4.464	0.048	4.455	0.039	4.440	0.044
35007	4.325	0.046	4.319	0.037	4.313	0.042
35079	4.283	0.046	4.279	0.036	4.277	0.041
35104	4.142	0.044	4.143	0.034	4.150	0.040
35135	4.266	0.055	4.261	0.045	4.259	0.058
35215	4.466	0.071	4.475	0.058	4.476	0.077
35271	4.107	0.050	4.106	0.036	4.114	0.040
35299	4.395	0.048	4.392	0.038	4.385	0.043
35329	4.438	0.067	4.432	0.051	4.421	0.059
35337	4.395	0.048	4.392	0.038	4.385	0.043
35395	4.378	0.050	4.383	0.039	4.385	0.043
35501	4.099	0.071	4.093	0.055	4.096	0.074
35502	4.297	0.047	4.296	0.037	4.295	0.041
35575	4.318	0.046	4.316	0.037	4.313	0.042
35653	4.335	0.051	4.343	0.040	4.349	0.042
35671	4.236	0.045	4.227	0.035	4.222	0.041
35777	4.306	0.046	4.300	0.036	4.295	0.041
35792	4.288	0.046	4.282	0.036	4.277	0.041
35834	4.117	0.056	4.111	0.044	4.114	0.057
35899	4.275	0.046	4.266	0.036	4.259	0.041
35910	4.246	0.049	4.242	0.037	4.241	0.041
35912	4.317	0.046	4.315	0.037	4.313	0.042
35926	4.163	0.046	4.162	0.035	4.168	0.040
36133	4.324	0.046	4.319	0.037	4.313	0.042
36151	4.237	0.045	4.228	0.035	4.222	0.041
36166	4.389	0.048	4.380	0.038	4.367	0.043
36262	4.346	0.050	4.339	0.038	4.331	0.042
36267	4.233	0.045	4.226	0.035	4.222	0.041
36285	4.361	0.047	4.356	0.037	4.349	0.042
36310	4.253	0.046	4.245	0.036	4.241	0.041
36392	4.289	0.046	4.282	0.036	4.277	0.041
36429	4.251	0.046	4.244	0.036	4.241	0.041
36430	4.342	0.047	4.337	0.037	4.331	0.042
36487	4.214	0.046	4.207	0.035	4.204	0.040
36541	4.206	0.049	4.203	0.036	4.204	0.040
36627	4.190	0.046	4.185	0.035	4.186	0.040
36629	4.462	0.054	4.454	0.041	4.440	0.044
36653	4.282	0.045	4.279	0.036	4.277	0.041
36695	4.435	0.048	4.431	0.039	4.421	0.043
36741	4.351	0.047	4.342	0.037	4.331	0.042
36760	4.159	0.047	4.151	0.035	4.150	0.040
36824	4.319	0.046	4.316	0.037	4.313	0.042
36892	4.228	0.071	4.233	0.056	4.241	0.075
37032	4.516	0.053	4.519	0.043	4.512	0.045
37043	4.485	0.049	4.475	0.039	4.458	0.044
37076	4.076	0.068	4.072:	0.048	4.078	0.056
37151	4.157	0.044	4.150	0.034	4.150	0.040
37173	4.281	0.048	4.278	0.037	4.277	0.041
37209	4.401	0.048	4.395	0.038	4.385	0.043
37232	4.366	0.047	4.359	0.037	4.349	0.042
37320	4.095	0.043	4.090	0.034	4.096	0.040
37321	4.272	0.046	4.264	0.036	4.259	0.041
37334	4.287	0.047	4.281	0.036	4.277	0.041
37352	4.078	0.055	4.082	0.044	4.096	0.057

TABLE IV (*continued*).

HD	Log T1	ERT1	Log T2	ERT2	Log T3	ERT3
37366	4.618:	0.054	4.627:	0.045	4.620:	0.047
37367	4.276	0.048	4.276	0.038	4.277	0.041
37383	4.310	0.064	4.312	0.048	4.313	0.058
37397	4.319	0.046	4.316	0.037	4.313	0.042
37437	4.231	0.053	4.235	0.044	4.241	0.057
37438	4.264	0.047	4.270	0.036	4.277	0.041
37481	4.390	0.048	4.380	0.038	4.367	0.043
37525	4.293	0.080	4.284	0.059	4.277	0.075
37526	4.255	0.047	4.246	0.036	4.241	0.041
37606	4.067:	0.043	4.067:	0.034	4.078	0.039
37615	4.415	0.057	4.421	0.048	4.421	0.059
37635	4.208	0.045	4.204	0.035	4.204	0.040
37641	4.200	0.050	4.200	0.037	4.204	0.040
37700	4.198	0.046	4.190	0.035	4.186	0.040
37711	4.275	0.045	4.266	0.036	4.259	0.041
37744	4.395	0.048	4.392	0.038	4.385	0.043
37756	4.353	0.047	4.343	0.037	4.331	0.042
37776	4.365	0.048	4.358	0.038	4.349	0.042
37889	4.329	0.046	4.321	0.037	4.313	0.042
38017	4.313	0.073	4.314	0.058	4.313	0.075
38034	4.168	0.073	4.175	0.056	4.186	0.074
38062	4.232	0.071	4.235	0.056	4.241	0.075
38087	4.534:	0.052	4.527	0.042	4.512	0.045
38131	4.476	0.060	4.480	0.050	4.476	0.060
38188	4.228	0.059	4.233	0.045	4.241	0.057
38622	4.262	0.046	4.259	0.036	4.259	0.041
38658	4.496	0.063	4.500	0.051	4.494	0.060
38755	4.197	0.046	4.189	0.035	4.186	0.040
38909	4.346	0.050	4.349	0.039	4.349	0.042
39096	4.098	0.051	4.102	0.042	4.114	0.057
39136	4.241	0.066	4.249	0.048	4.259	0.058
39291	4.343	0.047	4.337	0.037	4.331	0.042
39698	4.291	0.048	4.293	0.037	4.295	0.041
39712	4.388	0.053	4.389	0.046	4.385	0.059
39764	4.210	0.039	4.214	0.033	4.222	0.041
39777	4.365	0.047	4.358	0.037	4.349	0.042
40005	4.357	0.048	4.364	0.038	4.367	0.043
40200	4.268	0.039	4.279	0.034	4.295	0.041
40893	4.606:	0.057	4.611:	0.051	4.602:	0.062
40894	4.374	0.049	4.382	0.039	4.385	0.043
40964	4.054:	0.048	4.051:	0.035	4.060	0.039
40983	4.157	0.050	4.150	0.037	4.150	0.040
41398	4.257	0.066	4.257	0.049	4.259	0.058
41534	4.304	0.041	4.316	0.034	4.331	0.042
41690	4.318	0.052	4.326	0.040	4.331	0.042
41814	4.287	0.046	4.281	0.036	4.277	0.041
41831	4.595:	0.058	4.596:	0.051	4.584:	0.062
42088	4.554:	0.052	4.557:	0.043	4.548:	0.046
42352	4.397	0.052	4.403	0.040	4.403	0.043
42368	4.108	0.053	4.117	0.043	4.132	0.057
42379	4.239	0.058	4.248	0.046	4.259	0.058
42400	4.138	0.048	4.141	0.036	4.150	0.040
42401	4.304	0.049	4.309	0.038	4.313	0.042
42597	4.271	0.047	4.273	0.037	4.277	0.041
42655	4.247	0.047	4.252	0.036	4.259	0.041
42690	4.301	0.046	4.307	0.036	4.295	0.041
42745	4.431	0.049	4.420	0.039	4.403	0.043
42966	4.430	0.056	4.419	0.047	4.403	0.059
43025	4.231	0.057	4.225	0.045	4.222	0.057
43044	4.052:	0.053	4.060:	0.043	4.078	0.056
43112	4.455	0.051	4.460	0.040	4.458	0.044
43317	4.287	0.048	4.291	0.037	4.295	0.041
43461	4.149	0.045	4.146	0.035	4.150	0.040
43496	4.151	0.046	4.157	0.035	4.168	0.040
43754	4.182	0.058	4.182	0.045	4.186	0.057
43818	4.457	0.059	4.462	0.050	4.458	0.060
43836	4.425	0.064	4.426	0.051	4.421	0.059
43954	4.543:	0.069	4.532:	0.053	4.512	0.061
44081	4.231	0.045	4.225	0.035	4.222	0.041
44112	4.291	0.046	4.293	0.036	4.277	0.041
44139	4.559:	0.064	4.560:	0.053	4.548:	0.061
44172	4.260	0.047	4.268	0.036	4.277	0.041
44173	4.152	0.046	4.157	0.035	4.168	0.040
44290	4.495	0.060	4.489	0.049	4.476	0.060
44498	4.288	0.049	4.291	0.038	4.295	0.041
44597	4.518	0.065	4.520	0.052	4.512	0.061
44700	4.264	0.047	4.270	0.036	4.277	0.041
44811	4.426	0.056	4.427	0.047	4.421	0.059
44965	4.252	0.059	4.254	0.047	4.259	0.058
45057	4.221	0.038	4.228	0.033	4.241	0.041
45337	4.423	0.052	4.425	0.040	4.421	0.043
45789	4.310	0.048	4.312	0.037	4.313	0.042
45796	4.150	0.038	4.163	0.032	4.168	0.040
45911	4.334	0.048	4.343	0.038	4.349	0.042
46064	4.315	0.046	4.305	0.036	4.295	0.041
46189	4.280	0.040	4.286	0.034	4.295	0.041
46328	4.413	0.043	4.418	0.036	4.421	0.043
46469	4.330	0.058	4.332	0.047	4.331	0.058
46592	4.554:	0.054	4.556:	0.043	4.548:	0.046
46660	4.511	0.060	4.516	0.051	4.512	0.061
46769	4.162	0.046	4.162	0.035	4.168	0.040
46792	4.252	0.039	4.262	0.033	4.277	0.041
46885	4.032:	0.045	4.041:	0.034	4.060:	0.039
46966	4.464	0.050	4.465	0.040	4.458	0.044
47240	4.314	0.049	4.314	0.039	4.313	0.042
47247	4.215	0.038	4.225	0.033	4.241	0.041
47299	4.349	0.048	4.341	0.038	4.331	0.042
47395	4.191	0.046	4.195	0.035	4.204	0.040
47417	4.429	0.049	4.437	0.040	4.440	0.044
48038	4.151	0.044	4.147	0.035	4.150	0.040
48215	4.185	0.047	4.193	0.035	4.204	0.040
48282	4.512	0.075	4.507	0.060	4.494	0.077
48434	4.385	0.048	4.387	0.039	4.385	0.043
48691	4.345	0.052	4.348	0.040	4.349	0.042
48879	4.241	0.047	4.249	0.036	4.259	0.041
48914	4.085	0.046	4.086	0.035	4.096	0.040
48977	4.296	0.048	4.305	0.037	4.313	0.042
49028	4.156	0.037	4.158	0.032	4.168	0.040
49567	4.233	0.047	4.236	0.036	4.241	0.041
50012	4.334	0.041	4.341	0.035	4.349	0.042
50093	4.312	0.041	4.321	0.034	4.331	0.042
51200	4.301	0.041	4.306	0.034	4.313	0.042
51507	4.212	0.048	4.216	0.036	4.222	0.041
51557	4.093	0.044	4.118	0.034	4.114	0.040
51756	4.522	0.051	4.532:	0.042	4.530	0.045
51782	4.047:	0.055	4.048:	0.043	4.060:	0.056
51823	4.318	0.040	4.324	0.035	4.331	0.042
51826	4.231	0.038	4.241	0.033	4.259	0.041
51892	4.147	0.046	4.155	0.035	4.168	0.040
52018	4.294	0.040	4.302	0.034	4.313	0.042
52092	4.266	0.039	4.270	0.033	4.277	0.041
52382	4.401	0.051	4.405	0.041	4.403	0.043
52533	4.600:	0.052	4.608:	0.043	4.602:	0.047
52559	4.145	0.046	4.154	0.035	4.168	0.040
52670	4.252	0.040	4.262	0.034	4.277	0.041
53344	4.328	0.041	4.338	0.035	4.349	0.042
53428	4.231	0.084	4.234	0.061	4.241	0.075
53456	4.427	0.049	4.427	0.040	4.421	0.043
53649	4.541:	0.070	4.541	0.054	4.530	0.061
53756	4.431	0.049	4.439	0.040	4.440	0.044
54031	4.242	0.039	4.248	0.033	4.259	0.041
54224	4.333	0.041	4.340	0.035	4.349	0.042
54493	4.352	0.048	4.352	0.038	4.349	0.042
54662	4.499	0.050	4.501	0.041	4.494	0.045
54879	4.419	0.050	4.423	0.040	4.421	0.043
54893	4.270	0.040	4.280	0.034	4.295	0.041
54911	4.370	0.048	4.371	0.038	4.367	0.043
54912	4.339	0.040	4.344	0.035	4.349	0.042
54967	4.210	0.038	4.214	0.033	4.222	0.041
55019	4.317	0.041	4.323	0.034	4.331	0.042
55522	4.269	0.040	4.280	0.034	4.295	0.041
55523	4.268	0.039	4.279	0.034	4.295	0.041
55538	4.334	0.049	4.343	0.038	4.349	0.042
55718	4.277	0.039	4.284	0.034	4.295	0.041
55856	4.381	0.042	4.384	0.036	4.385	0.043
55958	4.345	0.041	4.356	0.035	4.367	0.043
56013	4.308	0.041	4.311	0.035	4.313	0.042
56211	4.311	0.040	4.320	0.034	4.331	0.042
56310	4.358	0.042	4.363	0.036	4.367	0.043
56342	4.242	0.039	4.248	0.033	4.259	0.041
56733	4.273	0.039	4.282	0.034	4.295	0.041
56779	4.283	0.040	4.287	0.034	4.295	0.041
56868	4.053:	0.055	4.060:	0.043	4.078	0.056
57109	4.239	0.057	4.238	0.045	4.241	0.057
57193	4.483	0.045	4.483	0.038	4.476	0.044
57593	4.303	0.040	4.307	0.034	4.313	0.042
58286	4.231	0.040	4.250	0.033	4.259	0.041
58325	4.314	0.041	4.321	0.034	4.331	0.042
58657	4.037:	0.037	4.042:	0.031	4.060:	0.039
58766	4.276	0.040	4.284	0.034	4.295	0.041

TABLE IV (*continued*).

HD	Log T1	ERT1	Log T2	ERT2	Log T3	ERT3
58784	4.258	0.048	4.257	0.037	4.259	0.041
59211	4.211	0.046	4.215	0.036	4.222	0.041
59215	4.230	0.040	4.234	0.034	4.241	0.041
59446	4.062:	0.039	4.064:	0.032	4.078	0.039
59543	4.321	0.048	4.327	0.038	4.331	0.042
59550	4.295	0.040	4.303	0.034	4.313	0.042
59864	4.355	0.040	4.361	0.036	4.367	0.043
59882	4.361	0.049	4.365	0.038	4.367	0.043
60196	4.395	0.048	4.401	0.039	4.403	0.043
60429	4.325	0.045	4.336	0.037	4.349	0.042
60479	4.437	0.065	4.441	0.050	4.440	0.060
60498	4.296	0.040	4.303	0.034	4.313	0.042
60553	4.325	0.041	4.328	0.035	4.331	0.042
60753	4.255	0.038	4.263	0.034	4.277	0.041
61006	4.288	0.039	4.299	0.034	4.313	0.042
61068	4.365	0.042	4.367	0.036	4.367	0.043
61330	4.096	0.036	4.100	0.031	4.114	0.040
61333	4.316	0.040	4.323	0.035	4.331	0.042
61347	4.401	0.047	4.404	0.039	4.403	0.043
61641	4.306	0.040	4.317	0.034	4.331	0.042
61948	4.211	0.053	4.214	0.043	4.222	0.057
62193	4.300	0.043	4.305	0.036	4.313	0.042
62226	4.193	0.038	4.204	0.033	4.204	0.040
62483	4.352	0.042	4.360	0.037	4.367	0.043
62542	4.179	0.049	4.187	0.038	4.204	0.040
62747	4.339	0.042	4.345	0.036	4.349	0.042
63028	4.232	0.040	4.235	0.034	4.241	0.041
63118	4.110	0.037	4.116	0.032	4.132	0.040
63271	4.355	0.042	4.353	0.036	4.349	0.042
63308	4.288	0.039	4.299	0.034	4.313	0.042
63343	4.224	0.039	4.230	0.033	4.241	0.041
63465	4.261	0.039	4.267	0.034	4.277	0.041
63578	4.412	0.041	4.418	0.036	4.421	0.043
63655	4.097	0.045	4.101	0.034	4.114	0.040
63735	4.536:	0.062	4.538:	0.050	4.530	0.061
63806	4.268	0.039	4.279	0.034	4.295	0.041
63868	4.260	0.039	4.266	0.033	4.277	0.041
63896	4.199	0.065	4.200	0.048	4.204	0.057
63949	4.393	0.041	4.399	0.036	4.403	0.043
64202	4.346	0.044	4.356	0.037	4.367	0.043
64287	4.308	0.040	4.318	0.034	4.331	0.042
64365	4.340	0.041	4.353	0.035	4.367	0.043
64399	4.266	0.045	4.270	0.036	4.277	0.041
64484	4.033:	0.036	4.039:	0.031	4.060:	0.039
64503	4.303	0.041	4.308	0.035	4.313	0.042
64717	4.335	0.040	4.342	0.036	4.349	0.042
64722	4.397	0.041	4.410	0.036	4.421	0.043
65038	4.301	0.040	4.306	0.034	4.313	0.042
65041	4.303	0.047	4.308	0.037	4.313	0.042
65460	4.301	0.040	4.306	0.034	4.313	0.042
65551	4.252	0.039	4.262	0.033	4.277	0.041
65658	4.307	0.040	4.318	0.035	4.331	0.042
65930	4.326	0.040	4.336	0.035	4.349	0.042
66341	4.134	0.037	4.138	0.032	4.150	0.040
66464	4.292	0.039	4.301	0.034	4.313	0.042
66591	4.261	0.040	4.267	0.033	4.277	0.041
66594	4.185	0.046	4.192	0.035	4.204	0.040
66738	4.251	0.047	4.254	0.036	4.259	0.041
67385	4.302	0.040	4.307	0.034	4.313	0.042
67880	4.301	0.047	4.307	0.037	4.313	0.042
68099	4.140	0.045	4.141	0.035	4.150	0.040
68217	4.265	0.041	4.278	0.034	4.277	0.041
68371	4.223	0.047	4.229	0.037	4.241	0.041
68474	4.085	0.040	4.086	0.033	4.096	0.040
68520	4.159	0.045	4.160	0.035	4.168	0.040
68608	4.204	0.042	4.210	0.034	4.222	0.041
68657	4.277	0.039	4.284	0.034	4.295	0.041
68761	4.460	0.044	4.462	0.038	4.458	0.044
68895	4.256	0.039	4.264	0.033	4.277	0.041
68982	4.380	0.049	4.384	0.039	4.385	0.043
69106	4.448	0.043	4.447	0.037	4.440	0.044
69144	4.216	0.039	4.225	0.033	4.241	0.041
69253	4.466	0.044	4.465	0.038	4.458	0.044
69302	4.416	0.041	4.429	0.037	4.440	0.044
70556	4.352	0.042	4.352	0.036	4.349	0.042
70930	4.375	0.041	4.381	0.036	4.385	0.043
71015	4.374	0.042	4.372	0.036	4.367	0.043
71336	4.291	0.042	4.293	0.035	4.295	0.041
71518	4.239	0.047	4.248	0.036	4.241	0.041
71609	4.277	0.046	4.276	0.037	4.277	0.041
71634	4.142	0.038	4.151	0.033	4.168	0.040
71771	4.334	0.048	4.333	0.037	4.331	0.042
71801	4.310	0.041	4.312	0.035	4.313	0.042
71833	4.071:	0.046	4.078	0.035	4.096	0.040
72127	4.353	0.042	4.352	0.036	4.349	0.042
72771	4.345	0.043	4.348	0.036	4.349	0.042
72787	4.229	0.040	4.250	0.034	4.241	0.041
74375	4.303	0.039	4.307	0.034	4.313	0.042
74773	4.239	0.043	4.239	0.035	4.241	0.041
75112	4.222	0.040	4.221	0.034	4.222	0.041
75149	4.151	0.044	4.156	0.035	4.168	0.040
75241	4.234	0.041	4.236	0.034	4.241	0.041
75549	4.235	0.041	4.236	0.034	4.241	0.041
75821	4.454	0.044	4.458	0.038	4.458	0.044
75869	4.278	0.041	4.285	0.034	4.277	0.041
75991	4.556:	0.071	4.557:	0.054	4.548:	0.061
76004	4.229	0.040	4.233	0.034	4.241	0.041
76538	4.216	0.038	4.225	0.033	4.241	0.041
76566	4.247	0.040	4.251	0.034	4.259	0.041
76640	4.220	0.038	4.227	0.033	4.241	0.041
76805	4.221	0.040	4.220	0.034	4.222	0.041
77475	4.212	0.040	4.215	0.034	4.222	0.041
77581	4.219	0.064	4.219	0.048	4.222	0.057
77770	4.272	0.048	4.293	0.037	4.277	0.041
77904	4.234	0.053	4.235	0.043	4.241	0.057
78005	4.249	0.048	4.253	0.037	4.259	0.041
78985	4.290	0.048	4.292	0.037	4.295	0.041
79041	4.202	0.050	4.210	0.037	4.222	0.041
79241	4.129	0.046	4.136	0.035	4.150	0.040
79351	4.287	0.040	4.298	0.034	4.313	0.042
79421	4.265	0.039	4.269	0.034	4.277	0.041
79447	4.236	0.046	4.255	0.036	4.241	0.041
79694	4.176	0.040	4.178	0.033	4.186	0.040
80094	4.156	0.041	4.159	0.034	4.168	0.040
80781	4.193	0.040	4.196	0.033	4.204	0.040
81504	4.135	0.065	4.139	0.047	4.150	0.057
81753	4.207	0.046	4.213	0.036	4.222	0.041
81891	4.266	0.042	4.270	0.035	4.277	0.041
82111	4.255	0.058	4.256	0.045	4.259	0.058
82419	4.102	0.039	4.104	0.032	4.114	0.040
83865	4.259	0.041	4.258	0.034	4.259	0.041
83881	4.109	0.070	4.116	0.054	4.132	0.074
83944	4.031:	0.044	4.040:	0.034	4.060:	0.039
84228	4.202	0.040	4.201	0.033	4.204	0.040
84971	4.263	0.048	4.269	0.037	4.277	0.041
85953	4.294	0.041	4.294	0.035	4.295	0.041
86352	4.292	0.041	4.293	0.035	4.295	0.041
86440	4.124	0.038	4.125	0.032	4.132	0.040
86466	4.224	0.040	4.230	0.034	4.241	0.041
86606	4.435	0.051	4.440	0.040	4.440	0.044
86659	4.293	0.047	4.293	0.037	4.295	0.041
87026	4.268	0.041	4.271	0.035	4.277	0.041
87782	4.227	0.059	4.232	0.045	4.241	0.057
88015	4.257	0.047	4.256	0.036	4.259	0.041
88497	4.030:	0.072	4.047:	0.055	4.042:	0.074
88976	4.050:	0.051	4.049:	0.042	4.060:	0.056
89104	4.340	0.042	4.345	0.036	4.349	0.042
89403	4.362	0.051	4.365	0.039	4.367	0.043
89688	4.210	0.047	4.214	0.036	4.222	0.041
90087	4.406	0.060	4.407	0.047	4.403	0.059
91272	4.270	0.048	4.272	0.037	4.277	0.041
92287	4.245	0.040	4.250	0.034	4.259	0.041
92467	4.086	0.046	4.087	0.035	4.096	0.040
92536	4.129	0.041	4.136	0.033	4.150	0.040
92850	4.429	0.056	4.428	0.046	4.421	0.059
92936	4.335	0.044	4.334	0.036	4.331	0.042
93163	4.283	0.046	4.288	0.037	4.295	0.041
93484	4.255	0.044	4.256	0.036	4.259	0.041
93695	4.207	0.051	4.213	0.038	4.222	0.041
93714	4.320	0.047	4.326	0.037	4.331	0.042
93845	4.318	0.047	4.325	0.037	4.331	0.042
94144	4.222	0.047	4.229	0.037	4.241	0.041
94559	4.298	0.063	4.296	0.048	4.295	0.058
96088	4.324	0.042	4.328	0.035	4.331	0.042
96261	4.548:	0.076	4.553:	0.060	4.548:	0.078
97522	4.462	0.068	4.463	0.052	4.458	0.060
97557	4.215	0.045	4.217	0.036	4.222	0.041
97670	4.251	0.040	4.254	0.034	4.259	0.041
97991	4.381	0.049	4.385	0.038	4.385	0.043
98695	4.332	0.055	4.332	0.045	4.331	0.058

TABLE IV (*continued*).

HD	Log T1	ERT1	Log T2	ERT2	Log T3	ERT3
98763	4.108	0.049	4.116	0.036	4.132	0.040
99171	4.351	0.049	4.351	0.038	4.349	0.042
99416	4.525	0.068	4.523	0.052	4.512	0.061
99857	4.424	0.056	4.425	0.046	4.421	0.059
99872	4.370	0.050	4.369	0.039	4.367	0.043
99890	4.378	0.051	4.383	0.040	4.385	0.043
100600	4.286	0.047	4.290	0.037	4.295	0.041
100826	4.035:	0.057	4.041:	0.044	4.060:	0.056
100929	4.241	0.041	4.240	0.034	4.241	0.041
101545	4.396	0.044	4.401	0.037	4.403	0.043
101839	4.373	0.067	4.372	0.050	4.367	0.059
102475	4.475	0.061	4.479	0.049	4.476	0.060
102657	4.188	0.062	4.193	0.046	4.204	0.057
103079	4.292	0.041	4.293	0.035	4.295	0.041
103884	4.304	0.041	4.308	0.035	4.313	0.042
104631	4.258	0.056	4.258	0.045	4.259	0.058
105078	4.082	0.040	4.084	0.033	4.096	0.040
105139	4.375	0.060	4.381	0.047	4.385	0.059
105521	4.242	0.041	4.249	0.035	4.259	0.041
105580	4.210	0.044	4.214	0.035	4.222	0.041
106231	4.200	0.041	4.200	0.034	4.204	0.040
106337	4.223	0.043	4.221	0.035	4.222	0.041
106983	4.331	0.041	4.332	0.035	4.331	0.042
108002	4.317	0.048	4.315	0.038	4.313	0.042
108610	4.344	0.049	4.347	0.038	4.349	0.042
108769	4.347	0.052	4.349	0.040	4.349	0.042
110879	4.342	0.042	4.346	0.036	4.349	0.042
111226	4.118	0.040	4.121	0.033	4.132	0.040
111774	4.129	0.041	4.127	0.033	4.132	0.040
112364	4.382	0.060	4.385	0.047	4.385	0.059
112409	4.149	0.041	4.146	0.033	4.150	0.040
112481	4.483	0.063	4.492	0.049	4.494	0.060
113791	4.351	0.043	4.351	0.036	4.349	0.042
113902	4.072:	0.040	4.070:	0.033	4.078	0.039
114529	4.166	0.045	4.173	0.035	4.186	0.040
114981	4.302	0.043	4.307	0.036	4.313	0.042
115846	4.305	0.045	4.309	0.037	4.313	0.042
115967	4.240	0.048	4.248	0.037	4.259	0.041
116003	4.395	0.050	4.401	0.039	4.403	0.043
116226	4.075	0.044	4.081	0.034	4.096	0.040
116852	4.602:	0.056	4.608:	0.049	4.602:	0.062
116890	4.132	0.050	4.137	0.036	4.150	0.040
117856	4.546:	0.052	4.552:	0.043	4.548:	0.046
118991	4.059:	0.040	4.063:	0.033	4.078	0.039
119069	4.461	0.048	4.463	0.039	4.458	0.044
119338	4.299	0.076	4.306	0.058	4.313	0.075
119608	4.222	0.044	4.220	0.035	4.222	0.041
120307	4.372	0.044	4.380	0.037	4.385	0.043
120908	4.157	0.041	4.159	0.034	4.168	0.040
121263	4.395	0.044	4.401	0.037	4.403	0.043
121790	4.368	0.044	4.369	0.036	4.367	0.043
122879	4.388	0.055	4.389	0.046	4.385	0.059
123515	4.075	0.043	4.080	0.034	4.096	0.040
123884	4.216	0.065	4.217	0.048	4.222	0.057
124182	4.226	0.042	4.232	0.034	4.241	0.041
124197	4.279	0.041	4.277	0.035	4.277	0.041
124471	4.459	0.043	4.462	0.038	4.458	0.044
124771	4.299	0.047	4.306	0.037	4.313	0.042
125288	4.103	0.039	4.104	0.032	4.114	0.040
125669	4.091	0.064	4.097	0.047	4.114	0.057
125924	4.411	0.050	4.418	0.039	4.421	0.043
126341	4.363	0.043	4.366	0.036	4.367	0.043
126475	4.096	0.040	4.100	0.033	4.114	0.040
127381	4.374	0.044	4.381	0.037	4.385	0.043
128344	4.068:	0.052	4.068:	0.042	4.078	0.056
128345	4.244	0.042	4.250	0.035	4.259	0.041
129056	4.308	0.043	4.310	0.035	4.313	0.042
129092	4.279	0.041	4.278	0.035	4.277	0.041
129116	4.327	0.043	4.329	0.036	4.331	0.042
129557	4.359	0.042	4.364	0.036	4.367	0.043
129740	4.301	0.048	4.307	0.038	4.313	0.042
129954	4.388	0.049	4.388	0.039	4.385	0.043
130021	4.329	0.048	4.330	0.038	4.331	0.042
131491	4.202	0.040	4.201	0.034	4.204	0.040
131657	4.028:	0.040	4.029:	0.032	4.042:	0.039
132041	4.125	0.043	4.125	0.034	4.132	0.040
132907	4.236	0.058	4.236	0.045	4.241	0.057
132960	4.367	0.045	4.368	0.037	4.367	0.043
132984	4.404	0.044	4.406	0.037	4.403	0.043
133242	4.250	0.042	4.253	0.034	4.259	0.041
133399	4.296	0.042	4.295	0.035	4.295	0.041
133518	4.287	0.045	4.290	0.036	4.295	0.041
133955	4.284	0.042	4.289	0.035	4.295	0.041
134657	4.222	0.041	4.221	0.034	4.222	0.041
134687	4.314	0.043	4.314	0.036	4.313	0.042
135348	4.227	0.041	4.232	0.034	4.241	0.041
135737	4.311	0.048	4.311	0.037	4.313	0.042
135876	4.213	0.041	4.215	0.034	4.222	0.041
136003	4.272	0.052	4.274	0.039	4.277	0.041
136504	4.344	0.043	4.347	0.036	4.349	0.042
136664	4.283	0.042	4.288	0.035	4.295	0.041
138527	4.018:	0.040	4.015:	0.032	4.023:	0.039
138800	4.121	0.045	4.122	0.035	4.132	0.040
139094	4.126	0.043	4.125	0.034	4.132	0.040
139160	4.157	0.040	4.159	0.033	4.168	0.040
139432	4.169	0.045	4.175	0.035	4.186	0.040
140008	4.237	0.042	4.237	0.034	4.241	0.041
140873	4.185	0.041	4.183	0.034	4.186	0.040
141180	4.041:	0.054	4.045:	0.042	4.060:	0.056
141318	4.334	0.042	4.333	0.036	4.331	0.042
141774	4.059:	0.050	4.063:	0.036	4.078	0.039
142313	4.093	0.042	4.099	0.033	4.114	0.040
142378	4.267	0.042	4.271	0.035	4.277	0.041
143018	4.404	0.044	4.406	0.037	4.403	0.043
143567	4.022:	0.071	4.026:	0.055	4.042:	0.074
143699	4.207	0.041	4.212	0.034	4.222	0.041
145792	4.266	0.043	4.271	0.035	4.277	0.041
146001	4.197	0.041	4.198	0.034	4.204	0.040
146029	4.049:	0.052	4.049:	0.042	4.060:	0.056
146284	4.134	0.045	4.138	0.035	4.150	0.040
146332	4.050:	0.075	4.049:	0.056	4.060:	0.074
146416	4.024:	0.041	4.027:	0.033	4.042	0.039
146706	4.078	0.064	4.082	0.047	4.096	0.057
147152	4.171	0.043	4.167	0.034	4.168	0.040
148740	4.274	0.051	4.274	0.038	4.277	0.041
148860	4.108	0.064	4.107	0.047	4.114	0.057
149065	4.446	0.059	4.446	0.047	4.440	0.060
149363	4.416	0.045	4.421	0.038	4.421	0.043
149671	4.131	0.045	4.136	0.035	4.150	0.040
149711	4.331	0.044	4.331	0.036	4.331	0.042
149881	4.325	0.040	4.336	0.035	4.349	0.042
150742	4.289	0.043	4.291	0.036	4.295	0.041
151139	4.366	0.063	4.368	0.048	4.367	0.059
151310	4.426	0.052	4.435	0.040	4.440	0.044
151475	4.486	0.072	4.485	0.058	4.476	0.077
151564	4.479	0.054	4.481	0.042	4.476	0.044
151865	4.310	0.068	4.311	0.050	4.313	0.058
152614	4.059:	0.040	4.072:	0.032	4.078	0.039
153716	4.236	0.046	4.236	0.036	4.241	0.041
154643	4.430	0.052	4.428	0.041	4.421	0.043
154811	4.435	0.060	4.431	0.048	4.421	0.059
155217	4.514	0.053	4.517	0.042	4.512	0.045
155320	4.444	0.053	4.445	0.041	4.440	0.044
155403	4.290	0.053	4.292	0.044	4.295	0.058
155450	4.366	0.045	4.368	0.037	4.367	0.043
155506	4.486	0.048	4.485	0.040	4.476	0.044
155550	4.288	0.049	4.291	0.038	4.295	0.041
155600	4.170	0.061	4.166	0.046	4.168	0.057
155754	4.415	0.048	4.412	0.039	4.403	0.043
155805	4.193	0.061	4.196	0.046	4.204	0.057
155910	4.265	0.072	4.261	0.056	4.259	0.075
156004	4.467	0.047	4.466	0.039	4.458	0.044
156070	4.339	0.054	4.345	0.045	4.349	0.058
156256	4.355	0.063	4.353	0.048	4.349	0.058
156838	4.331	0.047	4.331	0.037	4.331	0.042
157170	4.058:	0.061	4.062:	0.045	4.078	0.056
157243	4.100	0.041	4.102	0.033	4.114	0.040
157317	4.178	0.045	4.179	0.035	4.186	0.040
157698	4.195	0.054	4.197	0.043	4.204	0.057
158078	4.280	0.057	4.287	0.045	4.295	0.058
158094	4.060:	0.044	4.083	0.034	4.078	0.039
158111	4.245	0.058	4.250	0.045	4.259	0.058
158148	4.189	0.037	4.193	0.032	4.204	0.040
158186	4.491	0.047	4.487	0.039	4.476	0.044
158661	4.396	0.055	4.402	0.046	4.403	0.059
158846	4.205	0.048	4.203	0.036	4.204	0.040
158859	4.259	0.051	4.258	0.038	4.259	0.041
159090	4.509	0.049	4.506	0.041	4.494	0.045
159707	4.054:	0.045	4.061:	0.034	4.078	0.039
159831	4.176	0.058	4.179	0.045	4.186	0.057

TABLE IV (*continued*).

HD	Log T1	ERT1	Log T2	ERT2	Log T3	ERT3
159864	4.389	0.057	4.389	0.046	4.385	0.059
160233	4.392	0.047	4.399	0.038	4.403	0.043
161165	4.108	0.057	4.115	0.044	4.132	0.057
161573	4.171	0.041	4.175	0.034	4.186	0.040
161733	4.272	0.051	4.282	0.039	4.295	0.041
161840	4.042:	0.040	4.045:	0.033	4.060:	0.039
161961	4.436	0.049	4.440	0.040	4.440	0.044
162028	4.179	0.038	4.188	0.033	4.204	0.040
162365	4.257	0.039	4.265	0.034	4.277	0.041
163641	4.015:	0.036	4.021:	0.031	4.042:	0.039
163685	4.235	0.043	4.236	0.035	4.241	0.041
164002	4.429	0.049	4.428	0.039	4.421	0.043
164103	4.299	0.048	4.296	0.037	4.295	0.041
164188	4.391	0.061	4.390	0.048	4.385	0.059
164353	4.130	0.040	4.127	0.033	4.132	0.040
164432	4.287	0.039	4.298	0.034	4.313	0.042
164455	4.296	0.044	4.295	0.036	4.295	0.041
164581	4.357	0.045	4.354	0.037	4.349	0.042
164716	4.064:	0.041	4.066:	0.033	4.078	0.039
164806	4.171	0.046	4.176	0.035	4.186	0.040
164833	4.470	0.049	4.467	0.040	4.458	0.044
164852	4.260	0.038	4.266	0.033	4.277	0.041
165016	4.442	0.046	4.444	0.039	4.440	0.044
165049	4.489	0.059	4.486	0.048	4.476	0.060
165516	4.410	0.046	4.409	0.038	4.403	0.043
165793	4.310	0.047	4.311	0.037	4.313	0.042
165938	4.215	0.052	4.217	0.043	4.222	0.057
166182	4.330	0.040	4.339	0.035	4.349	0.042
166192	4.571:	0.055	4.574:	0.044	4.566:	0.046
166540	4.431	0.050	4.429	0.040	4.421	0.043
166596	4.208	0.046	4.232	0.036	4.222	0.041
166689	4.313	0.070	4.313	0.050	4.313	0.058
166787	4.545:	0.082	4.542:	0.062	4.530	0.077
166803	4.445	0.050	4.445	0.040	4.440	0.044
167965	4.216	0.046	4.217	0.036	4.222	0.041
168199	4.178	0.037	4.187	0.032	4.204	0.040
168302	4.429	0.066	4.428	0.050	4.421	0.059
169033	4.043:	0.040	4.046:	0.033	4.060:	0.039
169578	4.034:	0.036	4.040:	0.031	4.060:	0.039
169990	4.101	0.041	4.103	0.033	4.114	0.040
170200	4.116	0.037	4.119	0.032	4.132	0.040
170385	4.313	0.048	4.313	0.037	4.313	0.042
170523	4.181	0.045	4.180	0.035	4.186	0.040
170580	4.198	0.038	4.207	0.033	4.222	0.041
170604	4.343	0.049	4.347	0.038	4.349	0.042
170650	4.091	0.036	4.097	0.031	4.114	0.040
170740	4.314	0.045	4.314	0.037	4.313	0.042
170978	4.270	0.048	4.272	0.037	4.277	0.041
171141	4.436	0.049	4.440	0.039	4.440	0.044
171301	4.075	0.036	4.088	0.031	4.096	0.040
171957	4.049:	0.043	4.049:	0.034	4.060:	0.039
172094	4.334	0.049	4.342	0.038	4.349	0.042
172140	4.573:	0.059	4.575:	0.049	4.566:	0.061
172488	4.349	0.065	4.350	0.049	4.349	0.058
173117	4.153	0.045	4.157	0.035	4.168	0.040
173198	4.345	0.046	4.356	0.039	4.367	0.043
173375	4.243	0.048	4.250	0.037	4.259	0.041
174069	4.292	0.045	4.293	0.036	4.295	0.041
174152	4.201	0.046	4.209	0.036	4.222	0.041
174298	4.304	0.039	4.308	0.034	4.313	0.042
174391	4.183	0.037	4.190	0.032	4.204	0.040
174403	4.433	0.053	4.439	0.041	4.440	0.044
174585	4.247	0.047	4.252	0.036	4.259	0.041
174959	4.166	0.046	4.173	0.035	4.186	0.040
175156	4.063:	0.044	4.065:	0.034	4.078	0.039
175426	4.254	0.047	4.255	0.036	4.259	0.041
175544	4.261	0.040	4.267	0.035	4.277	0.041
175803	4.268	0.039	4.279	0.034	4.295	0.041
176254	4.197	0.038	4.206	0.033	4.222	0.041
176853	4.294	0.048	4.293	0.037	4.295	0.041
176871	4.175	0.037	4.186	0.032	4.204	0.040
177003	4.308	0.047	4.311	0.037	4.313	0.042
177109	4.266	0.047	4.271	0.036	4.277	0.041
177566	4.542:	0.057	4.550:	0.048	4.548:	0.061
177624	4.158	0.040	4.168	0.034	4.186	0.040
177817	4.121	0.045	4.122	0.034	4.132	0.040
177863	4.171	0.046	4.176	0.035	4.186	0.040
177880	4.154	0.038	4.157	0.033	4.168	0.040
178129	4.182	0.058	4.189	0.045	4.204	0.057
178322	4.166	0.046	4.173	0.035	4.186	0.040
178329	4.214	0.047	4.216	0.036	4.222	0.041
178370	4.287	0.057	4.290	0.045	4.295	0.058
178849	4.298	0.047	4.306	0.037	4.313	0.042
179007	4.375	0.064	4.382	0.048	4.385	0.059
179202	4.280	0.050	4.287	0.038	4.295	0.041
179588	4.075	0.036	4.080	0.031	4.096	0.040
180499	4.219	0.049	4.219	0.037	4.222	0.041
180554	4.206	0.037	4.211	0.033	4.222	0.041
180642	4.376	0.045	4.381	0.038	4.385	0.043
180885	4.236	0.046	4.236	0.036	4.241	0.041
181360	4.208	0.038	4.212	0.033	4.222	0.041
181409	4.404	0.049	4.406	0.039	4.403	0.043
181492	4.248	0.047	4.252	0.036	4.259	0.041
181558	4.193	0.045	4.196	0.035	4.204	0.040
182032	4.251	0.042	4.261	0.035	4.277	0.041
182078	4.251	0.040	4.261	0.034	4.277	0.041
182489	4.093	0.038	4.098	0.032	4.114	0.040
182618	4.209	0.036	4.206	0.029	4.204	0.026
182975	4.250	0.041	4.261	0.035	4.277	0.041
183013	4.347	0.041	4.356	0.036	4.367	0.043
183133	4.276	0.047	4.285	0.036	4.295	0.041
183227	4.068:	0.036	4.076	0.031	4.096	0.040
183261	4.311	0.039	4.320	0.034	4.331	0.042
183282	4.047:	0.049	4.056:	0.037	4.078	0.039
183419	4.157	0.039	4.159	0.033	4.168	0.040
183459	4.051:	0.040	4.058:	0.033	4.078	0.039
183561	4.166	0.042	4.165	0.035	4.168	0.040
183570	4.189	0.048	4.194	0.036	4.204	0.040
183899	4.342	0.066	4.346	0.049	4.349	0.058
184502	4.252	0.038	4.262	0.034	4.277	0.041
184927	4.322	0.039	4.319	0.034	4.313	0.042
184930	4.144	0.037	4.152	0.032	4.168	0.040
185268	4.174	0.036	4.169	0.029	4.168	0.025
185330	4.175	0.046	4.188	0.035	4.186	0.040
185423	4.138	0.037	4.140	0.032	4.150	0.040
185507	4.217	0.038	4.225	0.033	4.241	0.041
185607	4.132	0.050	4.136	0.038	4.150	0.040
185780	4.434	0.050	4.440	0.039	4.440	0.044
185784	4.237	0.044	4.245	0.036	4.259	0.041
185859	4.331	0.042	4.339	0.037	4.349	0.042
185915	4.107	0.037	4.114	0.032	4.132	0.040
185936	4.191	0.037	4.195	0.032	4.204	0.040
186205	4.265	0.042	4.269	0.035	4.277	0.041
186412	4.197	0.037	4.206	0.033	4.222	0.041
186536	4.179	0.040	4.188	0.034	4.204	0.040
186568	4.021:	0.034	4.033:	0.027	4.023:	0.024
186587	4.233	0.045	4.243	0.036	4.259	0.041
186660	4.242	0.038	4.248	0.033	4.259	0.041
186837	4.252	0.046	4.254	0.036	4.259	0.041
186994	4.437	0.051	4.441	0.040	4.440	0.044
187459	4.276	0.040	4.276	0.035	4.277	0.041
187536	4.252	0.068	4.254	0.049	4.259	0.058
187640	4.188	0.036	4.186	0.029	4.186	0.025
187879	4.211	0.046	4.215	0.036	4.222	0.041
188252	4.310	0.048	4.312	0.037	4.313	0.042
188461	4.301	0.048	4.307	0.037	4.313	0.042
188503	4.094	0.039	4.091	0.032	4.096	0.040
188504	4.264	0.052	4.261	0.044	4.259	0.058
188665	4.209	0.046	4.214	0.036	4.222	0.041
188891	4.331	0.049	4.331	0.038	4.331	0.042
189103	4.297	0.047	4.305	0.037	4.313	0.042
189316	4.033:	0.042	4.032:	0.033	4.042:	0.039
189432	4.192	0.036	4.188	0.029	4.186	0.025
189550	4.248	0.039	4.251	0.034	4.259	0.041
189846	4.087	0.039	4.087	0.032	4.096	0.040
189847	4.154	0.036	4.150	0.028	4.150	0.025
189957	4.499	0.052	4.500	0.041	4.494	0.045
190001	4.183	0.037	4.182	0.032	4.186	0.040
190047	4.103	0.035	4.104	0.028	4.114	0.024
190114	4.105	0.036	4.106	0.031	4.114	0.040
190256	4.108	0.038	4.107	0.032	4.114	0.040
190336	4.374	0.049	4.373	0.040	4.367	0.043
190427	4.586:	0.059	4.591:	0.050	4.584:	0.062
190549	4.210	0.050	4.206	0.038	4.204	0.040
190570	4.046:	0.040	4.047:	0.033	4.060:	0.039
191024	4.149	0.040	4.147	0.033	4.150	0.040
191139	4.346	0.048	4.340	0.039	4.331	0.042
191201	4.231	0.054	4.226	0.044	4.222	0.057
191243	4.011:	0.037	4.011:	0.031	4.023:	0.039
191263	4.246	0.038	4.250	0.033	4.259	0.041

TABLE IV (*continued*).

HD	Log T1	ERT1	Log T2	ERT2	Log T3	ERT3
191291	4.142	0.037	4.142	0.032	4.150	0.040
191395	4.315	0.044	4.314	0.037	4.313	0.042
191423	4.339	0.046	4.337	0.038	4.331	0.042
191456	4.250	0.039	4.245	0.034	4.241	0.041
191473	4.351	0.047	4.351	0.039	4.349	0.042
191494	4.141	0.056	4.142	0.044	4.150	0.057
191530	4.083	0.042	4.085	0.034	4.096	0.040
191566	4.257	0.059	4.257	0.047	4.259	0.058
191612	4.362	0.047	4.358	0.039	4.349	0.042
191639	4.380	0.041	4.392	0.036	4.403	0.043
191746	4.194	0.037	4.189	0.032	4.186	0.040
191811	4.170	0.038	4.167	0.032	4.168	0.040
191877	4.272	0.047	4.274	0.036	4.277	0.041
191917	4.320	0.044	4.318	0.037	4.313	0.042
192003	4.349	0.048	4.350	0.039	4.349	0.042
192039	4.528	0.049	4.525	0.043	4.512	0.045
192079	4.469	0.063	4.467	0.051	4.458	0.060
192225	4.068:	0.044	4.068	0.034	4.078	0.039
192322	4.251	0.042	4.246	0.035	4.241	0.041
192422	4.225	0.067	4.222	0.050	4.222	0.057
192516	4.053:	0.044	4.052:	0.034	4.060:	0.039
192517	4.241	0.038	4.240	0.033	4.241	0.041
192539	4.141	0.040	4.142	0.034	4.150	0.040
192584	4.112	0.058	4.109	0.044	4.114	0.057
192987	4.101	0.035	4.103	0.028	4.114	0.024
193032	4.514	0.066	4.509	0.053	4.494	0.060
193536	4.270	0.038	4.264	0.030	4.259	0.026
193814	4.070:	0.041	4.069:	0.033	4.078	0.039
193855	4.363	0.049	4.358	0.040	4.349	0.042
194092	4.424	0.047	4.425	0.040	4.421	0.043
194424	4.074:	0.038	4.072:	0.032	4.078	0.039
194636	4.175	0.045	4.177	0.035	4.186	0.040
195089	4.214	0.038	4.216	0.033	4.222	0.041
195810	4.132	0.037	4.145	0.032	4.150	0.040
195965	4.372	0.039	4.372	0.035	4.367	0.043
195986	4.191	0.036	4.187	0.029	4.186	0.025
196006	4.264	0.038	4.261	0.033	4.259	0.041
196025	4.313	0.039	4.321	0.034	4.331	0.042
196035	4.283	0.047	4.289	0.037	4.295	0.041
196421	4.459	0.061	4.462	0.049	4.458	0.060
196662	4.178	0.037	4.187	0.032	4.204	0.040
196740	4.176	0.045	4.179	0.035	4.186	0.040
197036	4.184	0.036	4.183	0.029	4.186	0.025
197226	4.139	0.036	4.141	0.028	4.150	0.025
197511	4.222	0.037	4.221	0.029	4.222	0.026
197512	4.350	0.049	4.351	0.039	4.349	0.042
197770	4.326	0.058	4.329	0.046	4.331	0.058
198414	4.121	0.038	4.122	0.032	4.132	0.040
198625	4.146	0.036	4.145	0.028	4.150	0.025
198781	4.318	0.048	4.325	0.037	4.331	0.042
198784	4.170	0.038	4.167	0.033	4.168	0.040
198846	4.439	0.049	4.442	0.039	4.440	0.044
198915	4.184	0.039	4.183	0.033	4.186	0.040
199081	4.219	0.037	4.219	0.029	4.222	0.026
199140	4.319	0.047	4.326	0.037	4.331	0.042
199479	4.025:	0.039	4.027:	0.032	4.042:	0.039
199661	4.283	0.048	4.288	0.037	4.295	0.041
199889	4.167	0.056	4.165	0.044	4.168	0.057
199890	4.139	0.039	4.141	0.032	4.150	0.040
200269	4.200	0.037	4.200	0.032	4.204	0.040
200340	4.153	0.037	4.157	0.032	4.168	0.040
200615	4.114	0.053	4.110	0.043	4.114	0.057
200804	4.505	0.055	4.504	0.048	4.494	0.060
200927	4.121	0.056	4.123	0.044	4.132	0.057
201269	4.053:	0.046	4.051:	0.035	4.060:	0.039
201320	4.009:	0.055	4.010:	0.043	4.023:	0.056
201359	4.042:	0.039	4.045:	0.032	4.060:	0.039
201522	4.201	0.049	4.201	0.038	4.204	0.040
201638	4.473	0.053	4.478	0.041	4.476	0.044
201795	4.441	0.049	4.443	0.039	4.440	0.044
201836	4.129	0.036	4.128	0.028	4.132	0.025
201910	4.247	0.038	4.243	0.033	4.241	0.041
202253	4.251	0.045	4.246	0.036	4.241	0.041
202347	4.355	0.039	4.354	0.035	4.349	0.042
202349	4.405	0.048	4.406	0.038	4.403	0.043
202654	4.266	0.044	4.261	0.035	4.259	0.041
202753	4.189	0.037	4.193	0.032	4.204	0.040
203245	4.160	0.042	4.179	0.034	4.168	0.040
203532	4.281	0.048	4.287	0.037	4.295	0.041
204076	4.287	0.053	4.290	0.044	4.295	0.058
204150	4.409	0.051	4.408	0.039	4.403	0.043
204536	4.248	0.044	4.242	0.035	4.241	0.041
204770	4.108	0.045	4.116	0.034	4.132	0.040
205139	4.271	0.048	4.273	0.037	4.277	0.041
205601	4.172	0.045	4.176	0.035	4.186	0.040
206259	4.272	0.053	4.273	0.044	4.277	0.058
206636	4.433	0.052	4.438	0.041	4.440	0.044
207330	4.233	0.043	4.235	0.035	4.241	0.041
207538	4.495	0.070	4.488	0.052	4.476	0.060
207563	4.263	0.046	4.269	0.036	4.277	0.041
207951	4.434	0.063	4.439	0.049	4.440	0.050
208218	4.144	0.060	4.144	0.045	4.150	0.057
208266	4.585:	0.067	4.581:	0.052	4.566:	0.061
208727	4.087	0.043	4.086	0.034	4.096	0.040
208761	4.447	0.052	4.446	0.040	4.440	0.044
208904	4.359	0.050	4.365	0.039	4.367	0.043
208947	4.313	0.048	4.313	0.037	4.313	0.042
208973	4.352	0.049	4.361	0.038	4.367	0.043
209008	4.231	0.046	4.234	0.036	4.241	0.041
209339	4.422	0.046	4.424	0.038	4.421	0.043
209419	4.161	0.044	4.161	0.035	4.168	0.040
209454	4.480	0.053	4.481	0.041	4.476	0.044
209819	4.096	0.036	4.100	0.031	4.114	0.040
209961	4.331	0.047	4.331	0.037	4.331	0.042
210424	4.172	0.037	4.175	0.032	4.186	0.040
210628	4.183	0.047	4.182	0.036	4.186	0.040
210809	4.453	0.062	4.449	0.049	4.440	0.060
211924	4.147	0.045	4.155	0.035	4.168	0.040
212043	4.207	0.044	4.203	0.035	4.204	0.040
212093	4.208	0.072	4.204	0.055	4.204	0.075
212183	4.153	0.064	4.148	0.047	4.150	0.057
212222	4.258	0.046	4.267	0.036	4.277	0.041
212883	4.356	0.048	4.363	0.038	4.367	0.043
213087	4.403	0.052	4.405	0.040	4.403	0.043
213236	4.081	0.037	4.083	0.032	4.096	0.040
213322	4.133	0.054	4.128	0.043	4.132	0.057
213571	4.323	0.048	4.328	0.037	4.331	0.042
214080	4.274	0.039	4.283	0.034	4.295	0.041
214240	4.240	0.046	4.248	0.036	4.259	0.041
214263	4.345	0.049	4.348	0.038	4.349	0.042
214652	4.341	0.048	4.346	0.038	4.349	0.042
214930	4.330	0.048	4.331	0.037	4.331	0.042
214993	4.373	0.048	4.381	0.038	4.385	0.043
215371	4.328	0.045	4.329	0.036	4.331	0.042
215733	4.308	0.049	4.311	0.038	4.313	0.042
216044	4.525	0.063	4.523	0.050	4.512	0.061
216200	4.273	0.047	4.274	0.036	4.277	0.041
216494	4.053:	0.036	4.059:	0.031	4.078	0.039
216534	4.398	0.054	4.403	0.046	4.403	0.059
216684	4.197	0.050	4.199	0.037	4.204	0.040
216916	4.332	0.047	4.342	0.037	4.349	0.042
217101	4.364	0.048	4.367	0.038	4.367	0.043
217227	4.278	0.048	4.286	0.037	4.295	0.041
217348	4.063:	0.046	4.065:	0.035	4.078	0.039
217811	4.281	0.047	4.287	0.037	4.295	0.041
217817	4.325	0.046	4.319	0.037	4.313	0.042
217966	4.217	0.067	4.217	0.048	4.222	0.057
218344	4.326	0.049	4.329	0.038	4.331	0.042
218407	4.366	0.048	4.368	0.038	4.367	0.043
218440	4.290	0.045	4.292	0.036	4.295	0.041
218537	4.328	0.045	4.329	0.036	4.331	0.042
218574	4.265	0.048	4.270	0.037	4.277	0.041
220016	4.446	0.054	4.445	0.041	4.440	0.044
220057	4.298	0.046	4.296	0.036	4.295	0.041
220222	4.162	0.045	4.172	0.035	4.186	0.040
220562	4.332	0.055	4.331	0.045	4.331	0.058
220598	4.293	0.048	4.294	0.037	4.295	0.041
220787	4.282	0.048	4.288	0.037	4.295	0.041
221253	4.318	0.045	4.315	0.036	4.313	0.042
221491	4.025:	0.045	4.027:	0.034	4.042:	0.039
221711	4.275	0.047	4.274	0.036	4.277	0.041
223128	4.344	0.045	4.338	0.036	4.331	0.042
223229	4.269	0.046	4.272	0.036	4.277	0.041
224151	4.365	0.053	4.367	0.040	4.367	0.043
224257	4.478	0.053	4.481	0.041	4.476	0.044
224572	4.376	0.048	4.382	0.038	4.385	0.043
224868	4.168	0.078	4.165	0.057	4.168	0.074
225094	4.235	0.054	4.235	0.044	4.241	0.057
225187	4.108	0.046	4.116	0.035	4.132	0.040
225190	4.258	0.051	4.267	0.038	4.277	0.041
225257	4.291	0.056	4.292	0.045	4.295	0.058
231970	4.329	0.052	4.338	0.040	4.349	0.042
250310	4.550:	0.061	4.555:	0.051	4.548:	0.061
251117	4.535:	0.063	4.538:	0.051	4.530	0.061
251847	4.457	0.068	4.461	0.052	4.458	0.060
252321	4.532:	0.058	4.536:	0.050	4.530	0.061
256413	4.508	0.079	4.515	0.062	4.512	0.077
257971	4.435	0.054	4.441	0.047	4.440	0.060
290385	4.339	0.056	4.336	0.045	4.331	0.058

Astron. Astrophys. 247, 447–454 (1991)

ASTRONOMY
AND
ASTROPHYSICS

A comparison of synthetic and observed Mg_2 indices for cool stars

R.K. Gulati[1], M.L. Malagnini[2], and C. Morossi[3]

[1] International School For Advanced Studies (SISSA), Strada Costiera 11, I-34100 Trieste, Italy
[2] Dipartimento di Astronomia, Universita' degli Studi di Trieste, Via Tiepolo 11, I-34131 Trieste, Italy
[3] Osservatorio Astronomico di Trieste, Via Tiepolo 11, I-34131 Trieste, Italy

Received December 10, 1990; accepted March 2, 1991

Abstract. Synthetic spectra, based on models computed by using Kurucz's ATLAS8 code, have been derived in the wavelength range 4820–5380 Å in order to synthesize the Mg_2 index, which measures the MgH and Mg b at 5177 Å features. The atmospheric parameters are chosen so as to represent intermediate type stars of solar chemical composition. For a sample of dwarf and giant stars, comparison between synthetic and observed fluxes in the three wavelength bands used to define the Mg_2 index shows systematic differences. The synthetic fluxes in the central band are generally lower than the observed ones, while in the blue and red bands they are systematically higher than the observed ones. Statistical tests reveal that the Mg_2 and the central bandpass flux discrepancies significantly correlate with both temperature and metallicity. The observed-to-synthetic spectra ratios are presented to illustrate the main features of the discrepancies. The grid of computed index values and their relationships with the basic atmospheric parameters effective temperature and surface gravity are also presented. Such a kind of results are a basic step towards the goal of providing a complete reference grid of spectral indices for the interpretation of the integrated light of stellar systems.

Key words: stellar content of the Galaxy – atmosphere of stars – population I stars

1. Introduction

The formation and evolution of stellar systems can be interpreted in terms of their stellar components histories. For a very limited number of nearby systems, stellar clusters and galaxies, observations and analyses of the individual stellar components can be performed, while for distant stellar systems the integrated light can only be gathered. In order to decode the integrated light into individual stellar components, many methods have been devised and extensively applied. In general, a complete reference grid of representative stars is required. Lack of observations of proper quality for all the stellar types needed to represent the different stellar populations call for the use of "synthetic" stars, namely atmosphere models, to fill in the gaps. At the same time, the use of models makes it possible to calibrate the empirically derived data in terms of the atmospheric parameters, effective temperature, surface gravity and metallicity. About the stellar components, it is well known that for individual nearby stars high resolution spectroscopy can be performed, and very detailed information gained through the spectrum synthesis technique (Kurucz, 1990a). Since quite a different level of resolution can be achieved in the observations of distant stellar systems, also for the stars to be used as templates for the different stellar populations, much lower resolution in the observations is required. Therefore, a loss of information is expected with respect to the case of high resolution spectroscopy but still the spectrum synthesis technique proves to be a very powerful tool for providing a grid of reference spectral features to be compared with observations (Tripicco and Bell, 1990).

Basically, conspicuous features should be extracted from the observed integrated spectra and related to the parameters which characterize the different stellar components. Features which can be easily distinguished and exhibit the characteristics of the stellar systems have been already identified and observed (Faber *et al.* ,1985, hereafter FFBG). One of these features, whose relevance for stellar population studies has been already emphasized (Burstein, 1985) is the Mg_2 index, as defined by FFBG, which has been derived from observations for a large sample of globular clusters and galaxies (Burstein *et al.*, 1984).

To investigate the behaviour of Mg_2 indices on the atmospheric parameters, effective temperatures and surface gravities, we present here a grid of synthetic Mg_2 index computed in the T_{eff} range 4000 - 6250 K, for log g values of 3.0 and 4.5, and solar chemical composition models.

In Sec. 2 the atmosphere models and the synthetic spectrum computation are described; in Sec. 3 the reference data and comparison with the theoretical ones are illustrated; analysis and conclusion are presented in Sec. 4.

2. The Theoretical Grid

2.1. Model Atmospheres

The starting point for the computation of synthetic spectra is a grid of stellar atmosphere models. Of the different sets of existing models, we have used Kurucz's one (Kurucz, 1979a), which has been widely tested for the absolute flux distributions in the stellar continuum and have been found to match the observed spectra of early type stars (Malagnini and Morossi, 1988, and references therein). For the present project, the grid of model atmosphere is chosen in such a way so as to represent main sequence and giant intermediate type stars of solar chemical composition; therefore we chose the surface gravity values of 4.5 and 3.0, effective

Send offprint requests to: M.L. Malagnini

Table 1. Reference stars used to calibrate synthetic Mg_2 index

HD	HR	Name	Sp. Type	T_{eff}	log g	[Fe/H]	No.	$v \sin i$	Mg_2^{obs}
1581	77	ζ TUC	F9V	6000	4.5	-0.10	1	0	0.084
1835	88	CET	G2V	5793	4.45	0.05	2	6	0.129
3443	160		G8V	5419	4.57	-0.16	1	2	0.170
13611	649	ξ^1 CET	G6II-III	5143	3.0	0.12	1	< 17	0.114
14802	695	κ FOR	G1V	5929	4.4	0.0	1	4	0.084
17925	857		K2V	5091	4.5	-0.15	1		0.280
18322	874	3 η ERI	K1III-IV	4710	2.8	0.20	1	< 17	0.223
20630	996	96 κ^1 CET	G5V	5793	4.45	0.23	2	< 17	0.130
22049	1084	18 ϵ ERI	K2V	5040	4.40	-0.23	3	< 17	0.297
22484	1101	10 TAU	F9V	6000	3.96	0.04	4	0	0.072
30495	1532	58 ERI	G1IV	6000	4.5	0.10	1		0.109
37160	1907	40 ϕ^2 ORI	K0IIIb	4667	2.57	-0.21	4		0.183
47205	2429	7 ν^1 CMA	K1III	4941	3.08	0.13	1	< 17	0.246
99491	4414	83 LEO	K1IV	5600	4.6	0.09	1		0.205
102634	4533		F8V	6072	4.3	0.12	2	6	0.071
102870	4540	5 β VIR	F8V	6072	4.3	0.21	8	3	0.068
191408	7703		K3V	4893	4.6	-0.07	1		0.357
192310	7722		K0V	4941	4.5	-0.08	2		0.334
216437	8701	ρ IND	G4IV-V	5929	4.4	0.10	1		0.108
219615	8852	6 γ PSC	K0III	4800	2.42	-0.18	2	7	0.142

Table 2. Synthetic spectral Mg_2 index ([M/H] = 0.0)

T_{eff}	log g	Mg_2^{syn}
4000	4.5	0.833
4250	4.5	0.739
4500	4.5	0.642
4750	4.5	0.534
5000	4.5	0.421
5250	4.5	0.321
5500	4.5	0.243
5750	4.5	0.185
6000	4.5	0.142
6250	4.5	0.109
4000	3.0	0.494
4250	3.0	0.460
4500	3.0	0.392
4750	3.0	0.305
5000	3.0	0.228
5250	3.0	0.175
5500	3.0	0.134
5750	3.0	0.101
6000	3.0	0.076
6250	3.0	0.057

temperature in the range of 4000–6250 K at 250 K step, and [M/H] = 0.0.

Kurucz (1979a,b) has already provided models with $T_{eff} \geq$ 5500 K in steps of 500 K at log g = 3.0 and 4.5 for metal abundance [M/H]= 0.0. We have extended this grid down to T_{eff} = 4000 K, at steps of 250 K. The VAX version 8 of the ATLAS code (Kurucz, 1970, 1979a), as described in Castelli (1988), has been used to compute the models at the effective temperature and surface gravity values reported in Table 2, columns 1 and 2, respectively. The computed models have the same characteristics of the "new convective" ones (Kurucz, 1979b): they take into account the optical thin formulation of mixing length theory, with α, the ratio of mixing length to the pressure scale height, equal to 1; 64 optical depth points are considered in the computations. The opacity distribution functions used in the computations refer to microturbulence velocity of ξ = 2 km s^{-1}. Each model has been computed with as many iterations as needed to ensure convergence to errors at each depth point within 3 % for the flux, and 10 % on its derivative. In this way we have set up a grid of models covering the temperature range 4000–6250 K; gravity values of 3.0 and 4.5, for solar chemical composition.

2.2. Synthetic Spectra

The grid of model atmosphere, as described in section 2.1, was used to compute a grid of corresponding synthetic spectra covering the wavelength range 4820-5380 Å, thereby spanning the range needed to compute the Mg_2 index.

For computation of synthetic spectra, Kurucz's spectrum-synthesis program (SYNTHE code, Kurucz and Avrett, 1981) was used. The advantage of this code is that one can change parameters as desired to generate the synthetic spectra. We took into account the contribution in the spectra due to atomic and molecular lines in the region of the Mg_2 index. Other parameters such as resolution, microturbulence velocity, and rotation velocity are also involved in the SYNTHE code. Molecular opacities are also considered in the Kurucz's spectrum-synthesis program in the treatment of the equation of state and to derive number densities; a total of 153 different species are taken into account, of which 85 refer to atoms and 68 to molecules, both in neutral and ionized form. Eventually, in order to compare synthetic spectra with observations, instrumental broadening is applied to the theoretical fluxes.

As far as the resolution for computing synthetic spectra is concerned, we made several tests with different $R = \lambda/\Delta\lambda$ values, such as 250,000, 125,000, 75,000, and 50,000, while developing the M.Phil. project of Gulati (1989). We found that, after instrumental broadening, there is no loss of spectral features in synthetic spectra with R = 50,000, therefore, to save computational time, we have used such value of resolving power.

As regards atomic line data, we have used the Kurucz's line lists (1988); a detailed description of them can be found in Castelli and Bonifacio (1990).

Concerning the Kurucz's (1987, 1990b) molecular line data, we have considered all hydrides, CN and C_2 molecular lines.

The effect of microturbulence velocity has been also investigated: for giant models, a ξ value of 2 km s^{-1} does not result in substantial difference in the computed spectra, after instrumental broadening and rebinning to the observational resolution, from those obtained with ξ = 0 km s^{-1}. Therefore, for each synthetic spectrum, we assume 0 km s^{-1} of microturbulence velocity.

With the parameters chosen as described above, for each model in the grid, the intensity spectra for 17 emergent angles were computed with a resolution $\lambda/\Delta\lambda$ = 50.000. The intensity spectra were interpolated and integrated over the disk to produce a flux spectrum for an assumed projected rotational velocity of 0 km s^{-1}.

2.3. Synthetic Mg_2 index

The Mg_2 index measures the strength of the features at about 5180 Å, including MgH and the Mg b triplet, and is defined as the ratio (expressed in magnitude) of the integrated flux at the central feature to the integrated flux interpolated between the blue and the red side continua, (see Fig. 1 and, for definition, see FFBG).

This kind of index was introduced by Faber (1973) in the form of $(Mg)_0$ and she had observed this for elliptical galaxies. In a first attempt to derive Faber's index from a theoretical point of view, Mould (1978) made use of different sets of models, including Kurucz's (1975) models, and adopted the atomic and molecular line data available at that time. He showed that the Mg index in an old stellar population is sensitive to metallicity and insensitive to the shape of the initial mass function.

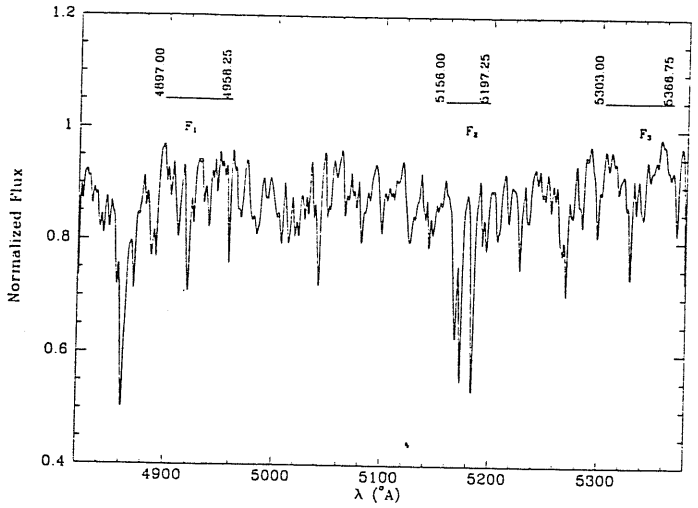

Fig. 1. Synthetic spectrum in the region of the Mg_2 index for atmospheric parameters (6000/4.5/0.0). Here F_1 and F_3 represent the fluxes in the side continuum bands and F_2 represents the flux in the central band. Integration wavelength extrema are reported

To study the old stellar populations, an analysis of K giant stars was done by Faber *et al.* (1985), who then, apart from other indices, introduced the actual Mg_2 index and showed that this index is the most accurate indicator of gravity. Mg_2 index is analogous to Faber (1973) $(Mg)_0$ index, and the transformation between them depends slightly on the luminosity.

Recently, Barbuy (1989) has studied the behaviour of different features constituting the Mg_2 index, in particular the effect of atmospheric parameters on the spectral features MgH, C_2, TiO and CN from a theoretical point of view.

Here we follow the combined approach, both theoretical as well as empirical to investigate the consistency of Kurucz's models to reproduce the observational Mg_2 index.

3. Reference data and comparison

3.1. Reference data

The stars listed in Table 1 have been used as a guide to check the consistency of the synthetic Mg_2 index with the one empirically determined. They have been observed with the Boller and Chivens spectrograph and CCD at the Cassegrain focus of the 1.5 m telescope at the ESO Observatory. The observations cover the wavelength region of 4500–5500 Å, including the Mg_2 index region; the grating used gives the dispersion of 59.5 Å/mm. The raw data have been calibrated in wavelength and rebinned at 0.8 Å step. This data is a sub sample of the complete data base by Buzzoni *et al.* (1990), kindly made available to us by the authors.

The effective temperature, surface gravity and chemical abundance, being the parameters which determine the spectral energy distribution of stars, are reported in columns 5, 6, and 7 of Table 1, respectively; the number of determinations of the parameters is given in Col. 8. The source is Cayrel's Catalog (Cayrel de Strobel *et al.*, 1985); for the parameters with more than one determinations, the average values are reported. In Col. 9, projected rotation velocity, v sin i, is listed, which is taken from Uesugi and Fukuda (1982). Columns 1 to 3 of Table 1 refer to identifiers of the reference stars, and Col. 4 to Spectral Type.

3.2. Comparison

To compare the observed spectra with the synthetic ones, model atmospheres corresponding to the T_{eff} and log g values reported in Table 1 are computed from the grid described in Sec 2.1 . Note that each model is computed starting from the nearest one in the grid.

As regards the metallicity parameter, stars with [Fe/H] in the range of -0.25 to 0.25 are represented by solar metallicity models. This choice is consistent with the fact that the uncertainty expected on this parameter is on the order of $\pm$ 0.25 dex (Cayrel de Strobel, 1985). For each star, the synthetic spectrum was then computed from the appropriate model with the parameters described in Sec. 2.2, and convolved with a gaussian profile of FWHM = 2 Å to match the resolution of the data (this figure was derived from the analysis of the Helium-Argon reference spectrum).

The projected rotational velocity, v sin i, is assumed to be 0 km s^{-1}, since the reference stars have values, listed in Col. 9 of Table 1, less than 17 km s^{-1} in the literature (Uesugi and Fukuda, 1982). Tests with two extreme values, v sin i = 0 km s^{-1} and 20 km s^{-1}, show hardly any difference in the synthetic spectra, owing to the low resolution of the data.

The data for the comparison stars are sampled at a wavelength step of 0.8 Å; therefore, in order to compare synthetic spectra with the observed ones, we rebinned the former with the observational step.

A template synthetic spectrum was constructed from each synthetic spectrum, exactly matching the starting wavelength, and wavelength step. In order to compare synthetic with observed data, it is necessary to normalize to the continuum the observed spectra, which are only calibrated in wavelength. It is difficult to locate continuum points , if any, by looking at the spectrum of late type stars, observed with a resolution power as low as R = 2225, due to the crowding of many molecular and atomic absorption lines. To normalize the observed spectrum, we divided the observed data points by the template synthetic spectrum, assuming that the atmosphere parameters of observed stars given in the literature are the correct ones to represent the spectral energy distribution of the star. A second order polynomial is fitted through the ratio points; all points with residuals in excess of 3 σ are rejected. The fitting procedure is iterated till no more points are discarded. Then the observed spectrum is normalized to the second order polynomial so derived. All the stellar spectra were normalized to the continuum following the above-described procedure.

As an example, Fig. 2 shows, in the case of the star HD 102634:

a. the observed spectrum;
b. its template synthetic spectrum;
c. the ratio of a. over b.; and
d. the "normalized" spectrum, together with its template synthetic spectrum.

At first glance, the synthetic spectrum seems to match well with the observed one with respect to the continuum and the wavelength calibration (see Fig. 2d).

The behaviour of the match between observations and models for the stars of our sample is illustrated in Figs. 3a-c for dwarfs, and in Fig. 3d for giants. The plots of C_λ/F_λ vs. wavelength are arranged in order of decreasing temperature; between any consecutive pair of data, which are normalized to the first point of the proper fitted polynomial, there is a constant offset of 2 on the vertical axis.

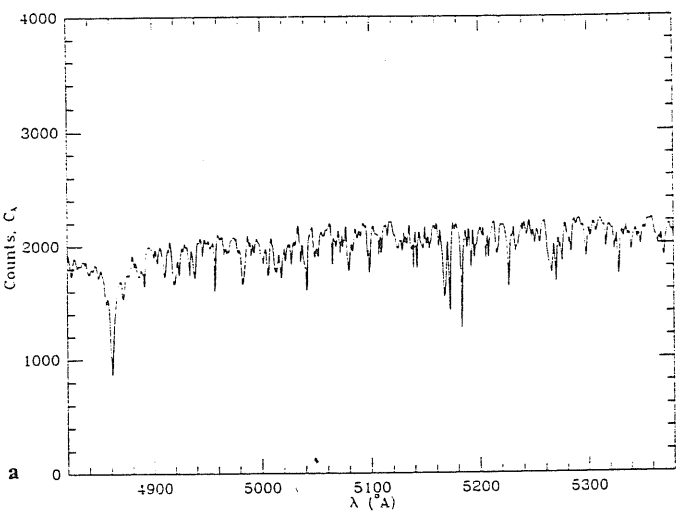

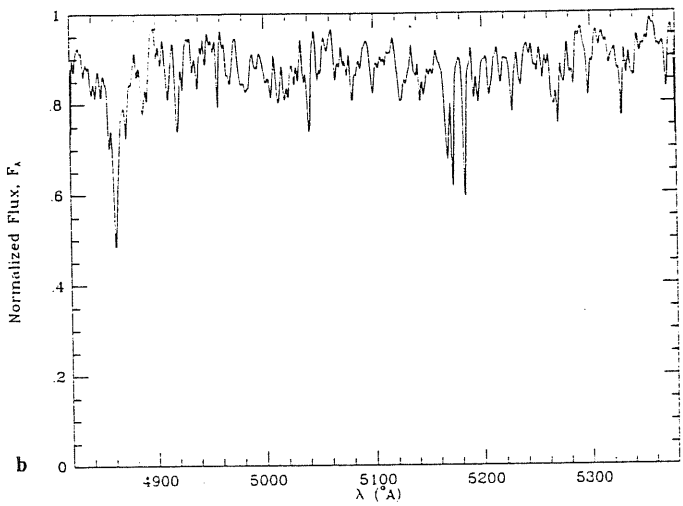

Fig. 2a. Observed Spectrum calibrated in wavelength for the star HD 102634

Fig. 2b. Normalized Synthetic Spectrum representative of the observed star (HD 102634) with atmospheric parameters (6072/4.3/0.0)

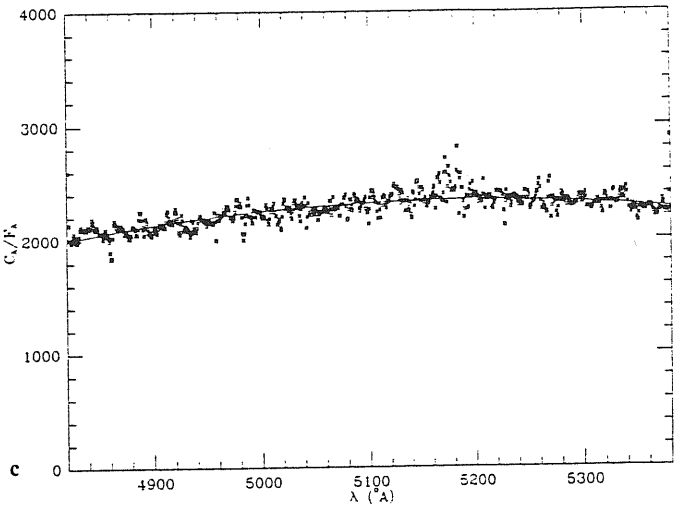

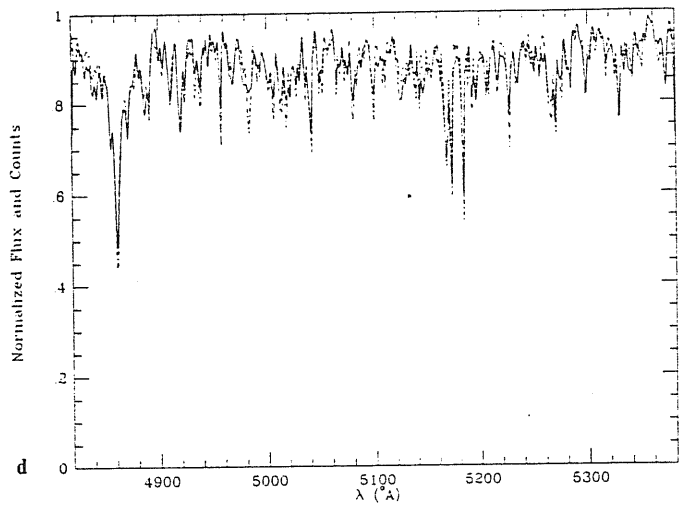

Fig. 2c. Ratio of pixel counts of the observed spectrum of the star HD 102634 to the fluxes for synthetic spectrum (6072/4.3/0.0) as a function of wavelength. Solid line is the second order polynomial through the ratio points

Fig. 2d. Comparison between normalized synthetic and observed spectra. Thick line refers to the synthetic spectrum, dashed line refers to the normalized observed one

Some general comments can be easily derived from these figures:

a. discrepancies between observations and models are present almost everywhere in the region, but are clearly more concentrated in the Mg b region;

b. the scatter is increasing, in particular in the Mg b region, with decreasing temperature;

c. the scatter seems to be sensitive to gravity, in the sense that it increases for giants with respect to dwarfs in the same temperature range; and

d. the behaviour of the giant HD 47205, particularly in the Mg b region, is quite different from the general trend. For this star we used T_{eff} = 4941 K, while recently Brown *et al.* (1989) have derived T_{eff}= 4700 K: this difference in T_{eff} may be responsible for that.

We have identified the C_λ/F_λ features for which discrepancies are more pronounced and found that, in all cases, they include strong Fe lines, apart from the Mg b triplet already mentioned; atomic data for all these lines are worth investigating.

In these spectra, at the sampling of the observations the spectral features are too crowded to be disentangled. It is beyond the scope of this paper to sort out such kind of features and match exactly all the spectral features, because of inadequate observational resolution. Thus our interest is limited to investigate the reliability of the present models in reproducing the observed Mg_2 indices.

For all the stars listed in Table 1, their empirical as well as synthetic Mg_2 indices are computed. The empirical values are listed in Table 1, Col. 10. The resulting two sets of values show significant differences, except for the star HD 47205, as illustrated in Fig. 4. To get more insight into such discrepancies, synthetic and observed integrated spectral fluxes in the individual bandpasses were compared: the integrated fluxes have been computed over the side continuum bandpasses $\lambda\lambda$ 4897–4958.25 Å, referred

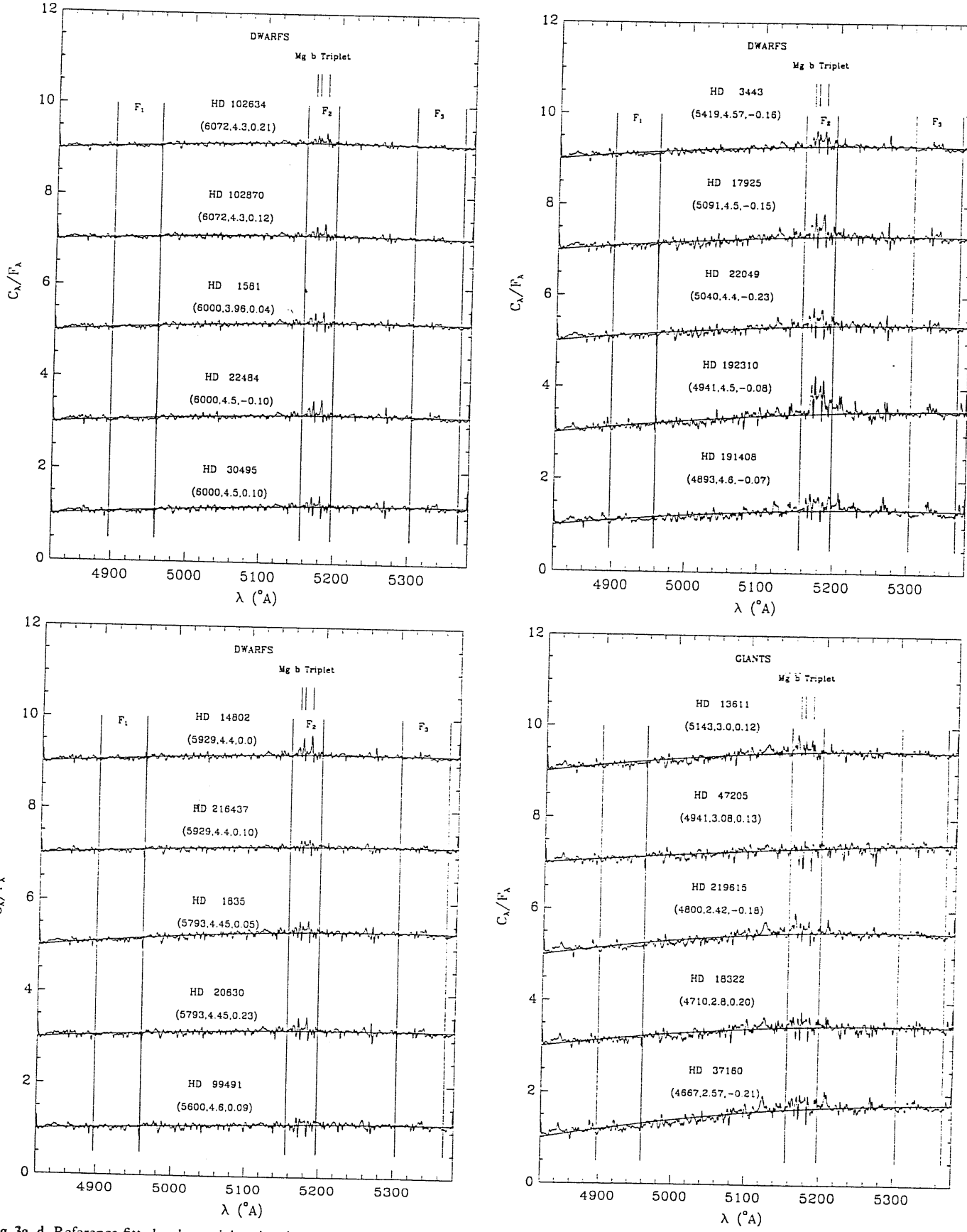

Fig. 3a–d. Reference fitted polynomial and ratio C_λ/F_λ, normalized to the first point of the polynomial, for dwarfs (3a–c) and giants (3d). A constant offset of 2 is applied on the vertical axis. The position of the Mg b triplet (5167.321 Å, 5172.684 Å and 5183.604 Å) and of the three passbands defining the Mg_2 index are marked

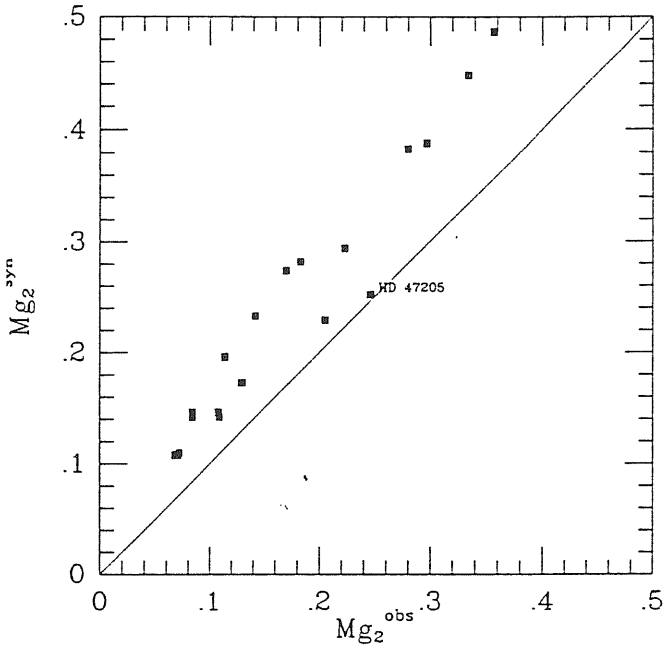

Fig. 4. Comparison between synthetic and observed Mg_2 indices. Solid line is drawn at 45°

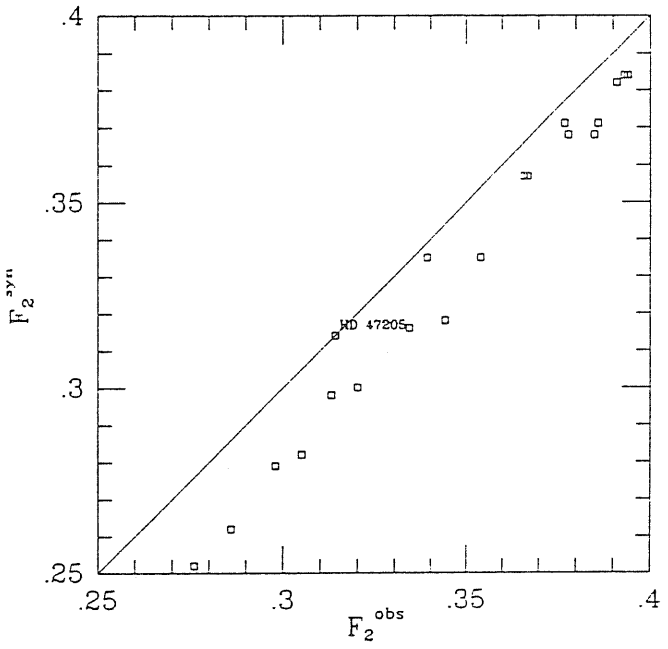

Fig. 6. Same as in Fig. 5 for the fluxes in the central band. F_2

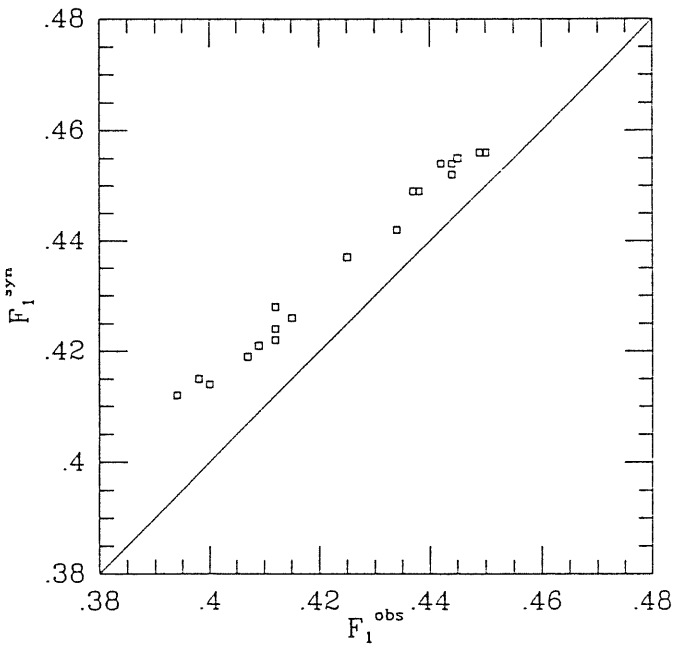

Fig. 5. Comparison between observed and synthetic fluxes in the blue band, F_1. Solid line is drawn at the angle of 45° to show the deviation of synthetic values from the observed ones

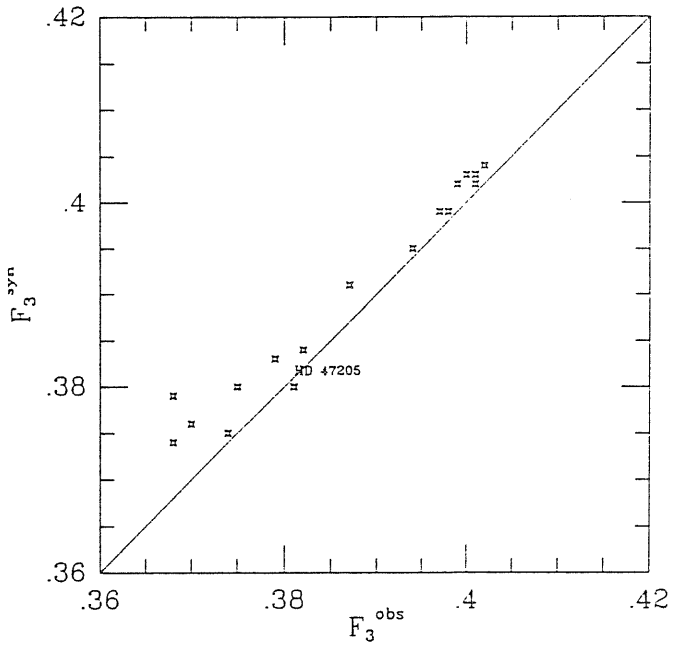

Fig. 7. Same as in Fig. 5 for the fluxes in the red band. F_3

to as blue bandpass , and ($\lambda\lambda$ 5303–5366.75 Å), referred to as red bandpass) and the central bandpass, ($\lambda\lambda$ 5156–5197.25 Å), and are denoted by F_1, F_3, and F_2 respectively. Figs. 5, 6 and 7 show the comparison between theoretical and empirical values in the three different bands. It is obvious from Fig. 5, that the synthetic fluxes in the blue band are higher than the observed ones in a systematic way. On the other hand, the synthetic fluxes in the central band are almost systematically lower than the observed ones (see Fig 6), except for the star HD 47205, which has a synthetic value equal to the observed one. While in the case of red band, synthetic fluxes are found to be slightly higher than the observed ones, except for HD 47205, which has a synthetic value lower than the observed one (see Fig. 7).

4. Analysis and Conclusion

At the resolution of the data, it is difficult to investigate the individual causes of discrepancies between observed and com-

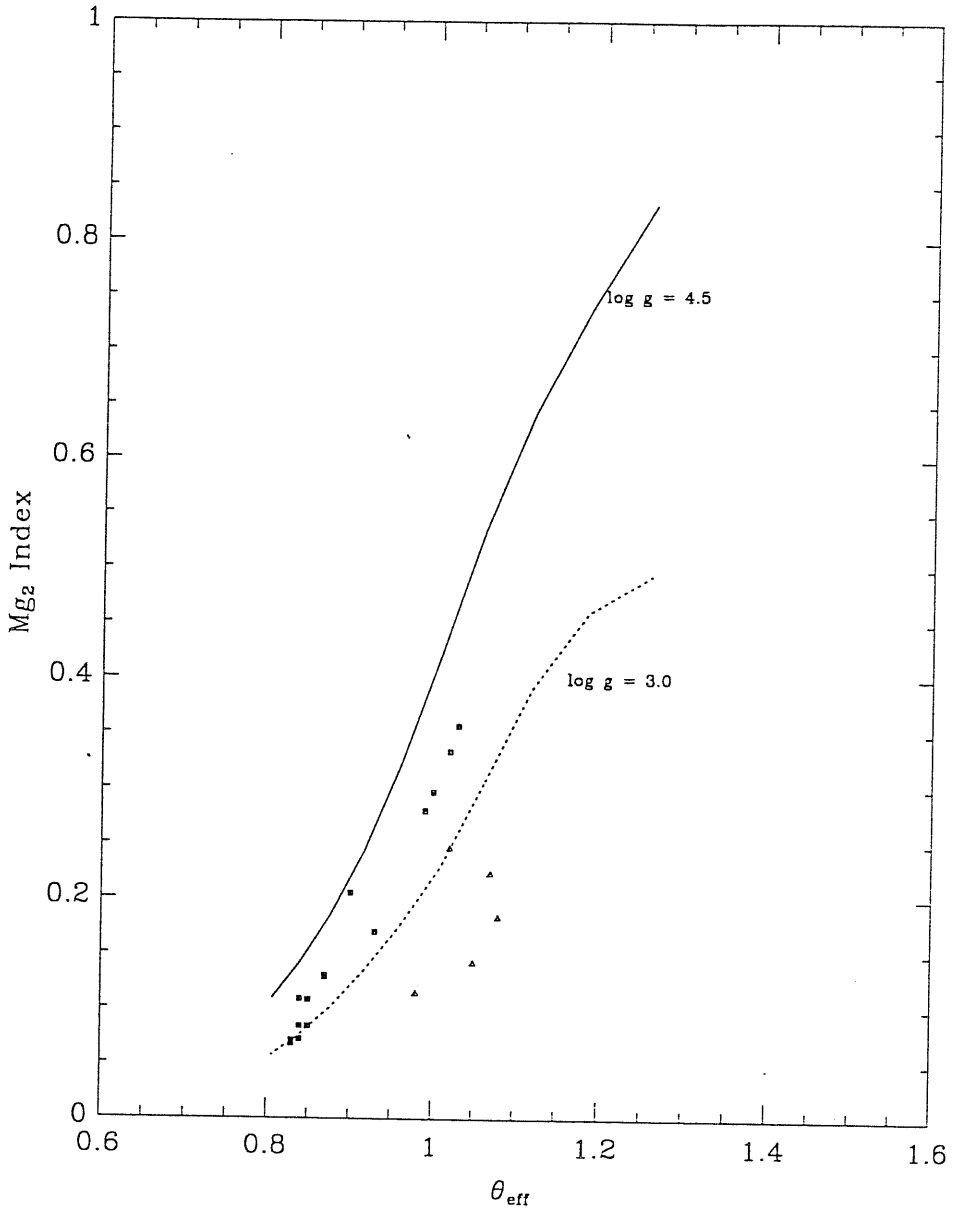

Fig. 8. Mg_2 index as a function of θ_{eff}: the solid line refers to synthetic values for surface gravity log g = 4.5 and the dashed one corresponds to log g = 3.0. Data for the comparison stars are also plotted (squares represent dwarfs, triangles refer to giants

puted fluxes in the three bands used to define the Mg_2 index. These might be attributed to inadequacies of the models, such as failure of the physical assumptions, incorrectness of atomic and molecular data, lack of opacity sources and so on. On the other hand, differences between synthetic and observed fluxes might be due to the uncertainties in the atmospheric parameters (T_{eff}, log g and [Fe/H]) adopted to represent the observed stars.

It is out of the scope of this paper to investigate in detail each of the possible causes above-mentioned, while we are interested in the investigation of their global influence on the Mg_2 index.

Therefore, in order to investigate possible trends of the overall discrepancies with the main atmospheric parameters, statistical tests have been performed. In particular, Pearson product-moment correlations have been computed to test the hypothesis that the residuals of the bandpasses and of the Mg_2 index are randomly distributed. It results that only the correlation coefficients for the residuals of the central bandpass fluxes (F_2) and of the Mg_2 index with respect to temperature and to metallicity are different from zero at the two-tailed 99.9 % confidence level. The same results hold when performing the tests on the reduced sample of 15 dwarfs. No significant correlations have been found versus gravity. It is worth reminding that our sample contains only 5 giants, one of which with a peculiar behaviour, thus preventing any sound conclusion of the role of gravity.

In Fig. 8 we show the trend of synthetic Mg_2 index and $\theta_{eff}=(5040/T_{eff})$, for the surface gravities log =4.5 and 3.0. On the same figure, the positions of the reference stars are plotted; dwarfs are represented by squares and giants by triangles.

The Mg_2 index shows a biparametrical behaviour, in the sense that this index depends both on T_{eff} and log g. The strength of Mg_2 index increases with the decrease of T_{eff}, while at the same temperature, there is a clear demarcation of Mg_2 indices with gravity. Thus Mg_2 index is shown to be an indicator of gravity; this result is consistent with that obtained by FFBG, who derived such a conclusion on the basis of empirical studies.

From the above discussion, we can draw the following conclusion: the current Kurucz stellar atmosphere models are not completely adequate to reproduce the observed Mg_2 indices for

solar metallicity dwarfs and giants in the temperature range 4000-6000 K.

Observations of reference stars covering a wider range of T_{eff}, log g and [Fe/H] are required to extend the comparison of the Mg_2 index to supergiants and non-solar chemical composition stars, and more molecular data have to be inserted in the models and in the synthetic spectra to analyze cooler stars.

Acknowledgements. This research is currently carried on under MURST and bilateral CNR grants. We are very grateful to Drs. R. L. Kurucz and F. Castelli for providing us with ATLAS8 and SYNTHE programs. We thank them and the referee, Dr. D. Burstein, for helpful suggestions.

References

Barbuy, B. : 1989, *Astrophy. Space Sc.* **157**, 111.
Brown, J.A., Sneden, C., Lambert, D.L.,Dutchover Jr., E. : 1989, *Astrophys. J. Suppl.* **71**, 293.
Burstein, D.: 1985 *Pub. Astron. Soc. Pacific* **97**, 89.
Burstein, D., Faber, S.M., Gaskell, C.M., Krumm, N.: 1984, *Astrophys. J.* **287**, 586.
Buzzoni, A., Gariboldi, G., Mantegazza, L.: 1990, *in preparation.*
Castelli, F.: 1988, *Pubbl. Osservatorio Astronomico di Trieste, N.* **1164**.
Castelli, F., Bonifacio, P. : 1990, *Astron. Astrophys. Suppl. Ser.* **84**, 259.
Cayrel de Strobel, G., Bentolila, C., Hauck, B., and Duquennoy : 1985, *Astron. Astrophys. Suppl. Ser.* **59**, 145.
Cayrel de Strobel, G.: 1985, *Calibration of Fundamental Stellar Quantities* **IAU Sym. 111**, 137.
Faber, S.M.: 1973, *Astrophys. J.* **179**, 731.
Faber, S.M., Burstein, D., Gaskell, C.M. : 1985, *Astrophys. J. Suppl. Ser.* **57**, 711.
Gulati R.K. : 1989, *M.Phil Thesis.* SISSA.
Kurucz, R.L.: 1970, *Smithson. Astrophys. Obs. Special Rep.* 309.
Kurucz, R.L. : 1975, *Dudley Obs. Report* **9**, 271.
Kurucz, R.L. : 1979a, *Astrophys. J. Suppl.* **40**, 1.
Kurucz, R.L. : 1979b, *Dudley Obs. Report* **14**, 363.
Kurucz, R.L. : 1987,in *The Second Conference on Fiant Blue Stars, IAU Colloquium No.95*, A. G. Davis Philip, D. S. Hayes, and J. W. Leibert eds., p. 129.
Kurucz, R.L. : 1988, *line list on magnetic tapes.*
Kurucz, R.L. : 1990a, *Harvard-Smithsonian Preprint Series* **No. 3060**.
Kurucz, R.L. : 1990b, *Molecular data on magnetic tapes*
Kurucz, R.L., Avrett, E.H. : 1981, *Smithson. Astrophys. Obs. Special Rep.* **391**.
Malagnini, M.L., Morossi, C.: 1988, in *New Direction in spectrophotometry*, A. G. Davis Philip, D.S. Hayes and S.J. Adelman eds, p. 187.
Mould, J. : 1978, *Astrophys. J.* **220**, 434.
Tripicco, M.J., Bell, R.A.: 1990, *Astron. J.* **99**, 691.
Uesugi, A., Fukuda, I. : 1982, *A revised Catalogue of Stellar Rotational Velocities.*

This article was processed by the author using Springer-Verlag LaTeX A&A style file 1990.

THE STELLAR POPULATIONS OF GALAXIES

IAU Symposium 149

Angra dos Reis, Brazil, August 5-9, 1991

A grid of synthetic Mg_2 indices for cool stars

R. K. GULATI

International School For Advanced Studies (SISSA), Strada Costiera 11, I-34100 Trieste, Italy

M.L. MALAGNINI

Dipartimento di Astronomia, Universita' degli Studi di Trieste, Via Tiepolo 11, I-34131, Trieste, Italy

and

C. MOROSSI

Osservatorio Astronomico di Trieste, Via Tiepolo 11, I-34131, Trieste, Italy

Abstract. A grid of synthetic spectra, based on Kurucz (1991) more recent models representative of cool stars, has been constructed in the wavelength region $\lambda\lambda$ 4850-5340 Å in order to synthesize the Mg_2 index. The behaviour of spectral features in the central band of the index, where the strong features of Mg b triplet and MgH show up, has been explored with respect to primary atmospheric parameters. The dependence of the synthetic Mg_2 index on effective temperature, surface gravity and metallicity is also investigated with the aim of understanding stellar populations of old stellar systems.

Key words: synthetic spectra- Mg_2 index

Method and Results

For the last decade, a large amount of attention is being paid to observe the region of the Mg_2 index spectroscopically at the moderate resolution for nearby stellar systems and individual stars, since this index is considered to be a good indicator of metallicity for stellar systems, and indicator of surface gravity for cool stars. On the theoretical side, recently Barbuy *et al.* (1991) and Gulati *et al.* (1991) have investigated the effect of temperature, surface gravity and metallicity on the synthetic spectra in the region of the Mg_2 index.

Kurucz (1991) has now computed new models which take into account the blanketing of 58 million lines including molecular components, which are important sources of opacity for cool stars. We synthesized a grid of flux spectra in the wavelength region of $\lambda\lambda$ 4850-5340 Å , with resolving power ($\lambda/\Delta\lambda$) of 250,000, for Kurucz new models representative of cool stars. A complete description of the input data and method will be presented in Gulati *et al.* (1991).

A preliminary study of line behaviour in the central region of the index suggests that in general the strength of features contributing to the integrated flux in the central band increases with the decrease of temperature; increases with the increase of surface gravity and decreases with the decrease of metallicity. This result is reflected on the dependence of Mg_2 index on basic atmospheric parameters.

References

Barbuy, B., Erdelyi-Mendes, Milone, A. : 1991, *submitted to Astron. Astrophys Suppl.*
Gulati, R.K., Malagnini, M.L., Morossi, C. : 1991, *Astron. Astrophys.* **247**, 447.
Gulati, R.K., Malagnini, M.L., Morossi, C. : 1991, *in preparation*
Kurucz, R.L. : 1991, *IAU Symposium 149.*